ESCUELA DE DOCTORADO
INTERNACIONAL DE LA USC

Iván
Alonso Fernández

Tesis doctoral

Andamiajes compuestos de ácido poliláctico y bioapatitas derivadas de dientes de tiburón fabricados mediante tecnología de impresión 3D. Ensayos preclínicos.

Lugo, 2024

Programa de doctorado en Investigación Básica y Aplicada en Ciencias Veterinarias

TESIS DOCTORAL

ANDAMIAJES COMPUESTOS DE ÁCIDO POLILÁCTICO Y BIOAPATITAS DERIVADAS DE DIENTES DE TIBURÓN FABRICADOS MEDIANTE TECNOLOGÍA DE IMPRESIÓN 3D. ENSAYOS PRECLÍNICOS.

Autor

Iván Alonso Fernández

Director: Antonio González Cantalapiedra y Fernando María Muñoz Guzón

Tutor/a: Antonio González Cantalapiedra

PROGRAMA DE DOCTORADO EN INVESTIGACIÓN BÁSICA E APLICADA EN CIENCIAS VETERINARIAS

LUGO

2024

DECLARACIÓN CONFLICTO DE INTERESES

Yo, Iván Alonso Fernández, con DNI 53520364-P y con domiciliación a efectos de notificación en Camino Molino, nº1, 1D (Castro Riberas de Lea, Lugo, Galicia), declaro que esta Tesis Doctoral no presenta conflictos de intereses.

En Lugo, a 3 de febrero de 2024.

Firmado: Iván Alonso Fernández

DECLARACIÓN DE TESIS CON EXPERIMENTACIÓN ANIMAL

Yo, Iván Alonso Fernández, con DNI 53520364-P y con domiciliación a efectos de notificación en Camino Molino, nº1, 1D (Castro Riberas de Lea, Lugo, Galicia), declaro que esta Tesis Doctoral se realizó bajo el amparo de proyectos de investigación aprobados por el Comité de Bioética de la Universidad de Santiago de Compostela y de la Xunta de Galicia conforme al marco legal establecido por la Unión Europea (Directiva 2010/63/UE) y por la legislación española (Real Decreto 53/2013). Los procedimientos experimentales que implicaron el manejo de animales vivos fueron realizados por el estudiante de doctorado y los profesores Fernando María Muñoz Guzón y Antonio González Cantalapiedra.

En Lugo, a 3 de febrero de 2024.

Firmado: Iván Alonso Fernández

FINANCIACIÓN

El estudio fue autofinanciado por el Grupo de Investigación “Cirugía, Radiología y Ecografía Experimental Veterinaria” (GI-1708), la ayuda de la Xunta de Galicia para la consolidación y estructuración de unidades de investigación competitivas y otras acciones de fomento en las universidades SUG-GRG (GRC ED431C 2021/19 y ED431C 2021/49) y el proyecto IBEROS+ de la Unión Europea (0072_IBEROS_MAIS_1_E) financiado por el programa FEDER POCTEP 2021-2027.

Durante el período de realización de la Tesis de Doctorado, Iván Alonso Fernández fue beneficiario de una Ayuda predoctoral de la Consellería de Cultura, Educación e Universidades de la Xunta de Galicia (Ref. ED481A 2021/137).

AGRADECIMIENTOS

Si cualquiera me pregunta cuánto tiempo me llevó terminar la Tesis, podría simplemente contestarle que fueron 4 años y 4 meses, sin embargo, me gusta pensar en este período de un modo ligeramente distinto.

Una opción, mi preferida, consiste en contabilizar el tiempo en campañas, concretamente esta Tesis Doctoral duró 5 campañas de maíz y 4 campañas de hierba, durante las cuales pude disfrutar de hacer una de las cosas que más me gusta, andar en tractor. Y, además, no en uno cualquiera… ¡Nunca en la vida habría imaginado que llegaría a conducir un Fendt! Así que no puedo despedir esta etapa sin acordarme de aquellos que lo hicieron posible: José Manuel, Mari Carmen, Nuria y sobre todo de Juanjo. Gracias por apoyarme y tratarme como uno más de la familia durante todo este tiempo, espero que aún nos queden muchas más campañas y momentos por disfrutar juntos.

Y la otra, consiste en desglosar este período en puestos de trabajo, y así poder recordar a la gente con la que pude compartir este camino. Todo comenzó con un año de internado, donde además de aprender, tuve la oportunidad de disfrutar de unos compañeros maravillosos ¡Gracias a todos! Después, el ideal de una vida tranquila y cómoda me llevo a intentar preparar una oposición, 5 meses tirados a la basura, que cosa más aburrida por favor, está claro que eso no es lo mío… Tras una temporada de contratos puntuales, y muchas, muchas, muchas horas de granja, la beca predoctoral de la Xunta de Galicia me dio el empujón (…y el dinero…) que necesitaba para poder centrarme en la Tesis. La disfruté durante 2 años y 6 meses, y tuve la suerte de coincidir con Estrella, Ana, Mónica y María. Sinceramente, fue una época que recordaré con mucho cariño y de la que espero llevarme amistades para toda la vida. Muchas horas de laboratorio, experimentales, cenas y alguna que otra fiesta, me he sentido infinitamente cómodo trabajando con vosotras, ¡gracias! Además, a lo largo de este período tuve la suerte de poder realizar una estancia en Noruega, allí conocí a dos de las personas que más me han ayudado para conseguir terminar la Tesis y pude disfrutar de viajes increíbles… Fiordos, lagos helados, auroras boreales, saunas y nieve, mucha nieve. Por ello, quiero dar las gracias a Håvard y a Liebert, quienes desde el momento de mi estancia se han mostrado siempre dispuestos a colaborar para que esto pudiera salir adelante, ¡Sin vosotros esto no habría sido posible! Actualmente, puedo decir que trabajo haciendo lo que más me gusta, Diagnóstico por Imagen, y con la suerte de disfrutar de la compañía de excelentes profesionales, pero sobre todo excelentes personas, Dani, María, Ali y Mó, creo que no hay palabras de cariño y agradecimiento suficientes para expresar lo que siento al poder trabajar cada día a vuestro lado.

Además, durante esta época también me tocó mudarme a la “preciosa” villa de Castro Riberas de Lea, lo que se hace por amor… Pero bueno, todo tiene su lado positivo, y en este caso fue conocer a personas que hacen que 360 días anuales de niebla y 2 dedos de moho en las paredes por culpa de la humedad se conviertan en minucias mientras pueda disfrutar de su compañía. Susi, Romina, Uxía, Andrea y Rober, ¡Gracias por vuestro apoyo y por muchos

buenos momentos! Por cierto, los miércoles son día de feria, se come un pulpo bueno, bonito y barato, os lo recomiendo.

Como veis, 4 años y 4 meses pueden dar para mucho, por ello quiero agradecerles a mis directores, Fernando y Antonio, su infinita paciencia conmigo y sobre todo su gran ayuda. Fer, a ti te tocó un poco más de cerca, así que gracias por tantas horas de charlas, por tu buen humor, tu positividad y por brindarme tu ayuda siempre que la necesité, poder contar con tu apoyo durante todo este tiempo me dio la fuerza y el ánimo para seguir adelante, cuando la opción más fácil habría sido dejarlo todo.

Quiero dar las gracias también a mi familia, a la que está y a la que se fue, que siempre creyó que podría sacar adelante este proyecto, que lo financió en momentos de crisis, y que tuvo prohibido hablar de él desde el mismo momento en que formalicé la matrícula. Papá, mamá, Andrés, solo vosotros sabéis lo que me lleváis aguantado y lo que os queda por aguantar, pero creedme cuando os digo que no os puedo querer más, y que sois lo más importante de mi vida. Como sé que habitualmente no os lo digo mucho, ahora os queda aquí por escrito para que no se os olvide nunca. Por último, tengo que dar las gracias a otras de las personas más importantes de mi vida, aquella con la que compartí los últimos 8 años, y con la que espero compartir los próximos 53 en base a la esperanza de vida media de los hombres en Lugo. Helena, gracias por ser como eres y por acompañarme durante este viaje, por quererme incondicionalmente, por cuidarme, por aguantarme, por respetarme, por animarme a dejar la Tesis cuando no quería seguir con ella y por animarme a acabarla cuando cambiaba de opinión, este trabajo es tan tuyo como mío, ¡Te quiero mucho! Espero que este solo sea el primero de los muchos objetivos que consigamos cumplir juntos.

Para finalizar, como he visto que se estila mucho lo de incluir frases profundas citadas por personajes célebres al inicio o final de los agradecimientos, me gustaría recordar unas palabras de nuestro querido Mariano, quien en contestación a la frase "*Si bien me quieres, Mariano, da menos leña y más grano*", concluyó:

"*Si quieres grano, Aitor, te dejaré mi tractor*"

ABREVIATURAS

AFM: Microscopio de fuerza atómica
AINE/NSAID: Antiinflamatorios no esteroideos
ALT: Estructura alterna
AM: Fabricación Aditiva
ARRIVE: "Animals in Research: Reporting In Vivo Experiments"
AW: Apatita-wollastonita
BCP: Fosfato cálcico bifásico
BG: Biovidrios
BIC: Contacto hueso-implante
BioCaP: Bioapatitas derivadas de los dientes de tiburón
BMPs: Proteínas óseas morfogenéticas
BMSCs: Células madre mesenquimales derivadas de la médula ósea
BS: Superficie ósea
BTE: Ingeniería de tejidos óseos
BV: Volumen óseo
CAD: Modelo matemático 3D
CAM: Membrana corioalantoidea
CaP: Fosfato cálcico
CCD: Dispositivo de carga acoplada
CDL: Defecto caudal izquierdo
CDR: Defecto caudal derecho
CG: Grupo control
COL-1: Colágeno tipo I
CRL: Defecto craneal izquierdo
CRR: Defecto craneal derecho
CSD: Defectos óseos de tamaño crítico
CSIC: Consejo Superior de Investigaciones Científicas
CT: Tomografía computarizada
DBM: Matriz ósea desmineralizada
DLP: Procesamiento digital de luz
DMLS: Sinterizado directo de metal por láser
DPSC: Células madre de la pulpa dental
EBM: Fusión por haz de electrones
eBM: Médula ósea mejorada
ECM: Matriz extracelular
EDS: Analizador por dispersión de energía de rayos X
EG: Grupo experimental
EMA: Agencia Europea del Medicamento
EMF: Campos electromagnéticos sinusoidales
FDA: "United States Food and Drug Administration"
FDM: Modelado por deposición fundida
FESEM: Microscopio electrónico de barrido de emisión de campo
FFF: Fabricación por deposición de filamento fundido
FGFs: Factores de crecimiento fibroblásticos
FTIR: Espectroscopía de infrarrojos por transformada de Fourier
GAGs: Glicosaminoglicanos
GPC: Cromatografía por permeación de gel
HA: Hidroxiapatita
HEL: Estructura helicoidal
hMSC: células madre mesenquimales humanas.
HSCs: Células madre hematopoyéticas
ICBG: Injerto óseo de cresta iliaca
IFN-γ: Interferón-γ
IIM: Instituto de Investigaciones Marinas
ILs: Interleuquinas
IM: Intramuscular
IMT: Técnica de Membrana Inducida
IP: intraperitoneal
IS: Superficie del implante
ISL: Microestereolitrografía
IV: Intravenoso
La: Lantano
LLFC: Cóndilo femoral lateral izquierdo
MD: Densidad mineral
MDS: Sistema de mini-deposición
MEB: Impresión 3D basada en micro-extrusión
MG-63 cell line: Línea cellular de osteoblastoma humano

MHDS: Sistemas de deposición de cabezales múltiples
Micro-CT: Microtomografía computarizada
MIT: Instituto de Tecnología de Massachusetts
MRI: Resonancia magnética
MSCs: Células madre mesenquimales
MSK: Musculoesquelética
n-HA: Nano-hidroxiapatita
NCPs: Proteínas no colágenas
NIR: Espectroscopía del infrarrojo cercano
Obj S/V: Superficie del objeto en función del volumen
OC: Osteocalcina
OCP: Octacalcio fosfato
PBS: Tampón salino fosfato
PCL: Policaprolactona
PDLA: Ácido poli-L,D-láctico
PEEK: Poliéter éter cetona
PGA: Ácido poliglicólico
PLA: Ácido poliláctico
PLGA: ácido poli(láctico-co-glicólico)
PLLA: Ácido poli-L-láctico
PCL: Policaporlactona
PPF: Polipropileno fumarato
rhBMP-2: Proteína ósea morfogenética recombinante humana-2
RLFC: Cóndilo femoral lateral derecho
ROI: Región de interés
SC: Subcutáneo
SD: Desviaciones estándar
SEM: Microscopía Electrónica de Barrido
SL: Estereolitografía
SLM: "Selective laser melting"
SLS: "Selective laser sintering"
St.Sp.: Separación entre líneas o "struts" / Tamaño de poro
St.Th.: Grosor de las líneas o "struts"
SYRCLE: "Systematic Review Centre for Laboratory animal Experimentation"
Tb.Pf.: Factor de Patrón Trabecular
Tb.Th.: Grosor trabecular
TE: Ingeniería de tejidos
TEM: Microscopía de transmisión de electrones
TGA: Análisis termogravimétrico
TNF-α: Factor de necrosis tumoral-α
TPP: Polimerización de dos fotones
TS: Superficie tisular
TV: Volumen tisular
UV: Ultravioleta
VOI: Volumen de interés
VPP: Técnica de fotopolimeración en cubeta
WD-10: 10-Dodeciltrimetoxisilano
WOS: "Web of Science"
XDR: Difracción de rayos X
β-TCP/TCP: β-fosfato tricálcico
2D: 2 Dimensiones
3D: 3 Dimensiones

ÍNDICE

SUMMARY

SUMMARY

The need for new treatments for patients with musculoskeletal pathologies has increased over the last few decades, attracting the research's community attention. Specifically, the regeneration of bone defects represents a significant challenge for modern medicine, given their implications on the patient's quality of life. Thus, once the healing physiologic capacity of the bone is surpassed or impaired, it becomes evident the need to develop alternative therapeutic strategies for bone generation.

To date, the "gold standard" technique have been autografts, however their use is limited by the existence of several drawbacks such as morbidity, deformities, limited availability, chronic pain, scarring or dysesthesia. Therefore, in recent decades, bone tissue engineering has focused on searching for clinically relevant bone substitutes to synthesize and/or regenerate the bone. For this purpose, a wide variety of biological and synthetic biomaterials have been tested. Among them, metals, polymers, bioceramics and composites have been the most frequently used ones. Furthermore, developing new 3D-printing techniques, such as Additive Manufacturing, has proven to be a promising alternative to satisfy the demand for customizable implants, since they allow the synthesis of porous three-dimensional structures with controlled shape and architecture. In addition, these structures can support cellular colonization, proliferation, and differentiation.

The main objective of the present Doctoral Thesis was to evaluate the use of 3D-printed scaffolds composed by polylactic acid (PLA) and bioapatites derived from shark teeth (bioCaP) manufactured by fused deposition modeling for the regeneration of bone defects in a rabbit model. To this end, the effects of the composition and design of the customized scaffolds on new bone formation were analyzed, to overcome the existing limitations so far in the field on bone tissue engineering. In addition, a systematic review was conducted regarding the use of PLA-bioceramic scaffolds in "in vivo" clinical trials, to better understand the effects, functioning and characteristics of the implanted materials.

The systematic review demonstrated the feasibility of synthesizing composite scaffolds from a combination of a polymeric matrix and a bioceramic material, with the obtained implants being biocompatible and suitable for their use in bone regeneration. Additionally, an increase of the implant's osteogenic capacity secondary to the addition of bioceramics to a polymeric matrix was observed. However, this work also showed the need for further manuscript refinement and standardization in terms of experimental design and anaesthetic protocol selection to obtain higher quality information for the research community.

Regarding to the experimental procedures, all the manufactured and implanted scaffolds demonstrated their biocompatibility for being used in the bone healing process. The scaffolds gradually enriched with bioCaP particles were implanted in rabbit calvarial defects without resulting in significamt enhancement of their osteogenic potential compared with PLA alone groups. Although their addition positively modifies scaffolds' characteristics, bone regeneration process could be probably impaired by the use of low proportions of bioCaP, an insufficient exposure of bioCaP particles on the scaffold's surface, or several drawbacks derived from the polymer, such as the appearance of mild inflammatory response or the

acidification of the environment. However, when designing and implanting scaffolds with alternate and helical designs in critical femoral defects, the results demonstrated that changes in scaffolds' architecture positively affected the new bone formation. These findings were probably occasioned by a greater porosity, pore size and accessible porosity of the helical structures. Nonetheless, the achievement of these characteristics is usually related to a sacrifice of the implant's mechanical properties, hence an adequate balance between porosity and mechanical properties is essential to obtain satisfactory results. Further investigations should be performed to the optimization of both, the composition and the design, as well as to evaluate the possible use of cell or other substances that may promote the osteogenic capacity of the implants.

INTRODUCCIÓN

1 INTRODUCCIÓN

1.1 JUSTIFICACIÓN

Uno de los principales objetivos de la investigación médica temporánea es la regeneración de tejidos dañados [1]. El incremento de la esperanza de vida y el envejecimiento de la población mundial están produciendo un aumento en el número de tratamientos relacionados con las patologías óseas y sus costes derivados [2,3]. Uno de los daños tisulares más frecuentes son los defectos óseos, posicionándolos como un importante problema clínico y socioeconómico, con efectos muy perjudiciales sobre la calidad de vida de los pacientes y la sociedad en general [4–6]. De hecho, el hueso es el segundo tejido más trasplantado después de la sangre [7].

Trastornos musculoesqueléticos tales como fracturas, infecciones óseas, tumores, malformaciones congénitas, patologías maxilofaciales o enfermedades reumáticas, son algunas de las alteraciones más comunes [2,3,8]. En la actualidad, el tratamiento de defectos óseos continúa siendo un reto en muchas cirugías reconstructivas [2,9], sobre todo en casos donde existe alguna condición que pueda retrasar o alterar el proceso de curación ósea, como por ejemplo defectos de gran tamaño o con riego sanguíneo comprometido. Es por ello que en las últimas décadas se ha incrementado la necesidad de nuevos tratamientos para pacientes con patologías musculoesqueléticas, atrayendo la atención de la comunidad investigadora [2,3,10]. En Estados Unidos y Europa, más de medio millón de pacientes se someten anualmente a cirugías de reparación de defectos óseos, suponiendo un coste estimado superior a los 3 mil millones de dólares [7].

La ingeniería de tejidos (TE) constituye un campo de investigación interdisciplinar que combina conocimiento biológico y de ingeniería, con el principal objetivo de desarrollar estrategias terapéuticas alternativas para la reparación y/o la reconstrucción de tejidos u órganos dañados [11,12]. Una de sus ramas de estudio es la ingeniería de tejidos óseos (BTE), cuyo objetivo es inducir la formación de nuevos tejidos óseos funcionales basándose en la comprensión de su biología y desarrollo [2,13,14]. Para ello, una de las principales herramientas es el uso de injertos, definidos como un material o una combinación de varios, que se implantan para promover la curación ósea [3].

Hasta el momento, el trasplante de tejido óseo autólogo ha sido la técnica *"*gold standard*"* para la regeneración de defectos. Sin embargo, su uso se ve limitado por la aparición de numerosas complicaciones que esta técnica puede producir en los pacientes [7]. La gran demanda de este tipo de sustitutos óseos, junto con la ausencia de otras alternativas disponibles actualmente en el mercado con una características idóneas, ha llevado a los investigadores al desarrollo de nuevos biomateriales [7,15]. Así mismo, la BTE ha propuesto un nuevo y esperanzador enfoque a dicho problema mediante el desarrollo de andamiajes 3D porosos, biomiméticos y con actividad osteoinductora [16].

La presente tesis doctoral trata de probar mediante la realización de una revisión bibliográfica sistemática y de un ensayo preclínico, la viabilidad del uso de andamiajes compuestos sintetizados a partir de ácido poliláctico (PLA) y biocerámicas para la regeneración de defectos óseos. Para ello, se utilizó una combinación de PLA y bioapatitas derivadas de

dientes de tiburón sintetizando andamiajes porosos compuestos mediante tecnología de impresión 3D.

1.2 PREVALENCIA DE LA ENFERMEDADES MUSCULOESQUELÉTICAS

La prevalencia de enfermedades musculoesqueléticas es un importante indicador de la calidad de vida entre la población. Un 17,4% de las personas entre los 45 y los 60 años padece alguna patología musculoesquelética (MSK), suponiendo uno de los primeros motivos de consulta a los profesionales de la salud, y ocupando el segundo lugar en cuanto a costes totales generados. Pese a que raramente son causantes de muertes o de ingresos en hospitales, este tipo de patologías se caracterizan por su cronicidad y sus efectos sobre la salud física y mental [17].

A nivel mundial, la prevalencia de casos relacionados con alteraciones MSK en el año 2017 fue de 1,3 billones. Concretamente en España, ese mismo año, fue de entre 18000 y 19000 casos por cada 100.000 habitantes. Generalmente, los trastornos musculoesqueléticos aumentan con la edad en ambos sexos, siendo más habituales en el caso de las mujeres [18]. Por ello, no es de extrañar que sea la condición incapacitante más común en los países de Occidente, y la segunda a nivel mundial. Se estima que las discapacidades ocasionadas por trastornos MSK aumentó un 45% entre 1990 y 2010, y se espera que esta cifra continúe incrementándose debido a una población cada vez más obesa, sedentaria y envejecida.

Algunas de las patologías más frecuentes son el dolor lumbar, dolor de cuello, osteoartritis, artritis reumatoide, gota u osteoporosis, siendo esta un factor de riesgo de fracturas [17–19]. Además, deben tenerse en cuenta las enfermedades profesionales y las lesiones derivadas del deporte, dado que pueden suponer patologías en sí mismas, o predisponer su aparición [20,21].

La cirugía ortopédica, concretamente, es una de las grandes contribuyentes a los costes generales relacionados con el tratamiento de las enfermedades musculoesqueléticas, siendo algunas de las más frecuentes y costosas la fijación de fracturas del cuello femoral en pacientes osteoporóticos, el manejo de fracturas traumáticas, las cirugías de reemplazo de cadera y rodilla, y los procedimientos de columna vertebral [21]. De acuerdo con estudios epidemiológicos, en el período comprendido entre 2010 y 2025, la prevalencia de fracturas en Europa se incrementará anualmente un 28%, suponiendo una carga económica adicional del 25% (Zhu *et al.,* 2021).

La importancia de este grupo de patologías ha sido también demostrada en medicina veterinaria, concretamente en perros y gatos. Así, un estudio realizado en el Reino Unido en 2014 demostró que las enfermedades musculoesqueléticas (MSK) constituían la tercera alteración más frecuente (11,8 %) en perros, tras las enteropatías (17,8%) y las alteraciones dermatológicas (15,5%). Además, otros trastornos como neoplasias, heridas traumáticas, obesidad o heridas por mordisco reportaron prevalencias del 9,5%, 9,0%, 6,1% y 3,8%, respectivamente, pudiendo todas ellas, a su vez, conllevar y/o desencadenar la aparición de trastornos MSK [22]. Años después, en 2021, el mismo autor publicó otro estudio incluyendo un mayor número de pacientes, y observó que los trastornos MSK descendían al cuarto lugar como grupo de patologías más frecuentes en perros con una prevalencia del 8,64%, después de alteraciones dentales (14,1%), desórdenes cutáneos (12,58%) y enteropatías (10,43%). El mismo estudio destacó una mayor aparición problemas MSK en perros machos y perros esterilizados [23]. Del mismo modo, un trabajo realizado en Estados Unidos basado en una encuesta telefónica, recogió como alteraciones más frecuentes en perros las enfermedades MSK, las dentales y las del tracto gastrointestinal o hepáticas; pudiendo deberse las discordancias entre ambos estudios a la fuente de información seleccionada y los métodos de extracción de los datos [23,24].

En el caso de los gatos, la interpretación de su bienestar puede suponer un desafío para los propietarios, dado el enmascaramiento de los signos clínicos, que pueden manifestarse únicamente como modificaciones comportamentales o en el estilo de vida, y que comúnmente suelen relacionarse erróneamente con la vejez. A modo de ejemplo, la osteoartritis, un problema relativamente frecuente en gatos, únicamente se diagnostica en un 2% de los mismos, sin ser la cojera una característica clínica común como ocurre en el caso de los perros. Esto es probablemente debido a su adaptación para ocultar signos de enfermedad, al tratarse tanto de un animal de presa, como depredador [25]. Como consecuencia, los estudios de prevalencia realizados en gatos mostraron que los desórdenes MSK eran mucho menos frecuentes, con una prevalencia del 3,2%. Sin embargo, otros procesos como las heridas traumáticas ocuparon la segunda posición como trastornos más habituales (12,9%), pudiendo estas inducir la aparición de alteraciones como fracturas, desgarros musculares, enfermedad articular degenerativa, etc. La obesidad y las neoplasias en el caso de los gatos presentaron prevalencias del 6,7% y 3,4% [26].

Datos actualizados publicados en el año 2021 elevaron la prevalencia de las enfermedades MKS en esta especie hasta el 4,1%, al igual que la de la obesidad y las neoplasias reportando porcentajes del 5,8% y 1,8%, respectivamente. Por el contrario, la aparición de heridas traumáticas se redujo hasta un 11,6%. Dicho estudio demostró además el efecto sobre la prevalencia de parámetros como el sexo de los animales, observándose un mayor riesgo de atropello, obesidad, cojeras y heridas por mordedura en gatos machos; y la edad, siendo más frecuentes en gatos jóvenes las heridas por mordedura y los atropellos [25].

1.3 EL TEJIDO ÓSEO

El hueso es un tejido biomineral, dinámico y altamente vascularizado que desarrolla múltiples funciones en la fisiología del organismo, incluyendo metabólicas (controlando la homeostasis mineral y ácido-base, almacenando calcio y fósforo, y albergando la médula ósea) y mecánicas (actuando como soporte estructural y de cargas, necesarios para la locomoción y la protección de los órganos internos). Se caracteriza por poseer una matriz extracelular (ECM) mineralizada, compuesta de fibras de colágeno, iones de calcio y fosfato, y proteoglicanos; en la cual se encuentran embebidas las células que componen la unidad básica multicelular [2,27–31]:

- Osteoblastos: Células derivadas de células progenitoras de origen mesenquimal especializadas en la formación de hueso, con un papel importante en el proceso de remodelación ósea por medio de la síntesis, deposición y mineralización de la matriz ósea.
- Osteocitos: Constituyen entre el 90% y el 95% del total de células ósea, son osteoblastos en una fase terminal de diferenciación que se encuentran embebidos en la matriz ósea.
- Osteoclastos: Células mieloides diferenciadas que se encuentra en las depresiones de la superficie ósea, son altamente migratorios y están adaptados únicamente para la reabsorción ósea.
- Células de revestimiento óseo: Se trata de osteoblastos en fase de quiescencia alineados en la superficie ósea. Poseen un papel esencial en la remodelación ósea permitiendo la comunicación con los osteocitos, y siendo responsables del acoplamiento entre formación y resorción ósea.

1.3.1 Composición y estructura ósea

La ECM del hueso constituye un entramado complejo que desempeña un papel crucial en sus propiedades mecánicas y su capacidad de adhesión celular. Se compone de una fracción orgánica (30%) y una inorgánica (70%). La fase orgánica está constituida principalmente de

fibras de colágeno (~90%), formadas por fibrillas de 35-60 nm de diámetro y 1 µm de longitud, las cuales a su vez se componen de moléculas de colágeno formando una triple hélice (triples hélices de tropocolágeno) (Figura 1). El ~10% restante está constituido por otras proteínas no colágenas tales como osteocalcina, osteonectina, fibronectina, etc. La fase inorgánica consiste esencialmente en cristales hexagonales de hidroxiapatita ($Ca_{10}(PO_4)_6(OH)_2$) que se localizan en el intersticio de las fibras de colágeno, proporcionándoles una mejora de sus propiedades mecánicas. Esta fase constituye un importante punto de almacenamiento de minerales, albergando el 99% del calcio del cuerpo, el 85% del fósforo y el 40-60% del magnesio y el sodio [10,30,31].

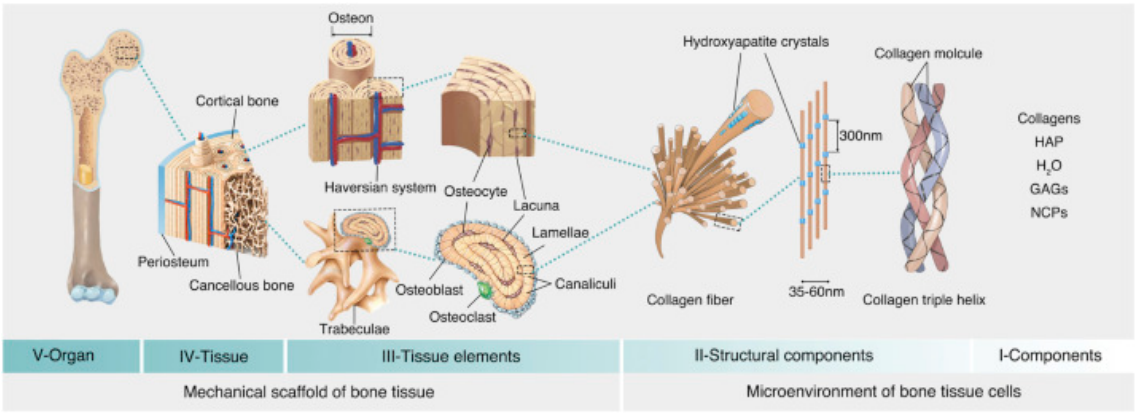

Figura1. Estructura del hueso. Las osteonas son la unidad funciona del tejido óseo, que se organizan para forma formal la cortical ósea. Así mismo, el hueso lamelar se organiza en trabéculas para formal es hueso esponjoso. Ambos son los encargados de proporcionar un soporte mecánico al tejido óseo. En cuanto a la ECM, está formada por una fase orgánica, esencialmente colágeno, y una fase inorgánica, compuesta de cristales de hidroxiapatita. HAP: hidroxiapatita; GAGs: glicosaminoglicanos, NCPs: proteínas no colágenas. "Reimpreso con permiso de [10] bajo los términos de la Licencia Creative Commons Attribution 4.0 International, CC BY-NC.ND 4.0".

El hueso lamelar representa una estructura jerárquica organizada en capas o lamelas. Las estructuras que conforma el hueso lamelar se componen esencialmente de hueso cortical denso y hueso trabecular esponjoso, cuya distribución varía entre las diferentes partes anatómicas [10,13,32].

- El hueso cortical posee una alta resistencia mecánica y rodea al hueso esponjoso en su periferia, proporcionándole estabilidad y soporte. A nivel microscópico, se compone de osteonas, unidad funcional del tejido óseo, que se disponen en círculos concéntricos longitudinalmente al eje largo del hueso, y en cuyo interior transcurren vasos sanguíneos y fibras nerviosas formando los Sistemas Haversianos (Figura 1).
- El hueso trabecular o esponjoso posee una estructura porosa (50-90% de porosidad) con baja resistencia mecánica, y a nivel microscópico se compone de trabéculas dispuestas formando una red similar a un panal de abeja, cuyo interior está relleno de vasos sanguíneos y médula ósea, donde se albergan a su vez las células madre hematopoyéticas (HSCs) y las células madre mesenquimales (MSCs). Este ofrece por tanto un espacio adecuado para el desarrollo del metabolismo óseo y la función hematopoyética (Figura1).

1.3.2 Proceso de curación ósea

Los huesos experimentan un crecimiento dinámico constante, con procesos de remodelación continuos a lo lago de la vida del individuo [2,10,27–29]. Por tanto, a diferencia de otros tejidos y órganos, el tejido óseo posee la capacidad de repararse de forma espontánea

tras una lesión recuperando su estructura y resistencia mecánica originales sin que exista la formación de una cicatriz, siempre que se encuentre bajo condiciones ambientales y fisiológicas adecuadas. Este fenómeno se conoce como proceso de curación ósea [6,10,33].

El proceso de formación ósea atiende a dos tipos de osificación, que comienza en ambos casos con la presencia de una condensación de células progenitoras mesenquimales, que actúan como una base para la posterior formación ósea. En la osificación intramembranosa dichas células se diferencian directamente a osteoblastos. Por el contrario, en la osificación endocondral estas se diferencian en condrocitos que son los responsables de depositar una plantilla cartilaginosa que posteriormente será mineralizada y reemplazada por hueso [13].

Con respecto al proceso de curación ósea existen dos mecanismos principales para la reparación de facturas: la remodelación directa, con formación mínima de callo óseo, y la remodelación indirecta, con formación de callo mediante una combinación de osificación intramembranosa y endocondral, que es la más frecuente. Generalmente este proceso incluye 3 fases superpuestas [6,13]:

- Fase Inflamatoria: Comienza en el momento en el que se produce la fractura con la formación del hematoma, acompañada de una respuesta inflamatoria cuyo pico se alcanza a las 24 horas, y el reclutamiento de moléculas señalizadoras involucradas en la regulación de la formación ósea (Interleuquinas (ILs), Factor de necrosis tumoral-α (TNF-α), factores de crecimiento fibroblásticos (FGFs), proteínas óseas morfogenéticas (BMPs), etc.).
- Fase de Formación Ósea o de Renovación: Tiene lugar 7-10 días después de la fractura. Las células madre mesenquimales proliferan y se diferencian en osteoblastos produciéndose una osificación intramembranosa inmediata a nivel del periostio y la corteza, estabilizando de este modo la fractura por medio de la formación del callo. A continuación, se inicia la condrogénesis en el tejido dañado (osificación endocondral), y al final de dicha fase el cartílago se calcifica y es sustituido por hueso inmaduro (*"*woven bone*"*). Una característica importante de la fase de renovación es la ausencia de mediadores inflamatorios.
- Fase de Remodelación Ósea: En la fase final, los osteoblastos y los osteoclastos ya diferenciados colaboran en el reemplazo del hueso inmaduro por hueso lamelar, por medio de procesos de formación y resorción ósea. En la regulación de la fase de remodelación están involucradas numerosas señales proinflamatorias, que pueden detectarse en la zona de fractura (ILs, TNF-α e interferón-γ (IFN-γ)).

1.4 INGENIERÍA TISULAR ÓSEA

Aunque la gran mayoría de los defectos óseos se pueden curar de forma espontánea bajo unas condiciones fisiológicas y ambientales adecuadas, la regeneración ósea es un proceso fisiológico complejo que dependerá, entre otras variables, del tipo y extensión de la lesión, la edad y el sexo del paciente [6,33]. En defectos de gran tamaño, también conocidos como defectos críticos, la curación puede verse afectada por las dimensiones del defecto, unas propiedades biomecánicas inestables, un entorno desfavorable de la herida o una técnica quirúrgica subóptima, así como por factores metabólicos, hormonales, nutricionales o de estrés [6,10,33]. En estas situaciones es necesaria la realización de intervenciones quirúrgicas terapéuticas debido al limitado potencial de regeneración [34].

Las limitaciones existentes a las que se deben hacer frente para lograr una adecuada reconstrucción y reparación óseas, han dado lugar a la aparición de la ingeniería de tejidos óseos como una solución emergente y prometedora [35,36], convirtiéndose en una de las piedras angulares de la investigación médica contemporánea desde su descripción en 1993. Durante las

últimas décadas ha tenido lugar un avance significativo en este campo, en busca del desarrollo de estructuras funcionales que promuevan la regeneración de órganos dañados o enfermos [27,36,37].

La ingeniería tisular ósea o ingeniería de tejidos óseos (BTE) es el campo de investigación más avanzado dentro de la ingeniería de tejidos, cuyo objetivo es inducir la formación de nuevos tejidos óseos funcionales basándose en la comprensión de su biología y desarrollo [2,13,14]. Para ello, busca crear injertos clínicamente relevantes, centrándose en métodos para sintetizar y/o regenerar hueso manteniendo, restaurando o incluso mejorando su funcionalidad "*in vivo*" [3,32]. Por ello, la capacidad regenerativa del hueso ha proporcionado un nuevo paradigma para el desarrollo de nuevas estrategias de regeneración ósea, postulándose el injerto óseo como una de las principales alternativas de tratamiento para lesiones óseas [3].

El objetivo es sintetizar un biomaterial, o una combinación de varios, con unas características inmunológicas, funcionales, estructurales y mecánicas, que se asemejen lo máximo posible al hueso nativo [1,38]. Para ser utilizado como injerto óseo, un biomaterial debe poseer ciertos requisitos biológicos esenciales como ser: biocompatible, osteoinductivo, osteoconductivo, no inmunogénico, seguro desde un punto biológico, mecánicanicamente resistente, con potencial angiogénico, y biorreabsorbible, para en última estancia ser completamente degradado y sustituido por hueso neoformado. Así mismo, existen otras características de gran interés tales como porosidad, estabilidad volumétrica, fácil disponibilidad, acceso y uso; larga vida útil, rentabilidad y costos de producción razonables [2,4,7,38,39]. Con el fin de cumplir estos criterios, se han ensayado gran variedad de biomateriales para la regeneración del tejido óseo "*in vivo*" [4,27]. Actualmente, existen cuatro tipos principales de injertos óseos: los injertos óseos autólogos o autoinjertos, los injertos óseos alogénicos o aloinjertos, los injertos óseos xenogénicos o xenoinjertos y los sustitutos de injertos óseos o sustitutos óseos.

Los autoinjertos son actualmente la técnica "gold standard" en regeneración ósea. Su composición, basada en células óseas y una matriz celular mineralizada con gran poder osteoconductor, le proporciona una gran capacidad osteoinductora, osteoconductora y osteointegradora, así como una ausencia de propiedades inmunogénicas, siendo la única alternativa que parece cumplir con todas las especificaciones requeridas para un injerto óseo ideal. Sin embargo, dicha técnica implica la realización de un procedimiento quirúrgico secundario que puede conllevar la aparición de numerosas complicaciones como morbilidad, deformidades, dolor crónico, infección, disestesia, cicatrices o hemorragias. Además, la técnica está también limitada por la cantidad de hueso disponible en el área donante del paciente [4,7,40,41].

Como técnicas alternativas a los autoinjertos, existen los aloinjertos y los xenoinjertos. Estos consisten en el trasplante de tejido óseo a partir de otros donantes humanos (cadáveres o donantes vivos), o de otras especies, respectivamente [7]. Sin embargo, la respuesta inmunológica, la falta de capacidad osteogénica con respecto a los autoinjertos, su alta tasa de fracasos y el riesgo de transmisión de enfermedades infecciosas representan una serie de inconvenientes que deben ser tenidos en cuenta y que limitan el uso de ambas opciones [7,40–42].

Frente a las limitaciones de los injertos óseos autólogos, alogénicos y xenogénicos, los sustitutos óseos han surgido como una posible solución para la obtención de nuevos biomateriales de origen biológico o sintético que puedan ser implantados para el tratamiento de defectos óseos, definiéndose un biomaterial como una matriz temporal que proporciona un entorno y arquitectura específica para el crecimiento y el desarrollo óseo. Si bien gran parte de los biomateriales disponibles comercialmente son osteoconductivos, solo unos pocos parecen

ofrecer realmente propiedades osteoinductivas, lo cual justifica la necesidad del desarrollo de nuevos biomateriales para su uso en ingeniería de tejidos óseos [2,4,7,15]. Ante esta situación, numerosos investigadores han explorado diferentes combinaciones de células, biomateriales y factores biológicos, tratando de conseguir nuevas estrategias terapéuticas para regeneración ósea [4,5,7]. Sin embargo, hasta el momento estos únicamente ofrecen una solución parcial para el manejo de la pérdida ósea.

Los implantes metálicos (aleaciones de titanio y acero inoxidable), por ejemplo, son actualmente utilizados para la fabricación de prótesis articulares, tornillos y placas de osteosíntesis, con el fin de brindar soporte mecánico y estructura en artroplastias, fracturas, etc. Sin embargo, estos biomateriales presentan ciertas limitaciones debido a su falta de biodegradabilidad, alta rigidez, fatiga, fractura, falta de integración en el tejido del hospedador y alto riesgo de infección [2].

1.4.1 Andamiajes para regeneración ósea

Tradicionalmente, la mayoría de los sustitutos óseos disponibles comercialmente se han presentado en forma de partículas, capaces de rellenar y adaptarse a cualquier defecto óseo [43–45]. Sin embargo, su uso se ha visto limitado por su baja estabilidad, siendo altamente vulnerables frente a la aplicación de fuerzas externas, con el subsecuente riesgo de colapso de la fractura. Por ello, estos biomateriales fracasaban en cuanto al mantenimiento del espacio, restringiéndose en gran medida su uso a aplicaciones concretas en zonas sin soporte de cargas para evitar resultados no deseados [45,46].

Esta situación llevó a la aparición de sustitutos óseos de tipo bloque, los cuales proporcionaban un mayor soporte mecánico, siendo capaces de mantener el volumen y el contorno óseos [29]. No obstante, la irregularidad y complejidad de los defectos óseos hace necesarios procesos de recorte y moldeado para que dichos biomateriales se ajusten al espacio que deben ocupar. Esto incrementa el riesgo de aparición de posibles infecciones con respecto a los biomateriales particulados, debido a una mayor manipulación de los mismos [29,43,45].

Con el paso del tiempo, y el avance y desarrollo de la técnicas de impresión 3D, surgió uno de los principales enfoques actuales en la ingeniería de tejidos óseos, como son los tratamientos basados en el uso andamiajes o “scaffolds” [34]. Estos se basan en el uso de estructuras porosas tridimensionales que pueden soportar y guiar activamente la regeneración del tejido óseo [7,38]. Al mismo tiempo, la demanda de sustitutos óseos personalizables se ha incrementado, en base a la ya mencionada necesidad de nuevos implantes que puedan adaptarse a la geometría ósea específica de los pacientes [29,36,47], fomentando la investigación de una herramienta capaz de crear andamiajes complejos y replicables a partir del uso de imágenes 3D obtenidas mediante técnicas de diagnóstico médico como la tomografía computarizada (TC) o la resonancia magnética (MRI) [35,38,48,49]. De este modo, la idea inicial de utilizar los andamiajes como simple sustitutos óseos que actúan rellenado un espacio, evolucionó a la búsqueda de estructuras complejas que tratan de replicar la composición físico-química y las propiedades mecánicas del hueso nativo [38].

Los andamiajes o “scaffolds” consisten en estructuras de soporte sólidas tridimensionales con una red de poros interconectados que debe soportar la colonización, proliferación, diferenciación y migración de las células óseas [2,3]. Al igual que los biomateriales para injertos óseos, los andamiajes deben poseer unas propiedades estructurales y fisicoquímicas adecuadas. Su objetivo principal es proporcionar un microentorno conductor que imite las propiedades de la matriz extracelular (ECM) nativa, con el fin de lograr una regeneración óptima del tejido [3,36,50]. A lo largo del último siglo, ha aumentado la disponibilidad comercial de andamiajes

sintéticos para la ingeniería de tejidos óseos. Sin embargo, a menudo existe una importante brecha entre la investigación y la aplicación clínica y comercialización [2,42].

En cuanto a un andamiaje ideal para la ingeniería de tejidos óseos, algunas de las características críticas son su arquitectura y método de fabricación, su composición, sus propiedades mecánicas, su tasa de degradación y su capacidad osteogénica (Figura 2). La estructura tridimensional debe tener un tamaño de poro, una arquitectura de poro, una porosidad y una interconectividad o permeabilidad (medida de líquido que puede fluir a través de una material poroso) adecuados para permitir la difusión de nutrientes, oxígeno y factores de crecimiento, así como el intercambio de productos de desecho. Otras características esenciales son que debe favorecer la infiltración vascular, la proliferación de células y el crecimiento óseo desde la periferia hasta la parte interna del andamio. [15,35,51]. Además, estas se encuentran estrechamente relacionadas con las propiedades mecánicas del andamiaje, proporcionando resistencia a la compresión suficiente y una elasticidad que permita la formación del hueso en regiones sometidas a soporte de cargas [7]. Del mismo modo, dichas estructuras deben facilitar la transmisión de cargas a los tejidos circundantes, proporcionando apoyo mecánico instantáneo al lugar del defecto tras la implantación [2,34,50]. La tasa de degradación del implante debe ser comparable a la tasa de formación de hueso nuevo, asegurando la reabsorción durante el proceso de remodelación del tejido óseo, mientras que mantiene el volumen del defecto [7,15]. Tambíen debe poder esterilizarse por métodos convencionales y ser reproducible por medio de procesos económicamente rentables [2]. En lo referente a la capacidad osteogénica de los andamiajes, esta será dependiente de múltiples factores como son el proceso de fabricación, sus características estructurales, los biomateriales que lo conformen y los requisitos biológicos del tejido [2]. Hasta la fecha, la mayoría de los andamiajes descritos en publicaciones científicas únicamente cumple algunos de esos criterios [12].

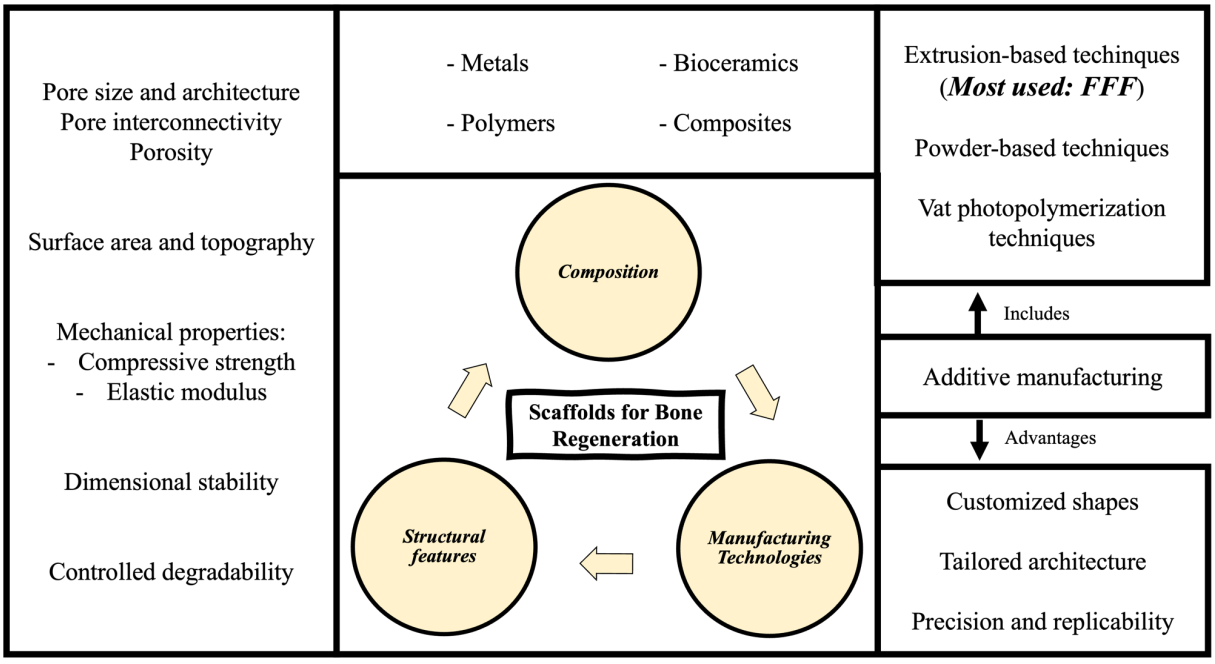

Figura 2. Características esenciales de andamiajes o "scaffolds" fabricados para regeneración ósea. FFF: fabricación por deposición de filamento fundido [1,2,7,32,36,38]. Modificado de Alonso-Fernandez *et al.* [8]

1.4.2 Fabricación aditiva para regeneración ósea

El desarrollo de injertos óseos anatómicamente personalizables ha reforzado la importancia clínica de la ingeniería de tejidos óseos, dado que las nano- y microarquitecturas juegan un papel crucial en la fisiología del tejido óseo nativo. Por ello, la posibilidad de fabricar nuevos andamiajes con dichas características ha dado origen a un importante campo de estudio e investigación [13]. La tecnología de impresión 3D fue desarrollada a inicios de los años 90 en el Instituto de Tecnología de Massachusetts (MIT) y consiste en la deposición por capas de materiales particulados, a través del uso de líquidos aglutinantes mediante un proceso automatizado para generar una estructura tridimensional [32,36].

La fabricación aditiva (AM) o "additive manifacturing" es actualmente un método prometedor de impresión 3D que permite la fabricación de estructuras porosas, demostrando su capacidad para satisfacer la creciente demanda de sustitutos óseos customizables para la regeneración ósea [29,47]. De este modo, se logra superar las limitaciones de técnicas de fabricación convencionales como "gas foaming", el método "sol-gel" o el "freeze-drying"; incapaces de incorporar una forma global, una arquitectura interna y una porosidad adecuadas a los andamiajes, independientemente de la complejidad de los defectos [38]. Dichas técnicas convencionales están basadas en el uso de métodos sustractivos, los cuales eliminan partes del material a partir de un bloque inicial hasta lograr la conformación deseada, limitando su capacidad para controlar formas y geometrías. Además, la necesidad de uso de solventes orgánicos puede comprometer la viabilidad o las funciones celulares, incluso cuando únicamente quedan residuos de los mismos [2].

Las técnicas de AM, también conocidas como técnicas "Rapid Prototyping","Solid Free-Form Techniques" o "3D printing" , son especialmente útiles en ingeniería de tejidos óseos, ya que permiten la fabricación de andamiajes con un control preciso de la arquitectura de la matriz, mejorando sus propiedades mecánicas, los efectos biológicos y la cinética de degradación. Se basan en la deposición de capas superpuestas para la fabricación del objeto final 3D, pudiendo utilizar materiales en forma de líquidos, sólidos o polvo. Para ello, se parte de un modelo matemático 3D (CAD), compuesto por una herramienta de digitalización/escáner que transforma la geometría en datos digitales (obtenidos como se mencionó anteriormente por medio de técnicas de imagen no invasivas como el CT o la MRI), un software que modifica los datos para que puedan ser utilizados por la máquina de fabricación y una tecnología que transforma dichos datos en el objeto deseado. Además, estas novedosas técnicas evitan el uso de solventes orgánicos tóxicos, mejorando de este modo la biocompatibilidad de los andamiajes [2,51,52]. Estas técnicas de fabricación permite la síntesis de andamiajes poliméricos, cerámicos y metálicos, y pueden clasificarse en 3 grupos principales [2,32,36,38,48,49]:

1.4.2.1 Técnicas basadas en materiales sólidos

Las técnicas basadas en materiales sólidos consisten en la deposición de un material termoplástico que es situado en una boquilla fijada a un brazo robotizado. Se conocen como técnicas basadas en la extrusión o "extrusion-based techniques", y permiten el uso de uno o varios materiales. Algunas de las más conocidas son el modelado por deposición fundida ("fused deposition modeling", FDM), el "robocasting" ("direct-write assembly" o "direct ink writing"), la "dispense plotting" ("material extrusion" o "bioplotting"), y los sistemas de deposición de cabezales múltiples ("multi head deposition system", MHDS).

Durante el proceso de fabricación por FDM los materiales son cargados en una boquilla fijada a un brazo robótico que se desplaza en los ejes X e Y, y que son dispensados por medio del uso de calor sobre una plataforma que se desplaza a lo largo del eje Z. De este modo, es posible la fabricación de andamiajes de porosidad y tamaño de poro controlados por medio de

la modificación del espacio entre trazados y la altura de la plataforma. En el caso de MHDS o "robocasting", el material se deposita en forma de pasta en una jeringa y es extrusionado por medio del uso de presión.

La técnica de AM más ampliamente empleada es la FDM, puesto que permite la impresión de gran variedad de biomateriales como polímeros, cerámicas o la combinación de ambos formando lo que se denomina compuesto o "composite", con un bajo coste, necesidad de un corto período de entrenamiento y una buena precisión (±0,5 mm). Además, otras de sus principales ventajas son la posibilidad de fabricar estructuras altamente porosas, con buena resistencia mecánica y sin ser necesario el uso de solventes tóxicos. Como aspectos negativos, podríamos destacar la incapacidad de producir estructuras con una resolución dimensional inferior a 100 μm, aunque esta puede ser en cierto grado dependiente de la técnica elegida; y la imposibilidad de imprimir materiales metálicos, debido al alto punto de fusión de estos materiales que no es posible alcanzar con dicha técnica.

Con respecto a los biomateriales poliméricos, estos suelen ser ampliamente accesibles en forma de filamentos o en forma de polvo/partículas que puede utilizarse para la síntesis de una pasta. Así mismo, las cerámicas suelen presentarse en forma de polvo/partículas que se utilizan para generar una pasta que pueda ser impresa mediante estas técnicas. Por último, los compuestos o "composites" formados por la mezcla de ambos suelen ser fabricados en forma de filamentos donde las partículas cerámicas están embebidas en una matriz polimérica.

1.4.2.2 Técnicas basadas en materiales particulados/en forma de polvo

Las técnicas basadas en materiales particulados/polvo necesitan del uso de un proceso de sinterizado o de unión química, para el paso del material en forma de polvo a la producción de un andamiaje.

Se han utilizado diferentes procedimientos para la síntesis de estructuras tridimensionales que pueden ser utilizadas en ingeniería de tejidos óseos, como son el "inkjet printing", "selective laser sintering" (SLS), "selective laser melting" (SLM), "direct metal laser sintering" (DMLS) y "electron beam melting" (EBM).

Durante el proceso de fabricación los materiales particulados se colocan en un colector, para a continuación esparcirlos sobre la plataforma de construcción y unirlos según la trayectoria estipulada mediante el uso, en función del procedimiento, de un láser de alta potencia (sinterización o "sintering") o una tinta ("ink") compuesta de un líquido aglutinante (unión química). Las capas posteriores son unidas a las ya depositadas hasta la síntesis completa de la estructura.

Dichas técnicas ofrecen gran precisión, con una resolución espacial variable en función de la técnica y el tamaño de las partículas, de aproximadamente 50 μm, siendo más precisa la fusión química que la sinterización. Por el contrario, necesita del uso de máquinas costosas y voluminosas, cuyo empleo requiere una formación específica.

En cuanto a los materiales que pueden ser impresos mediante estos métodos, puede ser utilizada en la fabricación de estructuras cerámicas, poliméricas, metálicas y compuestas o "composites"; siendo únicamente válida la sinterización para el caso de los metales, dado que el líquido aglutinante utilizado en la unión química no es capaz de lograr la fusión de los mismos.

1.4.2.3 Técnicas basadas en materiales líquidos

Las técnicas basadas en materiales líquidos consisten en la síntesis de objetos sólidos por medio de la impresión de sucesivas capas a partir de la fotopolimerización de una resina

líquida. Este proceso se denomina como "vat photopolimerization" o fotopolimerización en cubeta.

La estereolitografía (SL) es la principal técnica de fotopolimeración en cubeta (VPP). Para su realización se necesita una resina líquida fotosensible contenida en una cubeta, una plataforma de fabricación móvil que se desplaza a lo largo del eje Z y que permite la distribución de la resina en su superficie, un láser ultravioleta (UV) para irradiar la resina y un sistema dinámico de espejos. El proceso consiste en la deposición de capas seriadas de la resina, que se solidifican mediante el uso del láser UV dibujando el patrón diseñado en la laminadora o "*slicer*", y el posterior desplazamiento de la plataforma para la deposición de la siguiente capa. Estos pasos se repiten capa por capa hasta la fabricación completa del andamiaje 3D. La técnica requiere además de un tratamiento posterior una vez finalizada la impresión, en el que el andamiaje se lava para eliminar los restos de resina y se somete de nuevo a un proceso de curado bajo luz UV. En caso de que, en lugar de un láser UV, fuera utilizada una proyección de luz UV, pasaría a denominarse procesamiento de luz digital o "digital light processing" (DLP). Se pueden incluir otras novedosas técnicas tales como la microestereolitrografía ("micro-stereolithography", ISL) o la polimerización de dos fotones (TPP).

La SL y la DLP permiten la síntesis de andamiajes a partir de materiales fotosensibles como polímeros y cerámicas, no siendo posible la impresión de estas últimas por sí solas, así como en el caso de los metales. Se trata de técnicas versátiles, de uso intuitivo, con una resolución de 25 μm y una precisión de ±0,1 mm. Sin embargo, se ven limitadas por la citotoxicidad de las resinas.

Aunque las técnicas de AM se han utilizado ampliamente en investigación biomédica, hasta la fecha solo hay algunos productos disponibles en el mercado [38]. La selección del biomaterial es fundamental en el diseño del andamiaje, ya que, además de poseer unas características biológicas, fisicoquímicas y mecánicas adecuadas, deben poder ser impresos mediante alguno de los métodos indicados sin afectar negativamente a la precisión del proceso [53]. Esto justifica y reafirma la ya mencionada creciente demanda de desarrollo de biomateriales de alto rendimiento para la ingeniería de tejidos óseos. Algunos de los biomateriales típicamente seleccionados para la fabricación de andamiajes utilizados en regeneración ósea son las cerámicas, los metales, los péptidos de autoensamblaje y los polímeros sintéticos o naturales, de los cuales hablaremos más adelante [3,15]. Finalmente, debe señalarse pese a no ser objeto del presente trabajo la existencia de los métodos de bioimpresión o "bioprinting", que incluyen aquellos procedimientos capaces de imprimir capas seriadas de materiales biológicos como células, biomateriales o biomoléculas, con el fin de crear una estructura tridimensional [54].

Varios artículos han analizado a lo largo de los últimos años la importancia del uso de diferentes técnicas de impresión, materiales y diseños. Garot *et al.* [10] revisaron materiales y técnicas de fabricación aditiva o "additive manufacturing" utilizados específicamente para la reparación de defectos óseos. De manera similar, Amini *et al.* [41] revisaron los avances recientes y los desafíos existentes en cuanto a ingeniería de tejidos óseos. Además, en su trabajo realizan una discusión pormenorizada acerca de andamiajes compuestos o "composites" conformados a partir de algunos de los materiales empleados más frecuentemente en investigación, atendiendo también a sus propiedades estructurales e incluso al efecto de la incorporación de distintas moléculas y/o factores de crecimiento, realizado con el fin de mejorar las propiedades biomiméticas de los andamiajes. Asimismo, la arquitectura de los andamiajes fue estudiada entre otros por Ostrowska *et al.* [74], quienes analizaron *in vitro* el efecto de diferentes patrones de deposición impresos mediante tecnología 3D; Liang *et al.* [75], por

medio del diseño de 3 andamiajes diferentes impresos en 3D y la evaluación de sus aplicaciones clínicas *in vitro* e *in vivo*; y Gleadall *et al.* [76], realizando una revisión de la relación entre geometría y rendimiento de andamiajes de ingeniería de tejidos utilizando andamiajes fabricados mediante técnicas aditivas o "additive manufacturing".

1.4.3 Biomateriales para regeneración ósea

Un biomaterial puede ser definido como cualquier material utilizado para fabricar dispositivos que reemplacen una parte o una función del organismo de una forma segura, confiable, económica y funcionalmente aceptable. Algunos autores utilizan dicho término para referirse a materiales producidos por un sistema biológico como hueso, piel o una arteria, sin embargo, en nuestro caso los denominaremos "materiales biológicos". Los biomateriales han sido ampliamente usados en dispositivos médicos en forma de suturas, rellenos dentales, agujas, placas de osteosíntesis, etc. Otra definición similar de biomaterial es la de aquella sustancia sistemática y farmacológicamente inerte diseñada para la implantación o incorporación a sistemas vivos. Para ser empleados *in vivo,* los biomateriales deben ser aprobados por agencias como la FDA ("United States Food and Drug Administration") o la EMA (Agencia Europea del Medicamento) [55].

Un uso adecuado de los biomateriales requiere de una comprensión de las relaciones entre las propiedades, las funciones y las estructuras de los materiales biológicos. Por ello, generalmente su estudio está sujeto a tres aspectos esenciales como son los materiales biológicos, los materiales implantables y la interacción de ambos con el cuerpo humano. Así mismo, su éxito es altamente dependiente de sus propiedades y biocompatibilidad, el estado de salud del receptor, y la competencia del cirujano que lo implanta y supervisa su progreso [55].

Dentro de los materiales utilizados para la regeneración ósea podemos diferenciar cuatro clases: polímeros, metales, cerámicas y compuestos o "composites" [55]. Para el caso de los andamiajes fabricados mediante tecnologías 3D, los biomateriales utilizados más frecuentemente en ingeniería de tejidos óseos son los polímeros, las cerámicas bioactivas y los compuestos híbridos o "composites" de ambos [2]. A lo largo de la presente sección realizaremos un repaso de los mismos, profundizando más en aquellos que son objeto de la presente tesis doctoral.

Otra posible clasificación de los biomateriales sería diferenciando entre los derivados de productos biológicos, como por ejemplo la matriz ósea desmineralizada, las proteínas morfogenéticas óseas, el coral, etc.; y los sustitutos óseos sintéticos, como los cementos de fosfato cálcico (hidroxiapatita, HA), las cerámicas de fosfato tricálcico (β-fosfato tricálcico, β-TCP), los fosfatos de calcio bifásicos (sintetizados a partir de cerámicas de HA y β-TCP), vidrios bioactivos y sustitutos óseos basados en polímeros [4,56].

1.4.3.1 Metales

Los materiales metálicos han sido ampliamente utilizados en procedimientos dentales (implantes dentales), ortopédicos (prótesis, placas de osteosíntesis, etc.) o espinales (cajas intersomáticas), principalmente fabricados en titanio y sus aleaciones. Se trata de materiales biocompatibles, no degradables, y cuyas propiedades mecánicas son similares o incluso superiores a las del hueso nativo, lo cual puede ser beneficioso en situaciones de crecimiento óseo lento. Sin embargo, estos biomateriales poseen ciertos inconvenientes que limitan su uso *in vivo* como son su alto precio, la posible liberación de iones metálicos debido a un proceso de corrosión que puede originar una toxicidad a nivel local o sistémica, y la aparición de osteopenia asociada al uso de implantes o "stress shielding", dando lugar a una pérdida de tejido óseo como resultado del alto módulo elástico de los metales [38,57,58].

1.4.3.2 Biocerámicas

Las cerámicas, cerámicas bioactivas o biocerámicas poseen propiedades efectivas y seguras para promover la reconstrucción y remodelación ósea debido a sus similitudes con el hueso natural [7,59]. La capacidad de estos materiales para inducir la osteogénesis y la angiogénesis por medio de la liberación de iones biológicamente activos ha atraído gran interés entre los investigadores [30]. Se trata de compuestos con gran resistencia a la compresión, pero baja ductilidad, por lo que resisten la deformación aunque presentan gran fragilidad. Pueden ser de origen natural o sintético, siendo las más comunes las derivadas de corales, los fosfatos de calcio (CaP) o fosfatos cálcicos, los sulfatos de calcio y los vidrios bioactivos [2,49]. Entre ellos, los CaP como la hidroxiapatita (HA) y el fosfato beta-tricálcico (β-TCP), se utilizan comúnmente como materiales de injerto óseo, dadas su semejanzas con el principal componente inorgánico del hueso (fase mineral), la hidroxiapatita [7,39]. Las biocerámicas de CaP se caracterizan por su biocompatibilidad y bioactividad debido a su abundancia en el organismo, y a la disolución y liberación parcial de productos iónicos que aumentan la concentración de iones calcio y fosfato. Por tanto, tienen propiedades osteoconductoras e incluso osteoinductivas, estructura cristalina, alto punto de fusión y bajas características mecánicas. Su comportamiento frágil es un problema crítico que restringe su uso a localizaciones donde no deban soportar cargas [7,38,49,60].

Otro grupo prometedor son los biovidrios ("bioglasses", BG) o vidrios bioactivos, muchos de ellos basados en el sistema de Na_2O, CaO, P_2O_5 and SiO_2, y con un porcentaje en peso de SiO_2 menor del 55% [61–63]. Presentan una biocompatibilidad, bioactividad, y osteoconducción suficientes, actuando como fuente de minerales para las células óseas, y sin inducir una respuesta inflamatoria [36,57,61,62]. Además, los biovidrios pueden inhibir el crecimiento de numerosas cepas bacterianas, algunas de ellas incluso multirresistentes [61]. A pesar de esto, se trata de materiales frágiles, con una baja tasa de degradación y que carecen de características mecánicas (baja tenacidad a la fractura) para formar por sí mismos andamiajes de alta calidad [36,57].

El uso de materiales biocerámicos ha sido aprovado por la FDA, y pueden encontrarse diferentes productos comercialmente disponibles, como Cerapatite® (HA), Cerasorb® (β-TCP) o BonAlive® (Bioglass). Desde que la primera formulación recibió la aprobación en 1996, un total de 15 productos con HA, 21 con β-TCP y 11 con Bioglass han sido aprobados hasta diciembre del 2020 [64,65]. En cuanto al uso de dichas biocerámicas en medicina humana, Cannio *et al.* [63] realizaron una revisión bibliográfica sobre las aplicaciones de los vidrios bioactivos en ensayos clínicos en humanos, y Stachi *et al.* [66] compararon hidroxiapatita sintética con hueso bovino inorgánico en una técnica de elevación del seno maxilar en humanos, obteniendo resultados de regeneración ósea similares para ambos grupos (ClinicalTrials.gov Identifier NCT03077867).

Sin embargo, sigue siendo necesaria la búsqueda de nuevas biocerámicas alternativas a las cerámicas de fosfato cálcico para lograr una mejora de las propiedades de los biomateriales utilizados en regeneración ósea [67,68]. Frente a esta situación, las bioapatitas derivadas de los dientes de tiburón (bioCaP), también denominadas bioapatitas marinas, fosfatos cálcicos marinos bioderivados o biocerámicas de origen marino, han surgido como un material de injerto óseo alternativo que revaloriza subproductos de la pesca de *Isurus oxyrinchus* y *Prionace glauca*, dándoles una utilidad y proporcionándoles un valor añadido [67,69]. Esta biocerámica se obtiene tras unas fases de molienda, tamizado y pirólisis, y posee una estructura cristalina [70]. Su composición se basa en una combinación de una fase apatítica del 65-70 wt% (hidroxiapatita y fluorapatita), y una fase no apatítica del 25-30 wt% (β-TCP y whitlockite). Además, presenta elementos traza como F (1.0+-0.5 wt%), Na (0.9+-0.2 wt%) y Mg (0.65+-

0.04 wt%) en su estructura basada en apatita [69]. López-Álvarez *et al*. [69] demostraron por primera vez la biocompatibilidad *in vitro* de las bioapatitas derivadas de dientes de tiburón. Posteriormente, el mismo grupo realizó un ensayo preclínico en ratas, comparando esas bioapatitas con un injerto óseo comercial sintético bifásico HA/β-TCP (60/40%). Los resultados confirmaron una mayor osteointegración y crecimiento horizontal del tejido óseo, así como propiedades osteoconductivas y osteoinductivas [67]. Asimismo, García-González *et al.* [68] llevaron a cabo un ensayo clínico preliminar en perros y gatos con resultados exitosos, demostrando que las bioapatitas son candidatas adecuadas para la cirugía ortopédica en el ámbito veterinario.

1.4.3.3 Polímeros

Los polímeros pueden ser de origen natural o sintético. Los polímeros de origen natural como el ácido hialurónico, el quitosano o el colágeno se caracterizan por su buena biocompatibilidad, osteoconductividad y baja inmunogenicidad, pero que sin embargo se ven limitados por el difícil control de su tasa de degradación (habitualmente degradados por enzimas naturales entre 2 y 24 semanas) y su baja estabilidad química [2,7,30,38]. Por otro lado, los polímeros de origen sintético como el polipropileno fumarato (PPF), el policaprolactona (PCL), ácido poliláctico (PLA), poliéter éter cetona (PEEK) y ácido poliglicólico (PGA) muestran una tasa de degradación controlada, con la posibilidad de poder ser diseñados de acuerdo con las propiedades mecánicas del hueso, sintetizando estructuras complejas, que mejoran la adhesión celular e incluso con la capacidad de libera moléculas solubles. Además, pueden sintetizarse a costos reducidos y tienen una larga vida útil. Como principal desventaja, poseen una menor capacidad de interacción con las células en comparación con los polímeros naturales [2,7,30,71].

Los biopolímeros ofrecen una alterativa a los materiales biocompatibles tradicionales (cerámicos y metálicos) y a los polímeros no biodegradables [47]. El ácido poliláctico (PLA) es un biopolímero empleado comúnmente como materia prima en los procesos de impresión 3D. Concretamente, ha recibido gran atención su empleo en aplicaciones biomédicas utilizando técnicas de fabricación aditiva o "additive manufacturing", como el FDM, que permiten la fabricación de andamiajes de forma sencilla y con alta reproducibilidad. Desde su aprobación en 1970 por la Administración de Alimentos y Medicamentos en los EE.UU (FDA) para el contacto directo con fluidos biológicos, han sido utilizados en aplicaciones médicas relevantes como andamiajes para ingeniería tisular, dispositivos liberadores de fármacos, membranas de recubrimiento, fijación ósea, diferentes dispositivos médicos biorreabsorbibles y suturas. El PLA destaca por su biocompatibilidad, bajo coste, procesabilidad, un extenso perfil de propiedades mecánicas, biodegradabilidad y ausencia de efectos tóxicos o cancerígenos. Sin embargo, también presenta varios inconvenientes que deberán ser resueltos para lograr una adecuada regeneración ósea, como son una tasa de degradación lenta, un comportamiento hidrofóbico, una baja afinidad celular, o la liberación de subproductos ácidos derivados de su degradación que pueden dar lugar a la aparición de una respuesta inflamatoria en la zona de implantación, superior a la ocasionada habitualmente [7,42,45,47,49,50,72,73].

Dada su baja afinidad celular y la importancia de la adhesión de las células al polímero, las propiedades de superficie del biomaterial juegan un papel crítico, especialmente en la biocompatibilidad, permitiendo el crecimiento vascular, y la unión, migración y proliferación celular. Es por ello que se han desarrollado diferentes estrategias para la consecución de unas propiedades de superficie deseables en andamiajes sintetizados con PLA, como métodos físicos, químicos, inducidos por plasma o radiación; o la creación de recubrimientos ("coatings") o de compuestos ("composites") [7,47,73].

1.4.3.4 Biomateriales compuestos

Los biomateriales compuestos o "composites" consisten en una combinación de dos o más materiales con propiedades diferentes, generalmente una matriz y un agente de refuerzo, logrando un efecto sinérgico entre ambos [2,39,40].

Para superar las limitaciones de los polímeros y obtener una estructura más práctica y funcional, se han sintetizado "composites" combinando dos o más fases cuidadosamente integradas [48,74]. El uso de "composites" de PLA en lugar de polímeros puros, tiene el objetivo de aumentar su resistencia mecánica, actividad biológica y propiedades osteoconductivas [73,75]. Se fabrican incorporando un gran variedad de biomateriales como metales, cerámicas bioactivas, materiales orgánicos, inorgánicos, nanomateriales e incluso otros polímeros, en una matriz polimérica [73]. Algunos ejemplos de dichos "composites" son los fabricados mediante la combinación de matriz de PLA y otros materiales como el ácido hialurónico [45], policaprolactona (PCL) [76], HA [77,78], n-HA [62,79], biovidrios [78,80], cáscara de huevo [81] o β-TCP [82]. Típicamente, las combinaciones más utilizadas son las de polímero-polímero (copolímeros) o polímero-cerámica.

Los copolímeros derivan de la unión de dos o más monómeros, como por ejemplo la combinación del ácido poliláctico (PLA) y el ácido poliglicólico (PGA), que dan lugar al ácido poli(láctico-co-glicólico) (PLGA), considerado como un excelente candidato en ingeniería de tejidos óseos dada su biodegradabilidad y fácil fabricación [2,30,71]. Otro ejemplo es la combinación de PLGA y polifosfazenos que proporciona una posible solución a la necrosis tisular y al posible fracaso de la implantación derivadas de los productos ácidos de degradación del PLGA, por medio de la liberación de productos neutros o básicos, que ejercen un efecto tampón [2].

La combinación polímero-cerámica resulta en la síntesis de "composites" biomiméticos, una idea que surge de la base de que el hueso está compuesto de una mezcla de cristales inorgánicos de HA y un polímero de origen natural como es el colágeno [2]. La combinación de ambos materiales puede evitar algunas de las desventajas de cada uno, mejorando sus características individuales, propiedades físicas y mecánicas, tasa de degradación y bioseguridad; haciéndolos más atractivos para su uso en regeneración ósea [57,73,78].

La idoneidad de las biocerámicas para ser impresas mediante técnicas de fabricación aditiva permite su empleo en la producción de andamiajes compuestos [73,78], lo que optimiza la biocompatibilidad de los materiales poliméricos, manteniendo unas propiedades mecánicas adecuadas, y evitando su fragilidad [38]. Estas además, equilibrarán el entorno ácido que se origina durante la degradación del PLA y aumentarán su hidrofilicidad y tasa de degradación, con notables beneficios sobre la proliferación ósea y la regeneración celular [8].

Se han logrado fabricar con éxito compuestos de ácido poliláctico (PLA) y biocerámicas, demostrando mejorar la formación ósea *in vivo* [8]. A nivel comercial puede encontrase a la venta algún "composite" sintetizado a partir de PLA e HA, como el denominado SuperFIXSORB30® [64]. Sin embargo, no han sido encontrados ensayos clínicos publicado a cerca del uso de estos biomateriales.

Pese al gran avance realizado en la síntesis de "composites" fabricados a partir de PLA y biocerámicas, todavía existe una brecha de conocimiento en cuanto a la composición y estructura óptimas. El comportamiento de las biocerámicas en la matriz polimérica tiene un efecto dependiente de la dosis, por lo que la osteoconductividad y las propiedades mecánicas serán, respectivamente, directa e inversamente proporcionales a la cantidad de material cerámico añadido. Por lo tanto, es esencial equilibrar la fragilidad del CaP y la ductilidad del PLA para evitar la pérdida de la bioactividad del andamiaje [8,75,77]. Una vez solucionados dichos aspectos, y dada la necesidad de nuevos biomateriales para la regeneración ósea, los

"composites" de PLA-Biocerámicas podría llegar a adquirir gran importancia, llegando a equipararse con los autoinjertos [51].

En el caso de las bioapatitas marinas, también han sido utilizadas como agente de refuerzo de una matriz polimérica para la síntesis de materiales compuestos, y su posterior impresión mediante el uso de técnicas de fabricación aditiva [70]. Su adición supondrá una mejora sustancial de sus características físicas y biológicas, con efectos sobre las propiedades mecánicas, humectabilidad, topografía de las superficies, etc., todos ellos estrechamente relacionados con las propiedades osteoconductivas *in vivo* del andamio. Además, iones como el F y Mg presentes en el bioCaP, también favorecerán la regeneración ósea al potenciar la síntesis de factores de crecimiento celular y de la hormona paratiroidea, respectivamente [69].

1.4.4 Geometría de los andamiajes para regeneración ósea

Además de la importancia de la composición del "scaffold", en relación a los biomateriales utilizados, también son esenciales algunos aspectos específicos relacionados con el diseño de dichas estructuras para lograr la regeneración ósea. La hipótesis actual más aceptada hace referencia a que el proceso de curación dependa de la capacidad de los andamiajes para permitir o favorecer el transporte de fluidos, células o vasos sanguíneos, así como la difusión de nutrientes y productos de deshecho. Sin embargo, pese a los conocimientos existentes, no se ha logrado conseguir un diseño ideal para lograr una adecuada osteointegración [83,84].

La síntesis de andamiajes compuestos mediante impresión 3D para regeneración tisular es una alternativa prometedora en la regeneración de defectos óseos. Dada su amplia oferta de características biológicas, mecánicas y estructurales, puede servir como nicho para la proliferación celular y la formación tisular. La Tabla 1 muestra de forma resumida algunas de las características esenciales que se requieren de un andamiaje para su uso en regeneración de defectos óseos. Algunos de estos aspectos ya han sido mencionados anteriormente, y así mismo serán analizados de nuevo a lo largo del presente trabajo [12]. Concretamente, los métodos de deposición capa por capa, como el FDM, están siendo utilizados en la actualidad con gran efectividad en el diseño de la arquitectura, porosidad e interconectividad de los andamiajes. Mediante estos sistemas de fabricación, es posible la producción de "scaffolds" complejos con diseños bien definidos y una interconectividad de poro optimizada [13].

Tabla 1. Propiedades de los andamiajes en relación con su diseño. Modificado de Pedrero *et al.* [30]

Área de superficie	Crucial para las interacciones entre células y andamiajes, facilitando la vascularización e infiltración celular.
	La macroporosidad podría promover la osteogénesis a través de la facilitación del transporte celular e iónico.
	La microporosidad mejora el área de superficie para la adsorción de proteínas, aumento de la solubilidad iónica y de los puntos de adhesión para los osteoblastos.
Tamaño de poro	Poros > de 300 µm facilita la neoformación ósea y la vascularización.
	Se piensa que tamaños de poro de 75-100 µm promueven la angiogénesis.
	Un tamaño de poro de 200 a 500 µm resulta en una óptima penetración tisular y vascular *in vivo*.
Interconectividad de poro	Estimula la tasa de deposición ósea y la profundidad de infiltración.
	Un diámetro óptimo de conexiones entre poros oscila entre 700 y 1200 µm.
Topografía de superficie	Las superficies rugosas promueven la osteointegración y favorecen la adhesión epitelial.
Propiedades mecánicas	Los valores del módulo de Young deben de ser cercanos a 7-30 GPa y los de la resistencia a la tracción a 50-151MPa.

	La resistencia a la compresión debe ser comparable a la del hueso cortical (100-230 MPa).
Propiedades mecánicas y tasa de degradación	La tasa de degradación debe coincidir con el crecimiento de la ECM nativa para asegurar el soporte mecánico del andamiaje.

Las características geométricas de los andamiajes 3D como la arquitectura de poro, el tamaño de poro, la porosidad, la interconectividad y las propiedades mecánicas, así como la relación existente entre todas ellas, puede tener una gran influencia en la capacidad de regeneración ósea [7,10,85]. Estas propiedades son esenciales para la migración, proliferación y diferenciación de los osteoblastos y las células mesenquimales. Además, la interconectividad de poro o permeabilidad es esencial para favorecer el crecimiento hacia el interior del andamiaje, debido a que permite la invasión de vasos sanguíneos y el suministro de nutrientes [86].

Los "scaffolds" también deben proporcionar un efecto de soporte estructural adecuado en el lugar del defecto [87]. Las propiedades mecánicas van a ser en gran medida dependientes, además de los biomateriales que componen el andamiaje, de la porosidad, forma y tamaño del poro, grosor de filamentos, etc.; de modo que estas características determinarán el grado de estímulo mecánico que será capaz de soportar la estructura [84]. A su vez, todos estos parámetros estarán influidos por el diseño del "scaffold", a través de la modificación de la posición y orientación de las fibras, dando lugar a estructuras con filamentos alineados o escalonados, filamentos en capas repetidas, o filamentos con diferentes orientaciones (como por ejemplo 0º/90º o 0º/60º/120º), dependiendo del patrón de impresión [88]. La variabilidad de dichos parámetros se encuentra ejemplificada en la Figura 3.

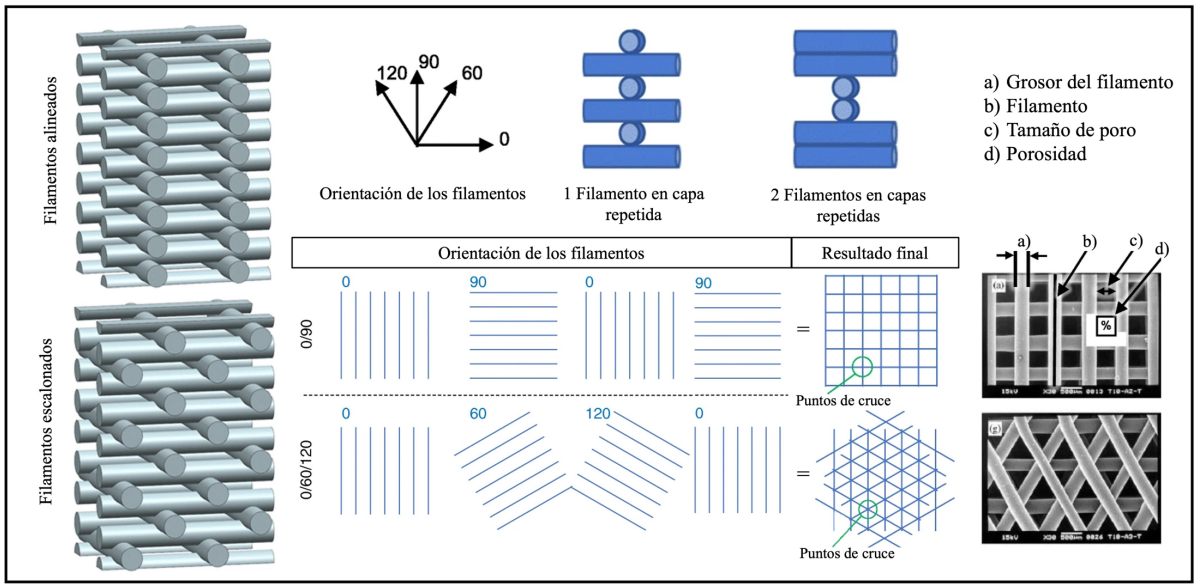

Figura 3. Ejemplo de algunas de las estrategias de impresión 3D con respecto a la arquitectura de los andamiajes 3D. Modificado de Gleadall *et al.* [88]. "Reimpreso con permiso de [88] bajo los términos de la Licencia Creative Commons Atribución 4.0 Internacional, CC BY-NC.ND 4.0."

Diferentes autores han estudiado el efecto de las modificaciones en el diseño de los "scaffolds" sobre la curación ósea *in vivo*. Algunos ejemplos son Berner *et al.* [34], que evaluaron el efecto de la arquitectura de los andamiajes en un modelo de regeneración ósea en hueso del cráneo, Lim *et al.* [43], que estudiaron el efecto de diferentes arquitecturas de poro, o Enterazi *et al.* [89], quienes demostraron que la manipulación del tamaño de poro y la permeabilidad de andamiajes impresos mediante tecnología 3D es una estrategia valiosa para mejorar los resultados obtenidos en un estudio de regeneración ósea.

Sin embargo, actualmente todavía existe una importante brecha entre la fabricación de "scaffolds" utilizando distintos patrones de impresión y su evaluación *in vivo* en estudios controlados, aislándose cualquier otro tipo de variable que pueda influir sobre el crecimiento óseo.

OBJETIVOS

2 OBJETIVOS

El objetivo general de la presente Tesis Doctoral es evaluar el uso de andamiajes compuestos de ácido poliláctico y bioapatitas derivadas de dientes de tiburón fabricados mediante tecnología de impresión 3D para la regeneración de defectos óseos en un modelo de conejo. Para ello se fijaron una serie de objetivos específicos que se corresponden con cada uno de los siguientes capítulos:

I. Analizar mediante una revisión sistemática de la literatura científica actual el uso de andamiajes compuestos de ácido poliláctico y biocerámicas impresos mediante tecnología 3D para la regeneración de tejidos óseos en modelos preclínicos *in vivo*.

II. Comparar el efecto sobre la regeneración ósea del enriquecimiento progresivo de andamiajes de ácido poliláctico con bioapatitas marinas en defectos óseos practicados en calvaria de conejo.

III. Evaluar la influencia de la geometría de los andamiajes sobre la regeneración ósea en defectos de tamaño crítico creados en cóndilo femoral lateral de conejo.

MATERIAL Y MÉTODOS

3 MATERIAL Y MÉTODOS

3.1 REVISIÓN BIBLIOGRÁFICA SISTEMÁTICA

La revisión bibliográfica sistemática fue realizada de acuerdo a las pautas establecida por las guías PRISMA ("Prefeered Reporting Items for Systematic Review and Meta-Analyses") [90].

3.1.1 Estrategia de búsqueda

Se realizó una búsqueda electrónica entre febrero y septiembre de 2022 en las bases de datos: MEDLINE (PubMed) y Web of Science (WOS), limitándose la misma a aquellos trabajos publicados en los últimos cinco años.

Para la identificación de los artículos objeto de estudio, se utilizaron diferentes estrategias de búsqueda basadas en permutaciones de los siguientes términos: "PLA", "Polylactic Acid", "PLLA", "poly (lactic) acid", "3D Print", "Three-dimensional print", "3D printing" "additive manufacturing" "material extrusion", "Scaffold", "Bone", "Bone regeneration", "Bone repair", "Bone reconstruction", "Bone tissue engineering", "In vivo" y "Animal".

Además, se incluyeron otros artículos relevantes obtenidos a partir del análisis de las referencias incluidas en los artículos revisados.

3.1.2 Criterios de inclusión y exclusión

La selección de los artículos objeto de la presente revisión se realizó a partir de una serie de criterios de inclusión y exclusión seleccionados previamente.

Criterios de inclusión:

- Artículos en inglés.
- Uso de implantes impresos mediante tecnología 3D.
- Inclusión de ensayos animales *in vivo*.
- Parámetros de estudio bien definidos, incluyendo evaluaciones microtomográficas o histológicas de la regeneración ósea.

Criterios de exclusión:

- Revisiones bibliográficas y capítulos de libros.
- Estudios donde únicamente se realizan evaluaciones *in vitro* o la caracterización de los implantes.
- Estudios que utilizan copolímeros de PLA o sintetizan materiales compuestos con materiales diferentes de las biocerámicas.
- Estudios en animales que emplean modelos de formación ósea ectópica (por ejemplo, subcutánea).
- Estudios que usan andamiajes combinados con agentes quimiterápicos, fármacos antiinflamatorios y antibióticos.
- Uso de dispositivos de PLA con una finalidad diferente a la regeneración ósea (por ejemplo, tornillos o clips para la fijación de fracturas).

3.1.3 Método de detección y extracción de la información

El proceso de detección y extracción de la información se desarrolló por medio de un cribado en 2 etapas, en base a los ya mencionados criterios de inclusión y exclusión. En primer lugar, se seleccionaron los artículos en base a sus títulos y resúmenes. Posteriormente, su elegibilidad fue cuidadosamente evaluada realizando una lectura en profundidad cada uno de los documentos. Finalmente, la información de interés fue extraída y registrada de acuerdo con varios formularios previamente diseñados, orientados a recopilar información relacionada con los biomateriales utilizados, los procesos de fabricación y caracterización de los implantes, y los ensayos preclínicos.

3.1.4 Evaluación de la calidad y riesgo de sesgo

La calidad y el riesgo de sesgo de los diferentes artículos fueron evaluadas por medio del uso de las directrices ARRIVE ("*Animals in Research: Reporting In Vivo Experiments*") [91] y la herramienta SYRCLE ("*Systematic Review Centre for Laboratory animal Experimentation*") para estudios en animales [92].

En el caso de las directrices ARRIVE se utilizó el denominado "Cuestionario de Complimiento" para evaluar si los estudios cumplían con los "10 Elementos Esenciales de ARRIVE": diseño del estudio, tamaño de la muestra, criterios de inclusión y exclusión, aleatorización, enmascaramiento, medidas de los resultados, métodos estadísticos, modelo animal, procedimientos experimentales y resultados. Además, se agregó un ítem a mayores denominado "Efectos Adversos", debido a su importancia en ensayos preclínicos. Estos elementos fueron categorizados en cada uno de los artículos, y clasificados como: "citado", si se informó adecuadamente acerca de los mismos, "no citado", si no se informó adecuadamente, y "no claro" si se informó parcialmente o no se proporcionaron detalles suficientes.

En cuanto a la herramienta SYRCLE, las publicaciones fueron evaluadas para cada uno de los 10 elementos incluidos en su lista de verificación utilizando una serie de preguntas de señalización específicas. Esta lista incluye ítems como: generación de la secuencia de asignación, características basales, ocultación de la asignación, asignación aleatoria, cegamiento del cuidador/investigador, evaluación aleatoria de los resultados, datos de los resultados abordados incompletos, comunicación libre de informes selectivos de los resultados y libre de otras fuentes de sesgo. Por tanto, la calidad metodológica se analizó en base a una serie de preguntas de señalización específicas para cada ítem, clasificándose las respuestas a dichas preguntas como: "sí", si se considera un bajo riesgo de sesgo; "no", en caso de un alto riesgo de sesgo; o "no claro", para elementos donde el riesgo de sesgo no está claro.

3.2 PROCEDIMIENTO EXPERIMENTAL

3.2.1 Materiales de partida

Como material de partida se utilizó ácido poliláctico (SMARTFIL®, Smart Materials, Jaén, España) en forma de pellets ovalados, con dimensiones en torno a 5 y 3,5 mm en eje mayor y menor respectivamente. Este polímero se combinó con una biocerámica, concretamente con un fosfato cálcico de origen marino derivado de un subproducto de la pesca (bioCaP), concretamente dientes de tiburón de las especies *Isurus oxyrinchus* y *Prionace glauca* proporcionados por el Instituto de Investigaciones Marinas (IIM-CSIC, Vigo, España). Esta biocerámica fue procesada en el Grupo de Novos Materiais (Universidade de Vigo), según el método descrito previamente por López-Álvarez *et al.* [67]. Tras un ciclo de lavado, los dientes se trituraron y se sometieron durante 12 horas a un proceso de pirólisis a una temperatura de

1100ºC, para finalmente obtener un biomaterial en forma de granulado con partículas de diámetros comprendidos entre 20 y 63 µm (Figura 4).

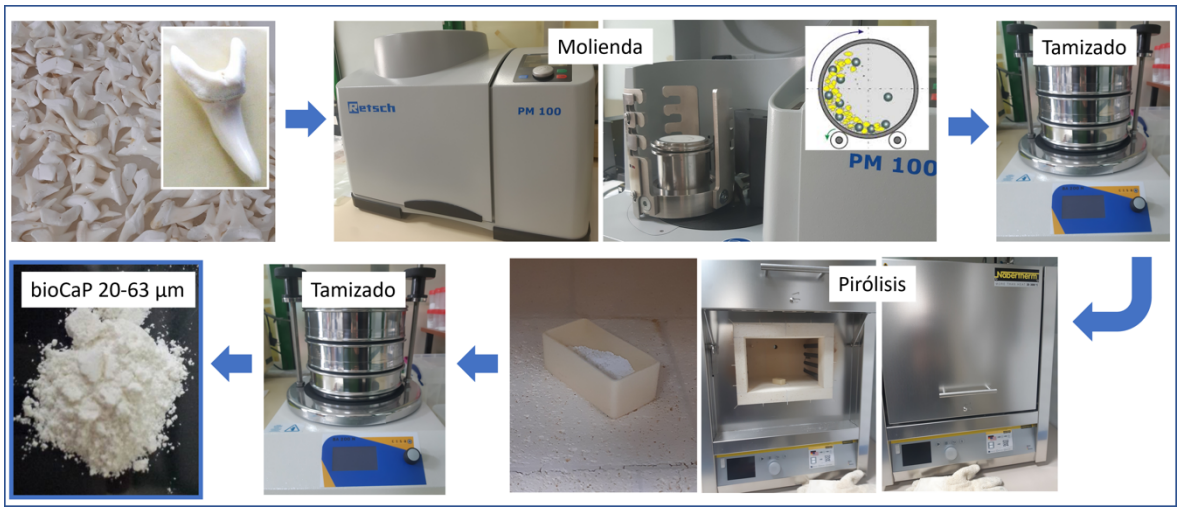

Figura 4. Esquema ilustrativo del proceso de obtención de la biocerámica de fosfato cálcico de origen marino (Imágenes cedidas por el Grupo Novos Materiais de la Universidad de Vigo).

3.2.2 Síntesis del filamento compuesto

Para la obtención del material compuesto o "composite" de PLA + bioCaP, los pellets de PLA fueron congelados a -80 ºC durante 20 minutos para facilitar su manipulación, sometidos a procesos de molienda y tamizado para reducir su tamaño hasta las 80-250 µm (Figura 5), aproximándolo lo máximo posible al tamaño de las partículas de bioCaP, para la obtención de una mezcla más homogénea. Ambos biomateriales (PLA y bioCaP) fueron combinados produciéndose "composites" con diferentes contribuciones de bioCaP. Para ello, se utilizó una mezcladora Turbula® (WAB, Nidderau, Alemania). Estos procesos fueron realizados en el Grupo I+D Farma (USC), y se encuentran descritos en mayor detalle en Rojas-Lozano *et al.* [70].

Figura 5. Esquema ilustrativo del proceso de obtención de la biocerámica de fosfato cálcico de origen (Imágenes cedidas por el Grupo Novos Materiais de la Universidad de Vigo).

A continuación, las distintas mezclas fueron sometidas, en el Grupo Novos Materiais (Universidad de Vigo), a un proceso extrusión para la síntesis de filamentos compuestos de las distintas formulaciones. Para ello se utilizó un kit de montaje básico de extrusión de la marca Filastruder (Filament2print, Snellville, Georgia) según lo publicado por Rojas-Lozano *et al.* [70].

Los filamentos fabricados constan de una base mayoritaria de PLA y una contribución variable de bioCaP. Además, se obtuvo un filamento íntegro de PLA para utilizar como material

control. En la Tabla 2 se muestran las diferentes contribuciones del material biocerámico y la nomenclatura utilizada en la presente Tesis Doctoral.

Tabla 2. Combinaciones de PLA y bioCaP en % en masa total por cada filamento obtenido, y la nomenclatura utilizada para cada uno de ellos.

PLA (% en masa total)	BioCaP (% en masa total)	Nomenclatura
100.00	0.00	PLA
98.29	1.71	PLA-1CaP
97.87	2.13	PLA-2CaP
87.34	12.66	PLA-12CaP

3.2.3 Fabricación de los andamiajes 3D

Los filamentos compuestos sintetizados fueron cortados a modo de pellets en secciones de menor tamaño e incorporados a una impresora 3D (Tumaker Voladora NX Pellet, Oiartzun, España) para la fabricación de los andamiajes en el Grupo de Novos Materiais (Universidade de Vigo) (Figura 6). Esta impresora 3D-FDM (modelado por deposición fundida o "fused deposition modeling") trabaja con dos puntos de control de temperatura (T1 y T2), los cuales deben de ser ajustados en función del material extruido durante el proceso de impresión. En nuestro caso, se establecieron en 140 ºC la T1 y en 220 ºC la T2, siendo la temperatura de la base de impresión de 65 ºC y el diámetro de boquilla de 0,8 mm. Con estos parámetros fueron fabricados andamiajes porosos 3D en forma de tapón craneal y cilindro para cada uno de los ensayos realizados.

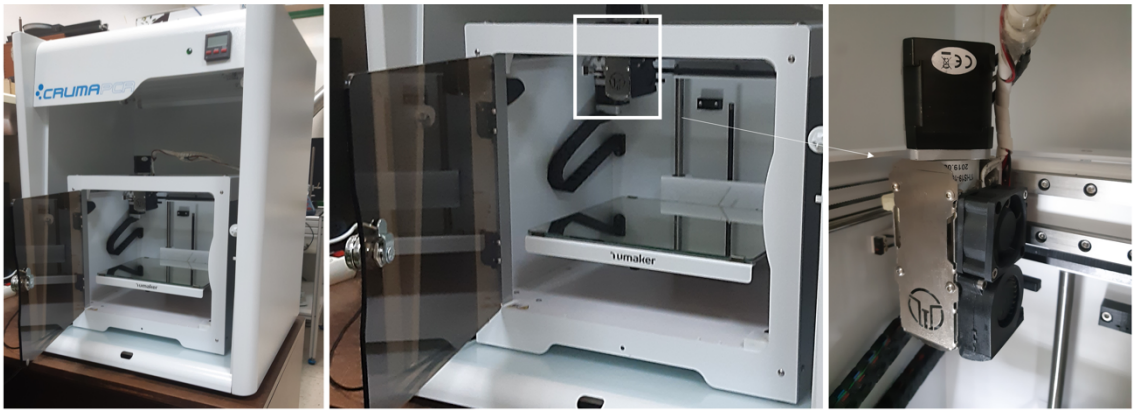

Figura 6. Impresora 3D, en cabina con lámpara germicida y detalle del extrusor, utilizada para la fabricación de los andamios composite PLA-bioCaP (Imágenes cedidas por el Grupo Novos Materiais de la Universidad de Vigo).

Los diseños de los andamiajes se realizaron utilizando el software SolidWorks 2016, los datos digitales se guardan como archivo STL para generar sets de código que se introducen en el software de la impresora: Simplify 3D Professional.

Para la evaluación del efecto sobre la regeneración ósea del enriquecimiento progresivo de andamiajes de ácido poliláctico con bioapatitas marinas derivadas de dientes de tiburón (*Capítulo II*), se utilizaron los filamentos de PLA, PLA-1CaP, PLA-2CaP y PLA-12CaP. Con los que se sintetizaron andamiajes porosos en forma de disco con un tapón ciego con dimensiones de 8 mm de diámetro y 1 mm de grosor en la tapa, y 6 mm de diámetro y 2 mm de grosor/altura en el cuerpo o sección interior que será introducida en el defecto, siguiendo un patrón de impresión alterno, donde cada una de cordones o "struts" es depositado perpendicularmente a la capa opuesta. La Figura 7 (a-d) muestra simulaciones del proceso de impresión y el resultado final del implante, utilizando el software "Simplify3D Professional".

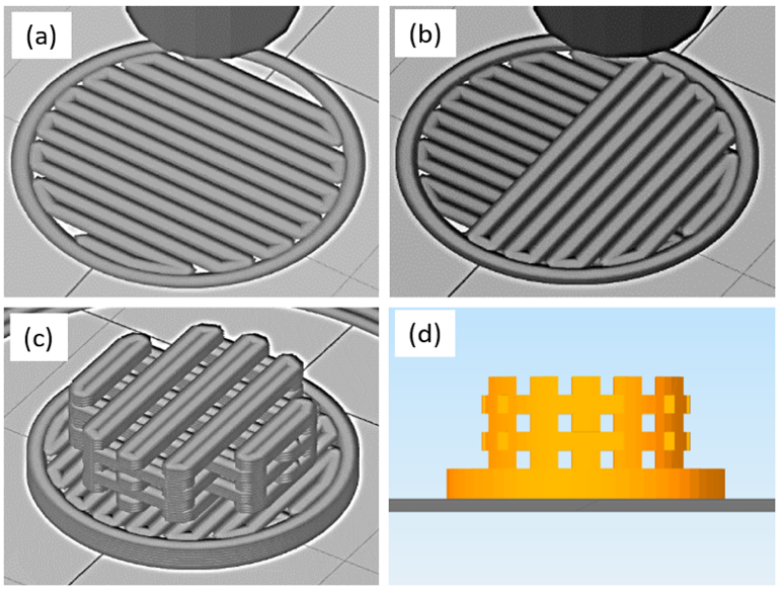

Figura 7. Ilustraciones del proceso de impresión obtenidas del software "Simplify3D Professional" (a-c), y del resultado final de la misma (d). Imagen propia.

Así mismo, con el fin de evaluar la influencia de la modificación de la arquitectura geométrica de los andamiajes sobre la regeneración ósea (*Capítulo III*), se seleccionaron únicamente filamentos de PLA-12CaP. En este caso, se sintetizaron andamiajes cilíndricos de 6 mm de diámetro y 10 mm de altura, utilizando dos patrones de impresión diferentes. Se fabricaron por un lado andamiajes porosos con un patrón de impresión alterno (denominándose dicha estructura alterna, ALT), variando el ángulo de deposición en 0º/90º/180º; y por otro lado andamiajes sintetizados siguiendo un ángulo de deposición de 0º/45º/90º/135º/180º, que se denominaron helicoidales (HEL). Al igual que en el caso anterior, el software "Simplify3D" fue utilizado para mostrar una simulación del proceso de impresión y el resultado final , como puede apreciarse en la Figura 8.

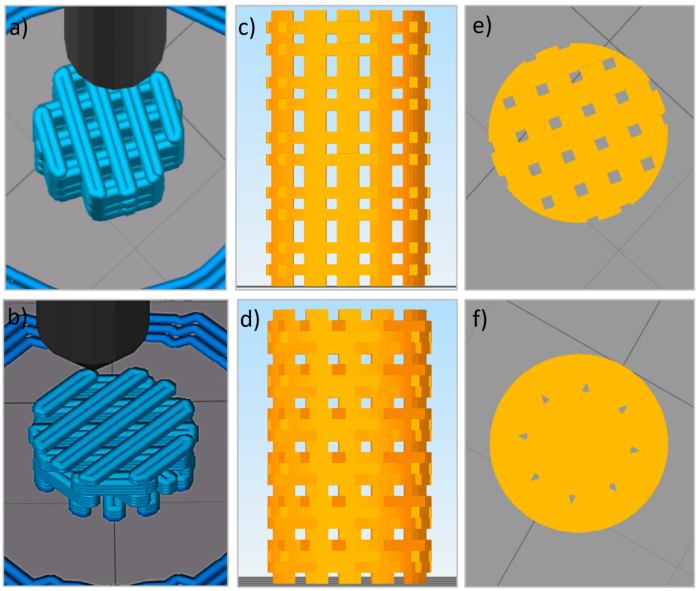

Figura 8. Ilustraciones del proceso de impresión obtenidas del software "Simplify3D Professional". Simulación de fabricación de estructuras alternas (a) y helicoidales (b), y resultado final, disposición alterna (c y e) y helicoidal (d y f). Imagen propia.

Finalmente, todas los andamiajes fueron envasados en condiciones de asepsia en una cabina de flujo laminar, y sometidos posteriormente a un proceso de esterilización mediante irradiación gamma utilizando una dosis de 15 kGy (Aragogamma, Barcelona).

3.2.4 Caracterización de los andamiajes

3.2.4.1 Ensayos de caracterización fisicoquímica y morfológica

La caracterización fisicoquímica de los andamiajes fue realizada sobre los discos fabricados mediante impresión 3D (PLA, PLA-1CaP, PLA-2CaP, PLA-12CaP), correspondientes al *Capítulo II*. Esta se llevó a cabo en el Grupo de Novos Materiais (Universidade de Vigo) mediante espectroscopía "FT-Raman" utilizando el instrumento B&WTEK i-Raman-785S (Metrohm, Herisau, Suiza) equipado con una sonda BAC 100 (785 mm), para identificar las vibraciones moleculares correspondientes a los principales grupos funcionales. Además, su estructura cristalina fue evaluada por medio de difracción de rayos X (XDR) utilizando un difractómetro Siemens D-5000 (Siemens AG, Munich, Alemania). La microestructura se analizó por Microscopía Electrónica de Barrido (SEM) con un equipo JEOL JSM-6700 FEG (JEOL Ltd., Tokyo, Japón) operando a un voltaje de aceleración de 5 kV. Para ello se tomaron micrografías de la parte superior de los implantes, previamente recubiertos de una fina capa de carbono. Las técnicas XRD y SEM se caracterizaron con los equipos de los Servicios Centrales (CACTI) de la Universidad de Vigo.

La topografía de la superficie de los andamiajes, y la exposición en la misma de las partículas de bioCaP fue del mismo modo evaluada por medio del uso de Microscopía Electrónica de Barrido (TM3030, Hitachi, Japón), en el Departamento de Biomateriales del Instituto de Odontología Clínica (Universidad de Oslo). Para ello, los implantes fueron montados sobre soportes de aluminio con una cinta de carbono conductora, y recubiertos con oro hasta conseguir una capa de 2 nm. Posteriormente, las imágenes fueron obtenidas con un voltaje de aceleración de 15 kV.

3.2.4.2 Análisis de la morfología del poro

La microestructura de los implantes fue determinada de manera no destructiva a partir de imágenes tridimensionales obtenidas mediante el uso de un microtomógrafo computarizado (micro-CT) "SkyScan" 1172 (Bruker Micro-CT NV, Kontich, Bélgica) en el Departamento de Biomateriales del Instituto de Odontología Clínica (Universidad de Oslo). Para ello, los parámetros de escaneo fueron establecidos en 70 kV y 141 mA para la fuente de rayos, seleccionando un filtro de aluminio de 0,5 mm y configurando un tamaño de píxel de 13,54 µm. Las muestras se rotaron 360º alrededor de su eje vertical, siendo recogidas las imágenes cada 0.4 grados. Éstas fueron a continuación reconstruidas utilizando el software "NRecon" (Bruker Micro-CT NV, Kontich, Bélgica) en base a tomografías seriadas con orientación coronal utilizando un algoritmo de retroproyección modificado [93]. Posteriormente, el software "CTAn" (Bruker Micro-CT NV, Kontich, Bélgica) fue empleado para el análisis cuantitativo de los andamiajes fabricados.

Los discos sintetizados para el desarrollo del Capítulo II fueron analizados a partir de secciones axiales transversales. El volumen de interés (VOI) fue definido como una región cilíndrica de 5,5 mm centrada en el andamiaje con una longitud total de 1,8 mm (133 cortes). Para el análisis, se utilizó un filtro de difusión anisotrópica seguido de la aplicación un método que establece un umbral de forma manual basándose en histogramas [94], estableciendo los valores de escala de grises entre 35 y 255 (siendo 0: negro y 255: blanco). A continuación, una herramienta de "despeckle" se empleó para eliminar los píxeles blancos excepto no incluidos en el objeto de mayor tamaño, y aquellos píxeles menores de 27 vóxels para eliminar el ruido existente en las imágenes. Finalmente, se llevó a cabo un análisis 3D y de parámetros morfológicos, obteniéndose mediciones de porosidad, diámetro de los "struts" (Grosor de las líneas o "struts"; St.Th.) y separación entre "struts" (tamaño de poro, St.Sp.). Así mismo, la interconectividad de los andamiajes fue calculada utilizando un algoritmo descrito previamente [95,96], el cual considera únicamente el volumen de poros abiertos y accesibles en el interior de la estructura. Este método permite cuantificar el crecimiento óseo hacia la parte interna del implante en función del tamaño de los poros accesibles basándose en su diámetro, obteniéndose por tanto la constricción o estrechez de poro que conecta cada vóxel con la periferia del andamio [97].

Los cilindros fabricados en el Capítulo III fueron igualmente analizados a partir de secciones axiales transversales. En este caso el volumen de interés fue definido como una región cilíndrica de 5,5 mm de diámetro y una longitud de 8 mm (591 cortes). Para su análisis, al igual que en caso anterior, se utilizaron un filtro de difusión anisotrópica, un método para establecer un umbral de forma manual basándose en histogramas y una herramienta de "despeckle", previamente a la cuantificación de parámetros específicos como la porosidad abierta, el ratio de la superficie del objeto en función del volumen (Obj S/V ratio), diámetro de los "struts" (St.Th.) y separación entre "struts" (tamaño de poro, St.Sp.). Del mismo modo, la interconectividad fue calculada con un algoritmo que considera únicamente el volumen de poros abiertos y accesibles dentro de la estructura, según lo previamente indicado en esta sección.

3.2.4.3 Ensayos mecánicos

Las pruebas de compresión mecánica (Zwicki, Zwick/Roell, Ulm, Alemania) fueron realizados en el Departamento de Biomateriales del Instituto de Odontología Clínica (Universidad de Oslo), para evaluar la resistencia mecánica de los andamiajes impresos mediante tecnología 3D. Para ello se utilizó una célula de carga de 1 kN, con una fuerza de precarga fijada en 0,5 N. Los discos (Φ6 x 2 mm) y los cilindros (Φ6 x 10 mm) se comprimieron a lo largo de su eje longitudinal a una velocidad de compresión de 1 mm/min hasta alcanzar el

fallo. La fuerza y el desplazamiento se registraron durante el proceso de compresión, y se transformaron en datos de tensión y deformación basándose en las dimensiones iniciales de los andamiajes. Finalmente, la resistencia a la compresión se midió al final del módulo elástico.

3.2.4.4 Ensayos de humectabilidad

La humectabilidad de los andamiajes, concretamente de los discos fabricados en el *Capítulo II*, fue determinada mediante la medición del ángulo de contacto estático con el agua utilizado el goniómetro "OCA Plus 20" (DataPhysics Instrument GmbH; Alemania) en el Departamento de Biomateriales del Instituto de Odontología Clínica (Universidad de Oslo). En torno a un 1 µl de agua destilada fue inyectado sobre la superficie de los implantes de cada grupo (n=2), y a continuación, tras la formación de la gotas, se obtuvieron imágenes de las mismas para llevar a cabo el análisis por medio de la técnica de la gota sésil en 3 puntos de cada una de las muestras.

3.2.5 Modelo animal y consideraciones éticas

Diez conejos adultos, esqueléticamente maduros, de la raza New Zealand White (Granja San Bernardo, Navarra, España) con un peso medio de 4,825 kg fueron utilizados en este estudio. El protocolo fue aprobado por el Comité de Ética de la Universidad de Santiago de Compostela (España) (Número de Referencia - 02/20/LU-002) y autorizados por la Xunta de Galicia. Así mismo, todos los experimentos animales fueron realizados según la normativa europea y española sobre la protección de animales utilizados con fines científicos (Directiva 2010/63/UE y Real Decreto 53/2013). Además, la descripción de la metodología experimental fue realizada según las directrices ARRIVE ("Animals in Research Reporting *In Vivo* Experiments") [91], para la correcta comunicación de los resultados obtenidos de estudios con animales.

Los procedimientos experimentales, así como el alojamiento de los animales, se llevaron a cabo en el Centro de Experimentación Animal de Universidad de Santiago de Compostela, REGA: ES270280331701 (Campus de Lugo, España), donde los animales fueron manejados y monitorizados por personal experimentado y debidamente cualificado (Iván Alonso Fernández, Antonio González Cantalapiedra y Fernando María Muñoz Guzón). Los animales fueron alojados en jaulas para conejos individuales (R-Suite, Tecniplast, Varese, Italia), ventiladas y enriquecidas mediante el uso de hierba esterilizada mediante autoclave, rollos de papel y palos de madera. Las salas donde se albergaban los animales se mantuvieron bajo unas condiciones de humedad y temperatura controladas, bajo un ciclo luz-oscuridad de 12 horas. En cuanto a su alimentación, se proporcionaron comida y agua *ad libitum*. Los animales fueron utilizados para le experimento tras un período de cuarentena/aclimatación de 3 semanas desde su llegada a las instalaciones.

Para la elección del tamaño muestral del estudio, se tomó como referencia en establecido en los estándares UNE-EN ISO 10993-6:2017.

3.2.6 Procedimiento experimental e implantación de los andamiajes

El protocolo anestésico fue diseñado específicamente para la realización de las cirugías, tratando de reducir al máximo el dolor y la angustia de los animales. Para ello, los conejos fueron premedicados mediante la administración intramuscular de una combinación de medetomidina (50 µg/kg IM, Domtor, Esteve, Barcelona, España), ketamina (25 mg/kg IM, Imalgène 1000, Merial, Toulouse, Francia) y buprenorfina (0.03 mg/kg IM, Buprex, RB Pharmaceuticals, Berkshire, Reino Unido). Y a continuación, la anestesia general fue inducida y mantenida por medio del uso de anestesia inhalatoria, concretamente de isoflurano

(Inspiratory Fraction ISO 2.5-4%, Isova-vet, Schering-Plow, Madrid, España). Adicionalmente se les administraron mediante inyección subcutánea durante el período preoperatorio enrofloxacino (5 mg/kg SC, Ganadexil 5%, Invesa, Barcelona, España) como profilaxis antibiótica, y meloxicam (0.2 mg/kg SC, Metacam, Boehringer Ingelheim, Barcelona, España) como fármaco analgésico adicional a la buprenorfina para el control del dolor y la inflamación.

Para la descripción de las cirugías llevadas a cabo durante el proceso experimental, procederemos a describir los procedimientos realizados para el cumplimiento de los objetivos correspondientes al *Capítulo II* y *Capítulo III*.

Capítulo II: Una vez anestesiados, la región frontoparietal de los conejos fue rasurada y desinfectada con una mezcla al 50/50 de alcohol y povidona iodada. Posteriormente, se realizó una incisión longitudinal en la calota a lo largo de la línea media sagital, y el hueso fronto-parietal de la calota fue expuesto por medio de la elevación de un colgajo mucoperióstico. Una vez identificadas las suturas sagitales y coronales que delinean los huesos frontal, parietal izquierdo y parietal derecho; se crearon cuatro defectos óseos circulares de 6 milímetros a cada lado de las suturas coronal y mediana, utilizando una tefrina (227B.204.060, Komet, Alemania) acoplada en una pieza de mano quirúrgica con abundante irrigación con solución salina fisiológica. La osteotomía fue realizada cuidadosamente para evitar dañar la duramadre expuesta subyacente. Finalmente, los segmentos óseos bicorticales fueron luxados utilizando un osteotomo, y a cada uno de los defectos se les asignó uno de los discos pertenecientes a los grupos de tratamiento según la aleatorización en bloques (Tabla 3): PLA (grupo control positivo), PLA-1CaP, PLA-2CaP y PLA-12CaP. La Figura 9 muestra imágenes relevantes del proceso quirúrgico correspondiente al *Capítulo II*.

Tabla 3. Aleatorización de los grupos de tratamiento en calota. CRL (Defecto Craneal Izquierdo), CRR (Defecto Craneal Derecho), CDL (Defecto Caudal Izquierdo) y CDR (Defecto Caudal Derecho)

	PLA (control)	PLA-1CaP	PLA-2CaP	PLA-12CaP
Conejo 1	CDR	CDL	CRL	CRR
Conejo 2	CDL	CRL	CRR	CDR
Conejo 3	CRL	CRR	CDR	CDL
Conejo 4	CRR	CDR	CDL	CRL
Conejo 5	CDR	CDL	CRL	CRR
Conejo 6	CDL	CRL	CRR	CDR
Conejo 7	CRL	CRR	CDR	CDL
Conejo 8	CRR	CDR	CDL	CRL

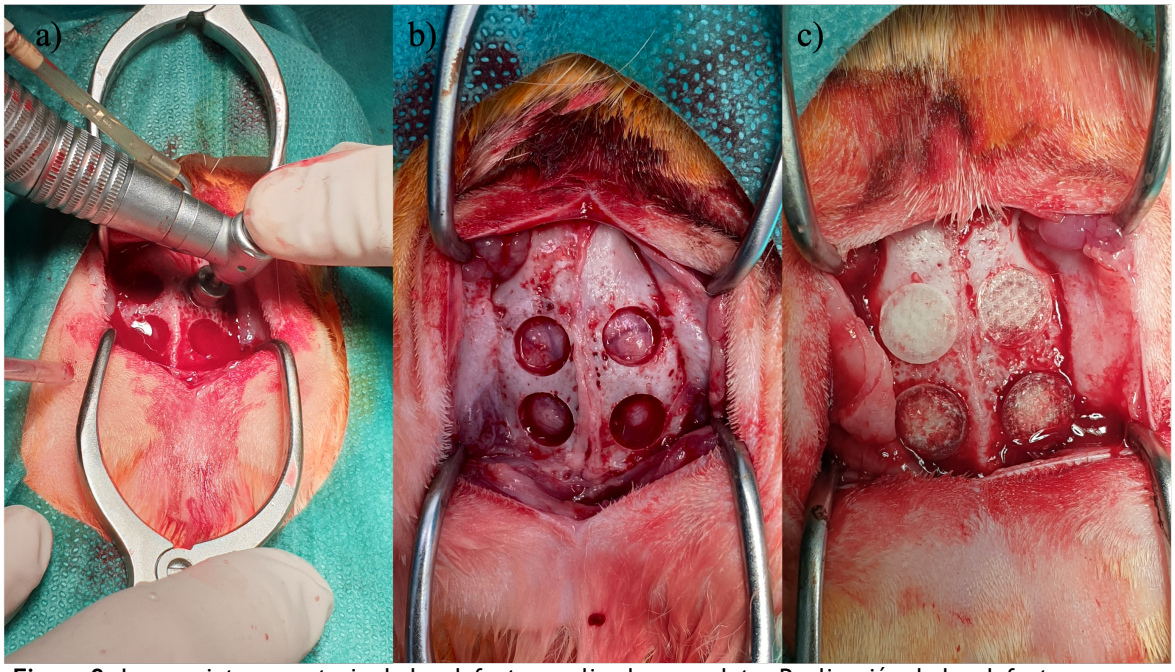

Figura 9. Imagen intraoperatoria de los defectos realizados en calota. Realización de los defectos con una fresa tefrina (a), imagen tras la luxación de los fragmentos óseos bicorticales (b) e implantación de los andamiajes (c). Imagen propia.

Capítulo III: En este caso, una región delimitada entre las diáfisis del fémur y la tibia fue rasurada y desinfectada. A continuación, la piel, el tejido subcutáneo y el músculo fueron incididos y diseccionados capa por capa, para la realización un defecto óseo circular de 6 mm de diámetro en el cóndilo femoral lateral de ambas extremidades con el uso una tefrina (227B.204.060, Komet, Alemania). Tras la luxación del fragmento óseo monocortical con un osteotomo, los cilindros fabricados con disposiciones ALT y HEL fueron implantados en cada uno de los defectos, según lo establecido en la aleatorización en bloques (Tabla 4): PLA-12CaP-ALT (estructura alterna) y PLA-12CaP-HEL (estructura helicoidal). La Figura 10 muestra imágenes relevantes del proceso quirúrgico correspondiente al *Capítulo III*.

Tabla 4. Aleatorización de los grupos de tratamiento en cóndilo femoral. RLFC (Cóndilo Femoral Lateral Derecho) y LLFC (Cóndilo Femoral Lateral Izquierdo).

	PLA-12CaP-ALT	PLA-12CaP-HEL
Conejo 1	RLFC	LLFC
Conejo 2	RLFC	LLFC
Conejo 3	RLFC	LLFC
Conejo 4	RLFC	LLFC
Conejo 5	LLFC	RLFC
Conejo 6	LLFC	RLFC
Conejo 7	LLFC	RLFC
Conejo 8	RLFC	LLFC

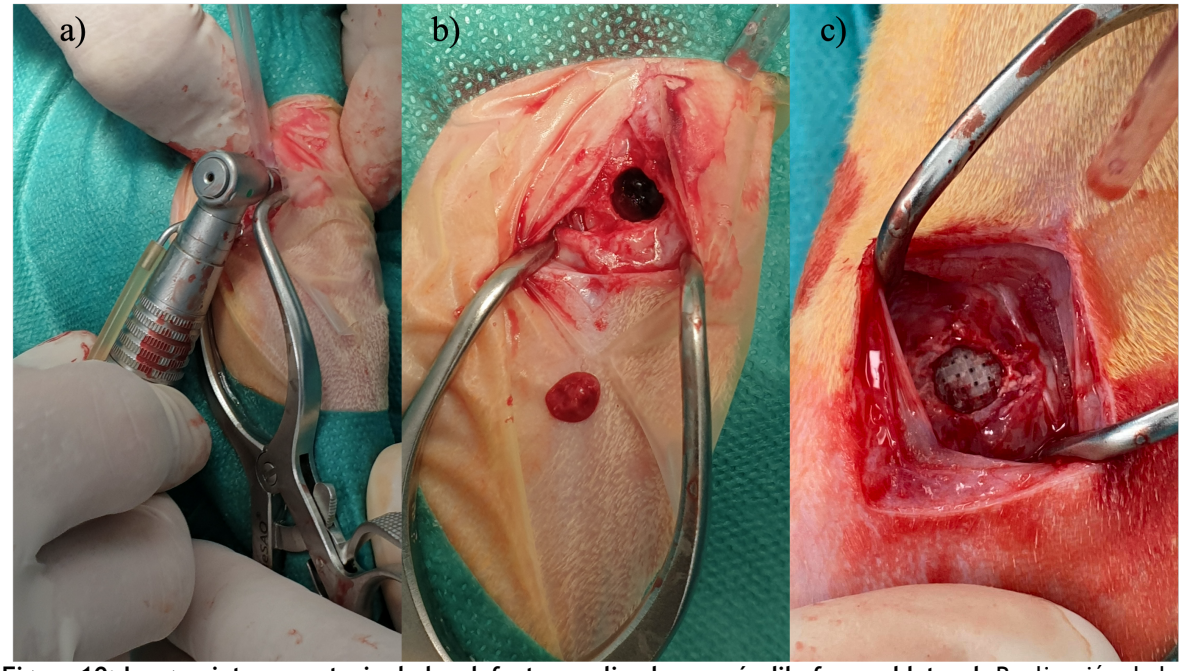

Figura 10: Imagen intraoperatoria de los defectos realizados en cóndilo femoral lateral. Realización de los defectos con una fresa tefrina (a), imagen tras la luxación del fragmento óseos monocortical (b) e implantación del andamiaje (c). Imagen propia.

Tras la implantación de los andamiajes, se utilizó un patrón de sutura continuo simple para cerrar los planos subcutáneo y muscular con VYCRYL 4/0 (Ethicon, Johnson & Johnson, Madrid, España). Y se seleccionó un patrón de puntos simples para el cierre de la piel con la misma sutura. Finalmente, se revirtió la sedación por medio de una inyección intramuscular de atipamezol (25 ug/kg IM, Nosedorm, Karizoo, Barcelona, España). Así mismo, como tratamiento postoperatorio durante los 5 días siguientes a la cirugía se administró a los conejos enrofloxacino (5 mg/kg, Ganadexil 10%, Invesa, Barcelona, España) por vía oral para evitar la aparición de infecciones, y meloxicam (0.1 mg/kg SC, Metacam, Boehringer Ingelheim, Barcelona, España) por vía subcutánea para el control del dolor. Los conejos fueron monitorizados semanalmente por veterinarios para la detección de dehiscencias, inflamación o infecciones, y la evaluación de su salud general hasta el momento del sacrificio.

12 semanas tras la implantación, los animales fueron sedados mediante una inyección intramuscular de medetomidina (50 ug/kg, Domtor, Esteve, Barcelona, España) y ketamina (25 mg/kg IM, Imalgène 1000, Merial, Toulouse, Francia), y posteriormente eutanasiados por medio de la inyección de pentobarbital sódico (100 mg/kg IV, Dolethal, Vétoquinol, Madrid, España) en la vena auricular lateral. Inmediatamente tras la eutanasia, las muestras de calvaria y fémur fueron disecadas de piel, tejidos blandos y músculo, y fijadas en formalina tamponada al 10% durante 2 semanas.

3.2.7 Evaluación de la regeneración ósea

3.2.7.1 Análisis con microtomografía computarizada

Una vez fijadas las muestras, estas fueron envueltas en una gasa humedecida con formalina tamponada al 10% y se escanearon previamente a ser procesadas para su análisis histológico.

Las muestras fueron escaneadas utilizando un instrumento de microtomógrafía computarizada de alta resolución (“Skyscan” 1172, Bruker micro-CT NV, Kontich, Bélgica),

equipado con una cámara CCD de 11-Mpixel. Los parámetros de adquisición fueron establecidos en 70 kV, 141 uA, filtro de aluminio de 0.5 mm, paso de rotación de 0.400º sobre un total de 360 º, y un tiempo de exposición de 1710 ms por proyección. La reconstrucción de las proyecciones de rayos X se realizó utilizando un algoritmo de retroproyección modificado [93], mediant el uso del software "NRecon" (Bruker Micro-CT NV, Kontich, Bélgica), obteniéndose un tamaño final de vóxel de 13,58 µm. El análisis quantitativos de la formación de hueso nuevo en los defectos se realizó mediante uso del software "CTAn" (Bruker Micro-CT NV, Kontich, Bélgica)

Para los andamiajes implantados en calota, correspondientes al *Capítulo II*, el volumen de interés (VOI) se definió a partir de cortes axiales como una región de cilíndrica de 5,96 mm, centrada en el defecto y ajustándose a los márgenes del mismo, y que transcurre desde la tapa del implante hasta su parte inferior excluyéndose los extremos. De este modo se obtiene una altura total de 1,45 mm (107 cortes).

En el caso de los cilindros sintetizados para su implantación en cóndilo femoral lateral, correspondientes al *Capítulo III*, el volumen de interés (VOI) fue establecido como una región cilíndrica centrada en el defecto de 5,98 mm de diámetro y 6 mm (442 cortes) de altura. Excluyéndose del análisis al igual que en el caso anterior los extremos.

Posteriormente, se aplicaron sobre las imágenes un filtro de difusión anisotrópica, se estableció el valor de la escala de grises de 80 a 255 (siendo 0: negro y 255: blanco)[94] y se empleó la herramienta "despeckle" para eliminar puntos blancos con un tamaño inferior a 27 vóxels. Esto nos permiten evaluar la formación de nuevo tejido mineralizado, y distinguirlo del implante y de otros tejidos conectivos fibrovasculares radiolúcidos adyacentes. Finalmente, para evaluar la capacidad de regeneración ósea de los andamiajes, se analizaron los siguientes parámetros:

- Volumen Óseo/Volumen Tisular (BV/TV): Esta medida cuantifica el hueso neoformado existente en un determinado volumen de interés con respecto a la cantidad total de tejido.
- Superficie Ósea/Volumen Óseo (BS/BV): Describe la relación entre la superficie de nuevo hueso formado y su volumen, y es un indicador del área disponible del hueso regenerado.
- Grosor Trabecular (Tb.Th.): Parámetro que indica el grosor medio del hueso trabecular regenerado.
- Factor de Patrón Trabecular (Tb.Pf.): Refleja cuantitativamente el ratio de conectividad intertrabecular.

3.2.7.2 Preparación y análisis histológico

Tras su análisis microtomográfico, las muestras se mantuvieron en formalina tamponada durante una semana más. Tras este período, fueron cuidadosamente cortadas a lo largo de las suturas sagital y coronal de la calota, y cada uno de cuatro defectos con su respectivo implante fueron individualizados. A continuación, se procedió a procesar cada uno de los especímenes según el método descrito por Donath [98], para la obtención de secciones histológicas sin descalcificar. Las muestras fueron deshidratadas por medio de una serie disoluciones con grados ascendentes de etanol (70-100% EtOH), y luego infiltradas e incluidas en una resina de metacrilato fotopolimerizable ("Technovit" 7200-VLC, Heraus Kulzer GmbH, Werheim, Alemania). Concretamente, estas fueron infiltradas primero en una serie de soluciones mixtas de alcohol etílico y resina, con concentraciones ascendentes de esta última, para posteriormente lograr una adecuada penetración de la resina por medio del uso de un

sistema de inclusión por vacío, y la fotopolimerización de la resina a través del uso de radiación UV.

En el siguiente paso, los bloques de resina fueron seccionados por la línea media del defecto (secciones centrales) utilizando una sierra de banda ("EXAKT", Apparatebau, Norderstedt, Alemania). La misma herramienta, fue utilizada a continuación para obtener secciones transversales de cada bloque con un grosor inicial de 250 ± 50 µm, que fueron pulidas con una micropulidora ("EXAKT", Apparatebau, Norderstedt, Alemania) empleando láminas de carburo de silicio con un tamaño de grano de 1200 y 4000 (Struers, Conpehagen, Dinamarca), hasta obtener sección con un grosor de aproximadamente 40 µm. Finalmente, estas fueron teñidas por el método de Lévai-Laczkó.

Para el análisis histológico, todas las muestras con andamiajes implantados en defectos en calota fueron evaluadas microscópicamente (Olympus BX41 microscope; Olympus Corporation, Tokyo, Japón) de acuerdo a lo establecido en los estándares UNE-EN ISO 10993-6:2017, para el análisis de los efectos locales existentes tras la implantación, como son la respuesta inflamatoria, la formación de nuevos vasos sanguíneos y la presencia de fibrosis o infiltrados grasos. Por consiguiente, los andamiajes implantados fueron clasificados en base a la siguiente escala de graduación como: no irritantes, levemente irritantes, moderado o severo. Además, también se realizó una descripción detallada de los hallazgos histológicos más relevantes.

3.2.7.3 Análisis histomorfométrico

Para los análisis quantitativos, las secciones al completo fueron capturadas con un microscopio "Olympus" BX51 (Olympus Corporation, Tokyo, Japón), con aumentos x10 en el caso de las muestras provenientes de calvaria (Capítulo II), y x4 para las muestras extraídas de cóndilo femoral lateral (Capítulo III). A continuación, las imágenes fueron coloreadas con el programa "Adobe Photoshop CS6" (Adobe Systems Incorporated, San Jose, EE.UU.), diferenciando el hueso nuevo regenerado, el hueso maduro, el material implantado y los tejidos blandos. Dichas imágenes coloreadas fueron posteriormente analizadas para medir los diferentes parámetros histomorfométricos que se expondrán a continuación utilizando el software "Olympus CellSens 1.5" (Olympus Corporation, Tokyo, Japón). Para dicha valoración, se definió una región de interés (ROI) entre los márgenes delimitados lateral y medialmente por el hueso nuevo y el hueso maduro, y dorsal y ventralmente por los extremos de los andamiajes. Los parámetros histomorfométricos evaluados fueron:

- Contacto Hueso-Implante (BIC): Este parámetro hace referencia al porcentaje de hueso en contacto con el implante, con respecto al perímetro total del mismo.
- Superficie del Implante/Superficie Tisular (IS/TS): Cuantifica la relación entre la superficie de implante y la superficie tisular total dentro de la ROI.
- Superficie Ósea/ Superficie Tisular (BS/TS): Evalúa la cantidad de hueso neoformado en la ROI, basándose en la relación entre la superficie del hueso regenerado y la superficie tisular total.

3.2.8 Análisis estadístico

El análisis realizado para la evaluación de los resultados se mostrará de forma individualizada para el *Capítulo II* y el *Capítulo III*. En ambos casos se llevó a cabo utilizando el software SigmaPlot 12.5 (Systat Software Inc., Chicago, IL, EE.UU.). Todos los datos se expresaron como medias ± desviaciones estándar (SDs).

Capítulo II: La normalidad de las variables fue evaluada utilizando la prueba de Shapiro-Wilk, y la prueba de Levene fue empleada para evaluar la igualdad de las varianzas de las

variables normales. La comparación estadística se realizó mediante un análisis de varianza unidireccional (ANOVA), seguido de una prueba post-hoc para las comparaciones múltiples por pares mediante el método Holm-Sidak. En el caso de variables no normales, una prueba de Friedman fue realizada para evaluar las comparaciones estadísticas, seguida de un análisis post-hoc utilizando una prueba de Tuckey. Además, se llevaron a cabo estudios de correlación utilizando el análisis de correlación de Pearson. El nivel de significación se fijón en $p<0,05$ para todos los parámetros.

Capítulo III: En el análisis estadístico de la morfología del poro y las pruebas mecánicas, la normalidad de las variables fue evaluada mediante las pruebas de Kolmogoron-Smirnov o Shapiro-Wilk, y las comparaciones estadísticas de los resultados obtenidos de los distintos grupos se realizó por medio de una prueba T pareada. Además, se llevaron a cabo estudios de correlación utilizando el análisis de correlación de Pearson. Sin embargo, en el caso de los resultados obtenidos de los análisis microtomográficos e histomorfométricos, la normalidad de las variables fue evaluada por medio de la prueba de Shapiro-Wilk, y continuación la igualdad de las varianzas se verificó mediante una prueba de Igualdad de Varianzas. En caso de que se superasen ambas pruebas, la comparación estadística de las muestras pertenecientes a ambos grupos se realizó mediante la prueba T de Student. Por el contrario, en aquellos casos donde las variables eran normales, pero no se superaba la prueba de Igualdad de Varianzas, la comparación estadística de los resultados se llevó a cabo mediante la prueba Mann-Whitney U. El nivel de significación se fijó en $p<0,05$ para todos los parámetros.

RESULTS

4 RESULTS

4.1 CHAPTER I

"USE OF 3D-PRINTED POLYLACTIC ACID/BIOCERAMIC COMPOSITE SCAFFOLD FOR BONE TISSUE ENGINEERING IN PRECLINICAL IN VIVO STUDIES: A SYSTEMATIC REVIEW."

The results included in this chapter have already been published as:

Alonso-Fernández[1], H.J. Haugen[2], M. López-Peña[1], A. González-Cantalapiedra[1], F. Muñoz[1], Use of 3D-printed polylactic acid/bioceramic composite scaffolds for bone tissue engineering in preclinical in vivo studies: A systematic review, *Acta Biomaterialia*. (2023). https://doi.org/10.1016/j.actbio.2023.07.013.

[1]Anatomy, Animal Production and Veterinary Clinical Sciences Department, Veterinary Faculty, Universidade de Santiago de Compostela, Campus Universitario s/n, 27002 Lugo, Spain

[2]Department of Biomaterials, Institute of Clinical Dentistry, Faculty of Dentistry, University of Oslo, Oslo, Norway

4.1.1 Study selection

The literature search resulted in an initial pool of 799 potentially eligible publications collected from Pubmed and Web of Science. Once duplicates were removed, the remaining manuscripts (n=626) were screened based on the tittle and the abstract, and after evaluating the inclusion and exclusion criteria, only 150 were included as potentially eligible. After full-text analysis, 122 reports were excluded (Table 5), and 15 were not retrieved. Finally, the assessment of the references included from the initial pool led to a total of 13 articles that were found suitable to be included, in addition, an article was added by hand-searching. Thus, a total 14 publications were selected to elaborate the present systematic review (Figure 11).

Table 5. Main Reason for exclusion after full-text screening. "Reprint with permission from [8] under the terms of the Creative Commons Attribution 4.0 International License, CC BY-NC.ND 4.0."

Main Reason for Exclusion	No.	References
Language	2	[99,100]
Implants' characterization and/or *in vitro* study	48	[16,37,61,78-82,101-140]
No additive manufacturing fabrication	3	[141-143]
Ectopic bone formation model	2	[144,145]
PLA Copolymers	32	[57,146-176]
No PLA bioceramic composites	34	[45,177-209]
Internal Fixation Clip	1	[210]

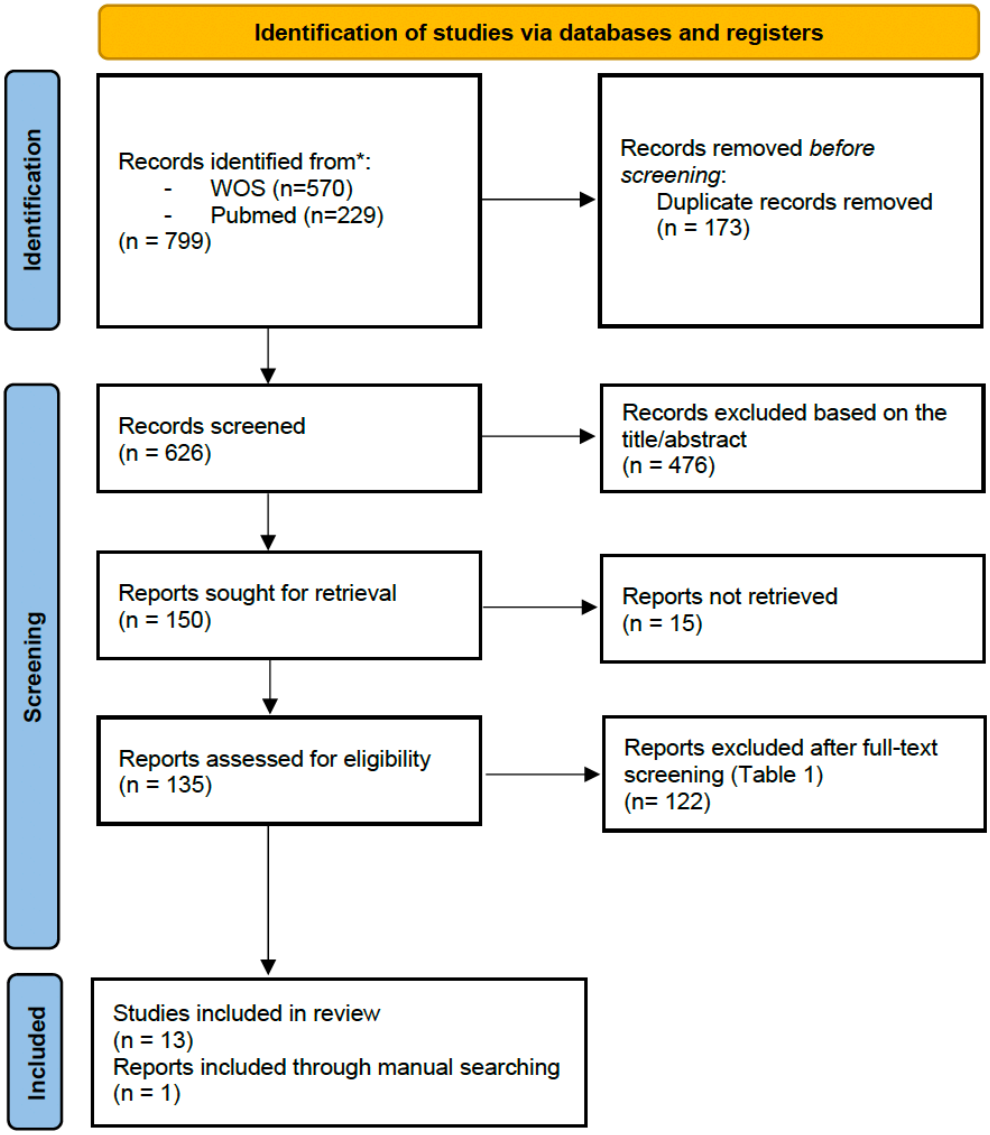

Figure 11. Flow chart of the article selection procedure. "Reprint with permission from [8] under the terms of the Creative Commons Attribution 4.0 International License, CC BY-NC.ND 4.0."

4.1.2 Study Characteristics

The manuscripts included in this systematic review were mainly published after 2020 (8/13). Indeed 3D-printed scaffolds have become a promising alternative for bone regeneration. Hence, the interest in this production method has been growing for years.

The qualitative data of the studies have been extracted and displayed in the following analytic tables. From a total number of 14 included articles, 7 of them were conducted in rabbits, in which New Zealand rabbits were used [77,211–216]. And another 7 ones in rats, where they used Wistar Strain in two papers [217,218], Spargue-Dawley in four [75,219–221] and in one the breed was not specificized [222]. According to the definition made by Brunello *et al.* [39], an intrabony defect of critical dimensions is not expected, by definition, to heal spontaneously within the lifetime of the animal. All the defects made in rats were performed in calvaria, but

only 3 could be considered as critical-sized bone defects (CSD). However, the ones in rabbits were performed in femur and radius, and only the ones in radius could be considered as CSD (Table 6). Zhang *et al.* [215], in contrast, did not make a defect, but rather developed a *in vivo* bioreactor model crossing the scaffold with a vascular bundle and transplanted it to tibial periosteum.

Table 6. Animal defects. "Reprint with permission from [8] under the terms of the Creative Commons Attribution 4.0 International License, CC BY-NC.ND 4.0."

Animal	Study Model	Number of Publications	Critical-Sized Defects	References
Rats (n=7)	Calvarial Bilateral Defect	1	1/1	[217]
	Calvarial Unilateral Defect	6	2/6	[75,218–222]
Rabbits (n=5)	Femoral diaphysis defect (cylindrical)	4	0/4	[77,211,213,214]
	Radius diaphysis segmental defect	2	2/2	[212,216]

As mentioned before, PLA is one of the main polymeric materials used in bone tissue engineering, and its isomeric composition may vary its characteristics. Only four out of fourteen articles specify the isomeric composition: PLLA (pure poly L-LA, n=3) [77,216,220] and PDLA (poly-D,L-LA, n=1) [221]. Likewise, hydroxyapatite was the main bioceramic chosen for synthesizing composites (n=10) [75,77,211–217,219], being used as a powder mixed in different ratios with the polymeric material. Besides, the HA particles' size varies among the publications, showing a nanometric size in 5 of them [77,211,213,214,219]. Other bioceramic materials employed were CaP (n=1) [218] as a biomimetic coating, β-TCP (n=1) [220], AW (n=1) [221] or OCP (n=1) [222].

Regarding the morphology of the scaffolds, the fabrication of 3D porous interconnected structures with different shapes and sizes has been the election in all the studies. These were probably selected for their advantages and crucial role in bone regeneration, simulating the properties of an extracellular matrix, to create a microenvironment conducive to optimal tissue regeneration. Among the wide range of production methods, additive manufacturing techniques, as mentioned before, can be divided in the following groups.

- Extrusion-based techniques, such as fused deposition modelling (FDM) or fused filament fabrication (FFF), robocasting, dispense plotting or bioplotting, multi-head deposition system (MHDS) or mini-deposition (MDS) system [36,38]. FDM or FFF was the most commonly used, as seen in 11 of the papers [75,77,211,213–219,221]. However, other alternatives when manufacturing 3D implants were also utilized, such as micro-extrusion based 3D-printing technology (n=1) [222] or 3D bioplotting (n=2) [212,220].
- Powder-based techniques, such as inkjet printing, selective laser sintering (SLS), selective laser melting (SLM), binder jetting/sintering, direct metal laser sintering (DMLS) and electron beam melting (EBM) [36,38]. Binder jetting/sintering (indirect 3D-printing) technique was selected for the synthesis of apatite-wollastonite (AW) disks [221].
- Vat photopolymerization techniques, which was not used in any of the included manuscripts.

Another important feature when synthesizing implants is the sterilization process since it is essential to prevent unsterile medical devices and also required to obtain regulatory approvals [38,223]. Among the different sterilization techniques, ethylene oxide sterilization was selected to sterilize PLA-bioceramic composite scaffolds in 7 of the included manuscripts [75,211,215–219], another paper utilized γ-irradiation [221], and in the remaining 6 studies the sterilization process was not reported [77,212–214,220,222]. Besides, Tcacencu *et al.* [221] used steam sterilization (also called autoclaving) to sterilize the apatite-wollastonite disks.

Scaffold's characterization is an essential step in bone tissue engineering due to the importance of key parameters that may influence the biological response and the bone healing process, such as mechanical strength, porosity, degradability, or *in vitro* trials (summarized in Table 7, included at the end of this Chapter).

First, mechanical strength, in terms of compressive strength and/or elastic modulus, is included in approximately 57% of the studies, and its importance lies in its ability to withstand the existing loads after implantation and provide sufficient support to bone growth. So it should be as similar as possible to the bone: Compressive strength of Trabecular bone 0.1-16 MPa and Compressive strength of Cortical Bone 130-200 MPa [224,225]. Likewise, porosity and/or pore size have been reported in all the articles included in the present review as a consequence of its main role in cell spreading and effective transport of nutrients, oxygen, waste, etc., favoring continuous ingrowth of bone tissue from the periphery into the inner part of the scaffold [13,35,226]. Indeed, high porosity and pore size promote bone regeneration, but reduce the mechanical properties of the implant [30,226]. The results include values of porosity and pore size ranging between 26.4% and 70% and 100 and 500 μm, respectively (See Table 7). However, the degradability of the scaffolds was only measured by 3 studies [77,213,220], even though it is an important parameter, since degradation by-products can influence the environment affecting bone formation and healing time. Furthermore, the degradability will also be related to porosity and mechanical strength, as higher porosity leads to higher degradability and, consequently, to lower mechanical resistance [30,226]. In two articles, the samples were soaked into PBS media (pH 7.4 +- 0.2) at an established temperature, and variations in weight, molecular weight and/or pH were measured at various time points [77,213]. And in the other one, the analysis was performed *in vivo*, through the measurement of non-degradation-related molecular weights by gel permeation chromatography (GPC) and near-infrared (NIR) fluorescence images [220]. Finally, *in vitro* trials were carried out in all studies except three (see Table 7); though no information was collected, they represent an essential intermediate step between material synthesis and characterization, and *in vivo* testing. Scanning electron microscopy (SEM) was the most commonly used characterization technique for the scaffolds. However, others can be found in Table 7, such as Micro-Computed Tomography (μCT), mechanical testing, Fourier Infrared Spectroscopy (FTIR), Energy Dispersive Spectroscopy (EDS), X-ray Diffraction Analysis (XDR), etc.

Furthermore, different substances can be applied to scaffolds to improve bone healing and regeneration by affecting bone metabolism. Two studies used bone marrow-derived stem cells (BMSCs) [215,219], one used dental pulp stem cells (DPSC) [217] and one used enhanced bone marrow (eBM) [212]. Human osteoblastoma cell line (MG-63 cell line) was also used in one of the reports [220], as well as recombinant human bone morphogenetic protein-2 (rhBMP-2) [218]. Substances such as lanthanum (La), a rare earth element with an important role in the bone remodeling cycle that can promote the proliferation of bone-building osteoblast, were used in one paper [222]. Specifically in this case, La may influence the hydrolysis of OCP to an HA structure, thus influencing OCP-mediated bone formation.

Likewise, many few procedures can also favor bone regeneration, such as sinusoidal electromagnetic fields (EMF) [219] or induced membrane technique (IMT) [212]. EMF triggered a higher new bone formation and vascularization. And IMT generated membranes similar to the periosteum, giving interesting results for treating large bone defects when combined with autografts [227].

There are different methods to assess bone healing in clinical trials. The ones utilized in selected studies were summarized in Tables 8 and 9. Histological evaluation was the most frequently used (n=14), being able to distinguish between a qualitative histological analysis (n=13), which described the results without the use of objective measurement techniques; and a quantitative or histomorphometric analysis (n=5), that supplies objective data about the parameters analyzed such as angiogenesis or osteogenesis. In addition, these procedures can be carried out by decalcifying the bone and embedding it in paraffin (n=10) or dehydrating and embedding it in a resin (n=4). Likewise, micro-computed tomography analysis was widely used (n=9), providing objective measurements to quantify bone regeneration. Other methods are radiographic evaluation, fluorescence imaging, immunohistochemistry (osteocalcin (OC), type I collagen (COL-1) or CD31) or biochemical analysis. Follow-ups varied between 4 and 16 weeks, a single observation time was reported in 4 out of 13 studies [77,216,217,221,222] and in the other ones, multiple observation times were utilized.

4.1.2.1 Studies in rats – main features

In vivo trials for testing biomaterials were conducted in the included reports through unilateral or bilateral defects in the calvaria of adult rats without any adverse reactions to the implanted scaffolds being reported. The main characteristics and results of the studies are summarized in Table 8 (Included at the end of this Chapter).

First, regarding the anaesthetic protocols, different drugs and their combinations were utilized by the authors. Intraperitoneal injection of pentobarbital was administered in two studies, as a single drug [222], or in combination with inhaled isoflurane [219]. Ketamine was used alone [75], combined with xylazine [217,221], or with xylazine and midazolam [218]. Kwon *et al.* [220] chose a mixture of tiletamine, zolazepam and xylazine. Besides, only one study reports the use of local anaesthesia, with lidocaine, and/or postoperative analgesia, in this case, buprenorphine [217]. Given the importance of the anaesthetic protocol, both from an ethical and experimental process point of views, it will be analyzed in more in detail in the discussion section.

HA was the main bioceramic added to a PLA matrix for synthesizing composites, which will be later used to produce 3D porous scaffolds via 3D-printing. They were tested in rats in three studies [75,217,219]. Gendviliene *et al.* [217] manufactured PLA-HA scaffolds and showed a low potential to induce bone growing (BV (mm^3) micro-CT: male 3.86±0.99, new bone (mm^2) histology: 2.90±0.06), that was slightly higher than PLA alone scaffolds and negative control, but less than the one showed by the Bio-Oss (BV (mm^3) micro-CT: male 4.24±0.51, new bone (mm^2) histology: 4.15±0.58). However, these results seemed to be improved by the incorporation of dental pulp stem cells to obtain cellularized scaffolds (PLA-HA-cells), or the production of decellularized extracellular matrix PLA-HA (PLA-HA-dECM) scaffolds. Thus, achieving a bone formation *in vivo* similar o even superior to that obtained with the Bio-Oss (PLA-HA-cells BV (mm^3) micro-CT: male 4.11±0.72, new bone (mm^2) histology: 3.66±0.29; PLA-HA-ECM BV (mm^3) micro-CT: male 5.09±1.27, new bone (mm^2) histology: 3.80±0.24). Interestingly, significant differences between male and female groups can be appreciated in relation to bone growth (Figure 12).

Results	Groups	Negative control	Bio-Oss	PLA	PLA/HA	PLA/HA cells	PLA/HAECM
BV (mm^3) μCT	female	2.31 ± 0.73	3.85 ± 0.10	1.50 ± 0.33	2.29 ± 0.27	2.47 ± 0.36	3.01 ± 0.26
	male	2.80 ± 0.39	4.24 ± 0.51	3.76 ± 0.43	3.86 ± 0.99	4.11 ± 0.72	5.09 ± 1.27
New bone (mm^2) Histology	female	2.04 ± 0.34	3.35 ± 0.26	1.90 ± 0.07	2.32 ± 0.09	2.81 ± 0.30	3.10 ± 0.27
	male	2.34 ± 0.96	4.15 ± 0.58	2.52 ± 0.33	2.90 ± 0.06	3.66 ± 0.29	3.80 ± 0.24

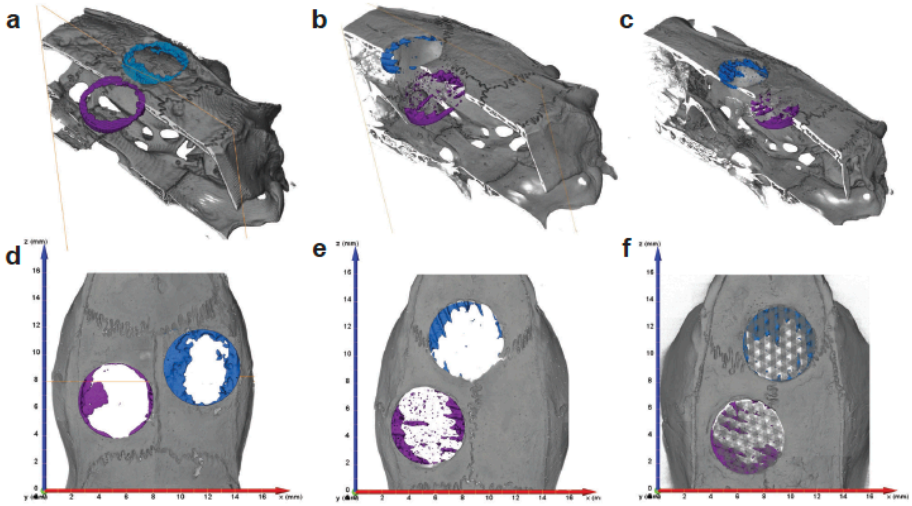

Figure 12. Micro-CT and histology results according to gender (All parameters are presented as mean SD). Processed micro-CT images taken with an X-Ray 3D Computer tomograph RayScan 250E. (a,d) Negative control (purple) and Geistlich Bio-Oss® (blue). (b,e) Pure PLA (blue) and PLA-HA (purple) scaffolds. (c,f) PLA-HA cellularized with dental pulp stem cells (blue) and PLA-HA-dECM scaffolds (purple) [217]. "Reprint with permission from [8] under the terms of the Creative Commons Attribution 4.0 International License, CC BY-NC.ND 4.0."

Nevertheless, Zhang *et al.* [75] demonstrated the osteogenic capability of 3D-printed PLA-HA scaffolds, as confirmed by histological examination and the results of the tomographic analysis, which was performed at 4 and 8 weeks, showing that scaffolds' bone volume per total volume (BV/TV) presented values around 45% at 8 weeks. On the other hand, defects filled with β-TCP presented the highest BV/TV value, almost reaching 50%, and those filled with demineralized bone matrix (DBM) and the empty ones got the lowest values.

Tu *et al.* [219] utilized nano-grade HA to manufacture 3D-printed PLA-HA composite scaffolds. Micro-CT results at 4 weeks after surgery indicate a BV/TV of about 10% approximately, a lower value than that obtained by Zhang *et al.* [75] at the same time point, approximately 20%. Histological and micro-CT results of the PLA-HA scaffold group were superior to the control group at both time points (PLA-HA BV/TV and New Bone Area Fraction (%) 4w and 8w: ~10% and ~20%). However, Tu *et al.* [219] applicated two different treatments to PLA-HA scaffolds to improve their bone regeneration capability, seeding rat bone marrow mesenchymal stem cells (BMSCs), applying electromagnetic fields (EMF) or both, thus generating another 3 experimental groups. The results showed a higher percentage of bone growth in all groups, being more notable in the one that combined BMSCs and EMF (PLA-HA BMSCs + EMF BV/TV; 4w and 8w: ~35% and ~70%; New Bone Area Fraction (%) 4w and 8w: ~30% and ~60%). When used independently, the amount of new bone is lower without significant differences between PLA-HA BMSCs and PLA-HA EMF groups at any time point (Figure 13).

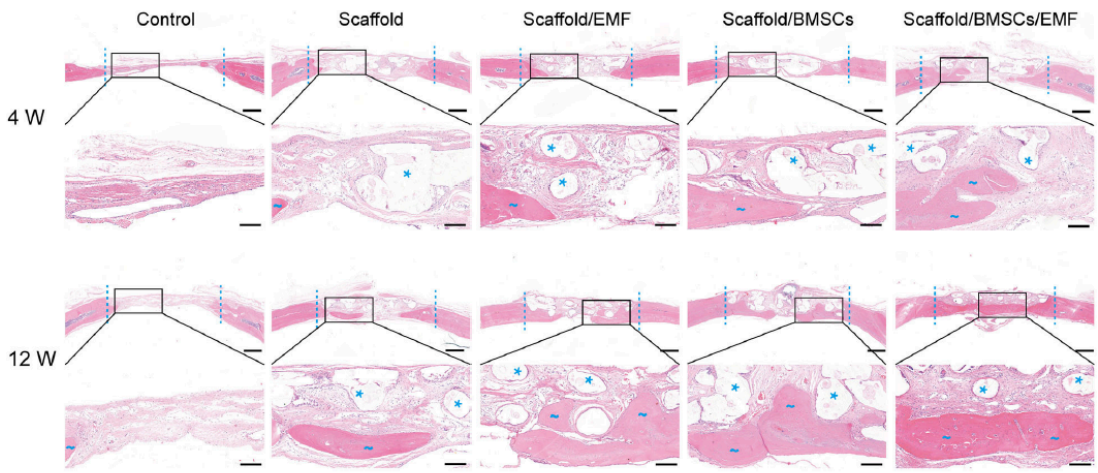

Figure 13. Bone regeneration evaluated by HE staining. Coronal HE stained sections in the calvarial defect region of different groups were taken 4 and 12 weeks post-operation. The dotted line indicates the boundary of the 6-mm defect. Blue wary lines designate newly formed bone, and asterisks point to residual scaffolds. Scale bars in lower magnification images represent 1000 μm, and scale bars in higher magnification images represent 250 μm [219]. "Reprint with permission from [8] under the terms of the Creative Commons Attribution 4.0 International License, CC BY-NC.ND 4.0."

Almost no direct comparisons could be performed among papers that used HA in rat's calvaria model [75,217,219], because of differences in time points, PLA-HA mixing ratios and the defects' number and/or size.

Octacalcium phosphate (OCP) is thought to be one of the precursors for the formation of bone apatite crystals, being converted to HA under physiological environments. OCP powders were synthesized and mixed with PLA to create 3D-printed porous scaffolds [222]. Likewise, OCP with different concentrations of Lanthanum (0.2/0.5/1La-OCP) were prepared via co-precipitation methods. *In vivo* trials showed that OCP promoted positive bone formation, an 0.2 La-OCP-PLA scaffolds showed an improvement in bone defect regeneration compared with the other groups.

β-tricalcium phosphate (β-TCP) was added to PLLA scaffolds by Kwon *et al.* [220], demonstrating effective support of bone regeneration. Micro-computed tomography showed a higher percentage of bone regeneration when a weight fraction (w.t.) of 30 TCP (~25% at 12 weeks) was used, compared with PLLA-TCP10 w.t. (~10% at 12 weeks) or PLLA (~0% at 12 weeks) at all time points. The same trend was maintained when MG-63 cells were added to the scaffold, reaching 45% of bone regeneration values in the PLLA-30TCP group at 12 weeks. Besides, Massons's trichrome staining of cranial bone showed the formation of new bone tissue with a typical mature bone structure when MG-63 cells are added.

CaP biomimetic coatings have shown their capability to confer osteoconductivity properties to scaffolds. Maia-Pinto *et al.* [218] developed and evaluated PLA scaffolds biomimetically coated with apatites, with and without loading rhBMP-2. After 6 months, trim bone formation levels were appreciated in PLA group (New formed bone: 11.2%), compared with PLA-CaP and PLA-CaP-BMP2 groups, which presented significantly better biological responses of newly formed bone, 31.2% and 44.85%, respectively. Besides, PLA-CaP-BMP2 groups presented bone tissue formation with a more advance degree of maturity filling larger areas, as compared to PLA-CaP group, nevertheless no significant degradation of the implants, was observed.

Finally, Tcacencu *et al.* [221] created a composite structure by manufacturing PLA and apatite-wollastonite (AW) disks combined with thermal bonding, creating AW/PLA porous

composite structures. Despite the confirmation by histological assessment of the *in vivo* biocompatibility of PLA, AW and AW/PLA scaffolds, the AW/PLA implants resulted in the group with the most considerable amount of newly formed bone, with a percentage of newly formed bone between 15 and 25%, versus other groups like AW disks, which showed percentages of 1-2%.

4.1.2.2 Studies in rabbits – main features

Studies in rabbits were performed on appendicular limbs, including the femur, tibia, and radius. No adverse effects were found when evaluating the behavior of the biomaterials. The main characteristics and results of the reports are summarized in Table 9 (Included at the end of this Chapter).

Curiously, 4 out of the 7 anaesthetic protocols selected in rabbits [77,212–214] included only an injection of pentobarbital, without the complementary administration of any drug. Regarding the other 3 studies, one reported the use of xylazine [211], and in the other one [215], no information about the anaesthetic protocol was provided. Eventually, Minto *et al.* [216] selected combination of ketamine, midazolam and morphine for preanaesthetic medication, besides they administered isoflurane for the induction and maintenance of the general anaesthesia, and performed a right brachial plexus block using lidocaine. Likewise, authors used tramadol and meloxicam for postoperative pain control.

As it was mentioned above, HA is the most commonly used bioceramic, having been selected in all the studies in rabbits [77,211–216]. Specifically n-HA, was utilized in 4 reports [77,211,213,214]; and 3 of them used a 5-millimeter circular defect in the femoral diaphysis to assess their bone regeneration properties [77,213,214]. Wang *et al.* [213] synthetized PLA-30%n-HA scaffolds and compared them with PLA-0%n-HA scaffolds. *In vivo* trials showed new bone tissue growing in all groups at any time points without inflammatory reaction or tissue necrosis, demonstrating the biocompatibility of the implant. Micro-CT results indicated a higher bone growth in PLA-30%n-HA groups at 4, 8 and 12 weeks, with BV/TV percentages of 40%, vs 30% in PLA-0%n-HA group. Wang *et al.* [214] manufactured 3D-printed porous scaffolds with a 5:5 mass ratio PLA-n-HA showing that high n-HA content composite materials were biocompatible and osteogenic inductors conducting new bone growth at 1,2 and 3 months. Statistical differences ($p<0.001$) were found when comparing BV/TV between PLA (~35% BV/TV at 3 months) and PLA-50%n-HA groups (~60% BV/TV at 3 months) (Figure 14). Likewise, these results were superior to those obtained by Wang *et al.* [213] at the same time point, 40% BV/TV PLA/30%n-HA vs 60% BV/TV PLA/50%n-HA, so a higher amount of n-HA on composites is related with an improved bone regeneration of femoral defects. Zhang *et al.* [77], for their part, reported the implantation during 4 weeks of porous PLLA/n-HA scaffolds loaded with 0%, 30% and 50% n-HA, and despite not having performed a quantitative analysis of the results, histological observations demonstrated that all the specimens were utterly integrated with surrounding host tissue, with a little bone tissue formation in the internal pores of PLLA/30% n-HA scaffolds and even less in PLLA ones, which presented the least new bone tissue. However, in the PLLA/50%n-HA scaffolds, all the pores were filled with new bone tissue, with signs indicating bone maturation. This reaffirms what was previously indicated about the relation between the presence of HA, and bone regeneration (Figure 15). The latest report on n-HA composites is the one carried out by Chen *et al.* [211], who developed porous PLA/n-HA composite scaffolds with the following PLA/n-HA mixing ratio 9:1 m/m, and evaluated their *in vivo* osteogenic effects by means of circular defects in the distal part of the femur. Quantitative analysis of micro-CT showed that BV/TV increased with the increased implant time, from 6% at 4 weeks to 20% at 12 weeks; besides the histological section indicated

no inflammation signs and the presence of bone in bone/implant contact region and inside the pores.

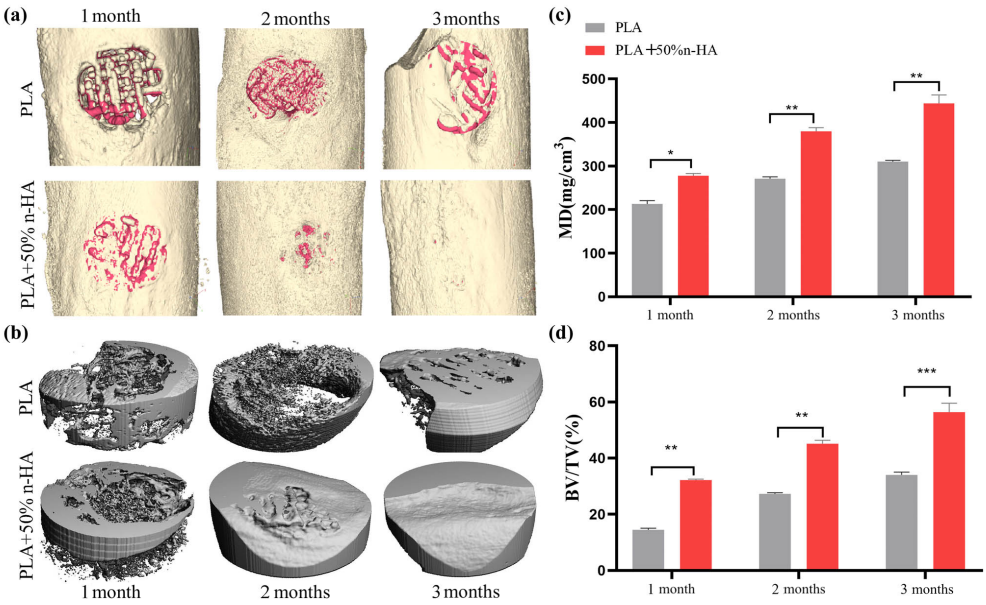

Figure 14: Micro-CT analysis of the implanted scaffolds. The PLA and PLA-n-HA composite scaffolds were implanted into the rabbit femoral defect. (a) At 1,2 and 3 months after scaffold implantation, the bone defect area was scanned using micro-CT, and 3D reconstruction was performed. The reconstructed scaffold was shown in red and the bone in gold; (b) the scaffold-implanted area of the cortical bone (5 mm in diameter and 2 mm in depth) was reconstructed in 3D; and (c and d) quantitative calculation of new bone growth based on micro-CT data, mineral density (MD), and bone tissue volume (BV)/total tissue volume (TV). *p<0.05; **p<0.01;***p<0.001. [214]. "Reprint with permission from [8] under the terms of the Creative Commons Attribution 4.0 International License, CC BY-NC.ND 4.0."

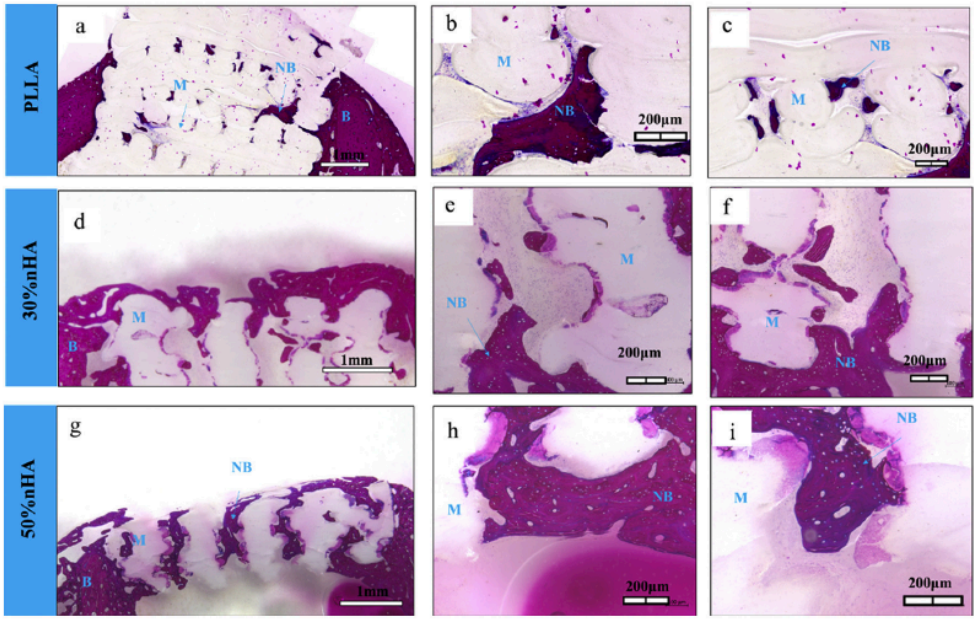

Figure 15: HE evaluation of PLLA-n-HA implanted scaffolds. Cross-section HE histological images of PLLA, 30%n-HA and 50%n-HA explants after 4 weeks implantation *in vivo* (a,d,g); high magnification images of PLLA cross-sections and new bone (b,c); high magnification images of 30%n-HA cross-section and new bone (e,f); high magnification images of 50%n-HA cross-sections and new bone (h,i) (M: materials cross-sections, NB: new bone) [77]. "Reprint with permission from [8] under the terms of the Creative Commons Attribution 4.0 International License, CC BY-NC.ND 4.0."

No nano-hydroxyapatite powders were utilized in 3 reports in rabbits. Liu *et al.* [212] designed a 3D-printed scaffold with a PLA-HA mass ratio of 7:3, and tested it in long bone defects, specifically in a segmental defect in the middle of the left radius. Besides, they studied the effect of its use with induced membranes (IM), alone and combined with enhanced bone marrow (eBM), or iliac crest bone graft (ICBG), which is considered the gold standard in bone regeneration to improve the bone healing process. Micro-tomographic analysis was performed at 16 weeks and showed the following results: PLA/HA group obtained the lowest BV/TV values (~30%), then IM+PLA-HA group (~50%), and finally IM+ICBG (~70%) and IM+PLA-HA+eBM (~70%), which had demonstrated the best effects on bone regeneration, without significative differences between them. Thus, IM and eBM significantly enhanced bone repair, achieving greater ratios of woven bone than PLA-HA and IM+PLA-HA groups. Likewise, histomorphometry results showed the same trend, with the following area ratios of WB at 8 weeks: PLA-HA (~20%) < IM+PLA-HA (~40%) < IM + ICBG (~70%) = IM + PLA-HA + eBM (~70%).

Minto *et al.* [216] manufactured a 3D-printed PLLA-HA non-porous scaffolds to fill a defect in the right radius diaphysis, and compared it with empty control and iliac crest autologous graft groups. No severe lameness was detected in any of the groups, however, the PLLA-HA ones showed grater lameness, edema, and pain, compared with the others. Likewise, radiographic, and histopathologic studies showed smaller bone callous and grater inflammation signs, respectively, when animals included in PLLA-HA group were analyzed. The autologous graft group, as expected, was the one which led to superior results.

Finally, 3D-printed PLA-HA composites scaffolds were combined with *in vivo* bioreactor strategies to generate vascularized tissue-engineered bone of customizable size and geometry by Zangh *et al.* [215]. The scaffolds were seeded with autologous BMSCs, crossed with a vascular bundle (experimental group, EG) or not (control group, CG) and inserted in a tibial periosteum capsule. The histological examination revealed neovascular formation and ossified tissue regeneration in both groups at 4 and 8 weeks. Microangiography and micro-CT measurements showed a higher vessel number and volume in the EG than CG at any time point. In the same way, BV/TV analysis of the EG was significantly greater than CG, 35% vs 20% at 4 weeks, and 70% vs 30% at 8 weeks.

4.1.3 Study qualitiy and risk of bias assessment

The quality assessment of the studies was performed according to the essential items of the ARRIVE guidelines, which are summarized in Figure 16. The individual analysis of the manuscripts showed that at item 3. “Inclusion and exclusion criteria”, 6. “Outcome measures”, 8. “Experimental Animals”, 9. “Experimental Procedures”, and 11. “Results” the information was adequate and reported with percentages of 85.7%, 78.6%, 85.7%, 64.3% and 64.3%; thus, it graded as “reported”. However, items 4. “Randomisation”, 5. “Blinding” and 10. “Adverse events” were considered as “not reported” because there is an evident lack of information in the reported studies, with frequencies 35.7%, 100% and 64.3%. Other items, such as 1. “Study Design”, 2. “Sample Size” and 7. “Statistical Methods”, were classified as “unclear reported”, due to incomplete items reported, insufficient experimental details provided, or no subitems included.

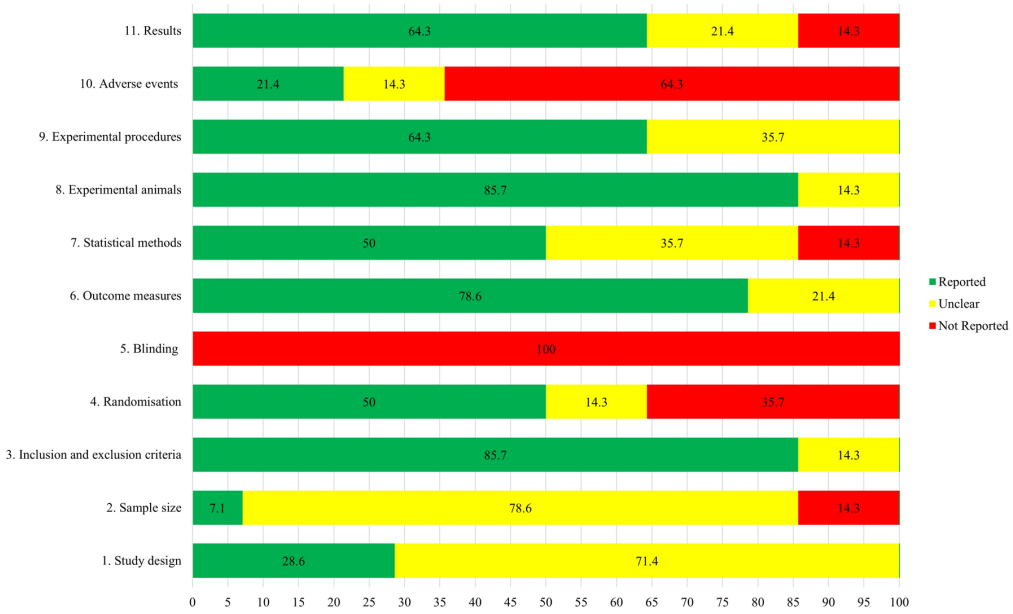

Figure 16. Study quality assessment (ARRIVE). "Reprint with permission from [8] under the terms of the Creative Commons Attribution 4.0 International License, CC BY-NC.ND 4.0."

The risk of bias was evaluated using the SYRCLE in all the included reports and is shown in the Figure 17, as a frequency distribution percent. Most of the questions were graded as "Low Risk of Bias", as shown in item 2. "Baseline characteristics", 6. "Random outcome assessment", 8. "Incomplete outcome data addressed", 9. "Free from selective outcome reporting" and 10. "Free from other sources of Bias", with percentages from 64.3% to 100%. By contrast, items 1. "Allocation sequence generation" and 5 "Blinding of care giver/investigator", were assigned as "High Risk of Bias" showing frequencies of 42.9% and 100%. Finally, "Unclear Risk of Bias" was detected at items 3 "Allocation concealment", 4 "Random housing" and 7 "Blinding of Outcome Assessor" with frequencies of 35.7%, 78.6% and 50%, respectively.

Figure 17. Risk of Bias Assessment (SYRCLE). "Reprint with permission from [8] under the terms of the Creative Commons Attribution 4.0 International License, CC BY-NC.ND 4.0."

Table 7. Characterization of the scaffolds in the studies. "Reprint with permission from [8] under the terms of the Creative Commons Attribution 4.0 International License, CC BY-NC.ND 4.0."

References	Biomaterials (s)	Mixing ratio (wt PLA: wt Bioceramic)	Bioceramic particle size	Production Method	Morphology	Porosity (%)	Pore Size (µm)	Elastic Modulus (GPa or MPa)	Compressive Strength (MPa)	In vitro	Degradability	Sterilization	Scaffolds analysis
[161]	PLA + HA	90: 10	50 µm	FFF	3D porous interconnected structure	58	450	-	-	-	-	Ethylene Oxide	SEM
[162]	PLA + CaP Coating	Uncoated 98: 2	-	FDM	3D porous interconnected structure	49.93+ -5.28 49.09±3.2	-	0.512±0.24 GPa 0.510±0.11 GPa	20.50±1.95 MPa 18.22±2.67 MPa	Yes	-	Ethylene Oxide	SEM, FTIR, XRD, TGA, Mechanical Test
[163]	PLA + n-HA	80:20	-	FDM	3D porous interconnected structure	70±2.23	-	10.12±1.24 GPa	31.18±4.86 MPa	Yes	-	Ethylene Oxide	SEM, Mechanical Test, Porosity evaluation
[164]	PLLA + β-TCP	100: 0 90: 10 70: 30	250 µm	3D Bioplotter	3D porous interconnected structure	~62	100		258±102MPa 310±40MPa 349±51MPa	Yes	PLLA/TCP30 % Remaining scaffold Week GPC NIR 4 ~87 ~91 8 ~79 ~84 12 ~71 ~69	-	SEM, µCT, Mechanical Test, Degradability test (GPC, NIR fluorescence imaging)
[165]	PLA + AW	70% AW AW+30%MD powder (maltodextrin) 50:50	55% - 90 µm 15% - 0-53 µm	AW- Binder jetting/sintering (Indirect 3D-printing) PLA-FFF	3D porous interconnected structure	AW disks 41.85+ -0.94% PLA 60%	-	-	-	Yes	-	AW – Autoclave PLA and composite – gamma radiation	SEM, µCT, Digital Microscope, XDR, Porosity evaluation (Archimedes method)
[166]	PLA + HA	85: 15	2.1±0.4 µm	MDS	3D porous interconnected structure.	60±1.5	500± 20	-	-	Yes	-	Ethylene oxide	SEM
[167]	PLA + OCP (octacalcium phosphate)	40: 60	-	MEB	3D porous interconnected structure.	-	500	-	1 MPa	Yes	-	-	FESEM, Mechanical Test
[156]	PLA + n-HA	100: 0 90: 10 80: 20 70: 30 60: 40 50: 50	50-80 nm	FDM	3D porous interconnected structure.	~50	-	-	~35MPa ~29MPa ~28MPa ~25 MPa ~23 MPa ~17 MPa	Yes	Degradation rate: Pn50>Pn 30>Pn0	-	SEM, XDR, TEM, Mechanical Test; Porosity evaluation (Archimedes method), Degradability test (GPC)
[157]	PLA + n-HA	100:0 50: 50	75±20 nm	FDM	3D porous interconnected structure.		300-400	-	35.41±2.07 MPa 17.8±1.92 MPa	Yes	-	-	TEM, AFM, SEM, EDS, µCT, Mechanical Test
[158]	PLLA + n-HA	100: 0 70: 30 50: 50	50-80 nm	FDM	3D porous interconnected structure.	60	-	43±0.09 MPa 45.54±0.11 MPa 44.31±0.10 MPa	44.02±6.85 MPa 29.68±1.92 MPa 14.22±0.20 MPa	Yes	Degradation rate and mass change: 50%n-HA>30%n-HA>0%n-HA	-	SEM, Contact angle, Mechanical test, Degradability test (GPC)
[155]	PLA + HA	70: 30	50 µm	3D Bioplotter	3D porous interconnected structure.	60	500	-	-	No	-	-	µCT, SEM
[154]	PLA + n-HA	90: 10	63±1.5nm	FDM	3D porous interconnected structure.	26.4	292±1.8	-	23.36±0.48 MPa	Yes	-	Ethylene oxide	SEM, EDS, Mechanical test, Porosity evaluation
[159]	PLA + HA	85: 15	2.1 ±1 µm	MDS	3D porous interconnected structure.	60	500	-	-	Yes	-	Ethylene oxide	-
[160]	PLA + HA	-	-	FDM	3D non-porous structure	-	-	-	-	No	-	Ethylene oxide	-

PLA: polylactic-acid); HA: hydroxyapatite; n-HA: nanohydroxyapatite; β-TCP: Beta-tricalcium phosphate; AW: apatite-wollastonite; OCP: octacalcium phosphate; wt: percentage by mass; FDM: Fused Deposition Modeling = FFF: Fused Filament Fabrication; MDS: Mini-Deposition System; MEB: Micro-extrusion based 3D-printing; SEM: scanning electron microscope; FTIR: Fourier transform infrared spectroscopy; XDR: X-ray diffraction; TGA: Thermogravimetric analysis; FESEM: field emission scanning electron microscope; TEM: Transmission Electron Microscope; AFM: Atomic Force Microscope; EDS: Energy-dispersive X-ray spectroscopy; µCT - Micro-computed tomography

Table 8. Main features of the studies in rats. "Reprint with permission from [8] under the terms of the Creative Commons Attribution 4.0 International License, CC BY-NC.ND 4.0."

Reference	Animal	Anesthetic Protocol	Biomaterial groups	Sample Size	Defect	CSD	Empty Control	Groups	Bone metabolisms substances	Sacrifice Weeks	Assessment method	Main findings
[161]	Rat Wistar 300 gr 4 m/o 1/2 female y 1/2 male	Anesthesia: Ketamine 2.4 ml/kg, and Xylacine 5 mg/kg (IP) Local anesthesia: 2% Lidocaine 0.25 ml (SC) Postoperative Analgesia: Buprenorphine 0.01 mg/kg(SC)	PLA/HA	24	Calvarial Bone Circular bilateral defect ø 5.5 mm.	Yes	Yes	Empty $n = 8$ Bio-Oss $n = 8$ PLA $n = 8$ PLA/HA ($n = 8$) PLA/HA + DPSC ($n = 8$) PLA/HA + ECM ($n = 8$)	DPSC ECM	8 w	µCT analysis Qualitative histological analysis Quantitative histological analysis Paraffin	PLA/HA ECM scaffolds presented bone-forming ability comparable to that of Bio-Oss, based on histology and µCT analysis. Otherwise, PLA/HA scaffolds can potentially be used in bone tissue engineering, especially combined with the ECM.
[162]	Rat Wistar 300-400 gr	Anesthesia: Ketamine 100 mg/kg, Xylazine 10 mg/kg and Midazolam 5 mg/kg (IM)	PLA/CaP	45	Calvarial Bone Circular unilateral defect ø 8 mm	Yes	No	PLA $n = 15$ PLA/CaP $n = 15$ PLA/CaP + rhBMP2 $n = 15$	rhBMP-2	1, 3 and 6 m	Qualitative histological analysis Histomorphometric analysis Paraffin	The clinical trials have shown that the PLA-CaP scaffolds have proven to be biocompatible, promoting new bone formation after 6 months, even without rhBMP-2, based on histological results.
[163]	Rat Sprague-Dawley 280-320 g weight 12-13 w/0 male	Anesthesia: Pentobarbital 35 mg/kg and Inhaled Isofluorane	PLA/n-HA	126	Calvarial Bone Circular unilateral defect ø 6 mm	No	Yes	Empty=24 PLA/n-HA $n = 24$ PLA/n-HA + EMF $n = 24$ PLA/n-HA + BMSCs $n = 24$ PLA/n-HA + EMF + BMSCs $n = 24$	BMSCs Sinusoidal EMF: 15 Hz, 1mT. 4h/day)	4 and 12 w	µCT analysis Quantitative histological analysis Paraffin	The histological and microtomographic analysis revealed that PLA+HA scaffolds + BMSCs with EMF exposure present the best bone integration among all the groups, positioning itself as a promising candidate for craniofacial reconstruction.
[164]	Rat Sprague-Dawley 320-350 g. 8 w/o	Anesthesia: Combination of tiletamine and zolazepam, and Xylazine, 1:1, 1,5 ml/kg	PLLA/β-TCP	90	Calvarial Bone Circular unilateral defect ø 5 mm	No	No	PLLA $n = 15$ PLLA/TCP10 $n = 15$ PLLA/TCP30 $n = 15$ PLLA+MG63 $n = 15$ PLLA/TCP10 + MG63 $n = 15$ PLLA/TCP30 + MG63 $n = 15$	MG-63	4,8 and 12 w	µCT analysis Qualitative histological analysis Paraffin	3D-printed PLLA+TCP scaffold effectively supports bone regeneration in rats. The results show a greater bone regeneration rate in those animals with higher percent of TCP, and after adding of MG-63 to the scaffolds.
[165]	Rat Sprague-Dawley 350 g. adult male	Anesthesia: Ketamine and Xylacine	PLA/AW	15	Calvarial Bone Circular unilateral defect ø 8 mm	Yes	No	PLA dics $n = 3$ AW discs $n = 6$ AW/PLA discs $n = 6$	-	12 w	Qualitative histological analysis Histomorphometric analysis Paraffin	All three types of scaffolds were biocompatible. AW/PLA, the ones with the largest amount of new formed bone. AW scaffolds showed excellent osseointegration with the formation of new bone, and PLA ones have been well tolerated but were not osteogenic.
[166]	Rat Sprague-Dawley 300-350 g. 8 w/o Male	Anesthesia: Ketamine	PLA/HA	32	Calvarial Bone Circular unilateral defect ø 5 mm	No	Yes	3DP PLA/HA $n = 8$ β-TCP $n = 8$ DBM $n = 8$ Blank control $n = 8$	-	4 and 8 w	µCT analysis Qualitative histological analysis Immunohistochemistry (OC and COL-1) Paraffin	The percentage of new bone area in 3DP PLA/HA scaffolds was larger than in DBM (demineralized bone matrix) and control groups but less than β-TCP (Beta-Tricalcium phosphate) groups. The same tendencies were found at 4 and 8 weeks. So, PLA/HA scaffolds might be a promising candidate for bone defect repair, with little inflammation response, relatively larger resorption rate and superior osteoinductive activity.
[167]	Rat 6-8 w/o	Anesthesia: Pentobarbital (IP)	PLA/OCP	?	Calvarial Bone Circular unilateral defect. ø 5 mm	No	Yes	Control $n = ?$ PLA/OCP $n = ?$ PLA/OCP + 0.2La $n = ?$ PLA/OCP + 0.5La $n = ?$ PLA/OCP + 1La $n = ?$	La	8 w	Qualitative histological analysis Paraffin	The scaffolds enhanced bone defect regeneration in vivo. 0.2La-OCP/PLA scaffolds are significantly more likely to enhance bone defect regeneration in vivo than other groups. Our study suggests that La-OCP/PLA porous scaffolds have markedly potential in clinical bone tissue engineering.

m/o: months old; w/o: weeks old; PLA: polylactic-acid; HA: hydroxyapatite; n-HA: nanohydroxyapatite; β-TCP: Beta-tricalcium phosphate; AW: apatite-wollastonite; OCP: octacalcium phosphate; IP: intraperitoneal injection; SC: subcutaneous injection; IM: intramuscular injection; PLA:; HA:; n-HA:; OCP:; DPSC: dental pulp stem cells; ECM: extracellular matrix; rhBMP-2: recombinant human bone morphogenetic protein-2; BMSCs: bone marrow mesenchymal stem cells; EMF: electromagnetic fields; MG-63: human osteoblastoma cell line; DBM: demineralized bone marrow; La: Lanthanum; months: m; weeks: w; OC: osteocalcin; COL-1: type I collagen; µCT: micro-computed tomography.

Table 9. Main features of the studies in rabbits. "Reprint with permission from [8] under the terms of the Creative Commons Attribution 4.0 International License, CC BY-NC.ND 4.0."

Reference	Animal	Anesthetic Protocol	Biomaterial	Sample Size	Defect	CSD	Empty Control	Groups	Bone metabolisms substances	Sacrifice Weeks	Assessment method	Main findings
[156]	Rabbit New Zealand White 2-3 kg, male	Anesthesia: Pentobarbital 40 mg/kg (IV)	PLA/n-HA	18	Femoral Diaphysis Circular Unilateral Defect ø 5 mm	No	No	PLA $n = 9$ PLA/n-HA30% $n = 9$	-	4, 8 and 12 w	µCT analysis Qualitative histological analysis Resin	PLA/n-HA can be printed when the n-HA ratio is less than or equal 50%, the increasing incorporation of n-HA doesn't affect significantly the overall mechanical strength in a limited range (0-30%), but it really enhances the osteogenesis in vivo.
[157]	Rabbit New Zealand White 2-3 kg, male	Anesthesia: Pentobarbital 40 mg/kg	PLA/n-HA	-	Femoral Diaphysis Circular ¿Unilateral? Defect ø 5 mm	No	No	PLA $n = ?$ PLA/n-HA 50% $n = ?$	-	1,2 and 3 m	µCT analysis Qualitative histological analysis Resin	The new bone growth of the composite material (PLA+50%n-HA) is significantly higher than that of the PLA group. Consequently, it has a high potential for use as implant for the critical bone defects
[158]	Rabbit New Zealand White 2-3 kg, male	Anesthesia: Pentobarbital 40 mg/kg (IV)	PLLA/n-HA	9	Femoral Diaphysis Circular bilateral Defect ø 5 mm	No	No	PLLA $n = 3$ PLLA/30%nHA $n = 3$ PLLA/50%nHA $n = 3$	-	4 w	Qualitative histological analysis Resin	The PLLA/50%n-HA has shown a preferable capability of bone regeneration, also supported by the discovery of the Harversian Canals, compared with the PLLA-30%n-HA specimens, which in turn have presented a bigger amount of new bone tissue than the PLLA ones.
[155]	Rabbit New Zealand White 2,5 +/- 0.25 kg, 6 m/o	Anesthesia: Pentobarbital 30 mg/kg (IM)	PLA/HA	36	Diaphysis Left Radius Segmental Unilateral Defect 15 mm	Yes	No	ICBG + IM $n = 9$ PLA/HA $n = 9$ IM + PLA/HA $n = 9$ IM + PLA/HA + eBM $n = 9$	eBM ICBG IMemb	4, 12 and 16 w	µCT analysis Qualitative histological analysis Histomorphometric Analysis Paraffin	The IM combined with 3D-printed PLA-HA scaffold and eBM has a bigger efficiency for treatment of large bone defects than the PLA-HA and the IM/PLA-HA groups, and similar to the IM/ICBG group (Gold Standard), based on the X-ray, µCT and histological results.
[154]	Rabbit New Zealand White 4.2+/-0.18 kg, male, adult	Anesthesia: Xylazine 0,.1 ml/kg (IM)	PLA/n-HA	3	Distal Right Femur Circular Unilateral Defect ø 4.5 mm and Depth 10-13 mm	No	No	PLA/HA $n = 3$	-	4, 8 and 12 w	µCT analysis Qualitative histological analysis Resin	In vivo trials confirmed that the printed PLA/n-HA scaffold can enhance osteogenesis and osteoconductivity. It was showing bone formation within the femoral defect at 4,8 and 12 weeks, and no inflammation signs.
[159]	Rabbit New Zealand White 2.5+/-0.2 kg., 6 m/o	-	PLA/HA	24	Tibial Diaphysis Periosteum. Cuboid shaped periosteal pockets 10 mm in length and 7.5 mm in diameter.	-	No	Experimental Group (EG) PLA/HA +BMSCs with blood vessel Control Group (CG) PLA/HA + BMSCs without blood vessel	BMSCs	4 and 8 w	µCT analysis Qualitative histological analysis Immunohistochemistry (OC and CD31) Paraffin	3D-printed PLA-HA composite scaffolds in an in vivo bioreactor prove to be a promising tool for the prefabrication of large volume, customized, vascularized bone tissues. Besides, adding a vascular bundle allows the construction of large vascularized bone grafts that translate into a bigger BV/TV, Tb.N and Tb.Th in the in vivo trials.
[160]	Rabbit 4-5.5 kg, female, > 7 m/o	Anesthesia: Ketamine 20 mg/kg, midazolam 2 mg/kg, and morphine 2 mg/kg (IM). Inhaled isoflurane Local anesthesia: 2% Lidocaine 6 mg/kg – Right brachial plexus block Postoperative Analgesia: Tramadol 4 mg/kg and meloxicam 0.1 mg/kg (SC)	PLA/HA	60	Diaphysis Right Radius Segmental Unilateral Defect 15 mm	Yes	Yes	Control Group $n = 20$ ICBG $n = 20$ PLA/HA Group $n = 20$	-	2, 4, 8 y 12 w	Radiographic analysis Qualitative histological analysis Paraffin	Scaffold created with anatomical characteristics similar to the radios proved to be biocompatible and allow cell multiplication around the composite. Despite of the fact that less bone callus and bone bridge was formed compared to the gold standard method (ICBG).

m/o: months old; w/o: weeks old; PLA: polylactic-acid; PLLA: poly-L-lactic-acid; HA: hydroxyapatite; n-HA: nanohydroxyapatite; IM: intramuscular injection; IV: intravenous injection; BMSCs: bone marrow mesenchymal stem cells; DBM: demineralized bone marrow; La: Lanthanum; eBM: enhanced bone marrow; ICBG: iliac crest bone graft; IMemb: induced membranes; w: weeks; m: months; OC: osteocalcin; µCT: micro-computed tomography; BV/TV: Bone Volume/Tissue Volume; Tb. N: Trabecular Number; Tb. Th: Trabecular thickness.

4.2 CHAPTER II

4.2.1 PLA-bioCaP scaffolds characterization

4.2.1.1 Physicochemical and morphological characterization

The morphology of the 3D printed blanking plug-shaped scaffolds can be observed at Figure 18, by optical images of PLA-0CaP and PLA-12CaP, and SEM micrographs from the top of the PLA-12CaP scaffold. A translucent appearance was showed in the free of bioCaP scaffolds becoming whiter for the PLA-12CaP scaffolds. The disposal of parallel lines of 0.8 mm thick with a separation between them of 0.4 mm perpendicularly alternating the direction of the processing lines between each overlapped layer is also shown (Figure 18, a-d). Moreover, the uniform distribution of open square-shaped pores of 0.4 x 0.4 mm forming a 3D cubic arrangement can also be observed.

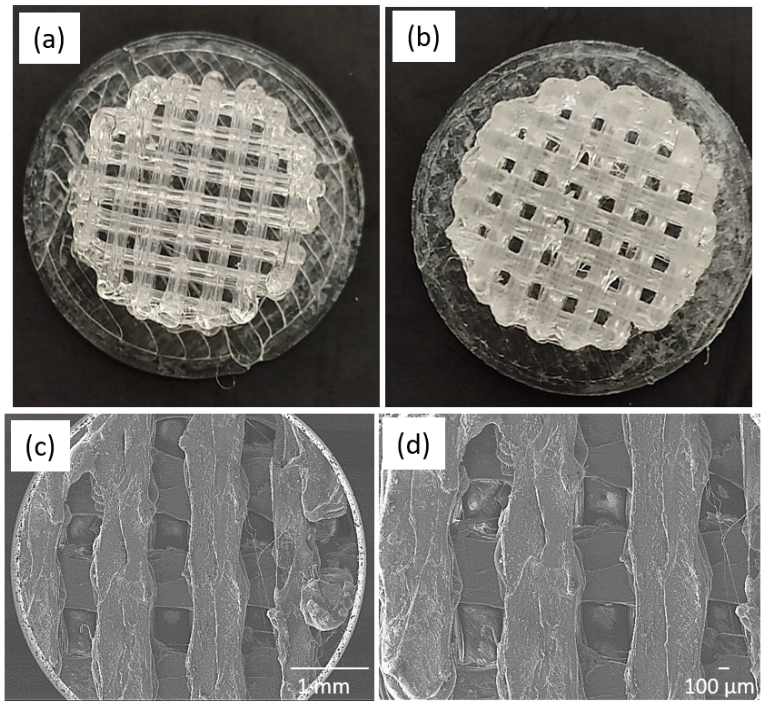

Figure 18. Optical images and SEM images of the scaffolds. Optical images x1 magnification of PLA scaffold with the porosity amplified for more detail (a) and the same for the PLA-12CaP scaffold (b). SEM micrographs of PLA-12CaP scaffold at x25 (c) and x33 (d) magnifications (Own Image).

The bonding configuration of PLA, PLA-1CaP, PLA-2CaP and PLA-12CaP scaffolds was characterized by Raman spectroscopy and presented in Figure 19. The characteristic spectrum of polylactic acid [228,229] was observed for PLA scaffolds (Figure 19 a) with leading strong bands registered, as expected, at: 872 cm-1 with an intense and sharp band attributed to C-COO stretching, 1769 cm-1 assigned to C=O asymmetric stretching, 1455 cm-1 to asymmetric bending CH3, 1126 cm-1 to asymmetric rocking CH3, 1043 cm-1 attributed to skeletal stretching C-CH3 and, finally, at 398 cm-1 and 298 cm-1 respectively assigned to bending CCO and COC. The Raman spectra obtained for PLA-1CaP, PLA-2CaP and PLA-12CaP scaffolds (Figure 19 a) presented the same PLA characteristic bands together with, as expected, the band near 960 cm^{-1} attributed to PO_4^{-3} symmetric stretching mode of calcium phosphates [230,231].

To continue with a more in-depth analysis, a quantitative evaluation from the Raman spectra was performed obtaining the bioCaP:PLA ratio for each of the 3D printed scaffolds. As it can be observed at Figure 19, b the gradually increasing contribution of calcium phosphates in the 3D printed scaffolds was proved.

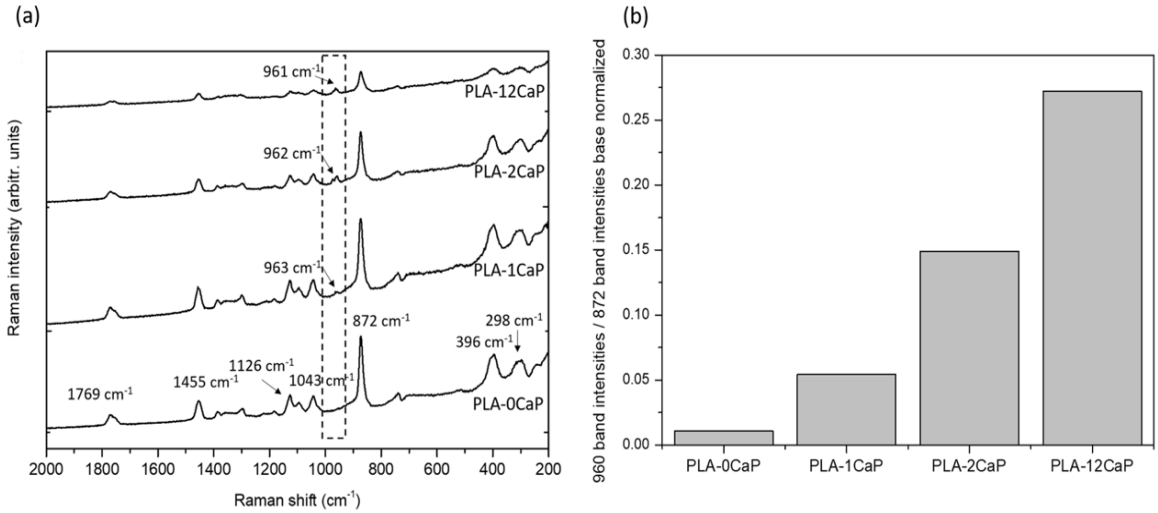

Figure 19. Raman spectra of PLA, PLA-1CaP, PLA-2CaP, PLA-12CaP scaffolds. Where main strong bands characteristic for PLA at the region 2000-200 cm-1 and spectra region (1000-900 cm-1) characteristic for main band of calcium phosphates (pointed square) are shown (a). Quantitative Raman evaluation to obtain the corresponding bioCaP:PLA ratio for the 3D printed scaffolds is also presented (b) (Own Image).

XDR determined the crystal structure of the 3D-printed scaffolds. At Figure 20 diffraction patterns for PLA and PLA-2CaP scaffolds are presented. In the case of the 3D-printed PLA scaffolds a wide band between 2θ angle of 10° and 25° was observed, with a main broad peak at 14.99°, instead of the characteristic main peak expected for neat PLA diffractogram at 16.8º and a less intense one at 19.5º [232]. The broadband obtained is attributed in the literature to an intermediate order in the polymer chains between the amorphous and crystalline forms, therefore, associated with the semi-crystalline nature of PLA [233–235]. When the 3D printed PLA-2CaP scaffold diffractogram was obtained, a weak band related to PLA appeared at 16.75º attributed to the α-form crystals at the plane (110)/(200), which implies a certain recrystallization of the polymer [232,236]. Moreover, sharp, and intense diffraction peaks located at the characteristic region near 32º of hydroxyapatite ($Ca_5(PO_4)_3(OH)$) were detected, in particular the three peaks 31.77º, 32.17º, 32.88º respectively corresponding to crystal planes of hexagonal hydroxyapatite (211), (112) and (300). Additionally, other diffraction peaks clearly attributed to hydroxyapatite [139,230,237] were also measured at 10.81º, 25.84º, 28.89º, 34.05º, 39.79º, 46.64, 49.44º and 53.18º, respectively attributed to (100), (002), (120), (202), (310), (222), (213) and (004). Finally, the diffraction peak observed at 28.02º is clearly attributed to β-tricalcium phosphate (β-TCP) or whitlockite (214), according to Jang *et al.* [238]. The diffraction patterns confirmed therefore, that the increase in the degree of the crystallinity of the 3D printed scaffolds promoted by incorporating the bioceramic produced a certain re-crystallization of the 3D printed PLA.

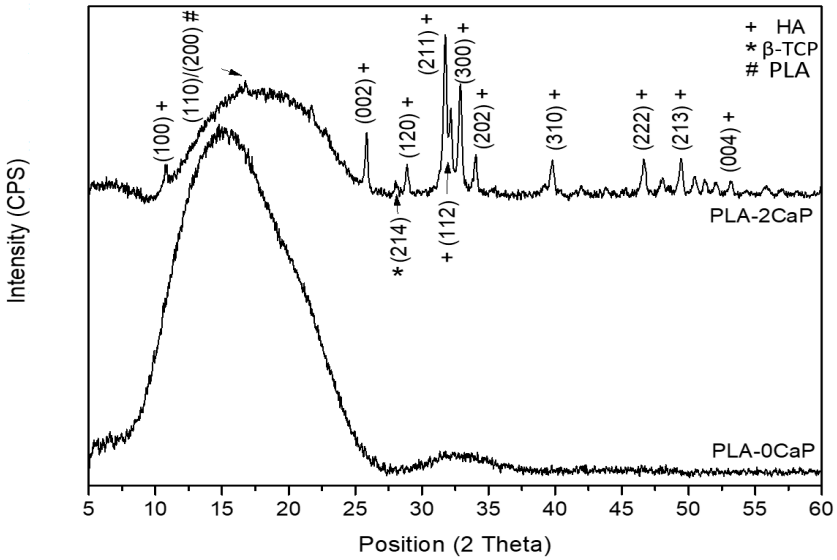

Figure 20. XRD patterns of PLA and PLA-2CaP scaffolds in the range of positions between 5º and 60º where crystal planes attributed to polylactic acid (PLA), hydroxyapatite and ß-tricalcium phosphate/whitlockite are indicated (Own Image).

Furthermore, printed samples were observed again under SEM to evaluate the roughness of the implant's surface. As seen in Figure 21, there was a clear difference in the surface topography of the scaffolds, being very smooth for the PLA group, and becoming rougher in PLA-2CaP and PLA12-CaP groups. A tendency to a rougher surface could be observed when increasing de wt% of bioCaP, with apparent differences between PLA-2CaP and PLA-12CaP implants. Likewise, despite being successfully dispersed, bioCaP particles tend to form agglomerates, whose size and appearance increased parallel to the percentage of bioCaP. Thus, the bioceramic material changes the surface from smooth to rough, so the higher the concentration of bioCaP, the greater the roughness.

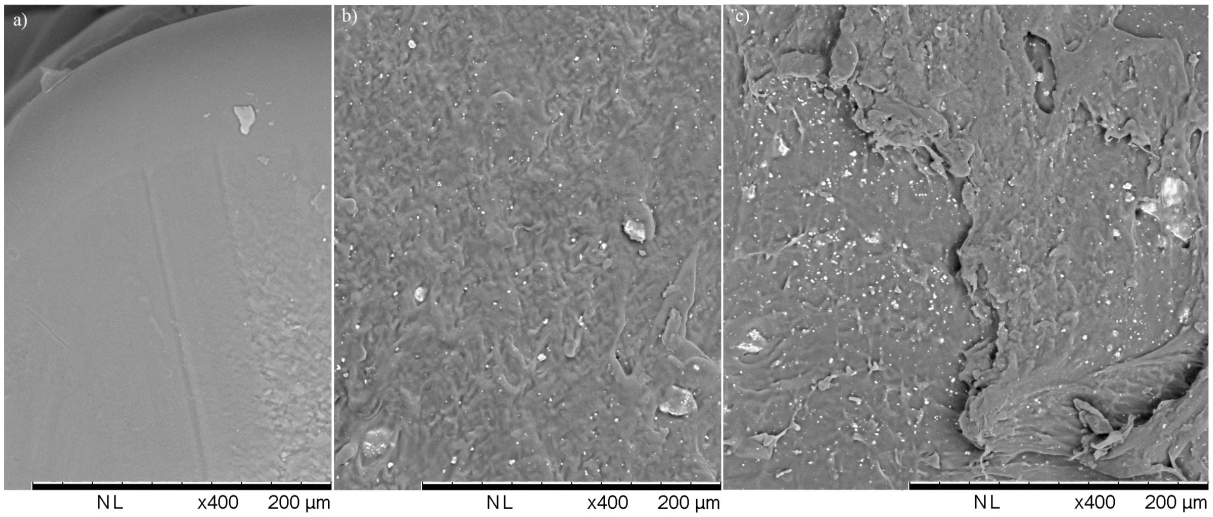

Figure 21. The surface morphology of the scaffolds observed by SEM (x400 magnification): PLA (a), PLA-2CaP (b) and PLA-12CaP (c) (Own Image).

4.2.1.2 Pore morphology

The scaffolds presented a highly interconnected square-shaped pore structure, as seen in SEM images (Figure 18), with open pores around their circumference, which favor cells and blood vessels growth toward the inner parts of the implants. 3D composite scaffolds synthesized by fused deposition modelling should be homogeneous, so we should be able to analyze the influence of different bioCaP proportions on porosity. The scaffolds' porosity was assessed for 2 samples of each group, obtaining a mean porosity value of 46±5%. The range of porosity measurements was between 40.30% and 51.38%, however, these differences seemed not to have any relationship with the amount of bioCaP added.

The distribution of the pore size and strut thickness along the scaffolds were represented in Figure 22. The mean values for all the groups of pore size and strut thickness were measured resulting in 390±10µm and 390±50µm, respectively. However, if we analyze the results, it may be interesting to point out that mean values did not represent those pore size or strut thickness values that appear with greater frequency. So, the mode was calculated, and obtained results were included in Table 10. Differences found between the size of the 3D-printer's nozzle and the strut thickness could be explained due to rheological factors [239]. Since struts were thicker in the area where they overlap with other ones, and narrower in the bridge areas (between two struts deposited perpendicularly). Affecting consequently to strut thickness and pore size measurements.

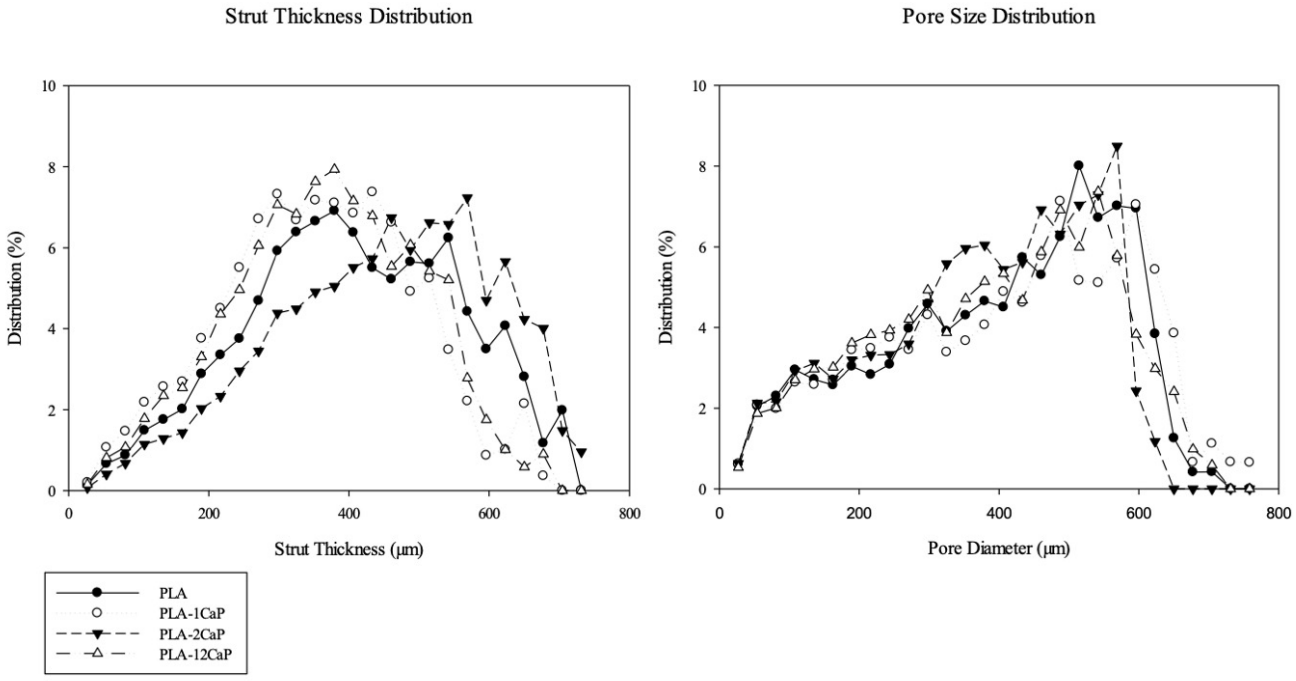

Figure 22. Strut Thickness and Pore Size Distribution of 3D printed composite scaffolds (Own Image).

Table 10. Pore morphology measurements in micro-CT. All parameters are represented as mean ± SD

		PLA	PLA-1CaP	PLA-2CaP	PLA-12CaP
Open Porosity	**%**	44±6	50.8±0.8	40.7±0.5	48±2
Strut Thickness (mean)	**µm**	410±70	360±20	449.2±0.9	370±20
Strut Thickness (mode)	**µm**	379.31	433.49	568.96	379.31
Pore Size (mean)	**µm**	400±10	410±20	377±4	388±1
Pore Size (mode)	**µm**	514.77	487.67	568.96	541.87

The dispersion of the bioCaP particles in the PLA struts along the longitudinal and cross-sectional axis was also assessed. Micro-tomographic images showed the particles homogeneously dispersed superficially and inside of the struts, which is in line with what was observed in the images obtained by SEM (Figure 23).

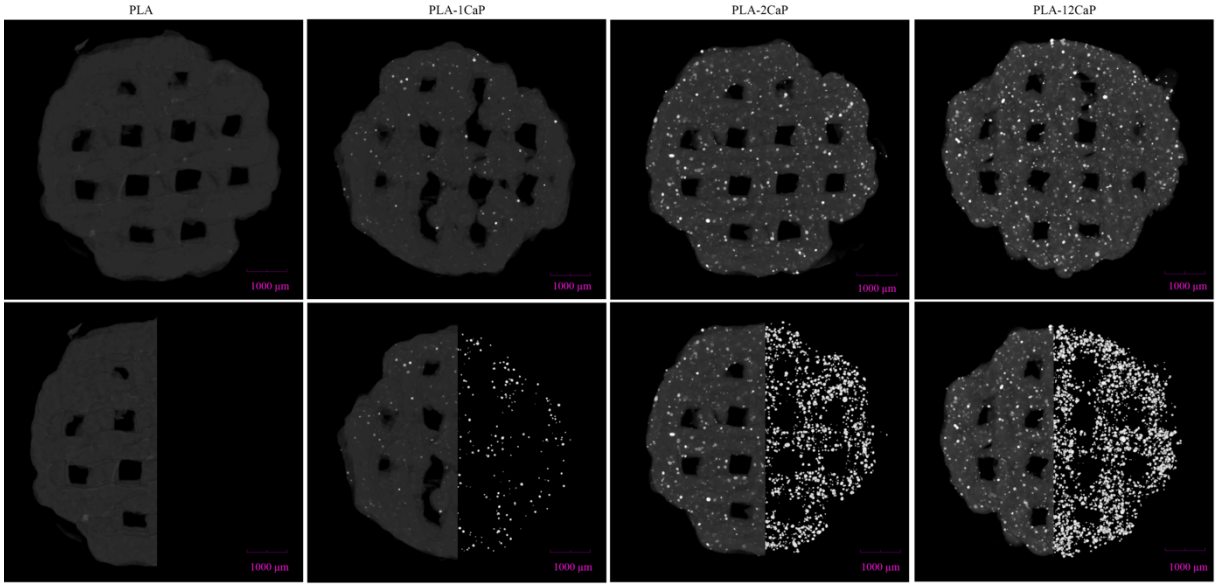

Figure 23. Micro-CT reconstruction of 3D printed composite scaffolds, showing the dispersion of the different amounts of bioCaP in different study groups (Own Image).

To obtain more data about the characteristics of the pores, a study was conducted on pore interconnectivity. This helps to denote the relations between two interlinked pores, indicating the level of connectivity of the porous structures. This attribute is vital to understanding the growth of cells. The connective porosity or accessible porosity consists of all the pores larger than the defined interconnective pore size. In this way, if the defined interconnection size was 0 (m), all the pores will be counted in the porosity, which means 100% of effective porosity [96].

All the scaffolds were highly interconnected, with values of the pore connected to the outside environment equal to or higher than 90% through openings smaller than 162.56 µm. Very slight changes among groups can be observed in the percentage of pore accessibility until a pore size less than 325.12 µm, with interconnectivity values still near 80%, as seen in the Figure 24. Regarding a minimum connection size of 596.05 µm, the PLA-2CaP group

represented the lowest interconnection values (18%). Variations in pore accessibility seem to be related to the implants' porosity.

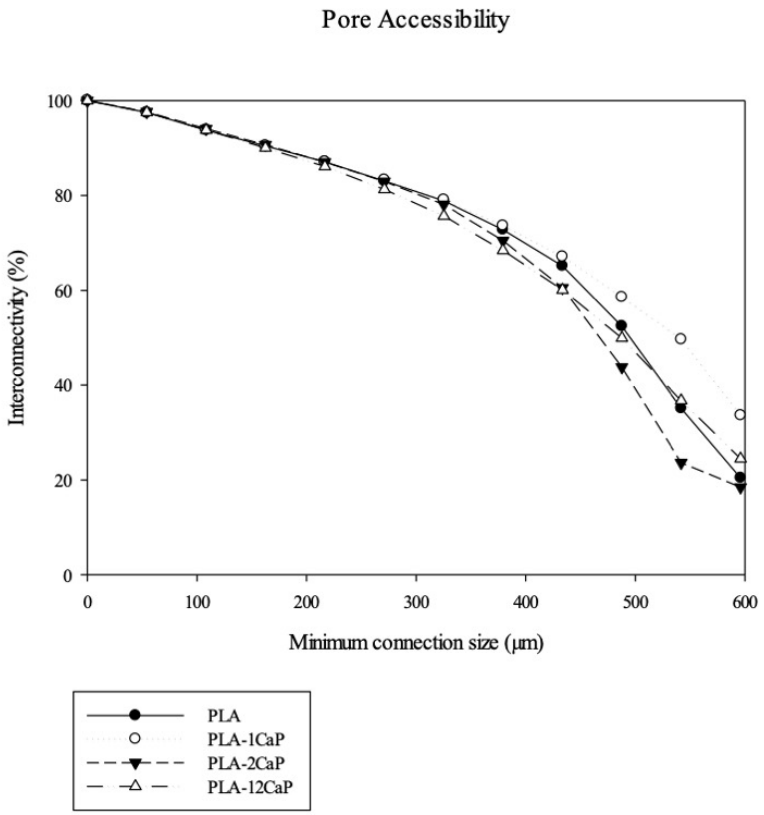

Figure 24. Pore accessibility assessment in micro-CT (Own Image).

4.2.1.3 Mechanical Test

Compressive strength was one of the most important scaffold properties, especially when these will be implanted in load-bearing sites. The mechanical properties were tested in scaffolds from the different groups (n=2): PLA, PLA-1CaP, PLA-2CaP and PLA-12CaP. The calculated strength was taken at the end of the linear elasticity phase. The results of compressive strength and elastic modulus are shown in Table 11.

Table 11. Mechanical Test Results. All parameters are represented as mean ± SD.

		PLA	PLA-1CaP	PLA-2CaP	PLA-12CaP
Compressive Strength	**MPa**	44±5	37± 1	49±5	28±4
Elastic Modulus	**MPa**	350±50	278±4	410±40	250±30

As seen, adding bioCaP reinforces the composite's mechanical properties when a 2% of bioCaP was used. However, implants belonging to PLA-12CaP group already presented a decrease in the compressive strength. A similar trend could be observed for the elastic modulus, since PLA-2CaP group was the one with the highest values (444.44MPa), which can be even compared with the ones of the human skull bone (450 MPa) [220]. The strain-stress curves (Figure 25) revealed a plastic material behavior in all the scaffolds, showing the typically three different

sections of porous materials: a linear elasticity phase, an intermediate plateau phase and further densification, with stress increasing with the strain.

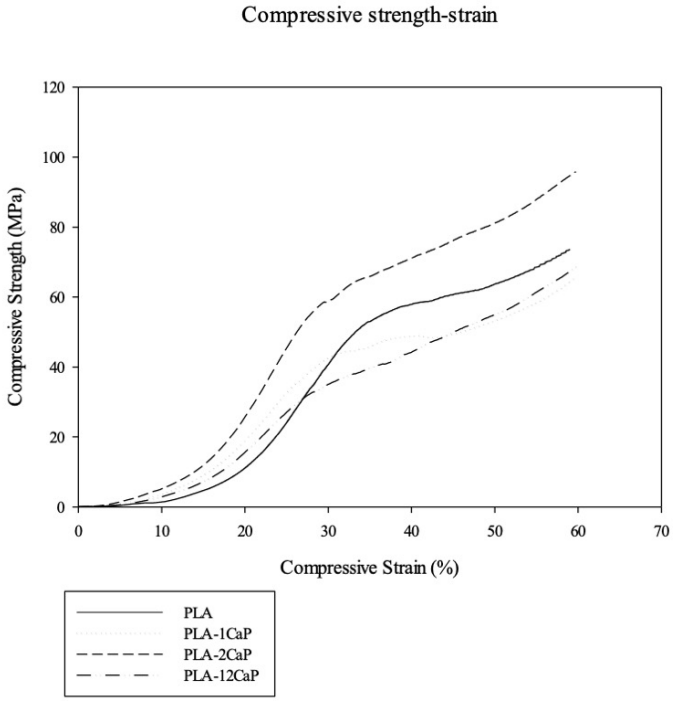

Figure 25. Compressive strength-strain curves of 3D printed scaffolds (Own Image).

Furthermore, compressive strength was correlated with several pore architectural characteristics of the scaffold (Table 12). As expected, strong correlations were found between compressive strength and open porosity, surface area-to-volume ratio, and strut thickness. Thus, the scaffolds' porosity influences their mechanical properties, so that by increasing open porosity or surface area to volume ratio, the compressive strength of the scaffold will decrease. And in contrast, when increasing strut thickness, the compressive strength will increase, too.

Table 12. Correlation study between compressive strength and pore architectural characteristics of the fabricated scaffolds (n=8, *p<0.05).

Pearson's correlation coefficient	Open Porosity	Surface area-to-volume ratio	Strut Thickness
Compressive Strength	-0.79*	-0.80*	0.80*

4.2.1.4 Wettability

The water contact angle of the scaffolds was measured, and the results are given in Table 13. Each value is the average of contact angle measurements in 3 points. As results showed, the increasing content of bioCaP in the composites is not enough to modify the hydrophobic behavior of PLA. Contrary to what was expected, adding CaP increases the scaffolds' hydrophobicity.

Table 13. Contact angle measurements. All parameters are represented as mean ± SD.

	PLA	PLA1CaP	PLA2CaP	PLA12CaP
Contact Angle (Degrees)	100±10	100±20	130±20	120±20

4.2.2 Animal model

Two animals suffered complications derived from the surgical intervention, and they death after accidentally incise the dura mater. So, both animals were excluded from both studies. The other rabbits did not present complications, and no other adverse effects were observed after implantation.

At the time of sacrifice, all the rabbits were healthy and did not present observable inflammatory reactions, furthermore, neurological reactions were absent.

During the necropsy, macroscopical examinations were conducted over all the implants, to ensure they had anchored adequately to the bone and fitted well in the defect. Furthermore, the absence of macroscopical signs of inflammation, hematoma or infection was confirmed. After the dissection of the implants' regions, only one rabbit presented adherences between the bottom of the implant and the dura mater, but it could be extracted without complications.

4.2.3 Micro-CT

Micro-tomographic analysis were performed to evaluate the bone morphometric parameters mentioned above (BV/TV, BS/BV, Tb.Th. and Tb.Pf.) in the stablished volume of interest. Results are shown in Figure 26. As it could be seen, there were no statistically significant differences for parameters referring to bone regeneration, such as BV/TV, which was higher for PLA (11.11 ± 3.26%) and PLA-12CaP (11.07 ± 4.33%) groups. In addition, there were no differences for bone surface-to-bone volume ratio (BS/BV), or trabecular thickness (Tb.Th.), which were very similar for all groups. PLA-12CaP group despite not being statistically significant, showed the highest trabecular values. Likewise, the same group showed statistically significant differences in terms of trabecular pattern factor (Tb.Pf) with PLA and PLA-1CaP groups. Representative images were included in Figure 27.

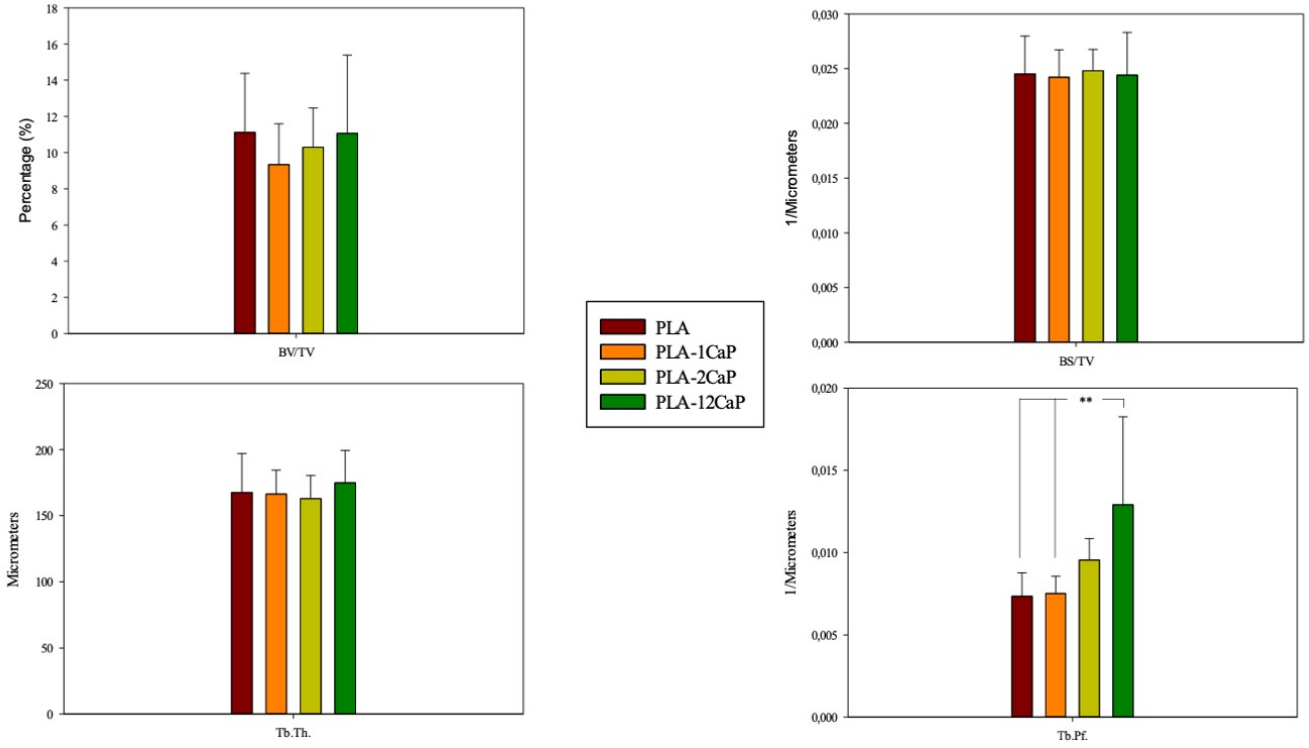

Figure 26. Micro-CT histomorphometric measurements. BV/TV: Bone Volume/Tissue Volume, BS/BV: Bone Surface/Bone Volume, Tb.Th.: Trabecular Thickness and Tb.Pf.: Trabecular Pattern Factor. **p<0.05 (Own Image).

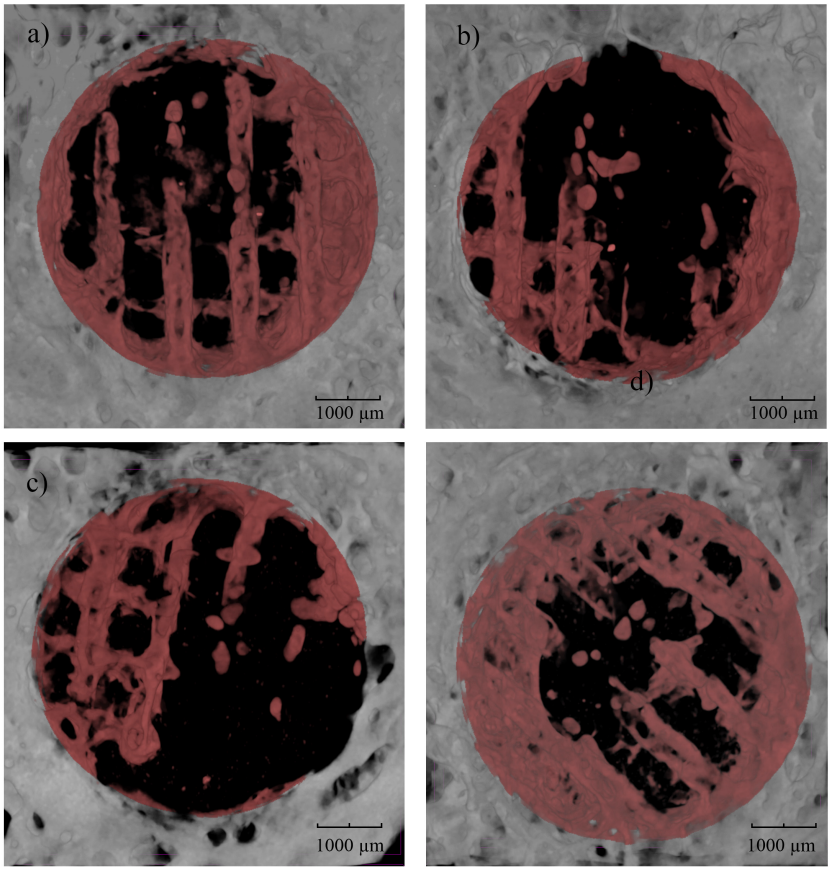

Figure 27. Representative micro-CT images of the effect of composite scaffolds on bone regeneration at 12 weeks in calvarial rabbit defects. The measured volume of interest (VOI) was highlighted in red color. PLA a), PLA-1CaP b), PLA-2CaP c) and PLA-12CaP d) (Own Image).

3D images demonstrated good biocompatibility of the different scaffolds implanted *in vivo.* Most presented good integration with the host bone without signs of rejection. Strongly mineralized tissue ingrowth within the scaffolds could be observed, initially at the edge of the bone defect and then gradually filling inwards and toward the center. Same samples showed isolated bone growing in the inner part of the scaffold, probably occasioned by the migration of bone marrow cells because of the bleeding and clot formation during the surgical procedure. Bone tissue ingrowth occurred through the pores and following its orientation, providing the scaffold with notable support to the host bone.

4.2.4 Histology

4.2.4.1 Qualitative histology

A rabbit model of calvarial defects was used to evaluate the osteogenic potential of rising concentrations of bioCaP mixed with PLA. Figure 28 shows optical images of the histological slides. For the histological assessment, Lévai-Laczkó stained slides were subjected firstly to semi-quantitative evaluation techniques to quantify the inflammatory response, new blood vessel formation, presence of fibrosis and fatty infiltrates, to assess the local effects after implantation following UNE-EN ISO 10993-6:2017 standards (Figure 29).

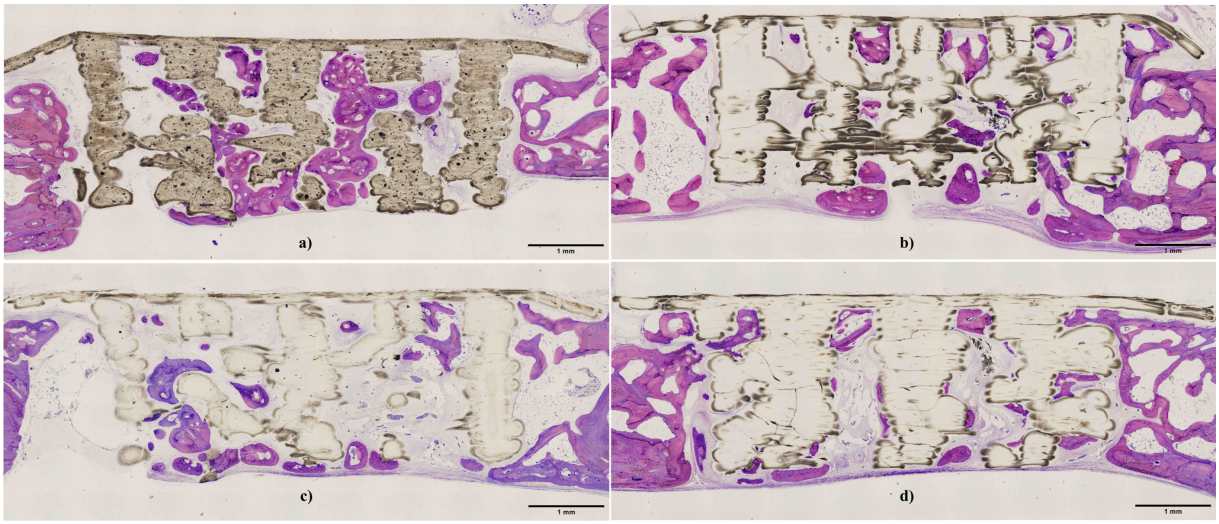

Figure 28. Histological sections of the calvarial bone after 12 weeks of healing (Lévai-Laczkó staining). Sections clearly show typical findings of the samples. PLA-12CaP a), PLA-1CaP c), and PLA b) and d). The bone grows from the edges to the defects' center through the pore. Connective tissue filling the empty space. Absence of bone growing when the scaffold is not in contact with the margin of the defect. Struts with different thicknesses were present depending on where the section was performed (Own Image).

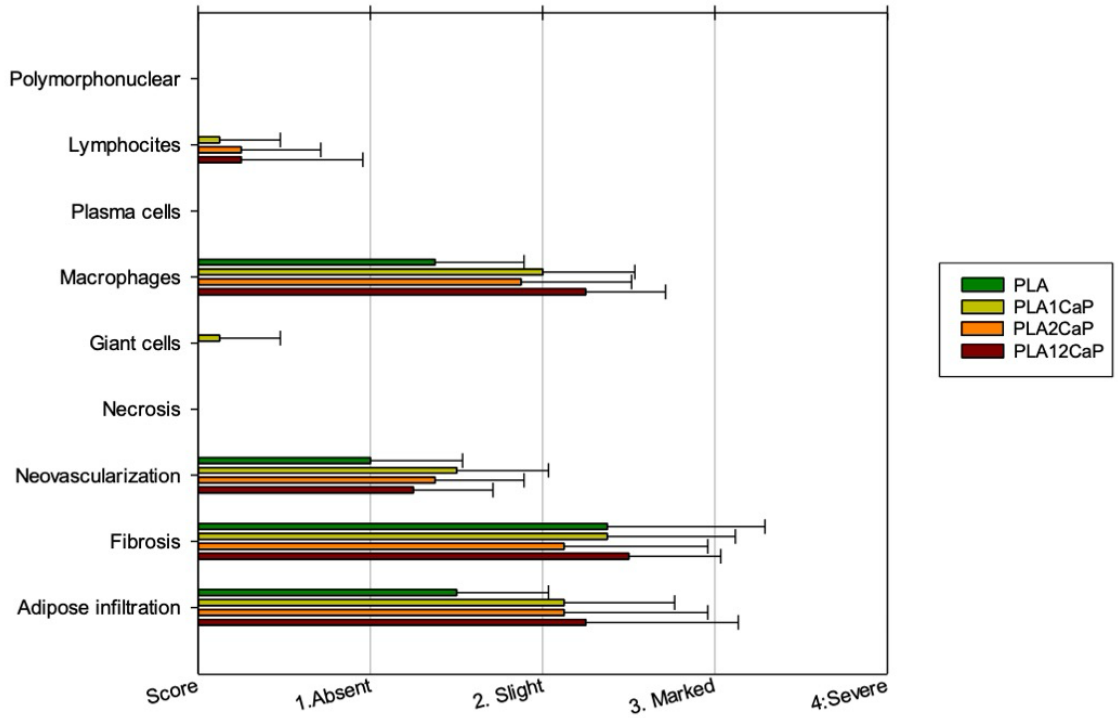

Figure 29: UNE-EN ISO 10993-6:2017 evaluation results summarized, classifying each parameter into different scores, being 0 equal to its absence, and 1, 2, 3, and 4, equal to slight, moderate, marked, and severe presence, respectively (Own Image).

Optical microscopy of the whole specimens was used to quantify cellular response by counting the number of polymorphonuclear cells, lymphocytes, plasma cells, macrophages and giant cells per high powered (400x) field (phf), focusing specifically on the biomaterials' contour (Figure 30). They were scored from 0 to 5, denoting absence, presence of 1-5 cells/phf, presence of 5-10 cells/phf, heavy infiltrates or packed, respectively. Among the mentioned inflammatory cells, macrophages were the main ones found in the different specimens and were usually very

close to the implant's surface, with scores between 1 and 3. In addition, lymphocytes were identified in 4 samples, being three of them scored as 1, and the other one as 2. Finally, 1 to 5 giant cells/phf appeared in one of the samples. There were no signs of necrosis in any of the specimens.

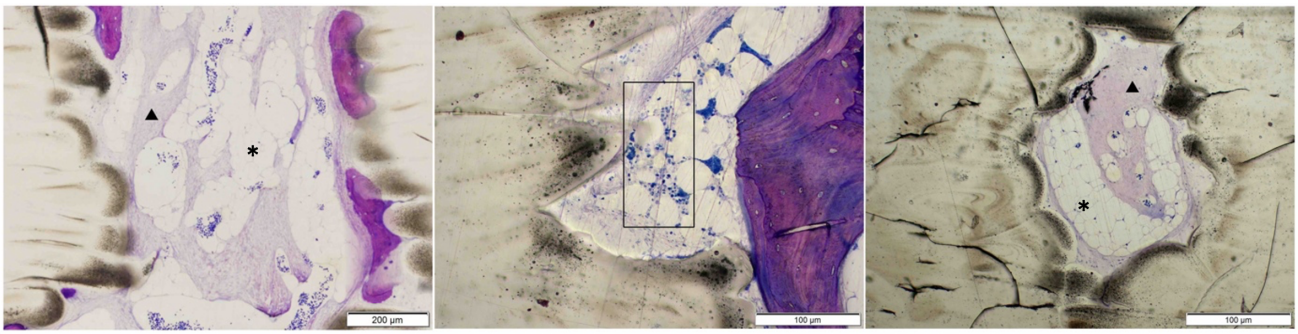

Figure 30. Lévai-Laczkó stained slides demonstrated the findings described during the semi-quantitative evaluation. Fatty infiltrates could be observed (*), as well as fibrous band with different thicknesses (▲), and macrophages were present near the composite material (black square) (Own Image).

Then, the rest of the parameters included in the UNE-EN ISO standards were evaluated. Firstly, fibrosis was the main finding in all the samples, narrow (1), to moderately thick (2) and even thick (3) bands were identified filling the inner part of the implants and avoiding bone-implant contact, both inside the implant pores and with the bony surface of the defect. Likewise, fatty infiltrates were found in all the samples, usually associated with fibrosis. Among minimal amounts of fat (1), and elongated and broad accumulations of fat cells (3) were observed filling the spaces inside the implants. The neovascularization was also a phenomenon shared by almost all the specimens, which was semi-quantified as focal minimal capillary proliferation (1), groups of 4 to 7 capillaries (2) or broad bands (3) with supporting fibroblastic structures (Figure 30). Besides, there was no evidence of traumatic necrosis or foreign debris.

Under the condition of this study, and in accordance with the provisions of the UNE-EN ISO 10993-6:2017 standards, the tested samples were considered as non-irritant (PLA-1%CaP and PLA-2%CaP groups), and slight irritant (PLA-12%CaP group) to the tissue as compared to PLA group (positive control). Furthermore, statistically significant differences among the different groups, were only found for the quantification of macrophages between the PLA and PLA-12%CaP groups ($p=0.042$), presenting the latter higher score values.

Another interesting aspect to highlight from the qualitative evaluation is the absence of bone growth in those points where the implants are not in contact with bone defect margins (Figure 28), since the defects were sometimes slightly bigger than implants. These findings may demonstrate the ability of the implants to stimulate bone growth and the proposal of the defect size as critical. As it was explained in Micro-CT section, usually new bone was formed from the edge towards the center, and the formation of bone bridges could be seen between scaffold's pores (Figure 28). Furthermore, isolated bone islands could be appreciated in the middle of the scaffolds, without connections with the newly formed bone present at the edges of the defect. All the scaffolds remained inside the defect, maintaining their structural integrity and without significant degradation observed.

4.2.4.2 Histomorphometric analysis

Histomorphometric parameters such as Bone-to-Implant Contact (BIC), Implant Surface to Tissue Surface (IS/TS) and New Bone Surface to Tissue Surface (BS/TS), were assessed inside the region of interest (ROI) for every single sample (Figure 31). The analysis

was performed after digital coloring of the images (Figure 32), and the following results were obtained.

Firstly, the percentage of implant surface inside the ROI was similar for all the groups without statistically significant p values, and mean values ranging between 41.52% ± 5.08 and 47.85% ± 8.78. This could indicate a similar degradation of the implants belonging to the different groups, even though there may be variations in these values since the arrangement of the struts could change depending on the place where the histological sections were performed, as it could be demonstrated in Figure 28.

Concerning BIC results, no statistical differences were found among the groups. PLA scaffolds showed the highest BIC values, 7.90% ± 7.22, and PLA-12CaP group obtained the lowest ones, 3.78% ± 4.41, despite of the fact that it was the group with a higher percentage of calcium phosphate added.

Finally, the measurement of the percentage of new bone surface (BS/TS) was performed in the assessed ROI. PLA group (18.23% ±5.70) was the one that had the greatest amount of newly formed bone, followed by scaffolds belonging to PLA-12CaP group (14.67% ± 5.26). In this case, statistically significant differences were found among PLA and PLA-2CaP groups (18.23% ±5.70 vs 11.69% ±3.06).

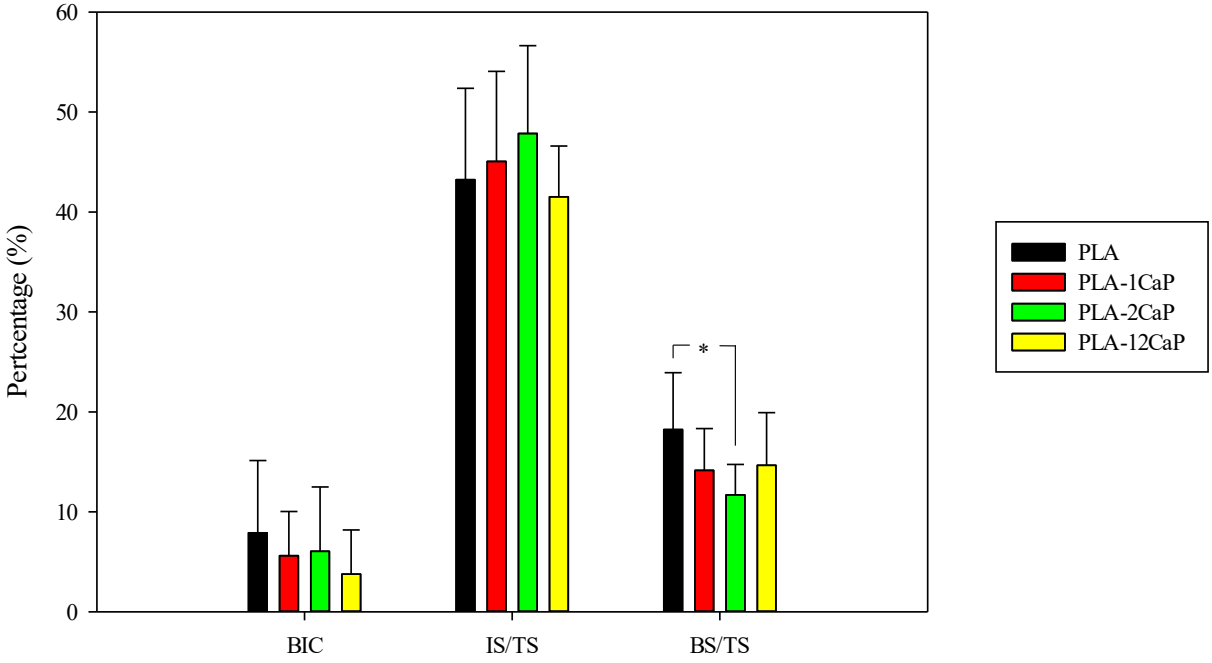

Figure 31. Histomorphometric measurements. BIC: Bone-to-Implant Contact, IS/TS: Implant Surface to Tissue Surface, BS/TS: New Bone Surface to Tissue Surface. *p<0.05 (Own Image).

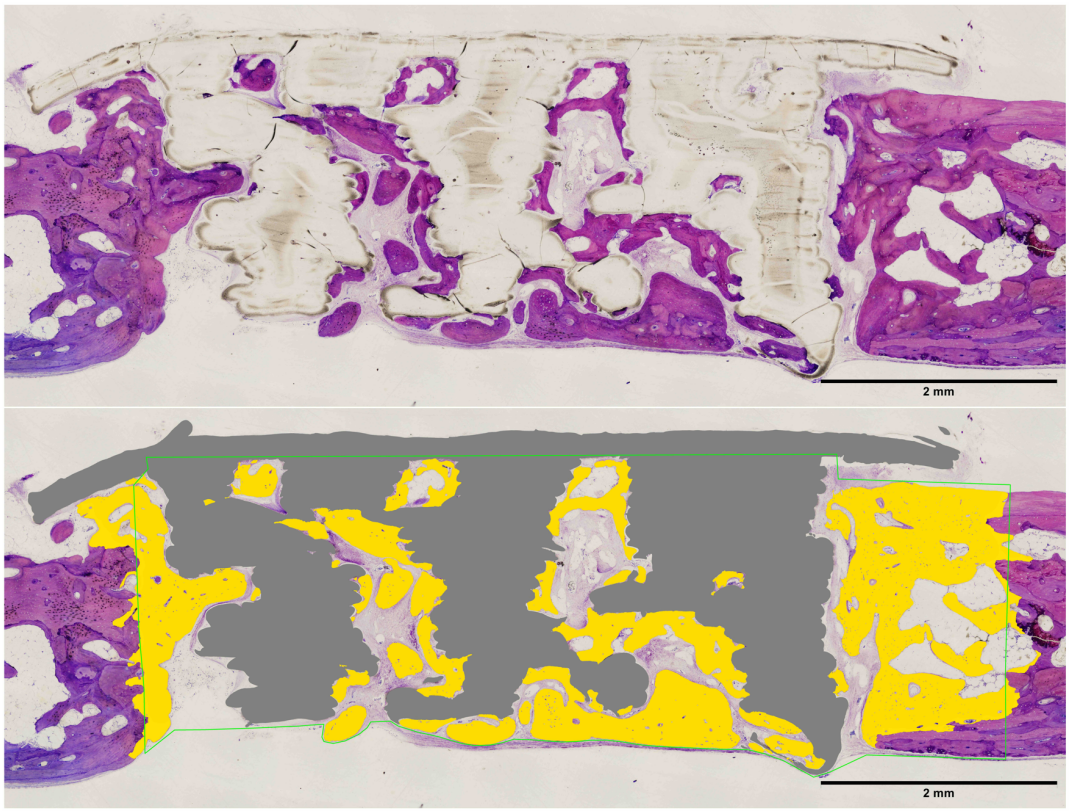

Figure 32. Histological Lévai-Laczkó stained sections, belonging to PLA group, before and after being colored and indicating the analyzed Region of Interest (Own Image).

4.3 CHAPTER III

4.3.1 Alternate and helical scaffolds characterization

BioCaP was successfully composited in the PLA matrix for the synthesized scaffolds with different laydown patterns through the fused deposition modeling technique. As mentioned before, the scaffold's design is a key factor for bone tissue engineering. The following results try to describe how the laydown pattern may affect varying implant characteristics.

Different laydown patterns of the 3D printed scaffolds could be observed macroscopically (Figure 33); both structures seemed to be highly interconnected along their circumferences, being this more significant for the helical one. The alternate structure (Figure 33, a) showed parallel lines of 0.8 mm thick with a separation between them of 0.4 mm perpendicularly alternating the direction of the processing lines between each overlapped layer. The helical structure (Figure 33, b) also exhibited 0.8 mm thick lines with a separation of 0.4 mm. However, their direction varied in 45 degrees about the already printed lines. This difference resulted in a higher separation among perpendicular struts and a higher pore size. In the case of the alternate structure, regular square-shaped pores could be seen from dorsally and lateral views. Nevertheless, the helical structure presented bigger and more irregular-shaped pores.

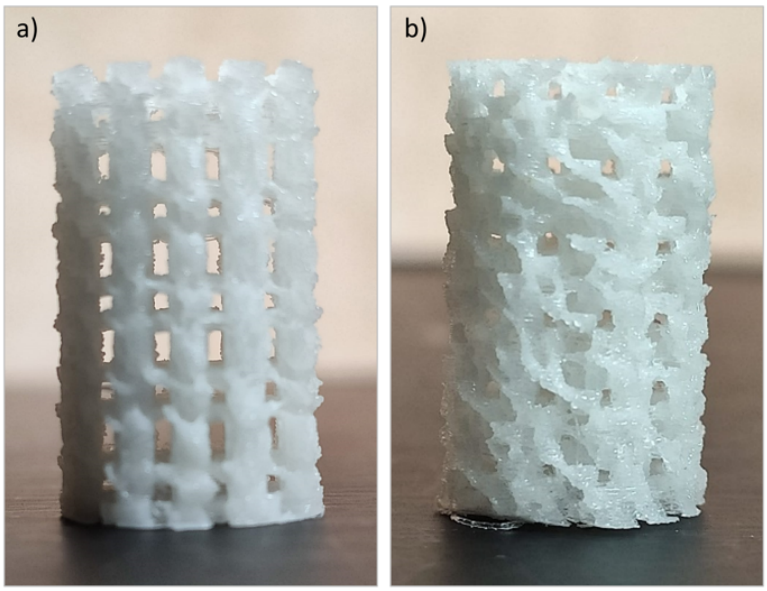

Figure 33. The macroscopic architecture of the 3D printed scaffolds (Ø: 6mm x h: 10 mm): alternate structure (a) and helical structure (b) (Own Image).

4.3.1.1 Pore morphology

3D micro-tomographic images confirmed the differences in the pores' size and shape. Furthermore, 3D analysis was performed to quantify them (Table 14). Firstly, printing patterns had great importance in the degree of infilling of the scaffolds, so this explained that alternate structures, with a higher infill ratio, presented higher scaffold volumes compared to helical ones (100 ± 10 mm^3 vs 70 ± 2 mm^3). Furthermore, the object surface per volume ratio (Obj S/V) was evaluated, and obtained information suggested that helicoidal structures provided more surface area available for biological contact than the alternate groups, with mean values of 10.6 ± 0.7 mm^{-1} and 8 ± 2 mm^{-1}, respectively. The porosity of the scaffolds was also evaluated in samples with alternate and helical structures, and the results confirmed what was suspected, obtaining mean porosity values of 45 ± 6 % and 63 ± 1 %, for alternate and helical groups. In addition, pore

size was measured, and mean values were established in 400±20 μm for alternate structures, and 560±6 μm for helical structures. Regarding pore size distribution (Figure 34), a more comprehensive range of pore sizes could be observed for helical structures, with peaks at 514.8 μm and 731.5 μm. However, this range is narrower in the case of alternate structures, with smaller pore sizes and a high peak at 460.6 μm. Thus, these issues provide the helical structure with better features to promote bone cells growth, neovascularization, and diffusion of nutrients, oxygen, and waste products.

Table 14. Pore morphology measurements in micro-CT. All parameters are represented as mean ± SD.

	Scaffold Volume	Obj S/V	Open Porosity	Strut Thickness	Pore Size
	mm^3	mm^{-1}	%	μm	μm
ALT	100±10	8±2	45±6	430±80	400±20
HEL	70±2	10.6±0.7	63±1	350±20	560±6

Besides, to confirm this statement, a detailed study of the interconnectivity was performed through the pore accessibility or open and accessible pore volume within the scaffold. This method, as explained before, gives the smallest pore constriction connecting every voxel of the scaffold, quantifying bone ingrowth as a function of accessible pore size [97]. Although both structures were highly interconnected, the analysis showed notable differences. As it could be seen in Figure 35, interconnectivity values lower than 90% were achieved at minimum connection sizes of 162.6 μm for the alternate structure, and 270.9 μm for the helical structure. Likewise, differences between them increased as the percentage of interconnectivity decreased, reaching values less than 80% when openings were greater than 270.9 μm in the alternate group, and 433.5 μm in the helical group. The highest pore throat studied was 650.2 μm, providing pore accessibility percentages of 26 % and 53 % for both structures, respectively.

Concerning strut thickness, higher mean values were appreciated in the alternate group compared with the helicoidal one (430±80 μm vs. 350±20 μm) (Table 14). Furthermore, apparent differences could also be observed between alternate and helical structures regarding strut thickness distribution (Figure 34). Even though both structures peaked at 352.2 μm, the alternate one presented a more comprehensive range of sizes, reaching strut thicknesses up to 800 μm. These results were probably caused due to the differences between both laydown patterns, since the filaments were aligned in the alternate structure, and they could merge and be interpreted as one during micro-tomographic analysis. Something that will hardly happen in the helical structure, due to a layer configuration which involves the deposition of staggered fibers varying 45 degrees.

The micro-tomographic evaluation also allowed us to confirm an adequate dispersion of the bioCaP particles along the longitudinal and cross-sectional axes of cylindrical structures. Figure 36 shows the homogeneous dispersion of the particles in the surface and the inner part of the struts.

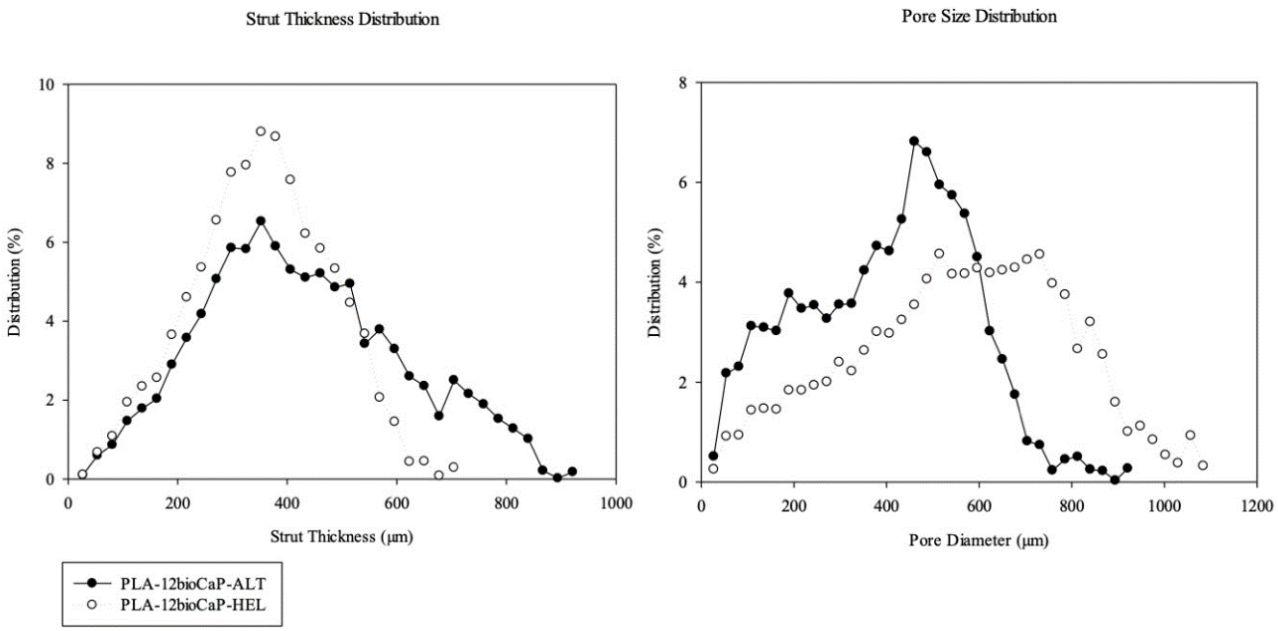

Figure 34. Strut Thickness and Pore Size Distribution of 3D printed composite scaffolds (Own Image).

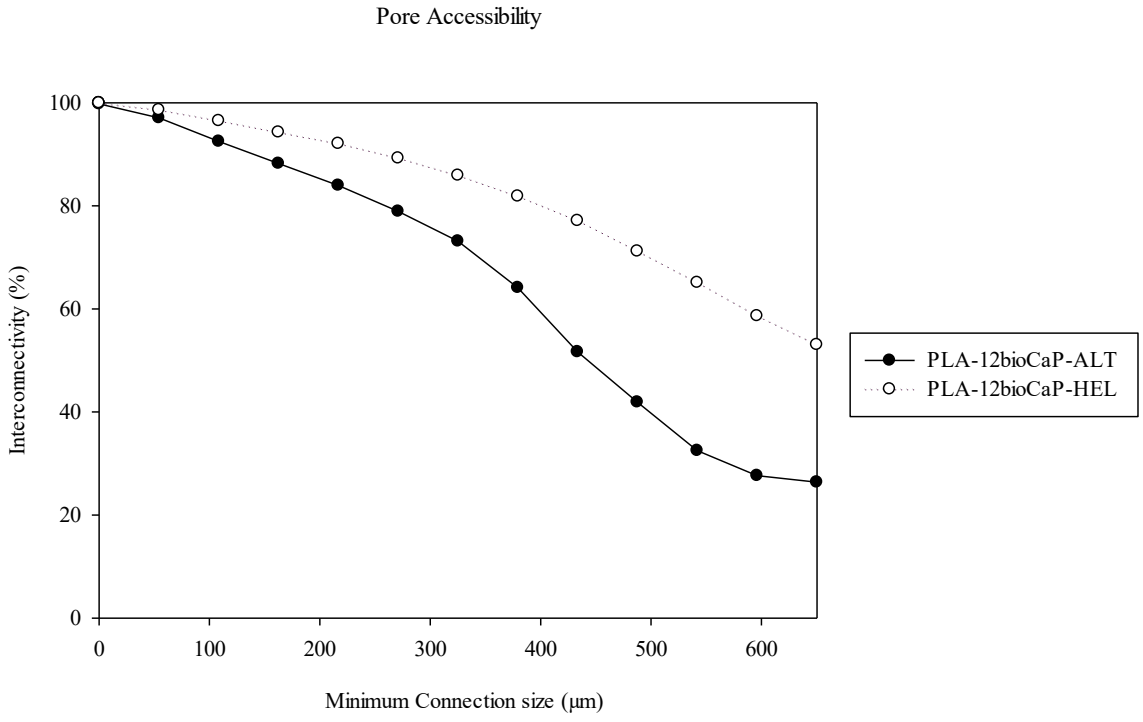

Figure 35. Pore accessibility assessment in micro-CT (Own Image).

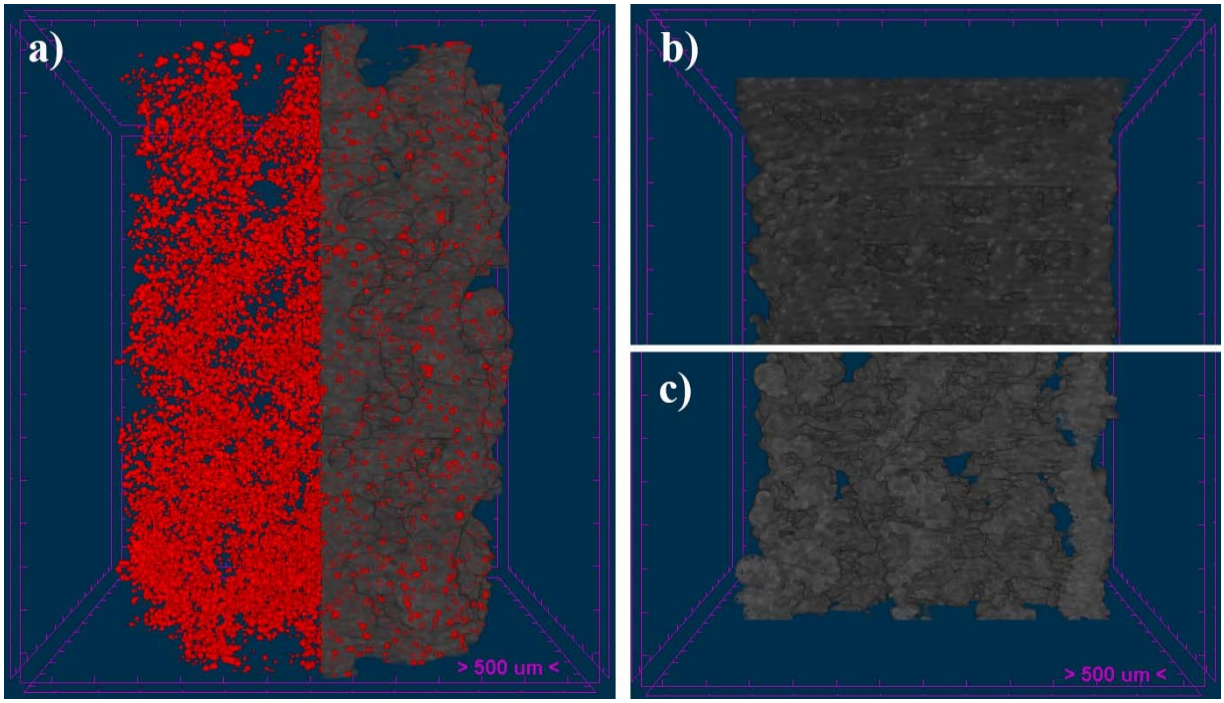

Figure 36. Micro-CT reconstruction of 3D printed scaffolds. Distribution of bioCaP particles (red dots) inside the struts along the scaffold (a), a cross-section of alternate (b) and helical (c) structures (Own Image).

4.3.1.2 Mechanical test

The implications of the laydown pattern in the compressive strength were also evaluated prior to scaffolds' implantation due to their great importance when facing bone regeneration in load-bearing sites. Four alternate and helical group samples were evaluated, and calculated strength, just like in the previous chapter, was obtained from the end of the linear elasticity phase. Results are visible in Table 15, showing a marked difference in compressive strength and elastic modulus values between both structures, which proved to be statistically significant. Therefore, the alternate structure will be significantly more resistant than the helical one.

Table 15. Results of mechanical tests. All parameters are represented as mean ± SD (*p<0.05).

	Compressive Strength	Elastic Modulus
	MPa	MPa
ALT	26±2*	300±100
HEL	5.8±0.3*	80±4

In addition, the correlation between the compressive strength and several micro-tomographic parameters, such as scaffold volume, porosity, and strut thickness, was also assessed. As demonstrated in Table 14, printed laydown patterns resulted in high differences in scaffold volume, and a positive correlation between these data and compressive strength was confirmed by Pearson's correlation method. Furthermore, a negative correlation with this parameter was found for the porosity but not the strut thickness (Table 16). Consequently, the weakness of the helicoidal structure could be closely related to its lower volume and increased porosity.

Table 16. Correlation study between compressive strength and scaffold's architectural characteristics (*p<0.05).

Pearson's correlation coefficient	Scaffold Volume	Porosity	Strut Thickness
Compressive Strength	0.98*	-0.98*	-0.85

4.3.2 Animal model

In vivo trials were performed without complications, and all the animals recovered adequately after the surgery. Furthermore, the skin healed normally, and no signs of infection, inflammation, or dehiscence were found. During the postoperative period, one of the rabbits presented a marked lameness of the left hind limb, although it could use the leg without problems. Despite being treated with analgesic drugs, it maintained a slight lameness until the time of euthanasia.

Macroscopically, mild to moderate signs of osteoarthritis, secondary to the surgical process, were observed in almost all the rabbits. Several related findings were described, such as thickening of the joint capsule, excessive synovial fluid, and loss of articular cartilage. During the necropsy, total and partial fractures of the lateral femoral condyle were detected in two knees; therefore, they were excluded from the analysis. Besides, macroscopical examinations confirmed that bone defects healed successfully, without signs of bone hematoma or infection being present, and the scaffolds seemed to be adequately anchored to the trabecular bone of the femoral condyle.

An in-depth analysis of these findings could demonstrate that both fractured femoral condyles were related to implanting scaffolds with a helical structure. The low mechanical resistance of the implants could lead to a collapse of the structure and a subsequent fracture of the bone when implanted in load-bearing sites.

4.3.3 Micro-CT

3D reconstructed images obtained by micro-CT showed appropriate osseointegration of the implants within the femoral condyle, with new bone formation occurring through the scaffolds. Representative images were included in Figure 37. Generally, no striking signs of inflammation or rejection were observed, with trabecular bone ingrowth inside the scaffold pores. Furthermore, three-dimensional views helped to clearly distinguish those samples where the femoral condyle and the scaffold were fractured (n=2) and those in which the implantation was performed in a more proximal femoral site and the scaffold was located inside the bone marrow and not in the trabecular Bone (n=1). These findings were also confirmed histologically, and both were considered criteria for excluding the analysis of the respective samples (Figure 38).

Bone regeneration inside the VOI was evaluated through a 3D analysis. Statistically significant differences between alternate and helical structures for any of the analyzed parameters were not found. As shown in Figure 39, the amount of newly formed Bone was higher for the helical structure than the alternate structure, with BV/TV percentages of 12.94±5.00 % and 9.65±2.3 %, respectively. Likewise, BS/BV and Tb.Pf. showed slight variations among structures, indicating that the available bone surface and the intertrabecular connectivity ratio were mildly higher in helical structures. However, regarding trabecular thickness, newly formed bone trabeculae seemed slightly thicker for alternate structures.

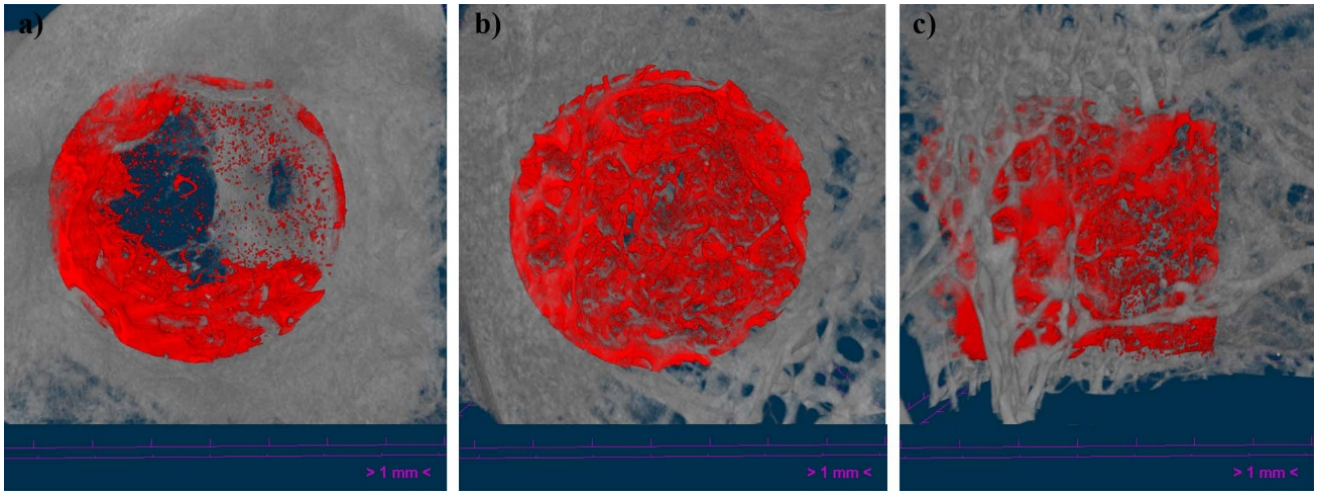

Figure 37. Representative micro-CT images of the implanted alternate (a) and helical scaffolds, in coronal (b) and sagittal (c) views, 12 weeks after the implantation. The measured volume of interest (VOI) was highlighted in red color (Own Image).

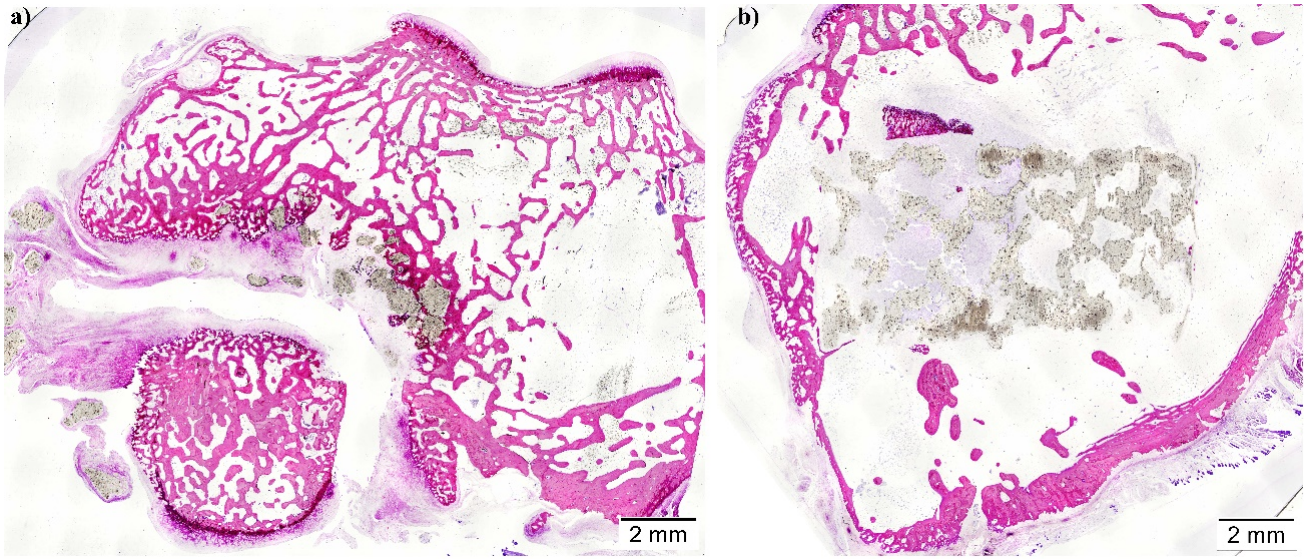

Figure 38. Histological sections of the samples were excluded from the analysis. Fractured femoral condyle and breakage of the scaffold (a) and scaffold implanted inside the bone marrow (Own Image).

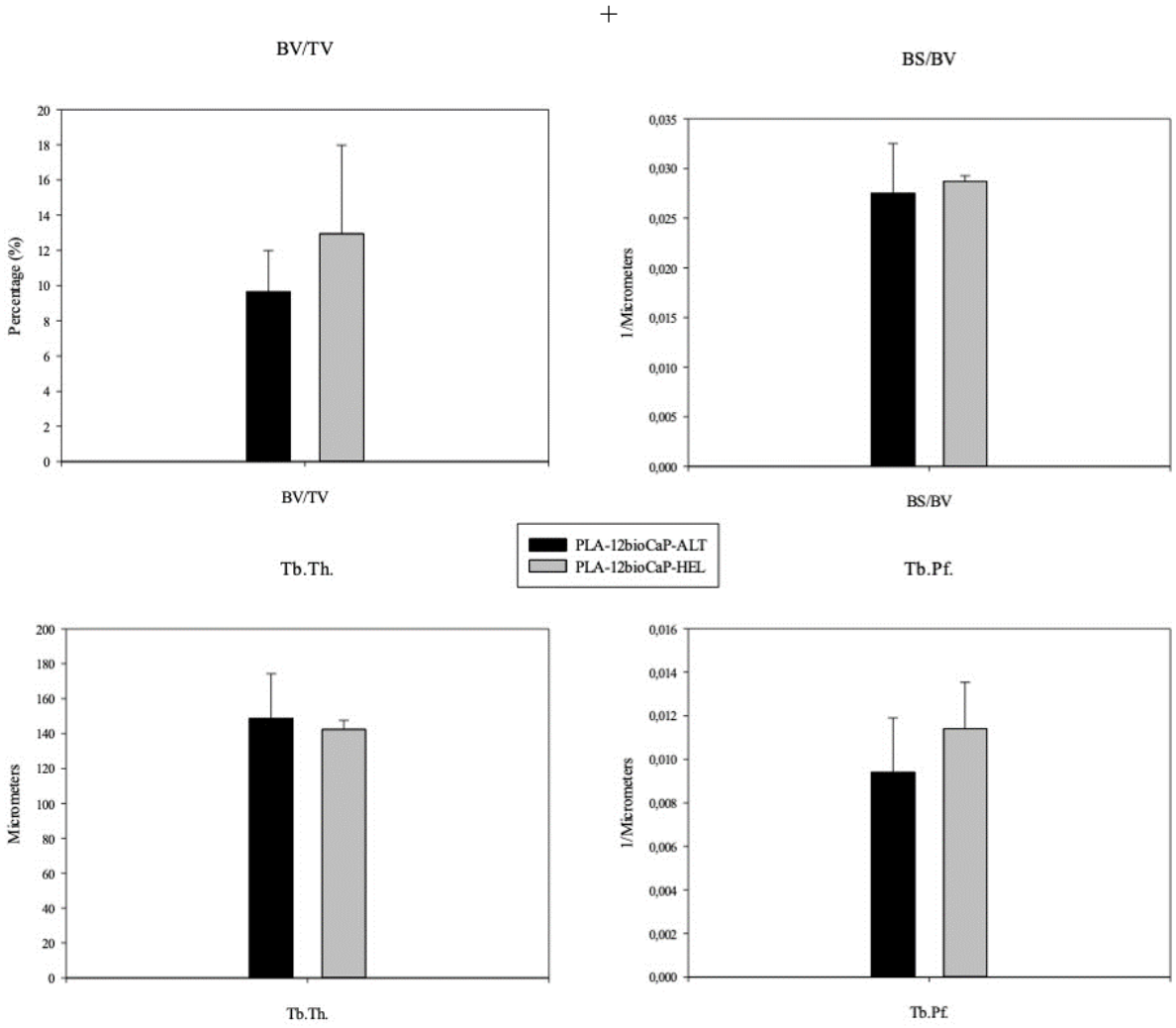

Figure 39. Micro-CT histomorphometric measurements. BV/TV: Bone Volume/Tissue Volume, BS/BV: Bone Surface/Bone Volume, Tb.Th.: Trabecular Thickness and Tb.Pf.: Trabecular Pattern Factor. *p<0.05 (Own Image).

4.3.4 Histomorphometric analysis

The structures' effect on bone regeneration was evaluated by creating bone-critical defects in a rabbit femoral condyle model. After twelve weeks of implantation, specimens were processed, and two slides were obtained from central sections of each sample. Then, they were stained with Lévai-Lazckó's protocol and evaluated histologically by optical microscopy. Representative histological images were included in Figure 40.

All the implants maintained their position in the center of the defect and were successfully osseointegrated into the host bone, showing good biocompatibility. The absence of other fractures or displacements of the grafting materials was described, except for those specimens in which a total or partial lateral condylar fracture occurred (Figure 38). Most of the bone-to-implant contacts were detected in the implant's periphery, where their surfaces were exposed and in contact with the trabecular condylar bone. In these sites, bone ingrowth could be appreciated through the pores to the inner parts of the scaffolds, more notably in those with a helical structure, probably due to its higher porosity and available surface. However, non-major differences were observed subjectively regarding the regenerative potential of both structures, which presented similar interconnected trabecular systems. The quantification of the newly

formed bone, the amount of remaining composite material, and the percentage of bone-to-implant contact were then performed objectively.

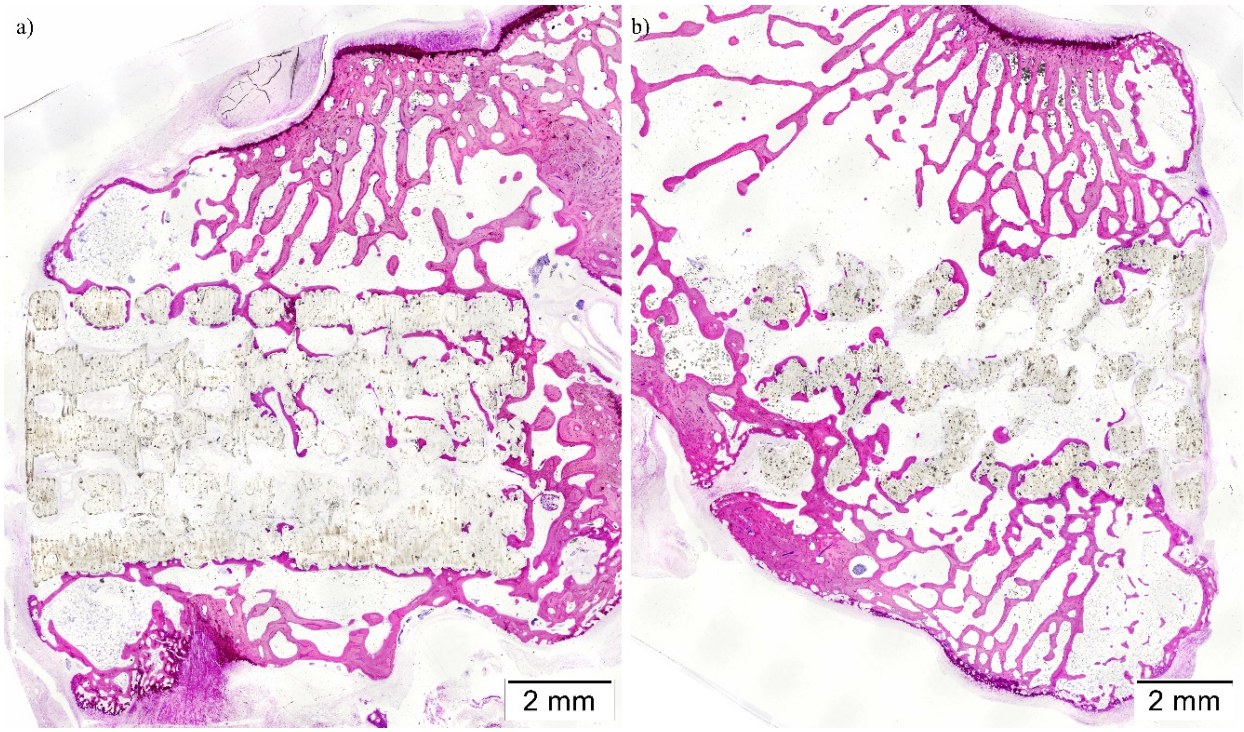

Figure 40. Histological sections showing the effect of 0°/90°/180° (a) and 0°/45°/90°/135°/180° (b) laydown patterns on bone regeneration 12 weeks after the implantation of the scaffolds in femoral condyle defects (Own Image).

Likewise, in those sites where the scaffolds were in contact with bone marrow or connective tissue, the pores showed an abundant infiltration with fatty and fibrous tissue. Neovascularization was described inside the pores, usually mixed with both fatty and fibrous tissues. Generally, inflammatory cells were mainly observed surrounding the composite material, specifically macrophages, which were more numerous in the slides from the helical group. Their presence is usually related to the degradation of resorbable biomaterials, and it seemed clear that the helical structure suffered a higher degree of degradation than the alternate one, which could explain the greater number of macrophages in the helical group. Besides, small infiltrates of lymphoplasmacytic cells were found embedded inside the connective tissue, and some neutrophils were occasionally observed. However, none of the signs suggested the presence of infection, tissue necrosis, or rejection.

Histomorphometric measurements were performed after coloring the images in a defined Region of Interest, delimited by the trephine bur's performed defect (Figures 41). In the images, these limits were represented as well-defined cuts in the lamellar bone perpendicular to the cortical bone. The results of the analysis are showed in Figure 42.

Bone-to-implant contact (BIC) was mainly restricted to the outer section of the cylinders. The percentage of BIC was similar for both studied types, without significant differences between them. Mildly lower values were found for the alternate structure (24.783±13.741 %) concerning the helical one (27.037±18.439 %).

Then, the amount of biomaterial inside the ROI, was measured. Statistically significant differences were found among structures for this parameter, and mean values were set at 50,950±6,023 % for alternate scaffolds, and 32.683±3.668 % for helical scaffolds. These

differences could be explained mainly by the discrepancies between both groups regarding the scaffold's volume. Nevertheless, the biodegradability of the implants should also be considered since a higher available surface for scaffold-environment contact will lead to further degradation, due to a greater surface area subjected to hydrolytic processes and the action of the macrophages, decreasing consequently the IS/TS obtained values.

Finally, regarding to bone Surface to Tissue Surface (BS/TS). Histomorphometric analysis revealed statistically significant differences between the helical and alternate structures when measuring the newly formed bone (BS/TS). Implanted scaffolds with a helical disposition achieved BS/TS mean values of 13.13±4.70 %, significative higher than the ones obtained by the alternate structures 9.246±2.64 %. Thus, the characteristics of the helical structures seemed to be more adequate to achieve a more significant osteogenic potential for bone regeneration in critical defects.

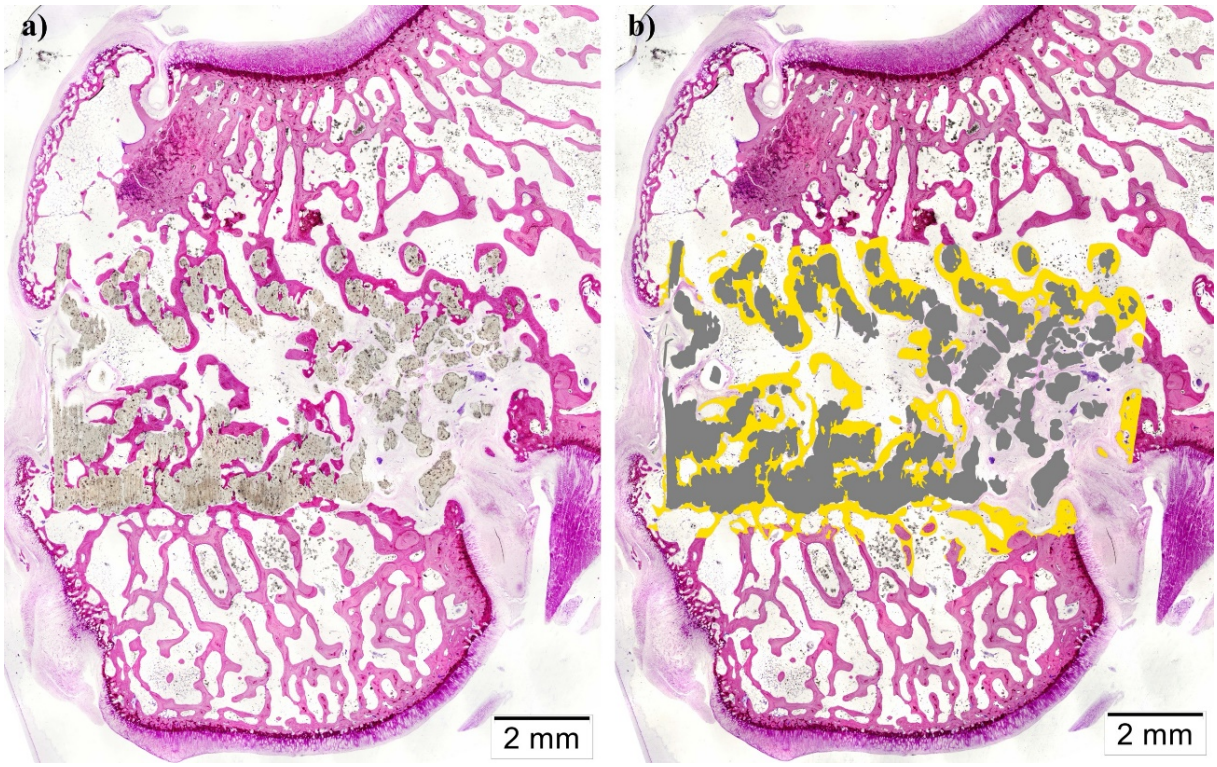

Figure 41. Histological stained colored and not colored sections of helical scaffolds implanted in rabbit's femoral condyle (Own Image).

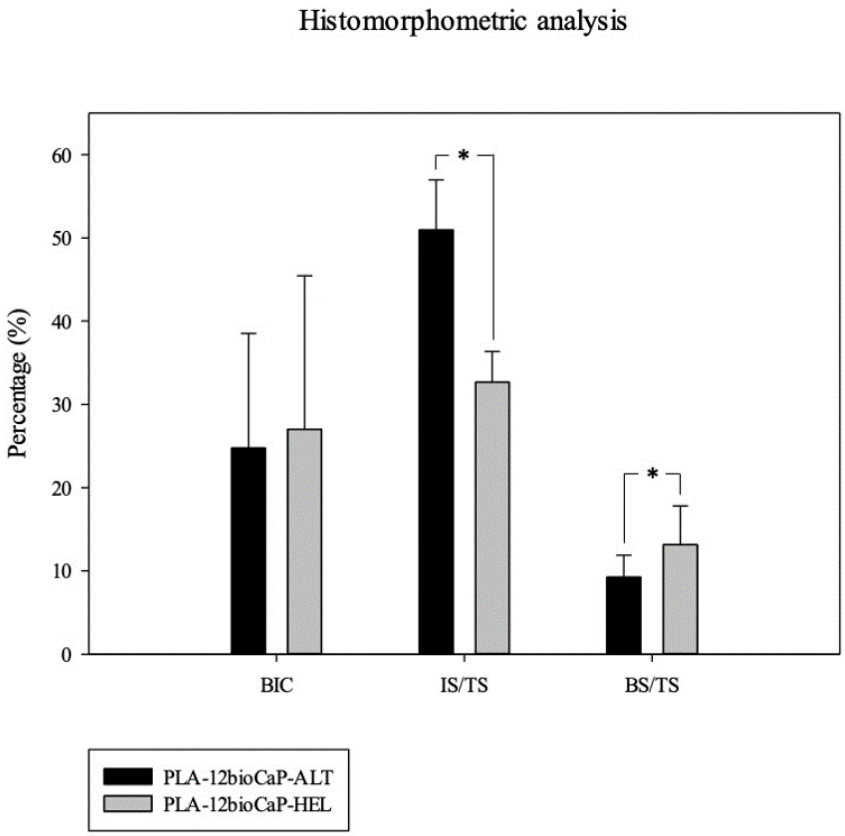

Figure 42. Histomorphometric measurements. BIC: Bone-to-implant Contact, IS/TS: Implant Surface to Tissue Surface, BS/TS: New Bone Surface to Tissue Surface. *p<0.05 (Own Image).

GENERAL DISCUSSION

5 GENERAL DISCUSSION

Bone tissue engineering is one of the main fields of biomedicine study, due to the tremendous impact of musculoskeletal disorders on people's quality of life. The importance of using scaffolds in bone tissue engineering has risen notably in recent years, to provide an alternative to autografts and allografts [75]. The development of additive manufacturing techniques has provided important advancements, since they allow the customization of the implants when dealing with complicated and irregular geometries, with precise control of the internal and external architecture [75,77,218,240].

Furthermore, bone substitutes should be tested *in vivo* before being implanted in human beings to ensure that it works effectively and safely. Rabbits are the most used preclinical model for bone tissue's testing, commonly for cortical and cancellous bone implant studies. In addition to their easy availability, housing, and handling, they reach skeletal maturity at an early age after puberty, present similarities in bone mineral density and fracture toughness with humans, and their bone turnover is faster than other species like primates or rodents. The calvarial bone defect model had been extensively used, mainly in rodent-models, when studying bone healing and regeneration processes. Due to its easy performance, there is no need for external fixation and it is possible to assess bone healing quickly using micro-CT and histology. However, it does not allow the evaluation of the scaffolds under physiological mechanical loads [217]. Likewise, femoral condyles support defects more significant than 3 mm to test biocompatibility and osteoinduction in cancellous bone, so they allow the performance of critical defects to test biomaterials in load-bearing conditions, which should be 6 mm according to the species and location. [33,241–244]. Critical size defects are defined as the smallest wound that does not heal spontaneously over a long period of time, so they are commonly performed to evaluate the scaffold's bone healing properties [8,33].

The purpose of the present Doctoral Thesis was firstly to review the feasibility of using 3D-printed PLA-bioceramic composite scaffolds as bone grafting materials, attending not only to results regarding newly formed bone, but also carefully analyzing the characterization of the implants and several aspects related to the *in vivo* trials, such as planification or the selection of the anaesthetic protocol. The systematic review provided us with the necessary knowledge for the correct design of the experimental procedures carried out below and for the understanding and discussion of the results obtained therein.

3D-printed PLA-bioCaP composite scaffolds were fabricated through FDM and studied carefully during both experimental processes, delving deeper in the understanding of the effect of modifications on the composition or the geometry of the scaffolds. The calvarial model was used to evaluate the effects of PLA's gradual enrichment with marine bioapatites over the characteristics of the scaffolds and their osteogenic capacity. Likewise, the femoral model sought to demonstrate that the structural existing differences between helical and alternate scaffolds derived from the modification of the laydown patterns, could have a notable effect on the characteristics of the implants and their capacity to induce bone regeneration. Even though scaffolds' osteogenic capabilities should be improved in future research, the absence of an inflammatory response that could harm bone regeneration, their high mechanical properties,

and their personalized architecture, allowed them to meet the vast majority of the requirements for a bone graft. Thus, positioning 3D-printing technology and composite materials as exciting alternatives to heal impaired fractures supports and favoring the growth of new bone and vascular tissue.

The results obtained from each chapter will be discussed throughout the following sections.

5.1 CHAPTER I: "USE OF 3D-PRINTED POLYLACTIC ACID/BIOCERAMIC COMPOSITE SCAFFOLDS FOR BONE TISSUE ENGINEERING IN PRECLINICAL *IN VIVO* STUDIES: A SYSTEMATIC REVIEW"

The main objective of the systematic review, as mentioned above, was to evaluate the possible use, as bone graft substitutes, of 3D-printed scaffolds synthesized form PLA/bioceramic composites in preclinical studies with animal models, as a promising approach to bone repair and reconstruction.

Other authors have reviewed over the last years the possible use in bone tissue engineering of several additive manufacturing technologies [35,36,38,73,245] and/or biomaterials, such as biopolymers [47,72], bioceramics [60] or composites [28,74]. However, most of them focused on the manufacturing process, characterization aspects, or applications without paying much attention to their behavior when used in preclinical trials with animal models, a key factor of translational research. Hassan *et al.* [27] evaluated the effect of using 3D-printed templates on bone tissue regeneration in critical bone defects induced in experimental animal studies, specifically in calvarial defect models. Their findings confirmed 3D-printed templates as an alternative for bone tissue regeneration, compared to conventional porous templates fabricated from the same material [27]. Likewise, bioceramic scaffolds, alone or combined with polymeric materials, have demonstrated better support of new bone formation, compared to untreated empty defects, and a similar bone growth compared to defects filled with deproteinized bovine-derived bone mineral [39], which is in agreement with the results obtained in the present systematic review.

Some of the scaffold's main studied parameters were the pore interconnection, overall porosity, and pore size. A wide range of pore sizes can be selected for bone regeneration. Generally, macroporosity promotes osteogenesis, and microporosity improves surface area for protein adsorption, providing attachment points for osteoblasts. Hence, studies suggested that pore size should range from 200 to 600 micrometers. Typically, pores should be higher than 300 μm to facilitate osteoblast proliferation and enhance neovascularization, and 100 μm is the very minimum size, since it is associated with the formation of non-mineralized osteoid or fibrous tissue, limiting oxygen and nutrient diffusion throughout the scaffolds [7,13,30,217,226]. Likewise, pore interconnectivity positively influences bone deposition rate and depth of infiltration, improving nutrient and oxygen supply to the scaffold's inner part and allowing cell growth [30,226]. Another feature that influences bone regeneration rate is pore's geometry, due to different morphologies giving rise to differences in pore width and curvature of the surface, leading to variations in tissue morphology and growth rate. For example, tissue formation favors concave surfaces compared with flat and convex regions [226].

Bioactive properties are also important, it was demonstrated that the addition of an appropriate amount of calcium phosphate to a PLA matrix provides the implant an improvement in its biological activity [213], by reducing possible inflammatory reactions that could limit PLA applications [75]. Likewise, the addition of bioceramics influenced mechanical properties and biodegradability.

Balancing PLA's ductility and CaP's brittleness is the key issue regulating composite's mechanical properties [77]. Kwon *et al.* [220] observed that adding β-TCP in mixture ratios of

10% and 30%, increased the compressive strength of the implants from approximately 258 MPa (PLA alone), to 310 MPa and 349 MPa, respectively. However, other studies observed that when higher concentrations of hydroxyapatite were added to a PLA matrix, the compressive strength of the implants decreased [77,213,214]. Zhang *et al.* [77] showed that PLA scaffolds had a compressive strength of around 44.02 MPa, which decreased progressively as hydroxyapatite was added, with 29.68 MPa and 14.22 MPa values for 30% and 50%HA concentrations, respectively.

An ideal biodegradable material should have a degradation rate matching the growth rate of native ECM, to ensure mechanical support throughout the lifecycle of the scaffold, while leaving space for tissue growth [30,75]. PLA is degraded by simple hydrolysis, and the degradation products are then transformed into non-toxic subproducts that are eliminated through regular cellular activity and urine [47]. Nevertheless, lactate's releasing triggers the acidification of the environment affecting the defect site's acid-base balance, which can lead to hampered biological response towards the scaffold [29,213]. Like other bioceramics, HA performed the neutralizing capacity to the acidic products formed *in vivo* by degraded polymers and partially blocked the unfavorable acidic environment [211,246]. Besides, HA is hydrophilic, increasing the ability to absorb the water, and accelerating the degradation process [213,217]. Wang *et al.* [213] observed that Pn50 group (PLA/50%HA) degraded faster than the other groups (Pn30, PLA/30%HA and Pn0, PLA/0%HA) after 7 days. Zhang *et al.* [77] also obtained similar results with higher mass and molecular weight losses in PLA/50%HA scaffolds than PLA/30% HA and PLA/0%HA ones. The higher content of HA seemed to alleviate environmental acidity, and the lowest pH values were found in samples without HA. By contrast, Kwon *et al.* [220] concluded from their *in vivo* degradability analysis that the degradation rates among PLLA, PLLA+TCP10, and PLLA+TCP30 scaffolds did not vary significantly.

Regarding to the modification of PLA scaffolds' characteristics, it is worth highlighting some of the other available possibilities that may be interesting for bone tissue engineering. Shuai *et al.* [165] concluded in their work that the addition of poly (glycolic acid) (PGA) to PLLA/HA scaffolds results in an improvement of the hydrophilic behavior, with higher water absorption and the degradation rate, increasing the contact area between PLLA and body fluid. Consequently, there is a higher exposure of the HA embedded in the PLA matrix, which contacts with body fluids to exchange ions, and therefore the deposition of bone-like apatites, providing a suitable environment for osteoblastic growth and proliferation. Another possibility is using a copolymer of the PLA, derived from natural monomers of lactide and glycolide, such as poly (lactic-co-glycolic acid) (PLGA). Its amorphous structure allows water molecules to diffuse easily into the scaffold, providing greater degradability and bioactivity compared to the ones made by PLA [247].

Generally, when manufacturing the implants, the bioceramic powders were mixed or dissolved with a PLA solution to be later printed using additive manufacturing techniques. However, Tcacencu *et al.* [221] synthesized apatite-wollastonite disks independently and then adhered them to PLA porous disks through a thermal bonding process; and Maia-Pinto *et al.* [218] biomimetically coated with apatite 3D-printed polylactic acid scaffolds. Regarding the manufacturing process of PLA-HA implants, the most frequent combination, and the variations among the mixing ratios, it could be seen that most of the studies chose one proportion [75,211,212,214,215,217,219], but readers do not know why it was selected. However, others tested different concentrations of HA to evaluate their influence on scaffolds' performance [77,213]. At this point, it was observed that when HA ratio was more significant than 50%, the composite material could not be printed coherently and stably due to its high brittleness, but

values less than or equal to 50% can be printed satisfactorily by FFF [77,213,214]. Zhang *et al.* [77] achieved a successful impression of a composite with 50% HA by using a silane couple agent called dodecyl trimethoxy silane (WD-10), which can combine with the polymer molecular chain more effectively. By contrast, Wang *et al.* [213] were able to print PLA/50%HA scaffolds but did not test them *in vivo*, probably because of the presence of apparent fractures in the cuboids, and the negative effects of proportions of HA higher than 30% had over the composite's ductility, as they reported.

Sterilization processes have a major significance when manufacturing scaffolds for bone regeneration and need to be raised at the beginning of implant development. For this purpose, there are many available options as steam sterilization (also called autoclaving), ethylene oxide sterilization, hydrogen peroxide sterilization, γ-irradiation, electron-beam irradiation (also called β-irradiation) and UV sterilization. However, not all of them can be used on biodegradable polymers and/or bioceramics, because it may produce adverse reactions such as physico-chemical and morphological changes or the formation of toxic byproducts by degrading the material [38,223]. UV exposure, γ-irradiation and β-irradiation are suitable processes to sterilize biodegradable polymers. Nevertheless, autoclaving, plasma sterilization and ethylene oxide, the most used process in the included papers, should be avoided because they produce respectively, a shrinkage of the materials, physical alterations, and toxicity [38,248–250]. Regarding bioceramics, γ-irradiation is the most indicate sterilization process. However, autoclaving and ethylene oxide have been demonstrated to degrade some calcium phosphate phases [38,60]. Therefore, neither has proven to be a suitable technique for sterilizing composites synthesized from PLA and bioceramics.

3D-printed templates have been shown to have adequate characteristics for their use in bone regeneration when composites originated from the addition of HA, β-TCP or octacalcium phosphate to a PLA matrix, the combination between PLA and apatite-wollastonite discs or the use of biomimetic CaP coatings, were utilized for their synthesis. Starting from this, we can extract certain ideas.

First of all, we could see that higher concentrations of HA [77,213] or β-TCP [220], as expected, will lead to higher percentages of new bone area. Furthermore, the addition of different substances to functionalize the scaffolds showed an improvement in the results compared with not functionalized groups. Ss Minto *et al.* [216] described in their paper:

> "A factor that could assist the scaffold would be the use of precursor cells for osteogenesis to optimize bone healing, since biologically active 3D implants are promising in tissue regeneration."

Dental pulp stem cells [217], bone marrow stem cells [215,219] or enhanced bone marrow [212] increased the migration of the stem cells to the site of the injury, and induce angiogenesis and osteogenic differentiation by the release of growth factors. Indeed, growth factors with great osteoinductive potential can also be applied, such as bone morphogenetic proteins (BMP) [218], which stimulate bone formation via recruiting osteoprogenitor cells. BMP-2 has been widely studied because of its ability to directly target BMP receptors at the cell surface and trigger stem cell differentiation in bone, and it has been demonstrated to be an alternative to stem cell implantation [49]. Likewise, other substances have demonstrated a positive effect on bone growth, such as human osteoblastoma cell lines [220], a potential osteoblast-like sourc that allows rapid bone proliferation; or lanthanum, a foreign ion capable of enhancing bone formation by influencing the hydrolysis of OCP to HA. Nevertheless, functionalizing substances is not the only strategy different authors use to stimulate bone regeneration.

Applying electric fields [219] and induced membranes technique [212] have also benefited bone healing. Among the substances that can be added to scaffolds to improve the biological effects, even the use of metals has been reported. Wang *et al.* [251] recently published the addition of lithium to PLA/n-HA composites, which plays an important role in bone development, homeostasis, osteoblast differentiation and bone formation via the activation of Wnt signaling pathway. Likewise, *in vivo* trials have demonstrated that in lithium doped groups presented higher osteogenic induction than not doped ones.

Regarding to animal models, Zeiter *et al.* [244] reported in their manuscript the massive variations in the chosen models used to test bone substitutes, in terms of animal species, strain or breed, age and gender. Rabbits and rats were the most frequently used models but without a clear preference for a specific gender. Besides, there is a high variability in the age of the animals, something with critical influence regarding the closure of growth plates and the skeletal maturity. Literature revealed that important information such as age or gender, was missed in many studies, hindering the interpretation and replicability of the results. These results were in agreement with those obtained in the present review. Al-allaq and Kashan [59] also reported more trials in rodents (rats, mice) than in the rest of the models, probably because of their ease of handling and small size. However, large animal models should be considered for future investigations due to the similarities with human clinical conditions, which are essential for investigating bone scaffold interactions.

Among the available species for the evaluation of bone formation, rats and rabbits were selected for testing different composite materials in the studied manuscripts, and information about age or gender was variable between them or was not reported or specified [75,77,211–222]. Calvaria and femur were the main anatomical regions selected to make the defects. However, because of protocol differences such as defect size, the number of defects, observation times or scaffolds composition, no cross-study comparisons could be performed, and the generalizability of the results was limited. Furthermore, the following limitations were found when evaluating the preclinical trials with animal models of the different reports:

- The sample size was not specified in two studies [214,222] and another one utilized only 3 animals [211], which is a deficient number of specimens to obtain significative statistical results.
- The critical-sized defect (CSD) model, commonly proposed for the evaluation of bone healing, was just observed in 5 papers [212,216–218,221].
- There was a lack of control groups since empty controls were only utilized in 5 of 14 studies [75,216,217,219,222], and iliac crest bone graft control or positive control was used in 2 [212,216].
- The low report of adverse effects, usually present in this kind of procedures, as seen in the study quality assessment.
- The absence of quantitative methods when evaluating bone regeneration among the different groups, such as micro-CT analysis, quantitative histologic analysis or histomorphometric analysis, was identified in 2 reports [77,216,222].

Likewise, the choice of the anaesthetic protocol is also an essential step in the design of any animal experiment, and must reach a state of unconsciousness, analgesia, and muscle relaxation. Scientists sometimes decide to leave the animals' pain untreated since using potent anaesthetic and analgesic drugs may strongly affect the animals' biology. However, animal pain management in laboratories is an ethical imperative [252], specifically when performing most orthopedic and wound healing models, since they produce moderate to severe pain [253]. Below, we will analyze some of the main features of the drugs used for surgical procedures.

Since pentobarbital is a barbiturate that produces hypnosis but has poorly analgesic properties, it is typically not used alone in painful procedures. In this case, it was administered alone in rabbits [77,212–214] and rats [222], although in the latter report, it was combined in one case with isoflurane (an inhalational anaesthetic with little or no analgesic activity) [219]. Ketamine is a dissociative anaesthetic that reaches high somatic analgesic levels. It was utilized in rats alone [75] or combined with other drugs, such as xylazine [217,221], xylazine and midazolam [218] or midazolam and morphine [216]. Xylazine is an alpha-2 agonist with powerful tranquillizing properties and moderate visceral analgesic action; midazolam, is a benzodiazepine with relatively low tranquillizing-sedative effects and no analgesic properties, which is usually utilized as an adjunctive drug to ketamine; and morphine is a pure opioid with potent analgesic action and bad hypnotic properties, which is very useful given its lasting effects for animal's premedication, but also for the postoperative period. Tiletamine, as well as ketamine, is a dissociative anaesthetic used commonly in conjunction with zolazepam, a benzodiazepine drug, providing sedation, but not so potent analgesia. It was administered to rats in combination with xylazine [220]. Furthermore, only two reports included the use of local anaesthesia or postoperative analgesia. Gendviliene *et al.* [217] selected respectively, lidocaine, a short-acting local anaesthetic commonly applied through the infiltration of the tissue, and buprenorphine, a partial agonist opioid which provides analgesia and is considered as an effective treatment for postsurgical pain. Buprenorphine is one of laboratory animals' most widely used analgesics [254]. Likewise, Minto *et al.* [216] administered lidocaine to perform a right brachial plexus block, a local anaesthesia technique; and used meloxicam and tramadol for the control of the pain during the postsurgical period. Meloxicam is a non-steroidal anti-inflammatory drug (NSAID) that provides a moderate analgesic action, usually used for the treatment of pain or inflammatory processes; and tramadol is another opioid commonly administered in rabbits to treat mild acute and chronic pain, that has a low activity at the mu-opioid receptors and inhibits noradrenaline and serotonin reuptake [255].

Once reviewed the anaesthetic protocols of the different studies, we can conclude that pain management is deficient in most of the articles, especially in the ones in rabbits. In addition, the use of local anaesthesia techniques and postoperative pain control are non-standardized practices.

But, what are the implications of choosing an ideal anaesthetic protocol that includes an effective pain management when designing an *in vivo* preclinical trial to evaluate biomaterials? Physiologic response to surgery and pain has been described as "surgical stress response". This phenomenon induced several changes in animals' physiology, such as muscle wasting, weight loss, impaired wound healing and a generalized state of immunosuppression, leading to the appearance of septic complications in the postoperative period. Furthermore, untreated pain can produce a reduction of food and water intake, disrupted sleep, and cause changes in activity and behavior in rodents, which also can delay bone healing [253]. In matter of orthopedic procedures, pain control is also essential, because it favors continued limb usage, and thus, stimulate bone healing [253,256]. So, this is why the concepts of balanced anaesthesia and multimodal analgesia become important, since on the one hand they will help us to achieve a quick recovery and bone healing, and prevent chronic pain [253]. And on the other hand, it will allow us to reduce the possible bias outcomes that pain and stress can exert on animal bone regeneration. The results of Carbone and Austin [252] also suggest that animal post-surgical pain is likely undertreated, likewise poor reporting of pain management can lead to the belief that analgesics are not or cannot be used, and as a consequence, other researchers published their work whit referring neither to pain or its treatment; so finally "under-reporting encourages under-treatment".

The urgent need to provide safe and effective biomaterials for clinical applications creates a demand for reproducible and technically simple bioassay for biomaterials' screening, which must be tested at all stages of preclinical development [257,258]. Animal models play a key role in basic medical research, and many different ones have been used for different applications. [259,260]. However, they encounter ethical, practical, and technical problems which limit their use [260]. For this reason, other alternative preclinical models have gained importance in recent years, thus promoting the incorporation of the 3Rs (Reduction, Replacement and Refinement) in submitted research proposals [258]. Cell cultures have been used as *in vitro* models for over a century and represents an indispensable tool to improve the understanding of cell biology and *in vivo* cell behavior mechanisms [259]. Different cell culture techniques have been developed. 2D monolayer models are simple and efficient to assess a biomaterial's biocompatibility, characterization, and functionality. However they not accurately mimic the natural 3D organization of cells and their extracellular matrix [258,259], and consequently do not fully predict *in vivo* outcomes. This is why 3D cell cultures were developed, offering an opportunity to replace animal models due to their success to replicate a higher number of *in vivo* features by mimicking living organ's organization and microarchitecture (organotypic culture/organoids) [258,259]. Thus, 3D cell cultures allow the study of cell-cell and cell-environment interactions mimicking *in vivo* physiology [258]. Likewise, the chorioallantoic-membrane (CAM) of the chick embryo have demonstrated to be a valuable, short-term, simple and cost-effective assay to test biomaterials, with results comparable to those obtained in mouse trials [257,258,260]. The CAM functions as an organ for gas exchange between the embryo and the environment [257]. Its most common application is examining the angiogenic response as an early indicator of biomaterials' performance *in vivo* [258], because of the close connection between osteogenesis and angiogenesis during bone healing [260]. But this model also allows the evaluation of biocompatibility based on the survival rate of the chick embryos at the experimental end-point, the integration of the implant within the CAM and the presence of a primitive inflammatory response [258]. Finally, another option for the study of angiogenesis is the generation of an arteriovenous loop. This model is helpful in investigating the angiogenesis and biocompatibility but also for the axial vascularization of scaffolds for tissue engineering purposes, in which engineered tissue can be transplanted with its vascular axis and connected to local vessels at the recipient site. The model provides the tissue with oxygen and nutrients immediately after transplantation [261].

5.2 Chapter II: Evaluation of the effect on bone regeneration in rabbit cranial defects of 3D-printed polylactic scaffolds gradually enriched with marine shark-teeth derived bioapatites.

Custom-designed 3D printed scaffold were developed to test the feasibility of shark teeth-derived bioapatites to promote bone regeneration when mixed with PLA for synthesizing composites in a rabbit calvarial defect model. Increasing bioCaP concentrations have been proven to produce several changes in the scaffold properties, some differing from what was expected. However, when implanted *in vivo*, no statistically significant differences were found after histologic and micro-tomographic new bone quantifications between composited and non-composited PLA groups.

When synthesizing 3D-printed composites with bioceramic materials, it should be clear that the main mechanism of bioceramics' bioactivity is the partial dissolution of ionic products *in vivo*, elevating the concentration of calcium and phosphate ions, directly linked with the precipitation of biological apatite on the surface. This precipitation may incorporate various proteins and growth factors that promote cell attachment and function eventually leading to new

bone formation. So, a greater surface area in contact with fluids will lead to faster dissolution rates [60]. Therefore, the improvement in osteogenic potential caused by the addition of the bioceramic materials will be closely related to the percentage of ceramic material exposed on the surface of the scaffold, either at the time of implantation or after the degradation of the polymeric matrix in this case. Since the composition and distribution of HA particles exposed on the surface are critical for cell-material interactions and osteoconductivity [262]. For this purpose, SEM analysis allows an exhaustive analysis of surface topography, identifying exposure points of bioCaP available to provide anchorage for cell spreading and adhesion. Possible control of point-exposed bioceramics in a composite enables the optimization of cell spreading and reduces the problem of deficient adhesion of bioceramics to PLA. However, although bioceramic particles can form a homogeneous suspension with the polymer, the amount of those particles that can appear on the surface may not reflect the average value of the bulk [262,263]. Furthermore, when working with biodegradable materials, factors related to polymer degradation products and their physicochemical and architectural changes must be carefully considered because of their effects on surrounding cells and tissues [263].

The apparition of bioCaP particles on the polymer's surface will have more implications on scaffolds' characteristics. As seen in SEM images, exposed particles increased surface roughness proportional to the amount of bioCaP added. A rougher surface has more area for cell to attach through proteins or integrins on the cell membrane and to proliferate better [262]. Our results are in agreement with those obtained by Corcione *et al.* [240], Wang *et al.* [214] or Wang *et al.* [213], where the addition of HA to a PLA matrix produces an increase in surface roughness.

The main purpose of tissue engineering scaffolding is to provide a platform for cells involved in bone regeneration, being conductive for blood vessel invasion, cell migration, proliferation, differentiation, and communication. Cancellous bone structure is an ideal template for BTE scaffolds, it is spongy and has a porosity of 50-90%, so resembling its mimicry seems to be a reasonable idea for the design of BTE scaffolds [10,214]. In the present study, Micro-CT analysis measured the open porosity of highly interconnected 3D printed composite scaffolds. Results showed a range of measures between 40.301% and 51.38%, which are similar to those obtained in other studies that synthesized 3D printed PLA/bioceramic composites, ranging from 26.4% to 70% [8]. The variations in mean porosity values for the different groups seemed unrelated to the added percentage of bioCaP. These observations were in agreement with those obtained by Wang *et al.* [213], who observed that there was no correlation between the proportion of n-HA and the porosity of the printed sample, being only influenced by the filling rate and shape of the blueprint. However, Corcione *et al.* [240], observed a discrepancy between the theoretical scaffold porosity (50%), and the results obtained for PLA group (39%) and PLA/HA (55%); according to the authors, these differences could be explained by the bigger thickness of the PLA struts and lower percentage of large pores, compared to PLA/HA ones.

In addition, other important biomimetic porous structure parameters, such as pore size or pore accessibility, were measured. Mean pore size value for all the scaffolds in the present study was established 390±10 μm. Optimal pore size is still inconclusive since the change in experimental conditions can yield different results. As discussed above, microporosity improves surface area for protein adsorption, providing attachment points for osteoblasts. Nevertheless, tiny pores are non-conductive to cell migration and communications, leading to non-mineralized osteoid and fibrous tissue formation. Desirable pore sizes for cell growth, blood flux, and adequate mechanical properties should vary between 200 and 600 μm [7,10,13,30,226].

While pore size is essential, the interconnectivity or pore accessibility of the complicated network of pores is crucial to bone ingrowth. Pore accessibility gives the smallest pore constriction between the scaffold edge and any voxel within the scaffold pore space, demonstrating the inability of bone to grow into pores accessible through narrow constrictions [97]. The fabricated scaffolds, according to pore accessibility results, have demonstrated high interconnectivity. Since, at least 87% of interconnectivity was measured through connections as large as 200 μm. Thus, these scaffolds are expected to guarantee sufficient transport of nutrients and metabolism products to allow tissue ingrowth and vascularization for bone regeneration [95]. No similar studies with PLA-Bioceramic composites, including pore accessibility analysis, were found. However, Tiainen *et al.* [95] reported that more than 92% of interconnectivity is achieved through 200 (m) openings in TiO_2 scaffolds with the same method.

Mechanical properties are one of the main scaffold requirements for bone regeneration. PLA is a biopolymer with relatively high strength and modulus, which may vary depending on its molecular weight and degree of crystallinity [72]. Its compressive strength (2 - 39MPa) is similar to that of natural bone (2-12 MPa) [213]. Micro- and nano-bioactive ceramic powders such as hydroxyapatite (HA) were incorporated to increase the printed PLA composites' mechanical strength and osseointegration properties. It has been reported an improvement of the mechanical properties when the content of HA is lower than 15% [50,73,213]. Thus, as indicated in the previous section, balancing the ductility of PLA and the brittleness of CaP is a key issue in regulating composites' mechanical properties [77]. However, Wang *et al.* [213] synthesized PLA-n-HA scaffolds with a percentage from 10 to 50% of the bioceramic material, and results showed that the greater proportion of n-HA, the lower the mechanical strength is. Similar results were obtained by other authors, such as Akindoyo *et al.* [264], who observed a reduction of tensile strength and flexible modulus when adding 5% and 20% of HA; or Corcione *et al.* [240] who appreciated a reduction of scaffold stiffness from 238 MPa to 124 MPa when adding 50% of mesoporous micron-sized spherical HA powder to a PLA matrix. These changes were attributed to morphological and microstructural differences between PLA and PLA-bioceramic groups, such as surface roughness or overall porosity. So, the particles increased the available surface area, but contrary to what was expected, they did not act as reinforcement for the PLA matrix, even when the percentages were lower than 15% [50,240]. Nevertheless, when adding 10%wt or 30%wt of β-TCP to a PLA matrix, synthesized scaffolds demonstrated an increase of the mechanical properties, with an increase of the compressive modulus from 258±102 MPa in PLA group to 349±51 MPa in PLA-30%β-TCP group, achieving values similar to human skull bone (450 MPa) [220].

In the present study, compressive strength and elastic modulus of the scaffolds decreased notably when 12% of bioCaP was added to a PLA matrix, compared to PLA alone, 44MPa vs 28MPa, respectively. However, these results should be analyzed cautiously since, according to the obtained results, changes in the mechanical properties are highly related to variations in open porosity, surface area-to-volume, and strut thickness. Similar correlations among porosity and compressive strength were found by Tiainen *et al.* [95] for TiO_2 scaffolds. Likewise, Chen *et al.* [211] suggested that changing the porosity can enhance the modulus of PLA-n-HA scaffolds. It should be noted that even with the addition of bioCaP particles, the mechanical properties of scaffolds were higher than that of pure HA (5.5 MPa) and natural trabecular bone (2-12 MPa).

Finally, surface wettability is another of the main parameters affecting protein adhesion to biomaterial surface and thus the biological response to an implanted material [265]. Superhydrophilic (contact angle < 2º) and superhydrophobic (contact angle > 150º) polymer surfaces are not favorable for cell attachment and growth [266]. Regarding the wettability of

the scaffolds, adding hydroxyapatite to synthesize a PLA/bioceramic composite is supposed to improve the hydrophilicity of the implant. Zhang *et al.* [77] obtained a reduction of the surface contact angle from 95.9º in PLA group to 87.2º in PLA-30%n-HA or 77.4º in PLA-50%n-HA. However, in our study, the results of the water contact angle showed a greater hydrophobicity of the scaffolds as the percentage of hydroxyapatite increases. This can be explained since as the roughness increases, the hydrophobicity or the hydrophilicity becomes stronger, as stated by the Wenzel model. A higher roughness of a surface will increase the surface area and, consequently, the interface between the liquid and the solid, exacerbating its surface properties. Thus, hydrophilic surfaces will appear more hydrophilic, while a hydrophobic surface will appear more hydrophobic [267,268].

Traditionally, 2D histological and radiographical techniques were used to evaluate the osteointegration of tissue-engineered scaffolds. Despite being unable to provide all the data of a standard histological analysis, micro-CT has emerged as a fast and non-destructive tool to characterize and measure the 3D properties of scaffold or tissue-engineered construct. This technique provides three-dimensional images of bone growing into scaffolds and allows its quantification in the hole volume of the defect region instead of only one slide. Furthermore, unlike bioceramic scaffolds, micro-CT allow an easy detection of newly bone formation in polymeric scaffolds due to its low attenuation [12,97,269]. Thus, it can be concluded that this technique cannot replace histology but can be used as a complementary evaluation method providing information of great interest. Likewise, the present work found a strong correlation between micro-tomographical and histomorphometric results ($p=0.000000837$) when measuring bone regeneration.

After the implantation of the scaffolds in the rabbit calvarial defects, bone regeneration was assessed by micro-tomographical and histomorphometric analysis. Micro-CT results demonstrated no differences among the four groups in BV/TV, BS/BV and Tb.Th; showing PLA-1CaP and PLA-2CaP groups the lowest values for the performed measurements. Likewise, regarding histomorphometric evaluations, statistically significant differences were found only for BS/TS, among PLA and PLA-2CaP groups. Therefore, contrary to what was expected, adding the already mentioned percentages of bioCaP did not seem to have a significant osteogenic effect. Similar studies were developed in rat's calvarial defects by other authors. On the one hand, Gendviliene *et al.* [217] found no statistically significant differences between PLA and PLA-10%HA groups according to micro-CT and histological results, although the amounts of regenerated bone were slightly higher when hydroxyapatite were added. On the other hand, Kwon *et al.* [220] fabricated 3D printed PLA scaffolds with increasing percentages of β-TCP (10% and 30%). *In vivo* trials demonstrated, 12 weeks after implantation, that higher concentrations of the bioceramic were related with higher percentages of newly formed bone (around 10 and 25%, respectively). Likewise, other studies performed in rabbit's femoral diaphysis defects showed similar results. Wang *et al.* [213] implanted 3D-printed PLA composite scaffolds with 10% and 30% of n-HA. It showed statistically significative differences among n-HA0 and n-HA30 groups when analyzing BV/TV in micro-CT, 1, 2 or 3 months after implantation. Finally, Wang *et al.* [214] implanted 3D-printed composite scaffolds with 50% of n-HA and reported also significative differences between PLA and PLA-n-HA groups after 1,2 and 3 months.

As described in the results' section, statistically significant differences were found between PLA and PLA-1CaP groups and PLA-12CaP group when measuring Tb.Pf in micro-CT. This index describes the connectedness of individual trabeculae in a two-dimensional section, thus quantitatively describing the intertrabecular connectivity ratio. Then, results indicate that the addition of bioCaP possessed a positive and significant influence in the connectivity of the

trabecular bone. The same trend was observed for Tb.Th., providing a higher trabecular thickness result for PLA-12CaP. However, no significant differences were found among the different groups when this parameter was micro-tomographically evaluated.

PLA is considered of satisfactory biocompatibility, although some cases of foreign body reactions and inflammatory reactions were reported [75,217,270]. From a qualitative histological analysis point of view, the implanted scaffolds in the present study seemed biocompatible, showing slightly inflammatory effects, without signs of necrosis or presence of foreign debris. Regarding the literature, different histological observations could be appreciated in papers referring to PLA and inflammation. On one side, Wang *et al.* [214] reported that no inflammatory cell aggregation was observed around the printed scaffolds, corroborating PLA's good biocompatibility. Likewise, Chen *et al.* [211] found no inflammatory response or formation of fibrous tissue near or inside the PLA/n-HA scaffold. And Zhang *et al.* [75] studied the cellular inflammatory reaction by hematologic analysis, and no significant differences were detected between treated and non-treated groups. On the other side, Maia-Pinto *et al.* [218] described the presence of connective tissue interspersed with biomaterial and rare inflammatory cells in defects filled with neat PLA, and Gendviliene *et al.* [217] signaled the presence of lymphocytes, mainly in PLA group, and the appearance of connective tissue with different thickness among the groups, which according to histological images seemed to appear between the scaffolds and the newly formed bone. Furthermore, Tcacencu *et al.* [221] synthesized a composite structure based on a PLA porous disk thermally mounted on a apatite-wollastonite (AW, bioceramic material) disk. After implantation, AW, PLA and AW/PLA groups demonstrated biocompatibility and were well integrated into the host tissue, with minimal evidence of inflammatory cell presence. However, when regarding histological images belonging to AW/PLA group, it could be appreciated that bone was mainly in touch with the bioceramic material (AW), and PLA's surface was essentially in contact with fibrous tissue. As it could be seen, the mentioned results agreed with those obtained in present study.

In addition to the aforementioned hydrolytic process, osteoclasts and macrophages are also responsible for resorbing or dissolving bone grafts [7], which could explain the notable presence of macrophages in the PLA-bioCaP scaffolds' periphery. Furthermore, macrophage colonization, giant cell engulfment, and cytokine secretion play a major role in the degradation of calcium phosphates. Thus, their presence is related to the release of calcium phosphate ions from biomaterials, which are very important to induce bone formation and maturation [41].

Regarding to bioceramic materials, the literature reported that they have been successfully used for medical applications in the form of cements, coatings, scaffolds and paste, chiefly bioceramics such as calcium phosphates (HA, β-TCP, etc.) due to their resemblance to bone's mineral phase [39,60]. Chen *et al.* [211] reported some of the reasons for choosing HA as an inorganic filler, which could be extrapolated for the rest of calcium phosphate bioceramics, such as its role in favoring bone reconstruction, improving PLA's osteogenic, osteoconductive, and mechanical properties, and buffering the acidic by-products produced during PLA's degradation, therefore blocking the unfavorable cellular environment. Thus, HA included in composite scaffolds will prolong PLA degradation, reducing the acidity and increasing osteoconductivity of the scaffolds [217]. In our case, the use of shark teeth-derived bioapatites also aims the improvement of PLA's physical and biological properties while simultaneously pursuing the revalorization of fishing by-products. Furthermore, this bioceramic material proved its feasibility to synthesize a composite material mixed with a polymeric matrix, showing mild or absent inflammation after being implanted *in vivo*.

To summarize, low osteogenic capabilities of the fabricated PLA-bioCaP composite implants could be explained as a mixture of the several reasons discussed above. Firstly, the

inflammatory effects of PLA and acidic by-products of its degradation can lead to an unfavorable environment for bone growth. Besides, the amount of bioCaP added to the scaffolds may not be enough to provide the already described buffering effect and modify the polymeric material's hydrophobic surface, since it was further proved that the high HA content (50%) could effectively reduce the acidity of the surrounding microenvironment [77]. Likewise, a low percentage of bioCaP will lead to a low exposure of the bioceramic particles and thus a decrease of the calcium and phosphate available ions for bone regeneration. Gendviliene *et al.* [217] also noticed that an increase in HA concentration can be expected to provide better osteoconductive potential, and be associated with higher levels of new bone formation.

5.3 CHAPTER III: EVALUATION OF THE INFLUENCE OF SCAFFOLD'S GEOMETRIC ARCHITECTURE MODIFICATIONS ON BONE REGENERATION IN CRITICAL-SIZED RABBIT LATERAL FEMORAL CONDYLE DEFECTS

3D-printed scaffolds with different laydown patterns were designed and fabricated in the present Doctoral Thesis to assess their morphological differences through the scaffold's characterization, and their capacity to promote bone regeneration when implanted in critical-sized bone defects. The results showed that helical structure presented higher values of pore size, porosity, and pore accessibility. However, the negative statistically significant correlation between porosity and compressive strength and how the struts were arranged in the helical scaffolds, resulted in lower mechanical properties than the alternate group. Regarding to bone regeneration, newly formed bone obtained results were similar for micro-tomographic and histomorphometric analysis. Respectively, the mean values for both measurements were 9.65±2.34% and 9.24±2,64% when scaffolds with alternate structures were implanted, and 12.94±5.04% and 13.13±4.70%, in the case of the scaffolds with helical structure.

During the last decades, the tissue engineering field has evolved from particulate materials to more complex structures called scaffolds, which provide mechanical support and promote cell growth and vascularization. Furthermore, custom-designed 3D-printings have elevated these structures to another dimension, allowing complete control over the geometry of the implants [29,43,45]. Thus, the scaffolds' design has been postulated as another key aspect when facing bone tissue engineering. So, by understanding how the architectural properties work, a better insight into the optimal structural design to improve bone regeneration could be provided [89].

The structural geometry or design of the scaffold is determined by the position and orientation of the fibers, affecting parameters such as pore size, porosity, mechanical properties, and biological performance [88]. The pore features of the 3D-printed scaffolds play an essential role in cell adhesion, proliferation, and migration [41]. As mentioned previously, a scaffold should be a 3D network with highly interconnected pores. Briefly, macroporosity promotes cell and ion transport, osteogenesis and vascularization; microporosity improves the surface area and roughness, providing attachment points for osteoblast [30,271]. However, currently no consensus on the optimal pore size has been achieved, and mainly approaches include regular and irregular pore structures [41,87]. In addition, porosity and connectivity are both critical parameters closely related to pore size. High porosity and large pores are supposed to enhance bone ingrowth and osseointegration [13,225,272,273]. Despite some reports showing differences in the osteogenic income of implants with different porosities, no beneficial effects of low porosities were reported. Other features, such as the materials' degradation rate and mechanical properties, should be considered when assessing porosity. Those materials with high degradation rates should not have high porosities (>90%) because higher surface areas interacting with host tissue will accelerate degradation due to macrophages via oxidation and/or

hydrolysis. However, those with low degradation rates and robust mechanical properties can be highly porous [271]. Trabecular bone is characterized by a highly trabecular foam-like cellular microstructure, with porosity levels ranging from 50 to 90% and pore sizes of 1 mm, surrounded by cortical bone creating a highly porous environment [41,274].

Alternate and helical structures resulted, respectively, in mean pore sizes of 400±20 μm and 560±6 μm, and porosity of 45±6% and 63±1%. And, after being implanted, helical PLA-bioCaP composite scaffolds achieved higher values of newly formed bone than alternate ones. According to what was stated above, the greater pore size and the larger porosity of the helical structure and a greater available surface area could explain the differences in bone regeneration between both groups. The effect on tissue formation of different 3D-printed scaffold designs has been extensively studied [19,31,35]. However, no similar studies *in vivo* with PLA composites were found.

Larger pore sizes do not always mean a higher percentage of bone regeneration, mainly when working with sizes greater than 800 μm. Liu *et al.* [41] manufactured macro-pore-sized (800, 1200, and 1600 μm) bioceramic scaffolds with identical porosity of 70%. For this purpose, they used biphasic calcium phosphate (BCP), the combination of HA and β-TCP, and they could isolate the importance of pore sizes in a rabbit calvarial defect model by maintaining a constant porosity. The results showed higher BV values for BCP 800 and 1200 groups than for BCP1600. This was explained because the surface area of porous scaffolds is closely related to bone formation, and the specific surface area of the scaffolds decreases with the increasing pore size. Nevertheless, in our study, the scaffolds with greater pore sizes also resulted in higher surface area values due to the differences between alternate and helical laydown patterns.

To study the effect of pore size and permeability, Entezari *et al.* [89] fabricated Strontium doped (Sr-HT-Gahnite) scaffolds with four different architectures, maintaining the same interconnectivity (100%) and similar porosity (49.3±1.9%). Architecture A was a conventional square mesh-like pattern; Architecture B was a double-lined pattern of bimodal pore sizes; Architecture C was a displaced double-layer pattern; and Architecture D was a quatrefoil pattern. Micro-tomographic results showed that architectures B and D presented greater volumes of regenerated bone. Likewise, both presented higher permeability and larger pore sizes than the other two architectures. Authors concluded that higher tortuosity induced by displacing the layers (C) limited nutrient transportation and formed pillar-shaped bone constructs to carry bone loads. They also found that pore sizes to enhance bone formation should range between 390 and 590 μm since larger pores did not show any improvements. Those findings agreed with our results.

Even though the permeability was not analyzed, an equivalent parameter, such as the pore accessibility, was measured. It varies as a function of the scaffolds' porosity and pore size [89], and as reported previously, it reflects the interconnectivity of the network of pores, giving the smallest pore connection (pore throat) between the scaffold edge and any voxel within the scaffold pore space [97]. Pore throat size determines whether cells can enter the pore structure smoothly and affects cell proliferation and differentiation functions since more pore accessibility provides the cells with a larger surface for attachment [87]. *In vivo* trials confirmed these statements, showing higher values of bone formation and better access of cells to the inner parts of the scaffolds in the helical structures, the ones with superior pore accessibility. However, based on the obtained results, both structures should be adequate to ensure mass transfer and oxygen perfusion to allow bone regeneration [88].

Regarding the effect of different laydown patterns, several authors studied their effects *in vitro* and *in vivo*. Domingos *et al.* [275] designed polycaprolactone (PCL) scaffolds varying the pore size from 550 to 750 μm and changing the deposition angle (0º/90º, 0º/60º/120º and

0º/45º/90º/135º), but maintaining a regular filament distance of 650 µm. Increasing the deposition angle achieves quadrangular, triangular, and complex polygonal internal pore geometries without modifying the scaffolds' porosity. Then, biological experiments were carried out using hMSCs (human mesenchymal stem cell) cultures, and a strong influence of pore size and geometry on cell viability was observed. Briefly, larger pore sizes could accommodate more viable cells, probably related to a large surface area and higher porosity. Regarding the influence of pore shape, decreasing deposition angles resulted in incremented cell viability, revealing that quadrangular pores (0º/90º) improved cell accessibility and colonization [275]. Similarly, Kook *et al.* [83] manufactured PCL scaffolds with combinations of different laydown patterns (0º/45º or 0º/90º) and pore sizes (150, 250, and 350 µm), and the optimum scaffold architecture was determined by an MMT assay to measure the proliferation of MC3T3-E1 cells. Nevertheless, highest cell proliferation was observed in scaffolds with 0º/45º strut layout pattern and 150 µm pore size; thus, based on these results, authors selected scaffolds with 45º/150 µm and 45º/350 µm for *in vivo* trials. Their results agreed with those obtained in the present study but were contrary to those obtained by Domingos *et al.* [275], who found that the most suitable laydown pattern *in vitro* was 0º/90º. After *in vivo* implantation, Kook *et al.* [83] found that the scaffolds with 150 µm pore size achieved higher amounts of newly formed bone than those with 350 µm, which is controversial considering the abovementioned results and reviewed literature. Variations in pore shape for bone regeneration were also studied by Berner *et al.* [34], who used different laydown patterns, and developed silanized polycaprolactone/tricalcium phosphate scaffolds with 0º/90º and 0º/60º/120º fiber orientations and implanted them in rat skull defects. The analysis showed that a higher degree of newly formed bone was observed in 0º/90º scaffolds, compared to 0º/60º/120º ones, where the bone formation was closer to the host bone with less ingrowth to the center of the scaffold. The authors reported that differences could not only be explained by the variations in higher porosity, large pore size, and lower surface area of the 0º/90º groups, but rather that struts' architecture must also play a main role in bone formation.

The absence of a unanimous agreement on optimal pore size and shape can be attributed to the variability in materials employed and the specific sites of implantation [10]. Additionally, the body of research examining scaffold geometry through *in vivo* studies is comparatively small.

In addition, one of the challenges when studying the effects of pore shape is the lack of isolation of architectural parameters. Mirkhalaf *et al.* [85] synthesized Baghdadite 3D-printed scaffolds with 5 different structures, maintaining similar values of pore size (500 µm), porosity (50%) and surface-to-volume ratio (10 mm^{-1}). They were implanted in rabbit cranial defects to assess the effects of the surface convexity (cylindrical struts with convex surfaces vs. concave surfaces), the relative orientation of the scaffold concerning the defect site (scaffolds with cubic pores vs. rotated cubic pores), and interconnectivity (body-centered cubic scaffold). The results showed that only pore interconnectivity significantly affected the scaffold's bone tissue regeneration capacity, which is in agreement with the data obtained from alternate and helical structures, where the one with greater interconnectivity got better results in bone regeneration trials.

Another important requirement for bone regeneration is the degradability of the implants, which, regardless of the material, is closely related to the porosity, the pore size, and the interconnectivity. In the present Doctoral Thesis, the degradation of the scaffolds was subjectively more evident in the helical group, with lower values of IS/TS and a lack of connection between the struts in the histological sections. As mentioned above, the degradation pattern of porous structures is linked to pore size, so smaller pores result in slower hydrolysis

and, thus, low degradation rates. As expected, the same happens with the porosity since higher values result in further permeability and faster degradation. Likewise, it was observed that scaffolds with large pore sizes and lower porosity degraded faster than those with smaller pore sizes and higher porosity due to the effect of higher available surfaces in scaffolds with macropores [41,226]. Besides, scaffolds with square pores provided faster degradability and higher weight loss than other pore morphologies such as triangular or parallelogram [276]. However, Domingos *et al.* [277] reported after *in vitro* degradation studies that the degradation rate of PCL scaffolds was notably affected by porosity and pore size, since 0º/90º and 0º/45º/90º/135º filament orientations resulted in similar degradation rates when porosity and pore size values remained similar.

The scaffold design also has an essential effect on the mechanical properties of the scaffolds since as porosity and mean pore size increase, the mechanical strength is sacrificed. Thus, an adequate balance among these parameters is essential for synthesizing an ideal scaffold for bone tissue engineering [13]. The present work shows that helical structures have demonstrated much lower mechanical properties than alternate structures. Furthermore, this lack of mechanical resistance in helical scaffolds could be the reason for the fracture of two femoral condyles after the scaffold's implantation in rabbits, even though their compressive strength values were within the range for those stipulated for natural bone (2-12 MPa) [213]. Similarly, Domingos *et al.* [275] reported that increases in pore size, reductions in laydown patterns' deposition angle or increases in the number of deposition angles (from 0º/90º to 0º/45º/90º/135º) resulted in scaffolds with lower compressive modulus, and therefore in weaker structures. Regarding to pore size, the compressive modulus decreases from 52.5±4.5 MPa to 23.1±2.8 MPa, and referring to deposition angle, the measurements showed reductions from 34.2±3.8 MPa to 19.1±2.8 MPa. The authors' explanation for these results was the larger fused area between struts occasioned by a reduced deposition angle, leading to lower local stress experienced by scaffolds and a greater ease of sliding, increasing consequently the scaffold's deformability [275,278,279]. Furthermore, high mechanical properties in scaffolds with 0º/90º and 0º/60º/120º laydown patterns are related to the aligned crossover points on every layer. By contrast, 0º/45º/90º/135º orientations produced misaligned crossover points among different layers, and thus the elastic modulus may be lower [88]. Nevertheless, Liu *et al.* [41], who synthesized scaffold using a brittle material such as BCP, observed that an increase in the size of the macropores resulted in similar compressive strength values.

Regarding differences between scaffolds with aligned or staggered fibers, many authors confirmed that staggered filaments had notably lower mechanical properties than aligned filaments, as reviewed by Gleadall *et al.* [88]. Specifically, Serra *et al.* [280] described that PLA-based composite scaffolds with staggered fibers showed 50-75% lower elastic modulus than others with aligned fibers. Likewise, regarding the mechanism by which scaffolds collapse, it could be appreciated that a solid column from the top to the bottom of the scaffolds, as it happened in those structures with 0º/90ª laydown patterns, provide them with a pillar that strongly resists compression. When fibers are staggered, such as 0º/45º/90º/135º/180º laydown patterns, filaments bend slightly and the structure easily collapses in a concertina manner [88].

The present chapter delved deeper into how specific scaffold designs resulted in significant changes in pore size, porosity, interconnectivity, available implant surface, and mechanical properties. But it also demonstrated, through the implantation of the scaffolds in an animal model, the effects of these modifications on bone regeneration, with their subsequent implications in the context of bone tissue engineering. Thus, the results confirmed the initial hypothesis since they demonstrated that scaffold architecture could influence bone regeneration capabilities. Critical defects were performed in a rabbit femoral condyle model, which allowed

us to confirm the advantages of using scaffolds with 0º/45º/90º/135º/180º (helical) orientations. As described above, laydown patterns have greatly influenced the implant's characteristics and suitability for bone graft use. Changes deriving from printing paths, which theoretically should trigger a series of biological changes *in vivo*, favored, or hindered bone ingrowth through different mechanisms. Mainly by facilitating or not facilitating the access of cells and new vessels to the inner part of the scaffolds, but also because of their differences in degradability rate.

5.4 LIMITATIONS OF THE STUDY

The impossibility of manufacturing scaffolds with bioCaP concentrations higher than 12% due to the selected nozzle size, limited us in obtaining implants with greater osteogenic capabilities. The lack of degradation analysis prevents us from ensuring different degradability rates among the synthesized structures, as well as analyzing its buffering capacities in an acidified environment and its implications on scaffold's mechanical integrity. And in addition, the absence of long-term clinical trials, the low number of animals used in the study, the absence of an empty negative control, and the variable distribution and limited amount of trabecular bone in rabbit models, represented some constrains that can limit the scope of the study and should be addressed in future investigations.

5.5 FUTURE RESEARCH

Controversial published results regarding scaffold's composition and architecture, as presented in this section, highlighted the importance of further investigations on this topic to validate and expand the knowledge.

Further research should be performed to improve implant's osteogenic capabilities. One widely used alternative is the addition of different substances to functionalize the scaffolds (growth factors, rhBMP-2, stem cells, etc.), showing successful results as reported in *Chapter I* of the present Doctoral Thesis. Another possible strategy could be the combination of the synthesis of composite scaffolds with a biomimetic mineralization by using calcium phosphate coatings, as described by Maia-Pinto *et al.* [218]. In addition, scaffold's surface hydrophobicity and environment acidification are some issues that should be addressed to avoid inflammation signs and favor the bone healing process.

Likewise, synthesizing and comparing a wider variety of scaffold laydown patterns could provide more interesting information regarding scaffold characterization and degradation analysis. Besides, the analysis of their osteogenic capabilities in *in vivo* trials is also crucial since *in vitro* findings are not always correlated to *in vivo* ones [38]. New alternative approaches may also be used to search highly porous and interconnected but, at the same time, resistant structures. A possible alternative are the bimodal pore topologies, described by Entezari *et al.* [35], which allowed the creation of larger pores without increasing porosity or sacrificing mechanical properties, or the combination of different laydown patterns, such as 0º/90º/180º and 0º/45º/90º/135º/180º orientations, to achieve porous structures that facilitate bone ingrowth without compromising its mechanical resistance.

Challenges in the clinical adoption of 3D-printed scaffolds include the need for medical-grade materials, fabrication costs for patient-specific products, clinician training, and scaffold sterilization [38]. Research and additive manufacturing efforts must focus on these areas to enhance clinical applicability. Adapting techniques for bone applications to weight-bearing sites, like long bone defects, is complex due to different bone environments and implant requirements. Therefore, extensive pre-clinical studies are crucial for clinical relevance, particularly on larger animals at intended implantation sites.

CONCLUSIONS

6 CONCLUSIONS

I. After being successfully tested in preclinical trials in rabbit and rat models, 3D-printed composite scaffolds have demonstrated to be a promising alternative for treating bone defects in human and veterinary medicine. Composite scaffolds have been proven to be biocompatible and mechanically resistant when implanted *in vivo*. Furthermore, no adverse reactions that could impair bone growth were reported, and the incorporation of higher amounts of bioceramics to a polymeric matrix was positively related with bone formation. The use of different substances and techniques to functionalize the scaffolds has also improved their biological activity and enhanced their bone regeneration capabilities. Nevertheless, a refinement and standardization on the design of experimental processes and anaesthetic protocols is needed to reduce the risk of bias and provide quality information to help the research community.

II. Gradually enriched PLA-bioCaP composite scaffolds were successfully manufactured using fused deposition modeling. The implants were characterized and despite their low hydrophilic behavior, they showed suitable properties for their use in bone tissue engineering. These findings were later corroborated, demonstrating a favorable biocompatibility and making evident their possible use as bone substitutes in repairing defects in humans and animals. However, the gradual enrichment of the polymeric matrix, contrary to what was expected, did not increase the scaffold's osteogenic potential. Something that should be addressed in future investigations to achieve an optimal application of the implants.

III. PLA-bioCaP composite scaffolds with alternate and helical laydown patterns were designed and fabricated to delve into the understanding of the impact of scaffold architectures on bone regeneration. The results revealed that both designs were biocompatible, and support and facilitate bone growth in load-bearing sites, with the helical structures showing a notable advantage in enhanced bone regeneration due to their larger pore size and increased porosity and accessible porosity. However, this architectural benefit comes at the cost of reduced mechanical strength, posing several limitations for their applications. These findings highlight scaffolds architecture's critical role in bone tissue engineering and the intricate balance required between mechanical stability and scaffold porosity for optimal bone healing. The insights gained from this work are instrumental for future advancements in scaffold design, particularly for applications involving critical-sized bone defects.

BIBLIOGRAFÍA

7 BIBLIOGRAFÍA

[1] Tumedei, Savadori, Del Fabbro, Synthetic Blocks for Bone Regeneration: A Systematic Review and Meta-Analysis, IJMS 20 (2019) 4221. https://doi.org/10.3390/ijms20174221.

[2] L. Roseti, V. Parisi, M. Petretta, C. Cavallo, G. Desando, I. Bartolotti, B. Grigolo, Scaffolds for Bone Tissue Engineering: State of the art and new perspectives, Materials Science and Engineering: C 78 (2017) 1246–1262. https://doi.org/10.1016/j.msec.2017.05.017.

[3] D. Tang, R.S. Tare, L.-Y. Yang, D.F. Williams, K.-L. Ou, R.O.C. Oreffo, Biofabrication of bone tissue: approaches, challenges and translation for bone regeneration, Biomaterials 83 (2016) 363–382. https://doi.org/10.1016/j.biomaterials.2016.01.024.

[4] G. Fernandez de Grado, L. Keller, Y. Idoux-Gillet, Q. Wagner, A.-M. Musset, N. Benkirane-Jessel, F. Bornert, D. Offner, Bone substitutes: a review of their characteristics, clinical use, and perspectives for large bone defects management, J Tissue Eng 9 (2018) 204173141877681. https://doi.org/10.1177/2041731418776819.

[5] A. Ho-Shui-Ling, J. Bolander, L.E. Rustom, A.W. Johnson, F.P. Luyten, C. Picart, Bone regeneration strategies: Engineered scaffolds, bioactive molecules and stem cells current stage and future perspectives, Biomaterials 180 (2018) 143–162. https://doi.org/10.1016/j.biomaterials.2018.07.017.

[6] M. Majidinia, A. Sadeghpour, B. Yousefi, The roles of signaling pathways in bone repair and regeneration, J Cell Physiol 233 (2018) 2937–2948. https://doi.org/10.1002/jcp.26042.

[7] H.J. Haugen, S.P. Lyngstadaas, F. Rossi, G. Perale, Bone grafts: which is the ideal biomaterial?, J Clin Periodontol 46 (2019) 92–102. https://doi.org/10.1111/jcpe.13058.

[8] I. Alonso-Fernández, H.J. Haugen, M. López-Peña, A. González-Cantalapiedra, F. Muñoz, Use of 3D-printed polylactic acid/bioceramic composite scaffolds for bone tissue engineering in preclinical in vivo studies: A systematic review, Acta Biomaterialia 168 (2023) 1–21. https://doi.org/10.1016/j.actbio.2023.07.013.

[9] S. Hosseinpour, M. Ghazizadeh Ahsaie, M. Rezai Rad, M.T. Baghani, S.R. Motamedian, A. Khojasteh, Application of selected scaffolds for bone tissue engineering: a systematic review, Oral Maxillofac Surg 21 (2017) 109–129. https://doi.org/10.1007/s10006-017-0608-3.

[10] G. Zhu, T. Zhang, M. Chen, K. Yao, X. Huang, B. Zhang, Y. Li, J. Liu, Y. Wang, Z. Zhao, Bone physiological microenvironment and healing mechanism: Basis for future bone-tissue engineering scaffolds, Bioactive Materials 6 (2021) 4110–4140. https://doi.org/10.1016/j.bioactmat.2021.03.043.

[11] M. Gazińska, A. Krokos, M. Kobielarz, M. Włodarczyk, P. Skibińska, B. Stępak, A. Antończak, M. Morawiak, P. Płociński, K. Rudnicka, Influence of Hydroxyapatite Surface Functionalization on Thermal and Biological Properties of Poly(l-Lactide)- and Poly(l-Lactide-co-Glycolide)-Based Composites, IJMS 21 (2020) 6711. https://doi.org/10.3390/ijms21186711.

[12] A.C. Jones, B. Milthorpe, H. Averdunk, A. Limaye, T.J. Senden, A. Sakellariou, A.P. Sheppard, R.M. Sok, M.A. Knackstedt, A. Brandwood, D. Rohner, D.W. Hutmacher, Analysis of 3D bone ingrowth into polymer scaffolds via micro-computed tomography imaging, Biomaterials 25 (2004) 4947–4954. https://doi.org/10.1016/j.biomaterials.2004.01.047.
[13] A.R. Amini, C.T. Laurencin, S.P. Nukavarapu, Bone Tissue Engineering: Recent Advances and Challenges, (2013).
[14] N. Xue, X. Ding, R. Huang, R. Jiang, H. Huang, X. Pan, W. Min, J. Chen, J.-A. Duan, P. Liu, Y. Wang, Bone Tissue Engineering in the Treatment of Bone Defects, Pharmaceuticals 15 (2022) 879. https://doi.org/10.3390/ph15070879.
[15] H. Shao, A. Liu, X. Ke, M. Sun, Y. He, X. Yang, J. Fu, L. Zhang, G. Yang, Y. Liu, S. Xu, Z. Gou, 3D robocasting magnesium-doped wollastonite/TCP bioceramic scaffolds with improved bone regeneration capacity in critical sized calvarial defects, J. Mater. Chem. B 5 (2017) 2941–2951. https://doi.org/10.1039/C7TB00217C.
[16] F. Gang, W. Ye, C. Ma, W. Wang, Y. Xiao, C. Liu, X. Sun, 3D Printing of PLLA/Biomineral Composite Bone Tissue Engineering Scaffolds, MATERIALS 15 (2022). https://doi.org/10.3390/ma15124280.
[17] C.H. Roux, Impact of musculoskeletal disorders on quality of life: an inception cohort study, Annals of the Rheumatic Diseases 64 (2005) 606–611. https://doi.org/10.1136/ard.2004.020784.
[18] S. Safiri, A. Kolahi, M. Cross, C. Hill, E. Smith, K. Carson-Chahhoud, M.A. Mansournia, A. Almasi-Hashiani, A. Ashrafi-Asgarabad, J. Kaufman, M. Sepidarkish, S.K. Shakouri, D. Hoy, A.D. Woolf, L. March, G. Collins, R. Buchbinder, Prevalence, Deaths, and Disability-Adjusted Life Years Due to Musculoskeletal Disorders for 195 Countries and Territories 1990–2017, Arthritis & Rheumatology 73 (2021) 702–714. https://doi.org/10.1002/art.41571.
[19] K. Storheim, J.-A. Zwart, Musculoskeletal disorders and the Global Burden of Disease study, Ann Rheum Dis 73 (2014) 949–950. https://doi.org/10.1136/annrheumdis-2014-205327.
[20] R. Govaerts, B. Tassignon, J. Ghillebert, B. Serrien, S. De Bock, T. Ampe, I. El Makrini, B. Vanderborght, R. Meeusen, K. De Pauw, Prevalence and incidence of work-related musculoskeletal disorders in secondary industries of 21st century Europe: a systematic review and meta-analysis, BMC Musculoskelet Disord 22 (2021) 751. https://doi.org/10.1186/s12891-021-04615-9.
[21] R.H. Osborne, M. Nikpour, L. Busija, V. Sundararajan, I.P. Wicks, Prevalence and cost of musculoskeletal disorders: a population-based, public hospital system healthcare consumption approach, J Rheumatol 34 (2007) 2466–2475.
[22] D.G. O′Neill, D.B. Church, P.D. McGreevy, P.C. Thomson, D.C. Brodbelt, Prevalence of Disorders Recorded in Dogs Attending Primary-Care Veterinary Practices in England, PLoS ONE 9 (2014) e90501. https://doi.org/10.1371/journal.pone.0090501.
[23] D.G. O'Neill, H. James, D.C. Brodbelt, D.B. Church, C. Pegram, Prevalence of commonly diagnosed disorders in UK dogs under primary veterinary care: results and applications, BMC Veterinary Research 17 (2021) 1–14. https://doi.org/10.1186/s12917-021-02775-3.
[24] L.M. Freeman, S.K. Abood, A.J. Fascetti, L.M. Fleeman, K.E. Michel, D.P. Laflamme, C. Bauer, B.L.E. Kemp, J.R. Van Doren, K.N. Willoughby, Disease prevalence among dogs and cats in the United States and Australia and proportions of dogs and cats that

receive therapeutic diets or dietary supplements, Javma 229 (2006) 531–534. https://doi.org/10.2460/javma.229.4.531.

[25] D.G. O'Neill, D. Gunn-Moore, S. Sorrell, H. McAuslan, D.B. Church, C. Pegram, D.C. Brodbelt, Commonly diagnosed disorders in domestic cats in the UK and their associations with sex and age, Journal of Feline Medicine and Surgery 25 (2023) 1098612X2311550. https://doi.org/10.1177/1098612X231155016.

[26] D.G. O'Neill, D.B. Church, P.D. McGreevy, P.C. Thomson, D.C. Brodbelt, Prevalence of disorders recorded in cats attending primary-care veterinary practices in England, The Veterinary Journal 202 (2014) 286–291. https://doi.org/10.1016/j.tvjl.2014.08.004.

[27] M.N. Hassan, M.A. Yassin, S. Suliman, S.A. Lie, H. Gjengedal, K. Mustafa, The bone regeneration capacity of 3D-printed templates in calvarial defect models: A systematic review and meta-analysis, Acta Biomaterialia 91 (2019) 1–23. https://doi.org/10.1016/j.actbio.2019.04.017.

[28] B.I. Oladapo, S.A. Zahedi, S.O. Ismail, D.B. Olawade, Recent advances in biopolymeric composite materials: Future sustainability of bone-implant, Renewable and Sustainable Energy Reviews 150 (2021) 111505. https://doi.org/10.1016/j.rser.2021.111505.

[29] J.-W. Kim, B.-E. Yang, S.-J. Hong, H.-G. Choi, S.-J. Byeon, H.-K. Lim, S.-M. Chung, J.-H. Lee, S.-H. Byun, Bone Regeneration Capability of 3D Printed Ceramic Scaffolds, IJMS 21 (2020) 4837. https://doi.org/10.3390/ijms21144837.

[30] S.G. Pedrero, P. Llamas-Sillero, J. Serrano-López, A Multidisciplinary Journey towards Bone Tissue Engineering, Materials 14 (2021) 4896. https://doi.org/10.3390/ma14174896.

[31] Histologia: texto y atlas correlación con biología celular y molecular, 8ª ed, Wolters Kluwer, Barcelona, 2020.

[32] S. Bose, S. Vahabzadeh, A. Bandyopadhyay, Bone tissue engineering using 3D printing, Materials Today 16 (2013) 496–504. https://doi.org/10.1016/j.mattod.2013.11.017.

[33] Y. Li, S.K. Chen, L. Li, L. Qin, X.L. Wang, Y.X. Lai, Bone defect animal models for testing efficacy of bone substitute biomaterials, Journal of Orthopaedic Translation 3 (2015) 95–104. https://doi.org/10.1016/j.jot.2015.05.002.

[34] A. Berner, M.A. Woodruff, C.X.F. Lam, M.T. Arafat, S. Saifzadeh, R. Steck, J. Ren, M. Nerlich, A.K. Ekaputra, I. Gibson, D.W. Hutmacher, Effects of scaffold architecture on cranial bone healing, International Journal of Oral and Maxillofacial Surgery 43 (2014) 506–513. https://doi.org/10.1016/j.ijom.2013.05.008.

[35] G. Brunello, S. Sivolella, R. Meneghello, L. Ferroni, C. Gardin, A. Piattelli, B. Zavan, E. Bressan, Powder-based 3D printing for bone tissue engineering, Biotechnology Advances 34 (2016) 740–753. https://doi.org/10.1016/j.biotechadv.2016.03.009.

[36] A.V. Do, R. Smith, T.M. Acri, S.M. Geary, A.K. Salem, 3D printing technologies for 3D scaffold engineering, Elsevier Ltd, 2018. https://doi.org/10.1016/B978-0-08-100979-6.00009-4.

[37] A. Saberi, A. Behnamghader, B. Aghabarari, A. Yousefi, D. Majda, M.V.M. Huerta, M. Mozafari, 3D direct printing of composite bone scaffolds containing polylactic acid and spray dried mesoporous bioactive glass-ceramic microparticles, International Journal of Biological Macromolecules 207 (2022) 9–22. https://doi.org/10.1016/j.ijbiomac.2022.02.067.

[38] C. Garot, G. Bettega, C. Picart, Additive Manufacturing of Material Scaffolds for Bone Regeneration: Toward Application in the Clinics, Adv. Funct. Mater. 31 (2021) 2006967. https://doi.org/10.1002/adfm.202006967.

[39] G. Brunello, S. Panda, L. Schiavon, S. Sivolella, L. Biasetto, M.D. Fabbro, The impact of bioceramic scaffolds on bone regeneration in preclinical in vivo studies: A systematic review, Materials 13 (2020) 1–26. https://doi.org/10.3390/ma13071500.
[40] L. Polo-Corrales, M. Latorre-Esteves, J.E. Ramirez-Vick, Scaffold Design for Bone Regeneration, J. Nanosci. Nanotech. 14 (2014) 15–56. https://doi.org/10.1166/jnn.2014.9127.
[41] F. Liu, Y. Liu, X. Li, X. Wang, D. Li, S. Chung, C. Chen, I.-S. Lee, Osteogenesis of 3D printed macro-pore size biphasic calcium phosphate scaffold in rabbit calvaria, J Biomater Appl 33 (2019) 1168–1177. https://doi.org/10.1177/0885328218825177.
[42] S. Hammouche, D. Hammouche, M. McNicholas, Biodegradable Bone Regeneration Synthetic Scaffolds: in Tissue Engineering, CSCR 7 (2012) 134–142. https://doi.org/10.2174/157488812799219018.
[43] H.K. Lim, S.J. Hong, S.J. Byeon, S.M. Chung, S.W. On, B.E. Yang, J.H. Lee, S.H. Byun, 3D-printed ceramic bone scaffolds with variable pore architectures, International Journal of Molecular Sciences 21 (2020) 1–12. https://doi.org/10.3390/ijms21186942.
[44] S.-H. Lee, K.-G. Lee, J.-H. Hwang, Y.S. Cho, K.-S. Lee, H.-J. Jeong, S.-H. Park, Y. Park, Y.-S. Cho, B.-K. Lee, Evaluation of mechanical strength and bone regeneration ability of 3D printed kagome-structure scaffold using rabbit calvarial defect model, Materials Science and Engineering: C 98 (2019) 949–959. https://doi.org/10.1016/j.msec.2019.01.050.
[45] J. Yun, J. Lee, C.W. Ha, S.J. Park, S. Kim, K. Koo, Y. Seol, Y. Lee, The effect of 3-D printed polylactic acid scaffold with and without hyaluronic acid on bone regeneration, Journal of Periodontology (2022) 1–11. https://doi.org/10.1002/jper.21-0428.
[46] H. Pae, J. Kang, J. Cha, J. Lee, J. Paik, U. Jung, B. Kim, S. Choi, 3D-printed polycaprolactone scaffold mixed with β-tricalcium phosphate as a bone regenerative material in rabbit calvarial defects, J. Biomed. Mater. Res. 107 (2019) 1254–1263. https://doi.org/10.1002/jbm.b.34218.
[47] M.S. Singhvi, S.S. Zinjarde, D.V. Gokhale, Polylactic acid: synthesis and biomedical applications, Journal of Applied Microbiology 127 (2019) 1612–1626. https://doi.org/10.1111/jam.14290.
[48] X. Wang, M. Jiang, Z. Zhou, J. Gou, D. Hui, 3D printing of polymer matrix composites: A review and prospective, Composites Part B: Engineering 110 (2017) 442–458. https://doi.org/10.1016/j.compositesb.2016.11.034.
[49] M. Bouyer, C. Garot, P. Machillot, J. Vollaire, V. Fitzpatrick, S. Morand, J. Boutonnat, V. Josserand, G. Bettega, C. Picart, 3D-printed scaffold combined to 2D osteoinductive coatings to repair a critical-size mandibular bone defect, Materials Today Bio 11 (2021) 100113. https://doi.org/10.1016/j.mtbio.2021.100113.
[50] M. Milazzo, N. Contessi Negrini, S. Scialla, B. Marelli, S. Farè, S. Danti, M.J. Buehler, Additive Manufacturing Approaches for Hydroxyapatite-Reinforced Composites, Adv Funct Materials 29 (2019) 1903055. https://doi.org/10.1002/adfm.201903055.
[51] X. Du, S. Fu, Y. Zhu, 3D printing of ceramic-based scaffolds for bone tissue engineering: an overview, J. Mater. Chem. B 6 (2018) 4397–4412. https://doi.org/10.1039/C8TB00677F.
[52] D.W. Hutmacher, M. Sittinger, M.V. Risbud, Scaffold-based tissue engineering: rationale for computer-aided design and solid free-form fabrication systems, Trends in Biotechnology 22 (2004) 354–362. https://doi.org/10.1016/j.tibtech.2004.05.005.

[53] J.M. Latimer, S. Maekawa, Y. Yao, D.T. Wu, M. Chen, W.V. Giannobile, Regenerative Medicine Technologies to Treat Dental, Oral, and Craniofacial Defects, Front. Bioeng. Biotechnol. 9 (2021) 704048. https://doi.org/10.3389/fbioe.2021.704048.
[54] L.M. Ricles, J.C. Coburn, M. Di Prima, S.S. Oh, Regulating 3D-printed medical products, Sci. Transl. Med. 10 (2018) eaan6521. https://doi.org/10.1126/scitranslmed.aan6521.
[55] J.B. Park, R.S. Lakes, Biomaterials: an introduction, 3rd ed, Springer, New York, 2007.
[56] W.R. Moore, S.E. Graves, G.I. Bain, Synthetic bone graft substitutes, ANZ J Surg 71 (2001) 354–361.
[57] Y. Zhang, T. Lin, H. Meng, X. Wang, H. Peng, G. Liu, S. Wei, Q. Lu, Y. Wang, A. Wang, W. Xu, H. Shao, J. Peng, 3D gel-printed porous magnesium scaffold coated with dibasic calcium phosphate dihydrate for bone repair in vivo, Journal of Orthopaedic Translation 33 (2022) 13–23. https://doi.org/10.1016/j.jot.2021.11.005.
[58] G. Turnbull, J. Clarke, F. Picard, P. Riches, L. Jia, F. Han, B. Li, W. Shu, 3D bioactive composite scaffolds for bone tissue engineering, Bioactive Materials 3 (2018) 278–314. https://doi.org/10.1016/j.bioactmat.2017.10.001.
[59] A.A. Al-allaq, J.S. Kashan, A review: In vivo studies of bioceramics as bone substitute materials, Nano Select 4 (2023) 123–144. https://doi.org/10.1002/nano.202200222.
[60] N. Eliaz, N. Metoki, Calcium Phosphate Bioceramics: A Review of Their History, Structure, Properties, Coating Technologies and Biomedical Applications, Materials 10 (2017) 334. https://doi.org/10.3390/ma10040334.
[61] E. Schätzlein, C. Kicker, N. Söhling, U. Ritz, J. Neijhoft, D. Henrich, J. Frank, I. Marzi, A. Blaeser, 3D-Printed PLA-Bioglass Scaffolds with Controllable Calcium Release and MSC Adhesion for Bone Tissue Engineering, Polymers 14 (2022) 2389. https://doi.org/10.3390/polym14122389.
[62] S. Sultan, N. Thomas, M. Varghese, Y. Dalvi, S. Joy, S. Hall, A.P. Mathew, The Design of 3D-Printed Polylactic Acid–Bioglass Composite Scaffold: A Potential Implant Material for Bone Tissue Engineering, Molecules 27 (2022) 7214. https://doi.org/10.3390/molecules27217214.
[63] M. Cannio, D. Bellucci, J.A. Roether, Dino.N. Boccaccini, V. Cannillo, Bioactive Glass Applications: A Literature Review of Human Clinical Trials, Materials 14 (2021) 5440. https://doi.org/10.3390/ma14185440.
[64] S. Dorozhkin, Medical Application of Calcium Orthophosphate Bioceramics, BIO 1 (2011) 1–51. https://doi.org/10.5618/bio.2011.v1.n1.1.
[65] S. Fukuba, M. Okada, K. Nohara, T. Iwata, Alloplastic Bone Substitutes for Periodontal and Bone Regeneration in Dentistry: Current Status and Prospects, Materials 14 (2021) 1096. https://doi.org/10.3390/ma14051096.
[66] C. Stacchi, T. Lombardi, F. Oreglia, A. Alberghini Maltoni, T. Traini, Histologic and Histomorphometric Comparison between Sintered Nanohydroxyapatite and Anorganic Bovine Xenograft in Maxillary Sinus Grafting: A Split-Mouth Randomized Controlled Clinical Trial, BioMed Research International 2017 (2017) 1–10. https://doi.org/10.1155/2017/9489825.
[67] M. López-Álvarez, E. Vigo, C. Rodríguez-Valencia, V. Outeiriño-Iglesias, P. González, J. Serra, *In vivo* evaluation of shark teeth-derived bioapatites, Clin. Oral Impl. Res. 28 (2017) e91–e100. https://doi.org/10.1111/clr.12934.
[68] M. García-González, F.M. Muñoz Guzón, A. González-Cantalapiedra, P.M. González-Fernández, R. Otero Pérez, J.A. Serra Rodríguez, Application of Shark Teeth–Derived Bioapatites as a Bone Substitute in Veterinary Orthopedics. Preliminary Clinical Trial in

Dogs and Cats, Front. Vet. Sci. 7 (2020) 574017. https://doi.org/10.3389/fvets.2020.574017.
[69] M. López-Álvarez, S. Pérez-Davila, C. Rodríguez-Valencia, P. González, J. Serra, The improved biological response of shark tooth bioapatites in a comparative *in vitro* study with synthetic and bovine bone grafts, Biomed. Mater. 11 (2016) 035011. https://doi.org/10.1088/1748-6041/11/3/035011.
[70] J. Rojas-Lozano, P. Días-Rodriguez, P. Barreiro, E. López-Senraa, C. Rodríguez-Valencia, M. López-Álvarez, M. Landín, P. González, P. Serra, Desarrollo de nuevos filamentos para impresión 3D basados en cerámicas bioinspiradoras., Materiales Compuestos 3 (2019) 65–69.
[71] H. Zhou, J.G. Lawrence, S.B. Bhaduri, Fabrication aspects of PLA-CaP/PLGA-CaP composites for orthopedic applications: A review, Acta Biomaterialia 8 (2012) 1999–2016. https://doi.org/10.1016/j.actbio.2012.01.031.
[72] V. DeStefano, S. Khan, A. Tabada, Applications of PLA in modern medicine, Engineered Regeneration 1 (2020) 76–87. https://doi.org/10.1016/j.engreg.2020.08.002.
[73] E.H. Tümer, H.Y. Erbil, Extrusion-Based 3D Printing Applications of PLA Composites: A Review, Coatings 11 (2021) 390. https://doi.org/10.3390/coatings11040390.
[74] R.A. Ilyas, S.M. Sapuan, M.M. Harussani, M.Y.A.Y. Hakimi, M.Z.M. Haziq, M.S.N. Atikah, M.R.M. Asyraf, M.R. Ishak, M.R. Razman, N.M. Nurazzi, M.N.F. Norrrahim, H. Abral, M. Asrofi, Polylactic acid (Pla) biocomposite: Processing, additive manufacturing and advanced applications, Polymers 13 (2021). https://doi.org/10.3390/polym13081326.
[75] H. Zhang, X. Mao, Z. Du, W. Jiang, X. Han, D. Zhao, D. Han, Q. Li, Three dimensional printed macroporous polylactic acid/hydroxyapatite composite scaffolds for promoting bone formation in a critical-size rat calvarial defect model, Science and Technology of Advanced Materials 17 (2016) 136–148. https://doi.org/10.1080/14686996.2016.1145532.
[76] Q. Yao, J.G.L. Cosme, T. Xu, J.M. Miszuk, P.H.S. Picciani, H. Fong, H. Sun, Three dimensional electrospun PCL/PLA blend nanofibrous scaffolds with significantly improved stem cells osteogenic differentiation and cranial bone formation, BIOMATERIALS 115 (2017) 115–127. https://doi.org/10.1016/j.biomaterials.2016.11.018.
[77] B. Zhang, L. Wang, P. Song, X. Pei, H. Sun, L. Wu, C. Zhou, K. Wang, Y. Fan, X. Zhang, 3D printed bone tissue regenerative PLA/HA scaffolds with comprehensive performance optimizations, MATERIALS & DESIGN 201 (2021). https://doi.org/10.1016/j.matdes.2021.109490.
[78] M. Alksne, M. Kalvaityte, E. Simoliunas, I. Rinkunaite, I. Gendviliene, J. Locs, V. Rutkunas, V. Bukelskiene, In vitro comparison of 3D printed polylactic acid/hydroxyapatite and polylactic acid/bioglass composite scaffolds: Insights into materials for bone regeneration., Journal of the Mechanical Behavior of Biomedical Materials 104 (2020) 103641. https://doi.org/10.1016/j.jmbbm.2020.103641.
[79] A. Smieszek, K. Marycz, K. Szustakiewicz, B. Kryszak, S. Targonska, K. Zawisza, A. Watras, R.J. Wiglusz, New approach to modification of poly (l-lactic acid) with nano-hydroxyapatite improving functionality of human adipose-derived stromal cells (hASCs) through increased viability and enhanced mitochondrial activity., Materials Science & Engineering. C, Materials for Biological Applications 98 (2019) 213–226. https://doi.org/10.1016/j.msec.2018.12.099.
[80] N. Soehling, S. Al Zoghool, E. Schaetzlein, J. Neijhoft, K.M.C. Oliveira, L. Leppik, U. Ritz, E. Doersam, J. Frank, I. Marzi, A. Blaeser, D. Henrich, In vitro Evaluation of a 20%

Bioglass-Containing 3D printable PLA Composite for Bone Tissue Engineering, International Journal of Bioprinting 8 (2022) 65–81. https://doi.org/10.18063/ijb.v8i4.602.

[81] S. Gnanamani Sankaravel, R.B. Syed, V. Manivachakan, In vitro and mechanical characterization of PLA/egg shell biocomposite scaffold manufactured using fused deposition modeling technology for tissue engineering applications, Polymer Composites 43 (2022) 173–186. https://doi.org/10.1002/pc.26365.

[82] E.H. Backes, L. de N. Pires, H.S. Selistre-de-Araujo, L.C. Costa, F.R. Passador, L.A. Pessan, Development and characterization of printablePLA/beta-TCPbioactive composites for bone tissue applications, Journal of Applied Polymer Science 138 (2021). https://doi.org/10.1002/app.49759.

[83] M.-S. Kook, H.-S. Roh, B.-H. Kim, Effect of oxygen plasma etching on pore size-controlled 3D polycaprolactone scaffolds for enhancing the early new bone formation in rabbit calvaria, Dental Materials Journal 37 (2018) 599–610. https://doi.org/10.4012/dmj.2017-318.

[84] A.C. Jones, C.H. Arns, D.W. Hutmacher, B.K. Milthorpe, A.P. Sheppard, M.A. Knackstedt, The correlation of pore morphology, interconnectivity and physical properties of 3D ceramic scaffolds with bone ingrowth, Biomaterials 30 (2009) 1440–1451. https://doi.org/10.1016/j.biomaterials.2008.10.056.

[85] M. Mirkhalaf, X. Wang, A. Entezari, C.R. Dunstan, X. Jiang, H. Zreiqat, Redefining architectural effects in 3D printed scaffolds through rational design for optimal bone tissue regeneration, Applied Materials Today 25 (2021) 101168. https://doi.org/10.1016/j.apmt.2021.101168.

[86] M. Mastrogiacomo, S. Scaglione, R. Martinetti, L. Dolcini, F. Beltrame, R. Cancedda, R. Quarto, Role of scaffold internal structure on in vivo bone formation in macroporous calcium phosphate bioceramics, Biomaterials 27 (2006) 3230–3237. https://doi.org/10.1016/j.biomaterials.2006.01.031.

[87] W. Peng, Y. Liu, C. Wang, Definition, measurement, and function of pore structure dimensions of bioengineered porous bone tissue materials based on additive manufacturing: A review, Front. Bioeng. Biotechnol. 10 (2023) 1081548. https://doi.org/10.3389/fbioe.2022.1081548.

[88] A. Gleadall, D. Visscher, J. Yang, D. Thomas, J. Segal, Review of additive manufactured tissue engineering scaffolds: relationship between geometry and performance, Burns & Trauma 6 (2018). https://doi.org/10.1186/s41038-018-0121-4.

[89] A. Entezari, I. Roohani, G. Li, C.R. Dunstan, P. Rognon, Q. Li, X. Jiang, H. Zreiqat, Architectural Design of 3D Printed Scaffolds Controls the Volume and Functionality of Newly Formed Bone, Adv Healthcare Materials 8 (2019) 1801353. https://doi.org/10.1002/adhm.201801353.

[90] M.J. Page, J.E. McKenzie, P.M. Bossuyt, I. Boutron, T.C. Hoffmann, C.D. Mulrow, L. Shamseer, J.M. Tetzlaff, E.A. Akl, S.E. Brennan, R. Chou, J. Glanville, J.M. Grimshaw, A. Hróbjartsson, M.M. Lalu, T. Li, E.W. Loder, E. Mayo-Wilson, S. McDonald, L.A. McGuinness, L.A. Stewart, J. Thomas, A.C. Tricco, V.A. Welch, P. Whiting, D. Moher, The PRISMA 2020 statement: an updated guideline for reporting systematic reviews, BMJ (2021) n71. https://doi.org/10.1136/bmj.n71.

[91] N. Percie du Sert, V. Hurst, A. Ahluwalia, S. Alam, M.T. Avey, M. Baker, W.J. Browne, A. Clark, I.C. Cuthill, U. Dirnagl, M. Emerson, P. Garner, S.T. Holgate, D.W. Howells, N.A. Karp, S.E. Lazic, K. Lidster, C.J. MacCallum, M. Macleod, E.J. Pearl, O.H. Petersen, F. Rawle, P. Reynolds, K. Rooney, E.S. Sena, S.D. Silberberg, T. Steckler, H.

Würbel, The ARRIVE guidelines 2.0: Updated guidelines for reporting animal research, PLoS Biol 18 (2020) e3000410. https://doi.org/10.1371/journal.pbio.3000410.
[92] C.R. Hooijmans, M.M. Rovers, R.B. de Vries, M. Leenaars, M. Ritskes-Hoitinga, M.W. Langendam, SYRCLE's risk of bias tool for animal studies, BMC Med Res Methodol 14 (2014) 43. https://doi.org/10.1186/1471-2288-14-43.
[93] L.A. Feldkamp, L.C. Davis, J.W. Kress, Practical cone-beam algorithm, J. Opt. Soc. Am. A 1 (1984) 612. https://doi.org/10.1364/JOSAA.1.000612.
[94] N. Otsu, A Threshold Selection Method from Gray-Level Histograms, IEEE Trans. Syst., Man, Cybern. 9 (1979) 62–66. https://doi.org/10.1109/TSMC.1979.4310076.
[95] H. Tiainen, S.P. Lyngstadaas, J.E. Ellingsen, H.J. Haugen, Ultra-porous titanium oxide scaffold with high compressive strength, J Mater Sci: Mater Med 21 (2010) 2783–2792. https://doi.org/10.1007/s10856-010-4142-1.
[96] H.-B. Wu, H.J. Haugen, E. Wintermantel, Supercritical CO_2 in injection molding can produce open porous polyurethane scaffolds – a parameter study, Journal of Cellular Plastics 48 (2012) 141–159. https://doi.org/10.1177/0021955X11432970.
[97] A. Jones, C. Arns, A. Sheppard, D. Hutmacher, B. Milthorpe, M. Knackstedt, Assessment of bone ingrowth into porous biomaterials using MICRO-CT, Biomaterials 28 (2007) 2491–2504. https://doi.org/10.1016/j.biomaterials.2007.01.046.
[98] K. Donath, The Diagnostic Value of the New Method for the Study of Undecalcified Bones and Teeth with Attached Soft Tissue, (Säge-Schliff, (Sawing and Grinding) Technique), Pathology - Research and Practice 179 (1985) 631–633. https://doi.org/10.1016/S0344-0338(85)80209-0.
[99] F. Ze-wen, Z. Xin-yu, Q. Shuai, W. Yan, G. Jing, Q. Hui-xin, X. Lan-juan, 3D printing of polylactic acid/poly ethylene glycol/hydroxyapatite porous bone scaffolds and their biocompatibility, Cailiao Gongcheng-Journal 0f Materials Engineering 49 (2021) 135–141. https://doi.org/10.11868/j.issn.1001-1381.2020.000390.
[100] S.M. Lebedev, D.M. Chistokhin, S. Shchadenko V, A.N. Dzuman, O.O. Nikolaeva, D. Mitrichenko V, A.B. Prosolov, I.A. Khlusov, Biodegradable polymer composites with osteogenic potential, Byulleten Sibirskoy Meditsiny 19 (2020) 119–129. https://doi.org/10.20538/1682-0363-2020-4-119-129.
[101] N. Ranjan, R. Singh, I.P.S. Ahuja, R. Kumar, D. Singh, S. Ramniwas, A.K. Verma, D. Mittal, 3D printed scaffolds for tissue engineering applications: Mechanical, morphological, thermal, in-vitro and in-vivo investigations, CIRP Journal of Manufacturing Science and Technology 32 (2021) 205–216. https://doi.org/10.1016/j.cirpj.2021.01.002.
[102] B. Ashwin, B. Abinaya, T.P. Prasith, S.V. Chandran, L.R. Yadav, M. Vairamani, S. Patil, N. Selvamurugan, 3D-poly (lactic acid) scaffolds coated with gelatin and mucic acid for bone tissue engineering., International Journal of Biological Macromolecules 162 (2020) 523–532. https://doi.org/10.1016/j.ijbiomac.2020.06.157.
[103] W. Clifton, E. Nottmeier, A. Damon, C. Dove, S.G. Chen, M. Pichelmann, A Feasibility Study for the Production of Three-dimensional-printed Spine Models Using Simultaneously Extruded Thermoplastic Polymers, Cureus 11 (2019). https://doi.org/10.7759/cureus.4440.
[104] M. Wan, S. Liu, D. Huang, Y. Qu, Y. Hu, Q. Su, W. Zheng, X. Dong, H. Zhang, Y. Wei, W. Zhou, Biocompatible heterogeneous bone incorporated with polymeric biocomposites for human bone repair by 3D printing technology, Journal of Applied Polymer Science 138 (2021). https://doi.org/10.1002/app.50114.

[105] H. Belaid, S. Nagarajan, C. Barou, V. Huon, J. Bares, S. Balme, P. Miele, D. Cornu, V. Cavailles, C. Teyssier, M. Bechelany, Boron Nitride Based Nanobiocomposites: Design by 3D Printing for Bone Tissue Engineering, ACS Applied Bio Materials 3 (2020) 1865–1874. https://doi.org/10.1021/acsabm.9b00965.

[106] C.R. Moreno, E.M. Santschi, J. Janes, J. Liu, D. Kim, A.S. Litsky, Compression generated by cortical screws in an artificial bone model of an equine medial femoral condylar cyst, Veterinary Surgery 51 (2022) 833–842. https://doi.org/10.1111/vsu.13814.

[107] H. Belaid, S. Nagarajan, C. Teyssier, C. Barou, J. Barés, S. Balme, H. Garay, V. Huon, D. Cornu, V. Cavaillès, M. Bechelany, Development of new biocompatible 3D printed graphene oxide-based scaffolds., Materials Science & Engineering. C, Materials for Biological Applications 110 (2020) 110595. https://doi.org/10.1016/j.msec.2019.110595.

[108] C.-H. Cheng, Y.-W. Chen, A. Kai-Xing Lee, C.-H. Yao, M.-Y. Shie, Development of mussel-inspired 3D-printed poly (lactic acid) scaffold grafted with bone morphogenetic protein-2 for stimulating osteogenesis, Journal of Materials Science: Materials in Medicine 30 (2019). https://doi.org/10.1007/s10856-019-6279-x.

[109] M.-M. Liu, Y. Zhong, Y. Chen, L.-N. Wu, W. Chen, X.-H. Lin, Y. Lei, A.-L. Liu, Electrochemical monitoring the effect of drug intervention on PC12 cell damage model cultured on paper-PLA 3D printed device, Analytica Chimica Acta 1194 (2022). https://doi.org/10.1016/j.aca.2021.339409.

[110] Z. Huan, H.K. Chu, H. Liu, J. Yang, D. Sun, Engineered bone scaffolds with Dielectrophoresis-based patterning using 3D printing., Biomedical Microdevices 19 (2017) 102. https://doi.org/10.1007/s10544-017-0245-5.

[111] R. Donate, M. Elena Aleman-Dominguez, M. Monzon, J. Yu, F. Rodriguez-Esparragon, C. Liu, Evaluation of Aloe Vera Coated Polylactic Acid Scaffolds for Bone Tissue Engineering, Applied Sciences-Basel 10 (2020). https://doi.org/10.3390/app10072576.

[112] K.S. Manjunath, K. Sridhar, V. Gopinath, K. Sankar, A. Sundaram, N. Gupta, A.S.S.J. Shiek, P.S. Shantanu, Facile manufacturing of fused-deposition modeled composite scaffolds for tissue engineering-an embedding model with plasticity for incorporation of additives., Biomedical Materials (Bristol, England) 16 (2020) 15028. https://doi.org/10.1088/1748-605X/abc1b0.

[113] A. Souness, F. Zamboni, G.M. Walker, M.N. Collins, Influence of scaffold design on 3D printed cell constructs., Journal of Biomedical Materials Research. Part B, Applied Biomaterials 106 (2018) 533–545. https://doi.org/10.1002/jbm.b.33863.

[114] F. Caronna, N. Glimpel, G.-P. Paar, T. Gries, A. Blaeser, K. Do, E.B. Dolan, W. Ronan, Manufacturing, characterization, and degradation of a poly(lactic acid) warp-knitted spacer fabric scaffold as a candidate for tissue engineering applications, Biomater. Sci. 10 (2022) 3793–3807. https://doi.org/10.1039/D1BM02027G.

[115] M.P. Bernardo, B.C.R. da Silva, A.E.I. Hamouda, M.A.S. de Toledo, C. Schalla, S. Rütten, R. Goetzke, L.H.C. Mattoso, M. Zenke, A. Sechi, PLA/Hydroxyapatite scaffolds exhibit in vitro immunological inertness and promote robust osteogenic differentiation of human mesenchymal stem cells without osteogenic stimuli, Sci Rep 12 (2022) 2333. https://doi.org/10.1038/s41598-022-05207-w.

[116] P. Kowalczyk, P. Trzaskowska, I. \Lojszczyk, R. Podgórski, T. Ciach, Production of 3D printed polylactide scaffolds with surface grafted hydrogel coatings., Colloids and Surfaces. B, Biointerfaces 179 (2019) 136–142. https://doi.org/10.1016/j.colsurfb.2019.03.069.

[117] R. Chung, D.M. Kalyon, X. Yu, A. Valdevit, Segmental bone replacement via patient-specific, three-dimensional printed bioresorbable graft substitutes and their use as

templates for the culture of mesenchymal stem cells under mechanical stimulation at various frequencies, Biotechnology And Bioengineering 115 (2018) 2365–2376. https://doi.org/10.1002/bit.26780.
[118] M.J. Dewey, E.M. Johnson, D.W. Weisgerber, M.B. Wheeler, B.A.C. Harley, Shape-fitting collagen-PLA composite promotes osteogenic differentiation of porcine adipose stem cells., Journal of the Mechanical Behavior of Biomedical Materials 95 (2019) 21–33. https://doi.org/10.1016/j.jmbbm.2019.03.017.
[119] K. Dave, Z. Mahmud, V.G. Gomes, Superhydrophilic 3D-printed scaffolds using conjugated bioresorbable nanocomposites for enhanced bone regeneration, Chemical Engineering Journal 445 (2022) 136639. https://doi.org/10.1016/j.cej.2022.136639.
[120] M. Alksne, E. Simoliunas, M. Kalvaityte, E. Skliutas, I. Rinkunaite, I. Gendviliene, D. Baltriukiene, V. Rutkunas, V. Bukelskiene, The effect of larger than cell diameter polylactic acid surface patterns on osteogenic differentiation of rat dental pulp stem cells., Journal of Biomedical Materials Research. Part A 107 (2019) 174–186. https://doi.org/10.1002/jbm.a.36547.
[121] S. Swetha, K. Balagangadharan, K. Lavanya, N. Selvamurugan, Three-dimensional-poly(lactic acid) scaffolds coated with gelatin/magnesium-doped nano-hydroxyapatite for bone tissue engineering., Biotechnology Journal 16 (2021) e2100282. https://doi.org/10.1002/biot.202100282.
[122] S. Pant, S. Thomas, S. Loganathan, R.B. Valapa, 3D bioprinted poly(lactic acid)/mesoporous bioactive glass based biomimetic scaffold with rapid apatite crystallization and in-vitro Cytocompatability for bone tissue engineering, International Journal of Biological Macromolecules 217 (2022) 979–997. https://doi.org/10.1016/j.ijbiomac.2022.07.202.
[123] B. Oladapo I, S.O. Ismail, M. Zahedi, A. Khan, H. Usman, 3D printing and morphological characterisation of polymeric composite scaffolds, Engineering Structures 216 (2020). https://doi.org/10.1016/j.engstruct.2020.110752.
[124] I. Buj-Corral, A. Bagheri, O. Petit-Rojo, 3D Printing of Porous Scaffolds with Controlled Porosity and Pore Size Values, Materials 11 (2018). https://doi.org/10.3390/ma11091532.
[125] L. He, X. Liu, C. Rudd, Additive-Manufactured Gyroid Scaffolds of Magnesium Oxide, Phosphate Glass Fiber and Polylactic Acid Composite for Bone Tissue Engineering, POLYMERS 13 (2021). https://doi.org/10.3390/polym13020270.
[126] C. Amnael Orozco-Diaz, R. Moorehead, G.C. Reilly, F. Gilchrist, C. Miller, Characterization of a composite polylactic acid-hydroxyapatite 3D-printing filament for bone-regeneration, Biomedical Physics & Engineering Express 6 (2020). https://doi.org/10.1088/2057-1976/ab73f8.
[127] R. Donate, M. Monzon, Z. Ortega, L. Wang, V. Ribeiro, D. Pestana, J.M. Oliveira, R.L. Reis, Comparison between calcium carbonate and beta-tricalcium phosphate as additives of 3D printed scaffolds with polylactic acid matrix, Journal Of Tissue Engineering And Regenerative Medicine 14 (2020) 272–283. https://doi.org/10.1002/term.2990.
[128] M.P. Bernardo, B.C. Rodrigues da Silva, L.H. Capparelli Mattoso, Development of three-dimensional printing filaments based on poly(lactic acid)/hydroxyapatite composites with potential for tissue engineering, Journal Of Composite Materials 55 (2021) 2289–2300. https://doi.org/10.1177/0021998320988568.
[129] V. Nadarajan, S.W. Phang, H.L. Choo, Fabrication of 3D-Printed Bone Scaffold of Natural Hydroxyapatite from Fish Bones in Polylactic Acid Composite, 13th International

Engineering Research Conference (13TH EURECA 2019) 2233 (2020). https://doi.org/10.1063/5.0001497.

[130] E.H. Backes, L.D.N. Pires, C.A.G. Beatrice, L.C. Costa, F.R. Passador, L.A. Pessan, Fabrication of Biocompatible Composites of Poly(lactic acid)/Hydroxyapatite Envisioning Medical Applications, Polymer Engineering And Science 60 (2020) 636–644. https://doi.org/10.1002/pen.25322.

[131] E. Salamanca, T.-C. Tsao, H.-W. Hseuh, Y.-F. Wu, C.-S. Choy, C.-K. Lin, Y.-H. Pan, N.-C. Teng, M.-C. Huang, S.-M. Lin, W.-J. Chang, Fabrication of Polylactic Acid/beta-Tricalcium Phosphate FDM 3D Printing Fiber to Enhance Osteoblastic-Like Cell Performance, Frontiers in Materials 8 (2021). https://doi.org/10.3389/fmats.2021.683706.

[132] G. Dubinenko, A. Zinoviev, E. Bolbasov, A. Kozelskaya, E. Shesterikov, V. Novikov, S. Tverdokhlebov, Highly filled poly(l-lactic acid)/hydroxyapatite composite for3Dprinting of personalized bone tissue engineering scaffolds, Journal of Applied Polymer Science 138 (2021). https://doi.org/10.1002/app.49662.

[133] Y. Zamani, G. Amoabediny, J. Mohammadi, B. Zandieh-Doulabi, J. Klein-Nulend, M.N. Helder, Increased Osteogenic Potential of Pre-Osteoblasts on Three-Dimensional Printed Scaffolds Compared to Porous Scaffolds for Bone Regeneration., Iranian Biomedical Journal 25 (2021) 78–87. https://doi.org/10.29252/ibj.25.2.78.

[134] H. Hwangbo, J. Lee, G. Kim, Mechanically and biologically enhanced 3D-printed HA/PLLA/dECM biocomposites for bone tissue engineering, International Journal of Biological Macromolecules 218 (2022) 9–21. https://doi.org/10.1016/j.ijbiomac.2022.07.040.

[135] X. Lacambra-Andreu, N. Dergham, M. Magallanes-Perdomo, S. Meille, J. Chevalier, J.-M. Chenal, A. Maazouz, K. Lamnawar, Model Composites Based on Poly(lactic acid) and Bioactive Glass Fillers for Bone Regeneration, Polymers 13 (2021). https://doi.org/10.3390/polym13172991.

[136] C.-A. Dascalu, F. Miculescu, A.-C. Mocanu, A.E. Constantinescu, T.M. Butte, A.M. Pandele, R.-C. Ciocoiu, S.L. Voicu, L.T. Ciocan, Novel Synthesis of Core-Shell Biomaterials from Polymeric Filaments with a Bioceramic Coating for Biomedical Applications, COATINGS 10 (2020). https://doi.org/10.3390/coatings10030283.

[137] C.E. Corcione, F. Scalera, F. Gervaso, F. Montagna, A. Sannino, A. Maffezzoli, One-step solvent-free process for the fabrication of high loaded PLA/HA composite filament for 3D printing, Journal of Thermal Analysis and Calorimetry 134 (2018) 575–582. https://doi.org/10.1007/s10973-018-7155-5.

[138] M. Bayart, M. Dubus, S. Charlon, H. Kerdjoudj, N. Baleine, S. Benali, J.-M. Raquez, J. Soulestin, Pellet-Based Fused Filament Fabrication (FFF)-Derived Process for the Development of Polylactic Acid/Hydroxyapatite Scaffolds Dedicated to Bone Regeneration, MATERIALS 15 (2022). https://doi.org/10.3390/ma15165615.

[139] I. Fernandez-Cervantes, M.A. Morales, R. Agustin-Serrano, M. Cardenas-Garcia, P.V. Perez-Luna, B.L. Arroyo-Reyes, A. Maldonado-Garcia, Polylactic acid/sodium alginate/hydroxyapatite composite scaffolds with trabecular tissue morphology designed by a bone remodeling model using 3D printing, Journal of Materials Science 54 (2019) 9478–9496. https://doi.org/10.1007/s10853-019-03537-1.

[140] T. Distler, N. Fournier, A. Gruenewald, C. Polley, H. Seitz, R. Detsch, A.R. Boccaccini, Polymer-Bioactive Glass Composite Filaments for 3D Scaffold Manufacturing by Fused Deposition Modeling: Fabrication and Characterization, Frontiers In Bioengineering And Biotechnology 8 (2020). https://doi.org/10.3389/fbioe.2020.00552.

[141] N.W. Pensa, A.S. Curry, P.P. Bonvallet, N.F. Bellis, K.M. Rettig, M.S. Reddy, A.W. Eberhardt, S.L. Bellis, 3D printed mesh reinforcements enhance the mechanical properties of electrospun scaffolds, Biomaterials Research 23 (2019). https://doi.org/10.1186/s40824-019-0171-0.
[142] H. Chen, H. Zhang, Y. Shen, X. Dai, X. Wang, K. Deng, X. Long, L. Liu, X. Zhang, Y. Li, T. Xu, Instant in-situ Tissue Repair by Biodegradable PLA/Gelatin Nanofibrous Membrane Using a 3D Printed Handheld Electrospinning Device., Frontiers in Bioengineering and Biotechnology 9 (2021) 684105. https://doi.org/10.3389/fbioe.2021.684105.
[143] V. Guduric, C. Metz, R. Siadous, R. Bareille, R. Levato, E. Engel, J.-C. Fricain, R. Devillard, O. Luzanin, S. Catros, Layer-by-layer bioassembly of cellularized polylactic acid porous membranes for bone tissue engineering., Journal of Materials Science. Materials in Medicine 28 (2017) 78. https://doi.org/10.1007/s10856-017-5887-6.
[144] X. Liang, J. Gao, W. Xu, X. Wang, Y. Shen, J. Tang, S. Cui, X. Yang, Q. Liu, L. Yu, J. Ding, Structural mechanics of 3D-printed poly(lactic acid) scaffolds with tetragonal, hexagonal and wheel-like designs, Biofabrication 11 (2019). https://doi.org/10.1088/1758-5090/ab0f59.
[145] F. Azadmanesh, M. Pourmadadi, J. Zavar Reza, F. Yazdian, M. Omidi, B.F. Haghirosadat, Synthesis of a novel nanocomposite containing chitosan as a three-dimensional printed wound dressing technique: Emphasis on gene expression., Biotechnology Progress 37 (2021) e3132. https://doi.org/10.1002/btpr.3132.
[146] J.A. Driscoll, R. Lubbe, A.E. Jakus, K. Chang, M. Haleem, C. Yun, G. Singh, A.D. Schneider, K.M. Katchko, C. Soriano, M. Newton, T. Maerz, X. Li, K. Baker, W.K. Hsu, R.N. Shah, S.R. Stock, E.L. Hsu, 3D-Printed Ceramic-Demineralized Bone Matrix Hyperelastic Bone Composite Scaffolds for Spinal Fusion., Tissue Engineering. Part A 26 (2020) 157–166. https://doi.org/10.1089/ten.TEA.2019.0166.
[147] D. Gao, Z. Wang, Z. Wu, M. Guo, Y. Wang, Z. Gao, P. Zhang, Y. Ito, 3D-printing of solvent exchange deposition modeling (SEDM) for a bilayered flexible skin substitute of poly (lactide-co-glycolide) with bioorthogonally engineered EGF., Materials Science & Engineering. C, Materials for Biological Applications 112 (2020) 110942. https://doi.org/10.1016/j.msec.2020.110942.
[148] R. Fairag, L. Li, J.L. Ramirez-GarciaLuna, M.S. Taylor, B. Gaerke, M.H. Weber, D.H. Rosenzweig, L. Haglund, A Composite Lactide-Mineral 3D-Printed Scaffold for Bone Repair and Regeneration, Frontiers In Cell And Developmental Biology 9 (2021). https://doi.org/10.3389/fcell.2021.654518.
[149] Y. Dou, J. Huang, X. Xia, J. Wei, Q. Zou, Y. Zuo, J. Li, Y. Li, A hierarchical scaffold with a highly pore-interconnective 3D printed PLGA/n-HA framework and an extracellular matrix like gelatin network filler for bone regeneration., Journal of Materials Chemistry. B 9 (2021) 4488–4501. https://doi.org/10.1039/d1tb00662b.
[150] H. Kang, X. Jiang, Z. Liu, F. Liu, G. Yan, F. Li, Biodegradable 3D Printed Scaffolds of Modified Poly (Trimethylene Carbonate) Composite Materials with Poly (L-Lactic Acid) and Hydroxyapatite for Bone Regeneration, Nanomaterials 11 (2021). https://doi.org/10.3390/nano11123215.
[151] S. Kurt, S. Selviler-Sizer, B. Onuk, M. Kabak, Comparison of sheep scapula models created with polylactic acid and thermoplastic polyurethane filaments by three-dimensional modelling, Anat Histol Embryol 51 (2022) 244–249. https://doi.org/10.1111/ahe.12784.

[152] M. Micic, D. Antonijevic, S. Milutinovic-Smiljanic, D. Trisic, B. Colovic, D. Kosanovic, B. Prokic, J. Vasic, S. Zivkovic, J. Milasin, V. Danilovic, M. Djuric, V. Jokanovic, Developing a novel resorptive hydroxyapatite-based bone substitute for over-critical size defect reconstruction: physicochemical and biological characterization and proof of concept in segmental rabbit's ulna reconstruction., Biomedizinische Technik. Biomedical Engineering 65 (2020) 491–505. https://doi.org/10.1515/bmt-2019-0218.

[153] J.W. Yun, S.Y. Heo, M.H. Lee, H.B. Lee, Evaluation of a poly(lactic-acid) scaffold filled with poly(lactide-co-glycolide)/hydroxyapatite nanofibres for reconstruction of a segmental bone defect in a canine model, Veterinarni Medicina 64 (2019) 531–538. https://doi.org/10.17221/80/2019-VETMED.

[154] B. Zhang, S. Shen, H. Xian, Y. Dai, W. Guo, X. Li, X. Zhang, Z. Wang, H. Li, L. Peng, X. Luo, S. Liu, X. Lu, Q. Guo, [Fabrication of poly (lactic-co-glycolic acid)/decellularized articular cartilage extracellular matrix scaffold by three-dimensional printing technology and investigating its physicochemical properties]., Zhongguo xiu fu chong jian wai ke za zhi = Zhongguo xiufu chongjian waike zazhi = Chinese journal of reparative and reconstructive surgery 33 (2019) 1011–1018. https://doi.org/10.7507/1002-1892.201901082.

[155] B. Li, C. Ruan, Y. Ma, Z. Huang, Z. Huang, G. Zhou, J. Zhang, H. Wang, Z. Wu, G. Qiu, Fabrication of Vascularized Bone Flaps with Sustained Release of Recombinant Human Bone Morphogenetic Protein-2 and Arteriovenous Bundle., Tissue Engineering. Part A 24 (2018) 1413–1422. https://doi.org/10.1089/ten.TEA.2018.0002.

[156] S. Pitjamit, W. Nakkiew, K. Thongkorn, W. Thanakulwattana, K. Thunsiri, Finite Element Analysis of Traditional and New Fixation Techniques of the 3D-Printed Composite Interlocking Nail in Canine Femoral Shaft Fractures, Applied Sciences-Basel 10 (2020). https://doi.org/10.3390/app10103424.

[157] S. Camarero-Espinosa, L. Moroni, Janus 3D printed dynamic scaffolds for nanovibration-driven bone regeneration., Nature Communications 12 (2021) 1031. https://doi.org/10.1038/s41467-021-21325-x.

[158] M. Deng, J. Tan, C. Hu, T. Hou, W. Peng, J. Liu, B. Yu, Q. Dai, J. Zhou, Y. Yang, R. Dong, C. Ruan, S. Dong, J. Xu, Modification of PLGA Scaffold by MSC-Derived Extracellular Matrix Combats Macrophage Inflammation to Initiate Bone Regeneration via TGF-β-Induced Protein., Advanced Healthcare Materials 9 (2020) e2000353. https://doi.org/10.1002/adhm.202000353.

[159] Y. Lai, Y. Li, H. Cao, J. Long, X. Wang, L. Li, C. Li, Q. Jia, B. Teng, T. Tang, J. Peng, D. Eglin, M. Alini, D.W. Grijpma, G. Richards, L. Qin, Osteogenic magnesium incorporated into PLGA/TCP porous scaffold by 3D printing for repairing challenging bone defect., Biomaterials 197 (2019) 207–219. https://doi.org/10.1016/j.biomaterials.2019.01.013.

[160] W.-X. Cheng, Y.-Z. Liu, X.-B. Meng, Z.-T. Zheng, L.-L. Li, L.-Q. Ke, L. Li, C.-S. Huang, G.-Y. Zhu, H.-D. Pan, L. Qin, X.-L. Wang, P. Zhang, PLGA/β-TCP composite scaffold incorporating cucurbitacin B promotes bone regeneration by inducing angiogenesis., Journal of Orthopaedic Translation 31 (2021) 41–51. https://doi.org/10.1016/j.jot.2021.10.002.

[161] W. Yu, R. Li, J. Long, P. Chen, A. Hou, L. Li, X. Sun, G. Zheng, H. Meng, Y. Wang, A. Wang, X. Sui, Q. Guo, S. Tao, J. Peng, L. Qin, S. Lu, Y. Lai, Use of a three-dimensional printed polylactide-coglycolide/tricalcium phosphate composite scaffold incorporating magnesium powder to enhance bone defect repair in rabbits, Journal Of Orthopaedic Translation 16 (2019) 62–70. https://doi.org/10.1016/j.jot.2018.07.007.

[162] J. Wei, Y. Yan, J. Gao, Y. Li, R. Wang, J. Wang, Q. Zou, Y. Zuo, M. Zhu, J. Li, 3D-printed hydroxyapatite microspheres reinforced PLGA scaffolds for bone regeneration., Materials Science & Engineering. C, Materials for Biological Applications (2021) 112618. https://doi.org/10.1016/j.msec.2021.112618.
[163] W. Chen, L. Nichols, L. Teer, K. Clinton, L.B. Priddy, A hybrid coating of polydopamine and nano-hydroxyapatite enhances surface properties of 3D printed poly(lactic-co-glycolic acid) scaffolds, JOURNAL OF MATERIALS SCIENCE 57 (2022) 13011–13026. https://doi.org/10.1007/s10853-022-07442-y.
[164] M. Lian, Y. Han, B. Sun, L. Xu, X. Wang, B. Ni, W. Jiang, Z. Qiao, K. Dai, X. Zhang, A multifunctional electrowritten bi-layered scaffold for guided bone regeneration., Acta Biomaterialia 118 (2020) 83–99. https://doi.org/10.1016/j.actbio.2020.08.017.
[165] C. Shuai, W. Yang, P. Feng, S. Peng, H. Pan, Accelerated degradation of HAP/PLLA bone scaffold by PGA blending facilitates bioactivity and osteoconductivity, Bioactive Materials 6 (2021) 490–502. https://doi.org/10.1016/j.bioactmat.2020.09.001.
[166] R. Donate, M. Monzon, M.E. Aleman-Dominguez, Additive manufacturing of PLA-based scaffolds intended for bone regeneration and strategies to improve their biological properties, E-POLYMERS 20 (2020) 571–599. https://doi.org/10.1515/epoly-2020-0046.
[167] J. Babilotte, B. Martin, V. Guduric, R. Bareille, R. Agniel, S. Roques, V. Héroguez, M. Dussauze, M. Gaudon, D. Le Nihouannen, S. Catros, Development and characterization of a PLGA-HA composite material to fabricate 3D-printed scaffolds for bone tissue engineering., Materials Science & Engineering. C, Materials for Biological Applications 118 (2021) 111334. https://doi.org/10.1016/j.msec.2020.111334.
[168] Z. Xu, N. Wang, P. Liu, Y. Sun, Y. Wang, F. Fei, S. Zhang, J. Zheng, B. Han, Poly(Dopamine) Coating on 3D-Printed Poly-Lactic-Co-Glycolic Acid/β-Tricalcium Phosphate Scaffolds for Bone Tissue Engineering., MOLECULES 24 (2019). https://doi.org/10.3390/molecules24234397.
[169] P.-C. Chang, H.-T. Luo, Z.-J. Lin, W.-C. Tai, C.-H. Chang, Y.-C. Chang, D.L. Cochran, M.-H. Chen, Preclinical evaluation of a 3D-printed hydroxyapatite/poly(lactic-co-glycolic acid) scaffold for ridge augmentation., Journal of the Formosan Medical Association = Taiwan Yi Zhi 120 (2021) 1100–1107. https://doi.org/10.1016/j.jfma.2020.10.022.
[170] S.-S. Cao, S.-Y. Li, Y.-M. Geng, K. Kapat, S.-B. Liu, F.H. Perera, Q. Li, H. Terheyden, G. Wu, Y.-J. Che, P. Miranda, M. Zhou, Prefabricated 3D-Printed Tissue-Engineered Bone for Mandibular Reconstruction: A Preclinical Translational Study in Primate., ACS Biomaterials Science & Engineering 7 (2021) 5727–5738. https://doi.org/10.1021/acsbiomaterials.1c00509.
[171] P.-C. Chang, H.-T. Luo, Z.-J. Lin, W.-C. Tai, C.-H. Chang, Y.-C. Chang, D.L. Cochran, M.-H. Chen, Regeneration of critical-sized mandibular defect using a 3D-printed hydroxyapatite-based scaffold: An exploratory study, Journal Of Periodontology 92 (2021) 428–435. https://doi.org/10.1002/JPER.20-0110.
[172] S.K. Lee, C.-M. Han, W. Park, I.H. Kim, Y.K. Joung, D.K. Han, Synergistically enhanced osteoconductivity and anti-inflammation of PLGA/β-TCP/Mg(OH)(2) composite for orthopedic applications., Materials Science & Engineering. C, Materials for Biological Applications 94 (2019) 65–75. https://doi.org/10.1016/j.msec.2018.09.011.
[173] H. Liu, H. Zhu, L. Cheng, Y. Zhao, X. Chen, J. Li, X. Xv, Z. Xiao, W. Li, J. Pan, Q. Zhang, C. Zeng, J. Guo, D. Xie, D. Cai, TCP/PLGA composite scaffold loaded rapamycin in situ enhances lumbar fusion by regulating osteoblast and osteoclast activity, Journal of

Tissue Engineering and Regenerative Medicine 15 (2021) 475–486. https://doi.org/10.1002/term.3186.

[174] R. Duan, Y. Wang, D. Su, Z. Wang, Y. Zhang, B. Du, L. Liu, X. Li, Q. Zhang, The effect of blending poly (l-lactic acid) on in vivo performance of 3D-printed poly(l-lactide-co-caprolactone)/PLLA scaffolds., Biomaterials Advances 138 (2022) 212948. https://doi.org/10.1016/j.bioadv.2022.212948.

[175] E. Akerlund, A. Diez-Escudero, A. Grzeszczak, C. Persson, The Effect of PCL Addition on 3D-Printable PLA/HA Composite Filaments for the Treatment of Bone Defects, POLYMERS 14 (2022). https://doi.org/10.3390/polym14163305.

[176] S. Pitjamit, K. Thunsiri, W. Nakkiew, T. Wongwichai, P. Pothacharoen, W. Wattanutchariya, The possibility of interlocking nail fabrication from FFF 3D printing PLA/PCL/HA composites coated by local silk fibroin for canine bone fracture treatment, Materials 13 (2020). https://doi.org/10.3390/ma13071564.

[177] J. Pizzicannella, F. Diomede, A. Gugliandolo, L. Chiricosta, P. Bramanti, I. Merciaro, T. Orsini, E. Mazzon, O. Trubiani, 3D Printing PLA/Gingival Stem Cells/ EVs Upregulate miR-2861 and -210 during Osteoangiogenesis Commitment., International Journal of Molecular Sciences 20 (2019). https://doi.org/10.3390/ijms20133256.

[178] Z.B. Velioglu, D. Pulat, B. Demirbakan, B. Ozcan, E. Bayrak, C. Erisken, 3D-printed poly(lactic acid) scaffolds for trabecular bone repair and regeneration: scaffold and native bone characterization., Connective Tissue Research 60 (2019) 274–282. https://doi.org/10.1080/03008207.2018.1499732.

[179] N. Söhling, J. Neijhoft, V. Nienhaus, V. Acker, J. Harbig, F. Menz, J. Ochs, R.D.R.D. Verboket, U. Ritz, A. Blaeser, E. Dörsam, J. Frank, I. Marzi, D. Henrich, N. Soehling, J. Neijhoft, V. Nienhaus, V. Acker, J. Harbig, F. Menz, J. Ochs, R.D.R.D. Verboket, U. Ritz, A. Blaeser, E. Doersam, J. Frank, I. Marzi, D. Henrich, N. Söhling, J. Neijhoft, V. Nienhaus, V. Acker, J. Harbig, F. Menz, J. Ochs, R.D.R.D. Verboket, U. Ritz, A. Blaeser, E. Dörsam, J. Frank, I. Marzi, D. Henrich, 3D-Printing of Hierarchically Designed and Osteoconductive Bone Tissue Engineering Scaffolds, MATERIALS 13 (2020). https://doi.org/10.3390/ma13081836.

[180] A. Lauer, P. Wolf, D. Mehler, H. Goetz, M. Ruezgar, A. Baranowski, D. Henrich, P.M. Rommens, U. Ritz, Biofabrication of SDF-1 Functionalized 3D-Printed Cell-Free Scaffolds for Bone Tissue Regeneration, International Journal Of Molecular Sciences 21 (2020). https://doi.org/10.3390/ijms21062175.

[181] S.H. Han, M. Cha, Y.-Z. Jin, K.-M. Lee, J.H. Lee, BMP-2 and hMSC dual delivery onto 3D printed PLA-Biogel scaffold for critical-size bone defect regeneration in rabbit tibia, BIOMEDICAL MATERIALS 16 (2021) 15019. https://doi.org/10.1088/1748-605X/aba879.

[182] C.-H. Yao, Y.-H. Lai, Y.-W. Chen, C.-H. Cheng, Bone Morphogenetic Protein-2-Activated 3D-Printed Polylactic Acid Scaffolds to Promote Bone Regrowth and Repair., Macromolecular Bioscience 20 (2020) e2000161. https://doi.org/10.1002/mabi.202000161.

[183] R.T. Anbu, V. Suresh, R. Gounder, A. Kannan, Comparison of the Efficacy of Three Different Bone Regeneration Materials: An Animal Study., European Journal of Dentistry 13 (2019) 22–28. https://doi.org/10.1055/s-0039-1688735.

[184] M. Zhu, J. Tan, L. Liu, J. Tian, L. Li, B. Luo, C. Zhou, L. Lu, Construction of biomimetic artificial intervertebral disc scaffold via 3D printing and electrospinning, Materials Science & Engineering C-Materials For Biological Applications 128 (2021). https://doi.org/10.1016/j.msec.2021.112310.

[185] M. Alksne, M. Kalvaityte, E. Simoliunas, I. Gendviliene, P. Barasa, I. Rinkunaite, A. Kaupinis, D. Seinin, V. Rutkunas, V. Bukelskiene, Dental pulp stem cell-derived extracellular matrix: autologous tool boosting bone regeneration, Cytotherapy 24 (2022) 597–607. https://doi.org/10.1016/j.jcyt.2022.02.002.
[186] B.N. Teixeira, P. Aprile, R.H. Mendonça, D.J. Kelly, R.M.D.S.M. Thiré, Evaluation of bone marrow stem cell response to PLA scaffolds manufactured by 3D printing and coated with polydopamine and type I collagen, Journal of Biomedical Materials Research - Part B Applied Biomaterials 107 (2019) 37–49. https://doi.org/10.1002/jbm.b.34093.
[187] X. Zhang, Q. Lou, L. Wang, S. Min, M. Zhao, C. Quan, Immobilization of BMP-2-derived peptides on 3D-printed porous scaffolds for enhanced osteogenesis., Biomedical Materials (Bristol, England) 15 (2019) 15002. https://doi.org/10.1088/1748-605X/ab4c78.
[188] L. Perez-Sanchez, M.A.O. De la O, P. Gonzalez-Alva, L.A. Medina, D. Masuoka-Ito, M.A. Alvarez-Perez, J. Serrano-Bello, In Vivo Study on Bone Response to 3D-Printed Constructs Designed from Microtomographic Images, Journal Of Materials Engineering And Performance 30 (2021) 5005–5012. https://doi.org/10.1007/s11665-021-05585-8.
[189] A. Sharma, S. Gupta, T.S. Sampathkumar, R.S. Verma, Modified graphene oxide nanoplates reinforced 3D printed multifunctional scaffold for bone tissue engineering, Biomaterials Advances 134 (2022) 112587. https://doi.org/10.1016/j.msec.2021.112587.
[190] K.-S. Liu, W.-H. Chen, C.-H. Lee, Y.-F. Su, Y.-W. Liu, S.-J. Liu, Novel Biodegradable 3D-Printed Analgesics-Eluting-Nanofibers Incorporated Nuss Bars for Therapy of Pectus Excavatum, IJMS 23 (2022) 2265. https://doi.org/10.3390/ijms23042265.
[191] J.L. Chakka, T. Acri, N.Z. Laird, L. Zhong, K. Shin, S. Elangovan, A.K. Salem, Polydopamine functionalized VEGF gene-activated 3D printed scaffolds for bone regeneration, RSC ADVANCES 11 (2021) 13282–13291. https://doi.org/10.1039/d1ra01193f.
[192] P. Wang, H.-M. Yin, X. Li, W. Liu, Y.-X. Chu, Y. Wang, Y. Wang, J.-Z. Xu, Z.-M. Li, J.-H. Li, Simultaneously constructing nanotopographical and chemical cues in 3D-printed polylactic acid scaffolds to promote bone regeneration, Materials Science & Engineering C-Materials For Biological Applications 118 (2021). https://doi.org/10.1016/j.msec.2020.111457.
[193] M. Bahraminasab, A. Talebi, N. Doostmohammadi, S. Arab, A. Ghanbari, S. Zarbakhsh, The healing of bone defects by cell-free and stem cell-seeded 3D-printed PLA tissue-engineered scaffolds, J Orthop Surg Res 17 (2022) 320. https://doi.org/10.1186/s13018-022-03213-2.
[194] F. Diomede, A. Gugliandolo, P. Cardelli, I. Merciaro, V. Ettorre, T. Traini, R. Bedini, D. Scionti, A. Bramanti, A. Nanci, S. Caputi, A. Fontana, E. Mazzon, O. Trubiani, Three-dimensional printed PLA scaffold and human gingival stem cell-derived extracellular vesicles: a new tool for bone defect repair, Stem Cell Research & Therapy 9 (2018). https://doi.org/10.1186/s13287-018-0850-0.
[195] M. Cha, Y.-Z. Jin, J.W. Park, K.M. Lee, S.H. Han, B.S. Choi, J.H. Lee, Three-dimensional printed polylactic acid scaffold integrated with BMP-2 laden hydrogel for precise bone regeneration, Biomaterials Research 25 (2021). https://doi.org/10.1186/s40824-021-00233-7.
[196] H. Chen, Q. Shi, H. Shui, P. Wang, Q. Chen, Z. Li, Degradation of 3D-Printed Porous Polylactic Acid Scaffolds Under Mechanical Stimulus, Frontiers In Bioengineering And Biotechnology 9 (2021). https://doi.org/10.3389/fbioe.2021.691834.

[197] P. Karimipour-Fard, R. Pop-Iliev, H. Jones-Taggart, G. Rizvi, G.U. Erinc, Design of 3D Scaffold Geometries for Optimal Biodegradation of Poly(lactic acid)-Based Bone Tissue, Proceedings Of The 35th International Conference Of The Polymer Processing Society (PPS-35) 2205 (2020). https://doi.org/10.1063/1.5142977.

[198] H. Shui, Q. Shi, N.M. Pugno, Q. Chen, Z. Li, Effect of mechanical stimulation on the degradation of poly(lactic acid) scaffolds with different designed structures, Journal Of The Mechanical Behavior Of Biomedical Materials 96 (2019) 324–333. https://doi.org/10.1016/j.jmbbm.2019.04.028.

[199] S.C. Cifuentes, L. Saldana, J. Luis Gonzalez-Carrasco, R. Benavente, A. Garcia-Penas, Effect of Thermal Processing on the Dynamic/Isothermal Crystallization and Cytocompatibility of Polylactic Acid for Biomedical Applications, Macromolecular Chemistry And Physics 222 (2021). https://doi.org/10.1002/macp.202100274.

[200] E. Mohan, M.S. Kumar, Experimental investigation on mechanical and tribological properties of the fused filament fabrication of poly-lactic acid parts with various print orientations, Applied Physics A-Materials Science & Processing 128 (2022). https://doi.org/10.1007/s00339-022-05579-w.

[201] Y. Zhang, C. Wang, L. Fu, S. Ye, M. Wang, Y. Zhou, Fabrication and Application of Novel Porous Scaffold in Situ-Loaded Graphene Oxide and Osteogenic Peptide by Cryogenic 3D Printing for Repairing Critical-Sized Bone Defect, Molecules 24 (2019). https://doi.org/10.3390/molecules24091669.

[202] A.C.D. Nascimento Jr., R.C.D.A.G. Mota, L.R.D. Menezes, E.O.D. Silva, Influence of the printing parameters on the properties of Poly(lactic acid) scaffolds obtained by fused deposition modeling 3D printing, Polymers & Polymer Composites 29 (2021) S1052–S1062. https://doi.org/10.1177/09673911211040770.

[203] B. Gao, H. Jing, M. Gao, S. Wang, W. Fu, X. Zhang, X. He, J. Zheng, Long-segmental tracheal reconstruction in rabbits with pedicled Tissue-engineered trachea based on a 3D-printed scaffold., Acta Biomaterialia 97 (2019) 177–186. https://doi.org/10.1016/j.actbio.2019.07.043.

[204] C. Pagano, L. Rebaioli, F. Baldi, I. Fassi, G.U. Erinc, Mechanical Behavior of Scaffold-Like Structures: Research of Relationships between Properties and Geometry, Proceedings of The 35th International Conference of The Polymer Processing Society (PPS-35) 2205 (2020). https://doi.org/10.1063/1.5142979.

[205] R. Baptista, M. Guedes, Morphological and mechanical characterization of 3D printed PLA scaffolds with controlled porosity for trabecular bone tissue replacement, Materials Science and Engineering C 118 (2021). https://doi.org/10.1016/j.msec.2020.111528.

[206] R. Baptista, M. Guedes, Porosity and pore design influence on fatigue behavior of 3D printed scaffolds for trabecular bone replacement, Journal of the Mechanical Behavior of Biomedical Materials 117 (2021). https://doi.org/10.1016/j.jmbbm.2021.104378.

[207] D. Singh, A. Babbar, V. Jain, D. Gupta, S. Saxena, V. Dwibedi, Synthesis, characterization, and bioactivity investigation of biomimetic biodegradable PLA scaffold fabricated by fused filament fabrication process, Journal of the Brazilian Society of Mechanical Sciences and Engineering 41 (2019). https://doi.org/10.1007/s40430-019-1625-y.

[208] K.-C. Feng, A. Pinkas-Sarafova, V. Ricotta, M. Cuiffo, L. Zhang, Y. Guo, C.-C. Chang, G.P. Halada, M. Simon, M. Rafailovich, The influence of roughness on stem cell differentiation using 3D printed polylactic acid scaffolds, Soft Matter 14 (2018) 9838–9846. https://doi.org/10.1039/c8sm01797b.

[209] A. Grivet-Brancot, M. Boffito, G. Ciardelli, Use of Polyesters in Fused Deposition Modeling for Biomedical Applications, Macromolecular Bioscience 22 (2022). https://doi.org/10.1002/mabi.202200039.
[210] Y.K. Yeon, H.S. Park, J.M. Lee, J.S. Lee, Y.J. Lee, Md.T. Sultan, Y.B. Seo, O.J. Lee, S.H. Kim, C.H. Park, New concept of 3D printed bone clip (polylactic acid/hydroxyapatite/silk composite) for internal fixation of bone fractures, Journal of Biomaterials Science-Polymer Edition 29 (2018) 894–906. https://doi.org/10.1080/09205063.2017.1384199.
[211] X. Chen, C. Gao, J. Jiang, Y. Wu, P. Zhu, G. Chen, 3D printed porous PLA/nHA composite scaffolds with enhanced osteogenesis and osteoconductivity in vivo for bone regeneration, Biomedical Materials 14 (2019). https://doi.org/10.1088/1748-605X/ab388d.
[212] Z. Liu, Y. Ge, L. Zhang, Y. Wang, C. Guo, K. Feng, S. Yang, Z. Zhai, Y. Chi, J. Zhao, F. Liu, The effect of induced membranes combined with enhanced bone marrow and 3D PLA-HA on repairing long bone defects in vivo, Journal Of Tissue Engineering And Regenerative Medicine 14 (2020) 1403–1414. https://doi.org/10.1002/term.3106.
[213] W. Wang, B. Zhang, M. Li, J. Li, C. Zhang, Y. Han, L. Wang, K. Wang, C. Zhou, L. Liu, Y. Fan, X. Zhang, 3D printing of PLA/n-HA composite scaffolds with customized mechanical properties and biological functions for bone tissue engineering, Composites Part B-Engineering 224 (2021). https://doi.org/10.1016/j.compositesb.2021.109192.
[214] W. Wang, B. Zhang, L. Zhao, M. Li, Y. Han, L. Wang, Z. Zhang, J. Li, C. Zhou, L. Liu, Fabrication and properties of PLA/nano-HA composite scaffolds with balanced mechanical properties and biological functions for bone tissue engineering application, Nanotechnology Reviews 10 (2021) 1359–1373. https://doi.org/10.1515/ntrev-2021-0083.
[215] H. Zhang, X. Mao, D. Zhao, W. Jiang, Z. Du, Q. Li, C. Jiang, D. Han, Three dimensional printed polylactic acid-hydroxyapatite composite scaffolds for prefabricating vascularized tissue engineered bone: An in vivo bioreactor model, Scientific Reports 7 (2017). https://doi.org/10.1038/s41598-017-14923-7.
[216] B.W. Minto, A.G. Sprada, J.A. Gonçalves Neto, B.M. de Alcântara, T.A.S. de S. Rocha, A.C.V. Hespanha, C. Quarterone, M. da R. Sartori, A. Hataka, R.A.R. Uscategui, L.G.G.G. Dias, Three-dimensional printed poly (L-lactide) and hydroxyapatite composite for reconstruction of critical bone defect in rabbits, Acta Cir. Bras. 36 (2021) e360404. https://doi.org/10.1590/acb360404.
[217] I. Gendviliene, E. Simoliunas, M. Alksne, S. Dibart, E. Jasiuniene, V. Cicenas, R. Jacobs, V. Bukelskiene, V. Rutkunas, Effect of extracellular matrix and dental pulp stem cells on bone regeneration with 3D printed PLA/HA composite scaffolds., European Cells & Materials 41 (2021) 204–215. https://doi.org/10.22203/eCM.v041a15.
[218] M.O.C. Maia-Pinto, A.C.B. Brochado, B.N. Teixeira, S.C. Sartoretto, M.J. Uzeda, A.T.N.N. Alves, G.G. Alves, M.D.M.D.M.D. Calasans-Maia, R.M.S.M. Thiré, R.M.S.M. Thire, R.M.S.M. Thiré, Biomimetic Mineralization on 3D Printed PLA Scaffolds: On the Response of Human Primary Osteoblasts Spheroids and In Vivo Implantation, POLYMERS 13 (2021). https://doi.org/10.3390/polym13010074.
[219] C. Tu, J. Chen, C. Huang, Y. Xiao, X. Tang, H. Li, Yongzhuang, J. Yan, W. Li, H. Wu, C. Liu, Effects of electromagnetic fields treatment on rat critical-sized calvarial defects with a 3D-printed composite scaffold, Stem Cell Research & Therapy 11 (2020). https://doi.org/10.1186/s13287-020-01954-7.

[220] D.Y. Kwon, J.H. Park, S.H. Jang, J.Y. Park, J.W. Jang, B.H. Min, W.-D. Kim, H.B. Lee, J. Lee, M.S. Kim, Bone regeneration by means of a three-dimensional printed scaffold in a rat cranial defect., Journal of Tissue Engineering and Regenerative Medicine 12 (2018) 516–528. https://doi.org/10.1002/term.2532.
[221] I. Tcacencu, N. Rodrigues, N. Alharbi, M. Benning, S. Toumpaniari, E. Mancuso, M. Marshall, O. Bretcanu, M. Birch, A. McCaskie, K. Dalgarno, Osseointegration of porous apatite-wollastonite and poly(lactic acid) composite structures created using 3D printing techniques, Materials Science & Engineering C-Materials for Biological Applications 90 (2018) 1–7. https://doi.org/10.1016/j.msec.2018.04.022.
[222] Z. Xu, B. Lin, C. Zhao, Y. Lu, T. Huang, Y. Chen, J. Li, R. Wu, W. Liu, J. Lin, Lanthanum doped octacalcium phosphate/polylactic acid scaffold fabricated by 3D printing for bone tissue engineering, Journal of Materials Science & Technology 118 (2022) 229–242. https://doi.org/10.1016/j.jmst.2021.09.069.
[223] N.P. Tipnis, D.J. Burgess, Sterilization of implantable polymer-based medical devices: A review, International Journal of Pharmaceutics 544 (2018) 455–460. https://doi.org/10.1016/j.ijpharm.2017.12.003.
[224] L.-C. Gerhardt, A.R. Boccaccini, Bioactive Glass and Glass-Ceramic Scaffolds for Bone Tissue Engineering, Materials 3 (2010) 3867–3910. https://doi.org/10.3390/ma3073867.
[225] K. Hayashi, M.L. Munar, K. Ishikawa, Effects of macropore size in carbonate apatite honeycomb scaffolds on bone regeneration, Materials Science and Engineering: C 111 (2020) 110848. https://doi.org/10.1016/j.msec.2020.110848.
[226] N. Abbasi, S. Hamlet, R.M. Love, N.-T. Nguyen, Porous scaffolds for bone regeneration, Journal of Science: Advanced Materials and Devices 5 (2020) 1–9. https://doi.org/10.1016/j.jsamd.2020.01.007.
[227] K.-W. Chong, C.Y.-L. Woon, M.-K. Wong, Induced Membranes—A Staged Technique of Bone-Grafting for Segmental Bone Loss: Surgical Technique, Journal of Bone and Joint Surgery 93 (2011) 85–91. https://doi.org/10.2106/JBJS.J.01251.
[228] G. Kister, G. Cassanas, M. Vert, Effects of morphology, conformation and configuration on the IR and Raman spectra of various poly(lactic acid)s, Polymer 39 (1998) 267–273. https://doi.org/10.1016/S0032-3861(97)00229-2.
[229] M.G. Gandolfi, F. Zamparini, M. Degli Esposti, F. Chiellini, C. Aparicio, F. Fava, P. Fabbri, P. Taddei, C. Prati, Polylactic acid-based porous scaffolds doped with calcium silicate and dicalcium phosphate dihydrate designed for biomedical application, Materials Science and Engineering: C 82 (2018) 163–181. https://doi.org/10.1016/j.msec.2017.08.040.
[230] H. Aguiar, S. Chiussi, M. López-Álvarez, P. González, J. Serra, Structural characterization of bioceramics and mineralized tissues based on Raman and XRD techniques, Ceramics International 44 (2018) 495–504. https://doi.org/10.1016/j.ceramint.2017.09.203.
[231] S. Koutsopoulos, Synthesis and characterization of hydroxyapatite crystals: A review study on the analytical methods, J. Biomed. Mater. Res. 62 (2002) 600–612. https://doi.org/10.1002/jbm.10280.
[232] S. Nanaki, P. Barmpalexis, A. Iatrou, E. Christodoulou, M. Kostoglou, D. Bikiaris, Risperidone Controlled Release Microspheres Based on Poly(Lactic Acid)-Poly(Propylene Adipate) Novel Polymer Blends Appropriate for Long Acting Injectable Formulations, Pharmaceutics 10 (2018) 130. https://doi.org/10.3390/pharmaceutics10030130.

[233] S. Mondal, T.P. Nguyen, V.H. Pham, G. Hoang, P. Manivasagan, M.H. Kim, S.Y. Nam, J. Oh, Hydroxyapatite nano bioceramics optimized 3D printed poly lactic acid scaffold for bone tissue engineering application, Ceramics International 46 (2020) 3443–3455. https://doi.org/10.1016/j.ceramint.2019.10.057.
[234] M. Tanase-Opedal, E. Espinosa, A. Rodríguez, G. Chinga-Carrasco, Lignin: A Biopolymer from Forestry Biomass for Biocomposites and 3D Printing, Materials 12 (2019) 3006. https://doi.org/10.3390/ma12183006.
[235] M.M. Rahman, S. Afrin, P. Haque, Md.M. Islam, M.S. Islam, Md.A. Gafur, Preparation and Characterization of Jute Cellulose Crystals-Reinforced Poly(L-lactic acid) Biocomposite for Biomedical Applications, International Journal of Chemical Engineering 2014 (2014) 1–7. https://doi.org/10.1155/2014/842147.
[236] M.A. Nazeer, O.C. Onder, I. Sevgili, E. Yilgor, I.H. Kavakli, I. Yilgor, 3D printed poly(lactic acid) scaffolds modified with chitosan and hydroxyapatite for bone repair applications, Materials Today Communications 25 (2020) 101515. https://doi.org/10.1016/j.mtcomm.2020.101515.
[237] JM. Hughes, M. Cameron, J. Rakovan, Structural variations in natural F,OH, and CL apatites, American Mineralogist 74 (1989) 870–876.
[238] H.L. Jang, K. Jin, J. Lee, Y. Kim, S.H. Nahm, K.S. Hong, K.T. Nam, Revisiting Whitlockite, the Second Most Abundant Biomineral in Bone: Nanocrystal Synthesis in Physiologically Relevant Conditions and Biocompatibility Evaluation, ACS Nano 8 (2014) 634–641. https://doi.org/10.1021/nn405246h.
[239] L. González-Rodríguez, S. Pérez-Davila, R. Lama, M. López-Álvarez, J. Serra, B. Novoa, A. Figueras, P. González, 3D printing of PLA:CaP:GO scaffolds for bone tissue applications, RSC Adv. 13 (2023) 15947–15959. https://doi.org/10.1039/D3RA00981E.
[240] C. Esposito Corcione, F. Gervaso, F. Scalera, S.K. Padmanabhan, M. Madaghiele, F. Montagna, A. Sannino, A. Licciulli, A. Maffezzoli, Highly loaded hydroxyapatite microsphere/ PLA porous scaffolds obtained by fused deposition modelling, Ceramics International 45 (2019) 2803–2810. https://doi.org/10.1016/j.ceramint.2018.07.297.
[241] M.R. Allen, Preclinical Models for Skeletal Research: How Commonly Used Species Mimic (or Don't) Aspects of Human Bone, Toxicol Pathol 45 (2017) 851–854. https://doi.org/10.1177/0192623317733925.
[242] L.M. Wancket, Animal Models for Evaluation of Bone Implants and Devices: Comparative Bone Structure and Common Model Uses, Vet Pathol 52 (2015) 842–850. https://doi.org/10.1177/0300985815593124.
[243] A. Pearce, R. Richards, S. Milz, E. Schneider, S. Pearce, Animal models for implant biomaterial research in bone: A review, eCM 13 (2007) 1–10. https://doi.org/10.22203/eCM.v013a01.
[244] S. Zeiter, K. Koschitzki, M. Alini, F. Jakob, M. Rudert, M. Herrmann, Evaluation of Preclinical Models for the Testing of Bone Tissue-Engineered Constructs, Tissue Engineering Part C: Methods 26 (2020) 107–117. https://doi.org/10.1089/ten.tec.2019.0213.
[245] A.T. Khalaf, Y. Wei, J. Wan, J. Zhu, Y. Peng, S.Y. Abdul Kadir, J. Zainol, Z. Oglah, L. Cheng, Z. Shi, Bone Tissue Engineering through 3D Bioprinting of Bioceramic Scaffolds: A Review and Update, Life 12 (2022) 903. https://doi.org/10.3390/life12060903.
[246] R.-S. Chen, S.-H. Hsu, H.-H. Chang, M.-H. Chen, Challenge Tooth Regeneration in Adult Dogs with Dental Pulp Stem Cells on 3D-Printed Hydroxyapatite/Polylactic Acid Scaffolds, CELLS 10 (2021). https://doi.org/10.3390/cells10123277.

[247] A.M. Maadani, E. Salahinejad, Performance comparison of PLA- and PLGA-coated porous bioceramic scaffolds: Mechanical, biodegradability, bioactivity, delivery and biocompatibility assessments, Journal of Controlled Release 351 (2022) 1–7. https://doi.org/10.1016/j.jconrel.2022.09.022.
[248] Y. Zhao, B. Zhu, Y. Wang, C. Liu, C. Shen, Effect of different sterilization methods on the properties of commercial biodegradable polyesters for single-use, disposable medical devices, Materials Science and Engineering: C 105 (2019) 110041. https://doi.org/10.1016/j.msec.2019.110041.
[249] N.S. Turker, A.Y. Özer, Ş. Çolak, B. Kutlu, R. Nohutçu, ESR investigations of gamma irradiated medical devices, Applied Radiation and Isotopes 130 (2017) 121–130. https://doi.org/10.1016/j.apradiso.2017.09.026.
[250] S. Pérez-Davila, L. González-Rodríguez, R. Lama, M. López-Álvarez, A.L. Oliveira, J. Serra, B. Novoa, A. Figueras, P. González, 3D-Printed PLA Medical Devices: Physicochemical Changes and Biological Response after Sterilisation Treatments, Polymers 14 (2022) 4117. https://doi.org/10.3390/polym14194117.
[251] W. Wang, J. Wei, D. Lei, S. Wang, B. Zhang, S. Shang, B. Bai, C. Zhao, W. Zhang, C. Zhou, H. Zhou, S. Feng, 3D printing of lithium osteogenic bioactive composite scaffold for enhanced bone regeneration, Composites Part B: Engineering 256 (2023) 110641. https://doi.org/10.1016/j.compositesb.2023.110641.
[252] L. Carbone, J. Austin, Pain and Laboratory Animals: Publication Practices for Better Data Reproducibility and Better Animal Welfare, PLoS ONE 11 (2016) e0155001. https://doi.org/10.1371/journal.pone.0155001.
[253] M.K. Huss, S.A. Felt, C. Pacharinsak, Influence of Pain and Analgesia on Orthopedic and Wound-healing Models in Rats and Mice, Comp Med 69 (2019) 535–545. https://doi.org/10.30802/AALAS-CM-19-000013.
[254] M. Guarnieri, C. Brayton, L. DeTolla, N. Forbes-McBean, R. Sarabia-Estrada, P. Zadnik, Safety and efficacy of buprenorphine for analgesia in laboratory mice and rats, Lab Anim 41 (2012) 337–343. https://doi.org/10.1038/laban.152.
[255] L. Benato, N.J. Rooney, J.C. Murrell, Pain and analgesia in pet rabbits within the veterinary environment: a review, Veterinary Anaesthesia and Analgesia 46 (2019) 151–162. https://doi.org/10.1016/j.vaa.2018.10.007.
[256] P. Leucht, J.-B. Kim, R. Wazen, J.A. Currey, A. Nanci, J.B. Brunski, J.A. Helms, Effect of mechanical stimuli on skeletal regeneration around implants, Bone 40 (2007) 919–930. https://doi.org/10.1016/j.bone.2006.10.027.
[257] N. Mangir, S. Dikici, F. Claeyssens, S. MacNeil, Using *ex Ovo* Chick Chorioallantoic Membrane (CAM) Assay To Evaluate the Biocompatibility and Angiogenic Response to Biomaterials, ACS Biomater. Sci. Eng. 5 (2019) 3190–3200. https://doi.org/10.1021/acsbiomaterials.9b00172.
[258] I. Moreno-Jiménez, J.M. Kanczler, G. Hulsart-Billstrom, S. Inglis, R.O.C. Oreffo, <sup/> The Chorioallantoic Membrane Assay for Biomaterial Testing in Tissue Engineering: A Short-Term *In Vivo* Preclinical Model, Tissue Engineering Part C: Methods 23 (2017) 938–952. https://doi.org/10.1089/ten.tec.2017.0186.
[259] P. Bédard, S. Gauvin, K. Ferland, C. Caneparo, È. Pellerin, S. Chabaud, S. Bolduc, Innovative Human Three-Dimensional Tissue-Engineered Models as an Alternative to Animal Testing, Bioengineering 7 (2020) 115. https://doi.org/10.3390/bioengineering7030115.

[260] E. Petrovova, Preclinical alternative model for analysis of porous scaffold biocompatibility in bone tissue engineering, Altex 36 (2019) 121–130. https://doi.org/10.14573/altex.1807241.
[261] A. Weigand, J.P. Beier, A. Arkudas, M. Al-Abboodi, E. Polykandriotis, R.E. Horch, A.M. Boos, The Arteriovenous (AV) Loop in a Small Animal Model to Study Angiogenesis and Vascularized Tissue Engineering, JoVE (2016) 54676. https://doi.org/10.3791/54676.
[262] L. Cai, A.S. Guinn, S. Wang, Exposed hydroxyapatite particles on the surface of photo-crosslinked nanocomposites for promoting MC3T3 cell proliferation and differentiation, Acta Biomaterialia 7 (2011) 2185–2199. https://doi.org/10.1016/j.actbio.2011.01.034.
[263] S.C. Rizzi, D.J. Heath, A.G.A. Coombes, N. Bock, M. Textor, S. Downes, Biodegradable polymer/hydroxyapatite composites: Surface analysis and initial attachment of human osteoblasts, Journal of Biomedical Materials Research 55 (2001) 445–669. https://doi.org/10.1002/1097-4636(20010615)55:4%3C475::AID-JBM1039%3E3.0.CO;2-Q.
[264] J.O. Akindoyo, M.D.H. Beg, S. Ghazali, H.P. Heim, M. Feldmann, Effects of surface modification on dispersion, mechanical, thermal and dynamic mechanical properties of injection molded PLA-hydroxyapatite composites, Composites Part A: Applied Science and Manufacturing 103 (2017) 96–105. https://doi.org/10.1016/j.compositesa.2017.09.013.
[265] B. Majhy, P. Priyadarshini, A.K. Sen, Effect of surface energy and roughness on cell adhesion and growth – facile surface modification for enhanced cell culture, RSC Adv. 11 (2021) 15467–15476. https://doi.org/10.1039/D1RA02402G.
[266] L.-C. Xu, C.A. Siedlecki, Effects of surface wettability and contact time on protein adhesion to biomaterial surfaces, Biomaterials 28 (2007) 3273–3283. https://doi.org/10.1016/j.biomaterials.2007.03.032.
[267] J. Wang, Y. Wu, Y. Cao, G. Li, Y. Liao, Influence of surface roughness on contact angle hysteresis and spreading work, Colloid Polym Sci 298 (2020) 1107–1112. https://doi.org/10.1007/s00396-020-04680-x.
[268] R.N. Wenzel, Resistance Of Solid Surfaces To Wetting By Water, Ind. Eng. Chem. 28 (1936) 988–994. https://doi.org/10.1021/ie50320a024.
[269] F. Peyrin, Evaluation of bone scaffolds by micro-CT, Osteoporos Int 22 (2011) 2043–2048. https://doi.org/10.1007/s00198-011-1609-y.
[270] K. Athanasiou, Sterilization, toxicity, biocompatibility and clinical applications of polylactic acid/ polyglycolic acid copolymers, Biomaterials 17 (1996) 93–102. https://doi.org/10.1016/0142-9612(96)85754-1.
[271] V. Karageorgiou, D. Kaplan, Porosity of 3D biomaterial scaffolds and osteogenesis, Biomaterials 26 (2005) 5474–5491. https://doi.org/10.1016/j.biomaterials.2005.02.002.
[272] C.M. Murphy, M.G. Haugh, F.J. O'Brien, The effect of mean pore size on cell attachment, proliferation and migration in collagen–glycosaminoglycan scaffolds for bone tissue engineering, Biomaterials 31 (2010) 461–466. https://doi.org/10.1016/j.biomaterials.2009.09.063.
[273] H. Qin, Y. Wei, J. Han, X. Jiang, X. Yang, Y. Wu, Z. Gou, L. Chen, 3D printed bioceramic scaffolds: Adjusting pore dimension is beneficial for mandibular bone defects repair, J Tissue Eng Regen Med 16 (2022) 409–421. https://doi.org/10.1002/term.3287.
[274] F. Zhao, M. Kirby, A. Roy, Y. Hu, X.E. Guo, X. Wang, Commonality in the microarchitecture of trabecular bone: A preliminary study, Bone 111 (2018) 59–70. https://doi.org/10.1016/j.bone.2018.03.003.

[275] M. Domingos, F. Intranuovo, T. Russo, R.D. Santis, A. Gloria, L. Ambrosio, J. Ciurana, P. Bartolo, The first systematic analysis of 3D rapid prototyped poly(ε-caprolactone) scaffolds manufactured through BioCell printing: the effect of pore size and geometry on compressive mechanical behaviour and *in vitro* hMSC viability, Biofabrication 5 (2013) 045004. https://doi.org/10.1088/1758-5082/5/4/045004.

[276] M. Xu, D. Zhai, J. Chang, C. Wu, In vitro assessment of three-dimensionally plotted nagelschmidtite bioceramic scaffolds with varied macropore morphologies, Acta Biomaterialia 10 (2014) 463–476. https://doi.org/10.1016/j.actbio.2013.09.011.

[277] M. Domingos, F. Chiellini, S. Cometa, E.D. Giglio, E. Grillo-Fernandes, P. Bartolo, E. Chiellini, Evaluation of *in vitro* degradation of PCL scaffolds fabricated via BioExtrusion – Part 2: Influence of pore size and geometry: The present study is to accurately investigate the influence of design parameters, such as filament distance (FD) and lay-down pattern, on the degradation behaviour and kinetics of PCL scaffolds, obtained via BioExtrusion, Virtual and Physical Prototyping 6 (2011) 157–165. https://doi.org/10.1080/17452759.2011.605839.

[278] D.W. Hutmacher, T. Schantz, I. Zein, K.W. Ng, S.H. Teoh, K.C. Tan, Mechanical properties and cell cultural response of polycaprolactone scaffolds designed and fabricated via fused deposition modeling, J. Biomed. Mater. Res. 55 (2001) 203–216. https://doi.org/10.1002/1097-4636(200105)55:2<203::AID-JBM1007>3.0.CO;2-7.

[279] L. Moroni, J.R. De Wijn, C.A. Van Blitterswijk, Three-dimensional fiber-deposited PEOT/PBT copolymer scaffolds for tissue engineering: Influence of porosity, molecular network mesh size, and swelling in aqueous media on dynamic mechanical properties, J Biomedical Materials Res 75A (2005) 957–965. https://doi.org/10.1002/jbm.a.30499.

[280] T. Serra, J.A. Planell, M. Navarro, High-resolution PLA-based composite scaffolds via 3-D printing technology, Acta Biomaterialia 9 (2013) 5521–5530. https://doi.org/10.1016/j.actbio.2012.10.041.

ANEXOS

8 ANEXOS

8.1 ANEXO I: PERMISOS PARA EL USO DE IMÁGENES

Las imágenes incluidas en la presente Tesis Doctoral obtenidas a partir de publicaciones de otros autores fueron utilizadas bajo los términos de la Licencia "Creative Commons Attribution 4.0 International, CC BY-NC.ND 4.0". El resto de las imágenes empleadas fueron realizadas por el autor (imágenes propias) o cedidas por el Grupo de Novos Materiais de la Universidade de Vigo. El origen de cada imagen fue especificado en el pie de figura junto a su descripción.

8.2 ANEXO II: LISTA DE VERIFICACIÓN ARRIVE

Lista de verificación para Tesis con animales de experimentación. **EXPERIMENTACIÓN ANIMAL ARRIVE**

Sí/no/NA		página
	Título	
Sí	Proporcionar una descripción tan exacta y concisa como sea posible sobre el contenido del trabajo.	Portada
	Resumen	
Sí	Proporcionar un resumen preciso de los antecedentes, los objetivos de la investigación, incluyendo detalles de la especie y cepa de los animales utilizados, métodos relevantes, hallazgos principales y conclusiones del estudio.	7-8
	Antecedentes	
Sí	Incluir suficientes antecedentes científicos (incluyendo las referencias pertinentes al trabajo anterior) a fin de comprender la motivación y el contexto para el estudio, y explicar las bases y el enfoque experimental.	11-28
Sí	Explicar cómo y por qué la especie y el modelo animal utilizados permiten abordar los objetivos científicos y, cuando sea apropiado, la relevancia del estudio para la biología humana.	89
	Objetivos	
Sí	Describir claramente los objetivos primarios y secundarios del estudio, o las hipótesis específicas que se van a probar.	31
	Declaración Ética	
Sí	Indicar el permiso del comité ético, y las leyes o decretos pertinentes para el cuidado y uso de animales, bajo las que se realiza la investigación.	42
	Diseño del estudio	
Sí	Número de grupos experimentales y control.	42-45
Sí	Cualquier medida adoptada para minimizar los efectos de sesgo subjetivo al asignar los animales a los grupos de tratamiento (por ej., procedimiento aleatorio) y al evaluar los resultados (por ej., si se hace, describir quiénes eran ciegos y cuándo).	42-45
Sí	La unidad experimental (por ej., un solo animal, grupos o jaulas de animales). Un diagrama cronológico o de flujo pueden ser útiles para ilustrar cómo se realizaron los diseños de estudio complejos.	42-45
	Procedimientos experimentales	
Sí	Cómo (por ej., formulación y dosis del tratamiento, el sitio y la vía de administración, anestesia y analgesia utilizadas [incluyendo la monitorización], procedimiento quirúrgico, el método de eutanasia). Proporcionar detalles de cualquier equipo especializado utilizado, incluyendo proveedor(es).	43-45
NA	Cuándo (por ej., la hora del día).	No procede
NA	Dónde (por ej., jaula de alojamiento, laboratorio, prueba del laberinto acuático).	No procede
Sí	Por qué (por ej., fundamentos para la elección del anestésico específico, la vía de administración, dosis del fármaco utilizado).	43-45
	Animales de experimentación	

Sí	Proporcionar detalles de los animales utilizados, incluyendo especie, cepa, sexo, etapa de desarrollo (por ej., edad media o mediana de edad y rango) y peso (por ej., media o mediana más rango de peso).	42
Sí	Proporcionar otra información pertinente, como la procedencia de los animales, nomenclatura internacional de la cepa, modificación genética (por ej., animal deficiente o transgénico), genotipo, estado de salud/inmune, si los animales han sido incluidos en estudios o recibido tratamientos anteriormente, procedimientos previos, etc.	42
	Animales	
Sí	Alojamiento (tipo de instalación por ej., libre de patógenos específicos [SPF], tipo de jaula o habitáculo, material del lecho, número de animales por jaula, forma y material del tanque, etc. para peces).	42
Sí	Condiciones de cría (por ej., programa de reproducción, ciclo de luz/oscuridad, temperatura, calidad de agua, etc. para peces, el tipo de alimentación, el acceso a los alimentos y al agua, enriquecimiento ambiental).	42
Sí	Evaluaciones e intervenciones relacionadas con el bienestar que se llevaron a cabo antes, durante o después del experimento	42-45
	Tamaño de la muestra	
Sí	Especificar el número total de animales utilizados en cada experimento, y el número de animales en cada grupo experimental.	42-45
Sí	Explicar cómo se determinó el número de animales. Proporcionar detalles del cálculo del tamaño muestral utilizado.	42
NA	Indicar el número de repeticiones independientes de cada experimento, si es pertinente.	No procede
	Asignación de animales a grupos experimentales	
Sí	Proporcionar detalles completos de la forma en que los animales fueron asignados a grupos experimentales, incluyendo distribución aleatoria o asignación específica, si así se hizo.	43-45
Sí	Describir el orden en el que los animales en los diferentes grupos experimentales fueron tratados y evaluados.	43-45
Sí	Resultados experimentales 12 Definir claramente los resultados primarios y secundarios evaluados (por ej., muerte celular, marcadores moleculares, cambios de comportamiento).	36-48
	Métodos estadísticos	
Sí	Proporcionar detalles sobre los métodos estadísticos utilizados para cada análisis.	47-48
Sí	Especificar la unidad de análisis para cada grupo de datos (por ej., un solo animal, grupo de animales, neurona individual).	42-45
Sí	Describir los métodos utilizados para evaluar si los datos corroboran las suposiciones del método estadístico.	47-48
	Datos basales	
Sí	Para cada grupo experimental, indicar las características relevantes y estado de salud de los animales (por ej., peso, estado microbiológico, si los animales han sido incluidos en estudios o recibido drogas anteriormente) antes de iniciar el tratamiento o prueba. (Esta información puede ser a menudo tabulada).	42
	Cantidades analizadas	
Sí	Indicar el número de animales en cada grupo incluido en cada análisis. Presentar números absolutos (por ej., 10/20, no 50 %2).	42-45
Sí	Si alguno de los animales o datos no fue incluido en el análisis, explicar por qué.	72, 82-84
	Resultados y Discusión	

Sí	Indicar los resultados de cada análisis llevado a cabo, con una medida de precisión (por ej., error estándar o intervalo de confianza).	65-87
	Eventos adversos	
Sí	Dar detalles de todos los eventos adversos importantes en cada grupo experimental.	42,72,82
NA	Describir las modificaciones a los protocolos experimentales realizadas para reducir los eventos adversos.	No procede
	Interpretación /implicaciones científicas	
Sí	Interpretar los resultados, teniendo en cuenta los objetivos y las hipótesis del estudio, la teoría actual y otros estudios pertinentes en la literatura.	91-106
Sí	Comentar las limitaciones del estudio incluyendo cualquier fuente potencial de sesgo, cualquier limitación del modelo animal y la imprecisión asociada con los resultados	95,106
Sí	Describir cualquier implicación de los métodos experimentales o hallazgos para el reemplazo, refinamiento o reducción (las 3 R) del uso de los animales en investigación.	96,97
	Capacidad de generalización/aplicabilidad	
Sí	Comentar si, y de qué forma, los hallazgos de este estudio son aplicables a otras especies o sistemas, incluyendo cualquier relevancia para la biología humana.	91-106, 109
	Financiación	
Sí	Listar todas las fuentes de financiación (incluyendo el número del proyecto) y el papel de la fuente(s) de financiación en el estudio.	Apartado Financiación

Basado en The ARRIVE guidelines: Animal Research: Reporting of In Vivo Experiments.

Firma Doctorando

8.3 ANEXO III: AUTORIZACIÓN DEL COMITÉ DE BIOÉTICA Y CERTIFICADOS DE CAPACITACIÓN

XUNTA DE GALICIA
CONSELLERÍA DO MEDIO RURAL

Xefatura territorial de Lugo
Servizo de Gandaría
Ronda da Muralla, 70
LUGO

galicia

RESOLUCIÓN DE AUTORIZACIÓN DE PROXECTOS DE EXPERIMENTACIÓN ANIMAL

Expediente núm: 02/20/LU-002
Interesado: **Fernando Muñoz Guzón**
Procedemento: RESOLUCIÓN DE AUTORIZACIÓN DE PROXECTOS DE EXPERIMENTACIÓN ANIMAL
Data de inicio: 5 de xuño de 2020
Forma de inicio: solicitude do interesado

ANTECEDENTES

O interesado, como responsable do proxecto "**Evaluación de biomateriales según norma UNE-EN ISO 10933-6:2017 (2020-2525)"** presentou, con data 15 de maio de 2020, solicitude para a realización do proxecto de experimentación animal cuxos datos se detallan a continuación:

Denominación do proxecto : Evaluación de biomateriales según norma UNE-EN ISO 10933-6:2017 (2020-2525).
Nome do centro usuario: animalario de Facultade de Veterinaria (AE-LU-002).
Persoa responsable do proxecto: Fernando Muñoz Guzón.
Establecemento onde se realizarán os procedementos do proxecto (ou lugar xeográfico no caso de traballos de campo) animalario de Facultade de Veterinaria (AE-LU-002).
Clasificación do proxecto : **Tipo I**

CONSIDERACIÓNS LEGAIS E TÉCNICAS

Real decreto 53/2013, de 1 de febreiro (BOE núm. 34, do 8 de febreiro), polo que se establecen as normas básicas aplicables para a protección dos animais utilizados en experimentación e outros fins científicos, incluíndo a docencia, establece no seu artigo 33 as condicións de autorizacións dos proxectos con animais de experimentación.

Artigo 88 da Lei 39/2015, do 1 de outubro, do procedemento administrativo común das administracións públicas (BOE núm. 236, do 2 de outubro) establece que a resolución que poña fin ao procedemento decidirá todas as cuestións formuladas polos interesados e aquelas outras derivadas del.

Esta xefatura territorial é competente para ditar resolución de conformidade co artigo 11 do Decreto 245/2009, do 30 de abril, polo que se regulan as delegacións territoriais da Xunta de Galicia e o Decreto 149/2018, do 5 de decembro, polo que establece a estrutura orgánica da Consellería do Medio Rural. O Servizo Provincial de Gandería de Lugo revisou a documentación presentada coa solicitude e visto o informe favorable da avaliación do proxecto, de data 12 de

maio de 2020 emitido polo órgano habilitado, e o Comité de Ética da Universidade de Santiago de Compostela, esta xefatura territorial resolve **AUTORIZAR** o proxecto solicitado.

A autorización deste proxecto terá unha duración de **5 ANOS** e unha vez que transcorran deberán renovala.

A autorización é unicamente válida nas condicións que figuran no expediente. Ante calquera cambio significativo no proxecto que poida ter efectos negativos sobre o benestar dos animais, deberá solicitar a confirmación da autorización ao Servizo Provincial de Gandería.

Esta autorización poderá ser suspendida no caso de que o proxecto non se leve a cabo de acordo coas condicións de autorización e retirala previo expediente tramitado ao que se lle dará audiencia.

Contra a presente resolución, que non pon fin á vía administrativa, poderá interpor recurso de alzada ante o conselleiro de Medio Rural da Xunta de Galicia no prazo dun mes contado a partir da recepción da notificación da presente resolución, conforme cos artigos 121 e 122 da Lei 39/2015, do 1 de outubro, do procedemento administrativo común das administracións públicas.

Documento asinado electronicamente á marxe

VICERREITORADO DE INVESTIGACIÓN
E INNOVACIÓN
Oficina de Investigación e Tecnoloxía

Edificio CACTUS – Campus universitario sur
15782 Santiago de Compostela
Tel. 981 547 040 - Fax 981 547 077
Correo electrónico: cittinfo@usc.es
http://imaisd.usc.es

Informe del Comité de Ética de Experimentación Animal (CEEA) de los centros usuarios de animales de experimentación de la USC en el Campus de Lugo

El CEEA de los centros usuarios de animales de experimentación de la USC en el Campus de Lugo, tras evaluar el Proyecto titulado "Evaluación de biomateriales según norma UNE-EN ISO 10993-6: 2017 (2020-2025)" del que es Investigador responsable D. Fernando Muñoz Guzón, acordó con fecha 12 de mayo de 2020 emitir

INFORME FAVORABLE

para la realización de dicho Proyecto, así como los procedimientos que incluye, en las instalaciones del establecimiento usuario Animalario de la Facultad de Veterinaria, con número de registro ES270280331701 (AE-LU-002), y siempre que, en cumplimiento del RD 53/2013, se obtenga la correspondiente autorización administrativa (en concreto, en relación con el artículo 27.2 y el apartado 1.b de la cláusula de salvaguardia enunciada en la disposición adicional segunda).

En Lugo, a 12 de mayo de 2020

Fdo.: La presidenta

Sonia Vázquez Rodríguez

Supervisora das instalacións de experimentación, cría e subministro de animais de laboratorio da Universidade de Santiago de Compostela

Responsable administrativo:	Nombre:Montserrat Valcárcel Armesto Cargo:Vicerreitora de Coordinación do Campus de Lugo	V°B° Firma y sello

VICERREITORÍA DE INVESTIGACIÓN
E INNOVACIÓN
Oficina de Investigación e Tecnoloxía
Servizo de Convocatorias e Recursos Humanos de I+S
Edificio CACTUS – Campus Vida
15782 Santiago de Compostela
Tel. 981 547 040 - Fax 981 547 077
Correo electrónico: cittinfo@usc.es
http://imaisd.usc.es

JOSÉ MANUEL CIFUENTES MARTÍNEZ, PRESIDENTE DEL COMITÉ DE BIOÉTICA DE LA UNIVERSIDAD DE SANTIAGO DE COMPOSTELA, cuya Sección de Experimentación animal ha sido designada como Órgano Habilitado para la evaluación de proyectos de experimentación animal por resolución de la Xunta de Galicia, con fecha 11 de noviembre de 2013, de acuerdo con lo exigido por el RD 53/2013 de 1 de febrero, por el que se establecen las normas básicas aplicables para la protección de los animales utilizados en experimentación y otros fines científicos, incluyendo la docencia,

INFORMA:

Que el proyecto de investigación titulado: **"Evaluación de biomateriales según norma UNE-EN ISO 10993-6: 2017 (2020-2025)"** del que es investigadora responsable **D. Fernando Mª Muñoz Guzón,** ha sido examinado por el Comité de Bioética de esta Universidad, Sección de Experimentación Animal, llegando a las siguientes conclusiones:

Con respecto a su finalidad, se trata de un proyecto de investigación que se enmarca dentro del desarrollo y fabricación de productos farmacéuticos, alimenticios, piensos y otras sustancias o productos así como la realización de pruebas para comprobar su calidad, eficacia y seguridad; cuyo objetivo es valorar la biocompatibilidad de nuevos materiales implantables. Dichos ensayos se hacen conforme a la norma UNE-EN ISO 10993-6:2017. Dicha norma específica los métodos de ensayo para la evaluación de los efectos locales después de la implantación de biomateriales implantables previstos para su utilización como productos sanitarios. La realización de los estudios mediante esta metodología permite que si en el futuro dichos materiales quieren comercializarse no es necesaria la repetición de los procedimientos para obtener el marcaje CE o FDA. Así mismo, al ser procedimientos normalizados permiten la comparación de resultados en el futuro.

- Con respecto a los requisitos de las 3Rs,
  - No cabe la posibilidad de reemplazo ya que no se han encontrado métodos o estrategias de ensayo que permitan llevar a cabo los experimentos propuestos en este trabajo.
  - La experimentación se realizará en un centro registrado como usuario de animales de experimentación por lo que la manipulación, manejo y supervisión de los animales durante todo el proyecto será llevada a cabo por personas capacitadas. El grupo investigador lo componen personas con capacitaciones a, b, c, d, e, y f, lo que asegura su preparación para garantizar el bienestar animales durante todos los procedimientos (requisito de refinamiento).
  - Finalmente, con respecto al requisito de reducción, se considera que el número de animales a utilizar es el mínimo imprescindible para la obtención de los resultados.
- La clasificación de los procedimientos en función de su grado de severidad es de "moderado".
- Con respecto al balance de los daños y los beneficios, los procedimientos se efectúan bajo analgesia y anestesia previa a las intervenciones por lo que se minimiza el dolor, angustia y

VICERREITORÍA DE INVESTIGACIÓN
E INNOVACIÓN
Oficina de Investigación e Tecnoloxía
Servizo de Convocatorias e Recursos Humanos de I+S
Edificio CACTUS – Campus Vida
15782 Santiago de Compostela
Tel. 981 547 040 - Fax 981 547 077
Correo electrónico: cittinfo@usc.es
http://imaisd.usc.es

sufrimiento. Los métodos de sacrificio descritos (sobredosis de anestesia previa sedación) se encuentran entre los indicados por el propio RD 53/2013.

- Se han examinado las situaciones y excepciones previstas en el punto e) del artículo 34. 2 encontrando que ninguna de ellas es aplicable en este proyecto.
- El proyecto se clasifica como tipo I por tanto no necesita ser sometido a evaluación retrospectiva.

Por todas estas razones, este Comité acordó emitir un **INFORME FAVORABLE.**

En la evaluación de este proyecto NO HA EXISTIDO CONFLICTO DE INTERESES.

Lugo, 13 de mayo de 2020

AXENCIA GALEGA DA CALIDADE ALIMENTARIA

Certificado de mantemento de capacitación en materia de protección de animais utilizados, criados ou subministrados con fins de experimentación e outros fins científicos, incluíndo a docencia conforme coa Orde ECC/566/2015 de 20 de marzo.

Certificado de mantenimiento de capacitación en materia de protección de animales utilizados, criados o suministrados con fines de experimentación y otros fines científicos, incluyendo la docencia conforme con la Orden ECC/566/2015 de 20 de marzo.

1. IDENTIFICACIÓN / *IDENTIFICACIÓN*

1.1. Apelidos / *Apellidos*

Alonso Fernández

1.2. Nome / *Nombre*	DNI / *DNI*
Iván	**53520364P**

1.3. Función / *Función*	1.4. Grupo ou grupos de especies* / *Grupo o grupos de especies**	1.5. Período de vixencia / *Período de vigencia*
"a"	**todos**	Do/*Del* **02/04/2023** ó/*al* **02/04/2031**

2. Nº DO CERTIFICADO / *Nº DEL CERTIFICADO*

m01a107

3.ORGANISMO QUE EXPIDE O CERTIFICADO / *ORGANISMO QUE EXPIDE EL CERTIFICADO*

3.1. Nome e enderezo do organismo que expide o certificado / *Nombre y dirección del organismo que expide el certificado*

AXENCIA GALEGA DA CALIDADE ALIMENTARIA
CONSELLERÍA DO MEDIO RURAL – XUNTA DE GALICIA
Rúa do Camiño Francés, 10 baixo
15781 Santiago de Compostela
A Coruña (España)

3.2. Teléfono / *Teléfono*	3.3. Fax / *Fax*	3.4. Correo electrónico / *Correo electrónico*
981 546 657	981 546 651	formacion.cmrm@xunta.gal

3.5. Data / *Fecha*	3.6. Lugar / *Lugar*
Ver sinatura / *ver firma*	**Santiago de Compostela**

3.7. Nome e sinatura / *Nombre y firma*

Santiago de Compostela,

O director da Axencia Galega da Calidade Alimentaria

Por delegación de sinatura (Resolución do 15/02/2022)

O xefe da Área de Formación, Innovación e Investigación Agraria

Manuel López Luaces

* Anexo II da Orde ECC/566/2015, do 20 de marzo: 1 (roedores), 2 (lagomorfos), 3 (carnívoros), 4 (équidos, ruminantes e porcino), 5 (primates), 6 (aves), 7 (réptiles), 8 (peixes e anfibios), 9 (cefalópodos), 10 (animais silvestres), 11 (outras especies).
* Anexo II de la Orden ECC/566/2015, de 20 de marzo: 1 (roedores), 2 (lagomorfos), 3 (carnívoros), 4 (équidos, rumiantes y porcino), 5 (primates), 6 (aves), 7 (reptiles), 8 (peces y anfibios), 9 (cefalópodos), 10 (animales silvestres), 11 (otras especies).
O mantemento da capacitación deberá solicitarse durante os oito meses anteriores á finalización do período de vixencia, preferiblemente entre os oito e os tres meses anteriores á finalización do mesmo. / *El mantenimiento de la capacitación deberá solicitarse durante los ocho meses anteriores a la finalización del periodo de vigencia, preferiblemente entre los ocho y los tres meses anteriores a la finalización del mismo.*

AXENCIA GALEGA DA CALIDADE ALIMENTARIA

Certificado de mantemento de capacitación en materia de protección de animais utilizados, criados ou subministrados con fins de experimentación e outros fins científicos, incluíndo a docencia conforme coa Orde ECC/566/2015 de 20 de marzo.

Certificado de mantenimiento de capacitación en materia de protección de animales utilizados, criados o suministrados con fines de experimentación y otros fines científicos, incluyendo la docencia conforme con la Orden ECC/566/2015 de 20 de marzo.

1. IDENTIFICACIÓN / *IDENTIFICACIÓN*

1.1. Apelidos / *Apellidos*

Muñoz Guzón

1.2. Nome / *Nombre*	DNI / *DNI*
Fernando	**02231460T**

1.3. Función / *Función*	1.4. Grupo ou grupos de especies* / *Grupo o grupos de especies**	1.5. Período de vixencia / *Período de vigencia*
"f"	**todos**	Do/*Del* **02/04/2023** ó/*al* **02/04/2031**

2. Nº DO CERTIFICADO / *Nº DEL CERTIFICADO*

m01f004

3.ORGANISMO QUE EXPIDE O CERTIFICADO / *ORGANISMO QUE EXPIDE EL CERTIFICADO*

3.1. Nome e enderezo do organismo que expide o certificado / *Nombre y dirección del organismo que expide el certificado*

AXENCIA GALEGA DA CALIDADE ALIMENTARIA
CONSELLERÍA DO MEDIO RURAL – XUNTA DE GALICIA
Rúa do Camiño Francés, 10 baixo
15781 Santiago de Compostela
A Coruña (España)

3.2. Teléfono / *Teléfono*	3.3. Fax / *Fax*	3.4. Correo electrónico / *Correo electrónico*
981 546 657	981 546 651	formacion.cmrm@xunta.gal

3.5. Data / *Fecha*	3.6. Lugar / *Lugar*
Ver sinatura / *ver firma*	**Santiago de Compostela**

3.7. Nome e sinatura / *Nombre y firma*

Santiago de Compostela,

O director da Axencia Galega da Calidade Alimentaria

Por delegación de sinatura (Resolución do 15/02/2022)

O xefe da Área de Formación, Innovación e Investigación Agraria

Manuel López Luaces

* Anexo II da Orde ECC/566/2015, do 20 de marzo: 1 (roedores), 2 (lagomorfos), 3 (carnívoros), 4 (équidos, ruminantes e porcino), 5 (primates), 6 (aves), 7 (réptiles), 8 (peixes e anfibios), 9 (cefalópodos), 10 (animais silvestres), 11 (outras especies).
* Anexo II de la Orden ECC/566/2015, de 20 de marzo: 1 (roedores), 2 (lagomorfos), 3 (carnívoros), 4 (équidos, rumiantes y porcino), 5 (primates), 6 (aves), 7 (reptiles), 8 (peces y anfibios), 9 (cefalópodos), 10 (animales silvestres), 11 (otras especies).
O mantemento da capacitación deberá solicitarse durante os oito meses anteriores á finalización do período de vixencia, preferiblemente entre os oito e os tres meses anteriores á finalización do mesmo. / *El mantenimiento de la capacitación deberá solicitarse durante los ocho meses anteriores a la finalización del periodo de vigencia, preferiblemente entre los ocho y los tres meses anteriores a la finalización del mismo.*

AXENCIA GALEGA DA CALIDADE ALIMENTARIA

Certificado de mantemento de capacitación en materia de protección de animais utilizados, criados ou subministrados con fins de experimentación e outros fins científicos, incluíndo a docencia conforme coa Orde ECC/566/2015 de 20 de marzo.

Certificado de mantenimiento de capacitación en materia de protección de animales utilizados, criados o suministrados con fines de experimentación y otros fines científicos, incluyendo la docencia conforme con la Orden ECC/566/2015 de 20 de marzo.

1. IDENTIFICACIÓN / *IDENTIFICACIÓN*

1.1. Apelidos / *Apellidos*

González Cantalapiedra

1.2. Nome / *Nombre*	DNI / *DNI*
Antonio	**09280718B**

1.3. Función / *Función*	1.4. Grupo ou grupos de especies* / *Grupo o grupos de especies**	1.5. Período de vixencia / *Período de vigencia*
"f"	**todos**	Do/*Del* **02/04/2023** ó/*al* **02/04/2031**

2. Nº DO CERTIFICADO / *Nº DEL CERTIFICADO*

m01f013

3.ORGANISMO QUE EXPIDE O CERTIFICADO / *ORGANISMO QUE EXPIDE EL CERTIFICADO*

3.1. Nome e enderezo do organismo que expide o certificado / *Nombre y dirección del organismo que expide el certificado*

AXENCIA GALEGA DA CALIDADE ALIMENTARIA
CONSELLERÍA DO MEDIO RURAL – XUNTA DE GALICIA
Rúa do Camiño Francés, 10 baixo
15781 Santiago de Compostela
A Coruña (España)

3.2. Teléfono / *Teléfono*	3.3. Fax / *Fax*	3.4. Correo electrónico / *Correo electrónico*
981 546 657	981 546 651	formacion.cmrm@xunta.gal

3.5. Data / *Fecha*	3.6. Lugar / *Lugar*
Ver sinatura / *ver firma*	**Santiago de Compostela**

3.7. Nome e sinatura / *Nombre y firma*

Santiago de Compostela,

O director da Axencia Galega da Calidade Alimentaria

Por delegación de sinatura (Resolución do 15/02/2022)

O xefe da Área de Formación, Innovación e Investigación Agraria

Manuel López Luaces

* Anexo II da Orde ECC/566/2015, do 20 de marzo: 1 (roedores), 2 (lagomorfos), 3 (carnívoros), 4 (équidos, ruminantes e porcino), 5 (primates), 6 (aves), 7 (réptiles), 8 (peixes e anfibios), 9 (cefalópodos), 10 (animais silvestres), 11 (outras especies).
* Anexo II de la Orden ECC/566/2015, de 20 de marzo: 1 (roedores), 2 (lagomorfos), 3 (carnívoros), 4 (équidos, rumiantes y porcino), 5 (primates), 6 (aves), 7 (reptiles), 8 (peces y anfibios), 9 (cefalópodos), 10 (animales silvestres), 11 (otras especies).
O mantemento da capacitación deberá solicitarse durante os oito meses anteriores á finalización do período de vixencia, preferiblemente entre os oito e os tres meses anteriores á finalización do mesmo. / *El mantenimiento de la capacitación deberá solicitarse durante los ocho meses anteriores a la finalización del periodo de vigencia, preferiblemente entre los ocho y los tres meses anteriores a la finalización del mismo.*

8.4 ANEXO IV: ARTÍCULO PUBLICADO

Año de publicación: 2023

Autores y filiación en orden: Iván Alonso Fernández [*1], Håvard Jostein Haugen[2] , Mónica López Peña[1], Antonio González Cantalapiedra[1], Fernando Muñoz Guzón[1].

[1]Departamento de Anatomía, Producción Animal y Ciencias Clínicas Veterinarias, Facultad de Veterinaria, Universidade de Santiago de Compostela, Campus Universitario s/n, 27002 Lugo, España.

[2]Departmento de Biomateriales, Instituto de Odontología Clínica, Facultad de Odontología, Universidad de Oslo, Noruega.

Referencia completa de la publicación: I. Alonso-Fernández, H.J. Haugen, M. López-Peña, A. González-Cantalapiedra, F. Muñoz, Use of 3D-printed polylactic acid/bioceramic composite scaffolds for bone tissue engineering in preclinical in vivo studies: A systematic review, *Acta Biomaterialia*. (2023). https://doi.org/10.1016/j.actbio.2023.07.013. S1742706123003999.
DOI: https://doi.org/10.1016/j.actbio.2023.07.013

Enlace: https://www.sciencedirect.com/science/article/pii/S1742706123003999

Editorial: Elsevier

Revista: *Acta Biomaterialia*

ISSN: 1742-7061

Índices de calidad:

- **Cuartil:** Q1
- **Factor de Impacto:** 9,7
- **CiteScore:** 17
- **Clasificación por categoría:**
  - Biochemistry Q1 (19/415)
  - Biomaterials Q1 (4/106)
  - Biomedical Engineering Q1 (11/229)
  - Biotechnology Q1 (17/282)
  - Molecular Biology (31/382)

Reproducido en el Capítulo I del apartado de resultados de la presente Tesis Doctoral.

Contribución doctorando: El doctorando contribuyó en la búsqueda de la información, la selección y el análisis de los artículos, la evaluación de su calidad y riesgo de sesgo, y la preparación y escritura del manuscrito.

Resumen: Los andamiajes compuestos impresos mediante tecnología 3D han surgido como una nueva alternativa frente a las limitaciones existentes en la reconstrucción de tejidos óseos. El objetivo del presente estudio fue revisar sistemáticamente la viabilidad del uso de andamiajes compuestos de ácido poliláctico (PLA)/biocerámicas como sustitutos óseos en modelos preclínicos "*in vivo*". Para ello se realizó una búsqueda en bases de datos electrónicas utilizando una serie de térmicos específicos, y catorce manuscritos fueron seleccionados para ser analizados en profundidad. La fabricación de los andamiajes se llevó a cabo principalmente mediante técnicas de extrusión, y la hidroxiapatita fue la biocerámica más utilizada para la síntesis de materiales compuestos al ser combinada con una matriz de PLA. Del total estudios incluidos en la revisión sistemática, siete fueron realizados en ratas y seis en conejos, sin embargo, la alta variabilidad existente en cuanto al diseño del proceso experimental dificultó la comparación entre los mismos. Con respecto a los resultados, los andamiajes compuestos de PLA/biocerámicas han demostrados ser biocompatibles y resistentes desde un punto de vista mecánico. Confirmándose mediante la realización de estudios preclínico que dichos andamiajes representan una alternativa prometedora para el tratamiento de defectos óseos. No obstante, con el objetivo de aumentar la calidad de la información obtenida en los estudios preclínicos y permitir una comparación adecuada de los resultados, es necesaria una estandarización de los procesos experimentales, prestando una mayor atención las fases de diseño y realización de los ensayos "*in vivo*".

Palabras Clave: Modelos animales, ácido poliláctico, biocerámicas, tecnología de impresión 3D, andamiajes compuestos, regeneración ósea.

Acta Biomaterialia 168 (2023) 1–21

Contents lists available at ScienceDirect

Acta Biomaterialia

journal homepage: www.elsevier.com/locate/actbio

Review article

Use of 3D-printed polylactic acid/bioceramic composite scaffolds for bone tissue engineering in preclinical in vivo studies: A systematic review

Iván Alonso-Fernández[a,*], Håvard Jostein Haugen[b], Mónica López-Peña[a], Antonio González-Cantalapiedra[a], Fernando Muñoz[a]

[a] Anatomy, Animal Production and Veterinary Clinical Sciences Department, Veterinary Faculty, Universidade de Santiago de Compostela, Campus Universitario s/n, 27002 Lugo, Spain
[b] Department of Biomaterials, Institute of Clinical Dentistry, Faculty of Dentistry, University of Oslo, Oslo, Norway

ARTICLE INFO

Article history:
Received 23 February 2023
Revised 11 July 2023
Accepted 12 July 2023
Available online 15 July 2023

Keywords:
Animal models
Polylactic acid
Bioceramic
3D-printing technology
Composite scaffolds
Bone regeneration

ABSTRACT

3D-printed composite scaffolds have emerged as an alternative to deal with existing limitations when facing bone reconstruction. The aim of the study was to systematically review the feasibility of using PLA/bioceramic composite scaffolds manufactured by 3D-printing technologies as bone grafting materials in preclinical in vivo studies. Electronic databases were searched using specific search terms, and thirteen manuscripts were selected after screening. The synthesis of the scaffolds was carried out using mainly extrusion-based techniques. Likewise, hydroxyapatite was the most used bioceramic for synthesizing composites with a PLA matrix. Among the selected studies, seven were conducted in rats and six in rabbits, but the high variability that exists regarding the experimental process made it difficult to compare them. Regarding the results, PLA/Bioceramic composite scaffolds have shown to be biocompatible and mechanically resistant. Preclinical studies elucidated the ability of the scaffolds to be used as bone grafts, allowing bone growing without adverse reactions. In conclusion, PLA/Bioceramics scaffolds have been demonstrated to be a promising alternative for treating bone defects. Nevertheless, more care should be taken when designing and performing in vivo trials, since the lack of standardization of the processes, which prevents the comparison of the results and reduces the quality of the information.

Statement of Significance

3D-printed polylactic acid/bioceramic composite scaffolds have emerged as an alternative to deal with existing limitations when facing bone reconstruction. Since preclinical in vivo studies with animal models represent a mandatory step for clinical translation, the present manuscript analyzed and discussed not only those aspects related to the selection of the bioceramic material, the synthesis of the implants and their characterization. But provides a new approach to understand how the design and perform of clinical trials, as well as the selection of the analysis methods, may affect the obtained results, by covering authors' knowledgebase from veterinary medicine to biomaterial science. Thus, this study aims to systematically review the feasibility of using polylactic acid/bioceramic scaffolds as grafting materials in preclinical trials.

1. Rationale

Bone defects are one of the most common tissue damages, originating from traumas, infections, tumor resection, reconstructive surgeries, congenital etiologies, etc. Resulting in significant detrimental effects on patient's quality of life and society [1–3]. Indeed, bone is the second most transplanted tissue after blood [4]. Al-

* Corresponding author at: Campus Universitario s/n, 27002 Lugo, Spain.
E-mail address: i.alonso.fernandez@usc.es (I. Alonso-Fernández).

https://doi.org/10.1016/j.actbio.2023.07.013

though the vast majority of bone defects can heal spontaneously under suitable physiological and environmental conditions, bone healing is a complex physiological process that depends on the type and extent of the injury and patient's age and gender [3,5]. Large defects, also known as critical bone defects, may not heal spontaneously due to the size of the defect or unstable biomechanical properties, unfavorable wound environment, suboptimal surgical technique, metabolic factors, hormones, nutrition and applied stress [5]. The existing limitations facing bone reconstruction and repair have given rise to bone tissue engineering as an emerging and promising solution [6,7], and it has become one of the cornerstones of contemporary medical research since it was described in 1993. Significant innovation in this field to build functional structures to promote the regeneration of damaged or diseased organs has occurred in recent decades [7–9]

The ideal goal for regeneration is a newly developed bone tissue with the same immunological, functional, structural and mechanical characteristics as the native bone [10,11]. Thus, bone substitutes should be biocompatible, bioresorbable, osteoconductive and osteoinductive; finally replaced by newly formed bone. Furthermore, it should be easy to use, safe and cost-effective [1,12]. In order to meet these criteria, a large variety of biomaterials have been tested for in vivo bone tissue regeneration [1,8]. However, none of the currently available bone grafts possesses all the desirable characteristics such a biomaterial should have [4].

Biopolymers offer an alternative to traditional biocompatible materials (metallic and ceramic) and non-biodegradable polymers [13]. Specifically, polylactic acid (PLA) is a biocompatible, biodegradable, low cost and no toxic or carcinogenic polymer. Besides, it has an extensible mechanical property profile, ease of production, and high reproducibility thanks to additive manufacturing techniques [13–15]. Since PLA products were approved by the US Food and Drug Administration (FDA), in 1970, for direct contact with biological fluids, they have been used in relevant medical applications such as tissue engineering scaffolds, delivery system materials, covering membranes, different bio-absorbable medical implants and sutures [13,14]. However, PLA also presents several drawbacks, such as its slow degradation rate, hydrophobicity, and low cell affinity. Sometimes an inflammatory response from the contacting surrounding tissue can occur and its degradation products may increase the resorption site because of its acidity. Likewise, due to the importance of cell adhesion to the polymer, surface properties play a critical role, especially in biocompatibility, allowing vascular ingrowth, and cell attachment, migration, and proliferation. That is why different surface modification strategies have been developed to create desirable surface properties of PLA biomaterials, such as physical, chemical, plasma and radiation-induced methods, and the formation of coatings or composites [4,13,15].

A composite generally consists of two parts, the matrix and the reinforcing agent [15]. Among the wide range of materials that have been used for the synthesis of PLA composites, we are going to focus on bioceramics, which include calcium phosphates, the most widely used bone grafting materials due to their resemblance to the bone mineral phase, such as hydroxyapatite (HA) and β-tricalcium phosphate (β-TCP) [11,12]; and another promising group, the bioglasses (BG) or bioactive glasses, most of them based on the Na_2O, CaO, P_2O_5 and SiO_2 system, and with a weight percent of SiO_2 less than 55% [16–18]. They present sufficient biocompatibility, bioactivity, and bone conductivity, acting as a source of minerals for bone cells and not promoting an inflammatory response [7,16,17,19]. Furthermore, bioglasses can suppress growth of many, even multi-resistant, bacterial strains [16]. Despite that, they are brittle, have a low degradation rate, and lack mechanical characteristics (low fracture toughness) to form a high-quality scaffold by themselves [7,19]. However, bioceramics are suitable to be manufactured through additive manufacturing techniques, allowing the synthesis of 3D-printable composites when mixed with a polymeric matrix. Combining both materials can negate some of each other's disadvantages, improving their individual characteristics, such as better physical and mechanical properties, degradation rates and biosafety. And thus making them more attractive for their use in bone regeneration [15,19,20].

As well as FDA has approved PLA, bioceramic materials for its clinical use in humans, and different commercially available products can be found, such as Cerapatite® (HA), Cerasorb® (β-TCP) or BonAlive® (Bioglass) Since, the first formulation received the approval in 1996, a total of 15 HA, 21 β-TCP and 11 Bioglass products have been approved as of December 2020; even one PLA/HA composite, called SuperFIXSORB30® [21,22]. No human clinical trials using PLA/HA composites were found, however, Cannio et al. [18] did a literature review regarding the bioactive glass applications in human clinical trials, and Stachi et al. [23] compared synthetic hydroxyapatite with and inorganic bovine bone in sinus floor elevation in humans (ClinicalTrials.gov Identifier NCT03077867).

The advancement and creation of additive manufacturing techniques have provided researchers with a tool to create intricate replicable scaffolds for tissue regeneration. The demand for customizable bone substitutes has increased, and this technology has been shown to be able to create 3D porous scaffolds used for bone tissue engineering, because it allows the adaptation of the implants to the patient's specific bone geometry [7,13,24], based on the combined use of 3D image analysis, and computed tomography (CT) or magnetic resonance imaging (MRI) techniques [6,11]. Additive manufacturing is a promising 3D-printing method that allows the fabrication of customized 3D templates with complete control over the architecture, unlike conventional techniques such as gas foaming, sol-gel method, or freeze-drying [11]. Thus, it provides the necessary porosity and interconnectivity to access fluids and cells, favoring their migration, adhesion and proliferation, and effective transport of nutrients, oxygen, wastes, and growth factors. Hence, stimulating the continuous ingrowth of bone tissue form the periphery into the inner part of the scaffold (Fig. 1) [6,11].

Furthermore, before use in human beings as bone substitute, it should be tested both in vitro and in vivo to ensure it works effectively and safely, and for ethical, safety, economic and regulatory concerns [5,27]. 2D in vitro studies allow us to understand the mechanisms of bone repair at the cellular level and to assess biomaterials' biocompatibility. However, they oversimplify in vivo situations and do not give an overview of the whole tissue response [28]. Thus, pre-clinical models are necessary to simulate a clinical situation in a reproducible and easy-to-control manner, allowing us to evaluate a biomaterial's bioactivity, biocompatibility, toxicity, potential adverse reactions, or viability and efficacy [27,28]. They are based on similarities and analogies between humans and animals, and generally, the more similarities, the more suitable model [27].

Many reports have been published over the last years reviewing the possible use in bone tissue regeneration of different additive manufacturing technologies [6,7,11,15,29] and/or biomaterials, such as biopolymers [13,14], bioceramics [30] or composites [31,32]. However, most of them were focused on the manufacturing process, characterization aspects, or applications without paying much attention to their behavior when used in preclinical trials with animal models, which is a key factor of translational research. Tree systematic reviews addressed these issues. Hassan et al. [8] evaluate the effect of using 3D-printed templates on bone tissue regeneration in critical bone defects induced in experimental animal studies, specifically in calvaria defect models. Brunello et al. [12] investigated the result of applying bioceramic scaffolds, in terms of bone regeneration, for treating critical side defects in vivo. And finally Al-allaq and Kashan [33] reported a large-scale

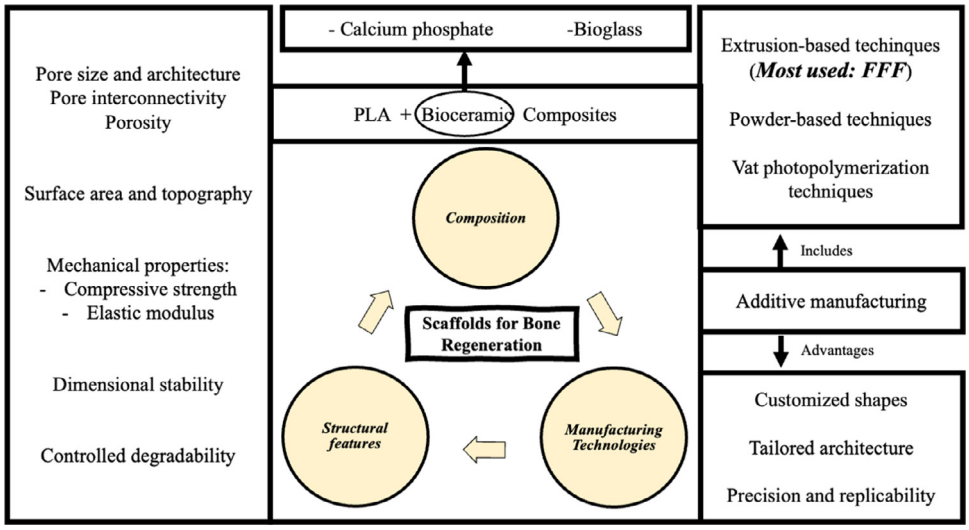

Fig. 1. Main features when synthesizing 3D-printed scaffolds for bone regeneration. PLA: polylactic acid; FFF: fused filament fabrication [4,7,10,11,25,26].

assessment of the capabilities of in vivo studies to generate an optimal regenerative process based on an analysis of the results after using bioceramics as bone substitute materials.

The purpose of the present study was to systematically review the feasibility of using PLA/bioceramic composite scaffolds manufactured by 3D-printing technologies as bone grafting materials in preclinical in vivo studies by evaluating their bone regeneration capabilities. However, this is not the only goal of the report, but also tries to carry out the importance of the different aspects to characterize when manufacturing 3D-printed scaffolds, and how they can affect to the bone healing process. Likewise, they authors highlight the importance of planning the clinical trials carefully, because of the implication that aspects such as the anesthetic protocol have on the result of the study.

2. Materials and methods

The present systematic review was conducted and reported according to the formal PRISMA guidelines ("Preferred Reporting Items for Systematic Reviews and Meta-Analyses"). However, ethics approval was not required for this review.

2.1. Search strategy

An electronic search was performed in the following health science databases: MEDLINE (PubMed) online library and Web of Science (WOS) database; it was carried out manually during February and September 2022. The search was limited to studies published in the last five years, considering the recent advancements in 3D-printing and biomaterial synthesis.

The studies were identified, based on different search strategies, using permutations of the following terms: "PLA", "Polylactic Acid", "PLLA", "poly (lactic) acid", "3D Print", "Three-dimensional print", "3D printing" "additive manufacturing" "material extrusion", "Scaffold", "Bone", "Bone regeneration", "Bone repair", "Bone reconstruction", "Bone tissue engineering", "In vivo", "Animal".

In addition, all the relevant articles found in the references and relevant review articles were checked and added as other sources.

2.2. Inclusion and exclusion criteria

2.2.1. Inclusion criteria

- Articles in English.
- Use of 3D-printed implants.
- In vivo animal model.
- Defined study parameters, including micro-tomographic (μCT) or histological evaluations of the bone formation.

2.2.2. Exclusion criteria

- Reviews and book chapters.
- In vitro studies or implants' characterization studies.
- Studies using PLA copolymers or non-bioceramic composites.
- Animal studies report ectopic bone formation models (e.g., subcutaneous).
- Studies using scaffolds loaded with chemotherapeutic agents, anti-inflammatory drugs and antibiotics.
- Use of PLA devices different from bone regeneration (e.g. screws or clips for fracture fixation).

Those studies including scaffolds with drugs/stem cells/substances affecting bone metabolism were not excluded.

2.3. Screening method and data extraction

A 2-stage screening was carried out. First, titles and abstracts were selected through an online search of inclusion. After removing duplicates, they were screened independently by two reviewers (I.A. and F.M.) using the inclusion and exclusion criteria. Next, the same two reviewers (I.A. and F.M.) carefully reviewed the full text of reports assessed for eligibility. For each study, relevant data were extracted and recorded on two previously designed data collection forms. One of them was dedicated to compiling the information referring to the biomaterials used, the manufacturing process of the scaffolds and their characterization; and the other one collected all the data related to the protocols for the in vivo preclinical test, grouping the animals according to the species, and the subsequent analysis of the obtained results. The final selection was based on the inclusion and exclusion criteria detailed above.

2.4. Quality assessment and risk of bias

Two independent authors (I.A. and F.M.) performed the quality and risk-of-bias assessments, and all authors resolved discrepancies with team consensus. To assess the quality of the included in vivo preclinical studies, we used the updated guidelines for reporting animal research: the ARRIVE guideline (Animals in Research: Reporting In Vivo Experiments) [34]. Specifically, we utilized the

"Compliance Questionnaire" to evaluate whether the reports complied with the ARRIVE Essential 10: Study design, sample size, inclusion and exclusion criteria, randomization, blinding, outcome measures, statistical methods, experimental animals, experimental procedures and results. Furthermore, we added the item "Adverse Events" because of its importance in a preclinical trial. Next, we categorized all the items as "reported", if the item was reported entirely, "not reported", if it was not reported, and "unclear" if it was partially reported or if insufficient details were provided.

The risk-of-bias in the manuscripts was assessed by using the SYRCLE (Systematic Review Centre for Laboratory animal Experimentation) tool [35] for animal studies in order to assign a judgment of low, high or unclear risk of bias to each of the 10 items included in the checklist evaluating 10 items: Allocation Sequence Generation, Baseline Characteristics, Allocation Concealment, Random Housing, Blinding of Care Giver/Investigator, Random Outcome Assessment, Blinding of Outcome Assessor, Incomplete Outcome Data Addressed, Free from Selective Outcome Reporting and Free from Other Sources of Bias. The methodological quality was analyzed by answering the main 10 questions as "yes", considered at low risk of bias, "no" which indicated a high risk of bias, or "unclear", for unclear items.

3. Results

3.1. Study selection

The literature search resulted in an initial pool of 799 potentially eligible publications collected from Pubmed and Web of Science. Once duplicates were removed, the remaining manuscripts ($n = 626$) were screened based on the tittle and the abstract, and after evaluating the inclusion and exclusion criteria, only 150 were included as potentially eligible for the present systematic review. After full-text analysis, 122 reports were excluded (Table 1), and 15 were not retrieved. Finally, the assessment of the references included from the initial pool led to a total of 13 articles that were found suitable to be included, in addition, an article was included by hand-searching. Thus, there are 14 publications to elaborate the present systematic review (Figure 2).

3.2. Study characteristics

Manuscripts included in this systematic review were mainly published after 2020 (8/13). Indeed 3D-printed scaffolds have become a promising alternative for bone regeneration. Hence, the interest in this production method has been growing for years.

The qualitative data of the studies have been extracted and displayed in the following analytic tables. From a total number of 14 included articles, 7 of them were conducted in rabbits, in which New Zealand rabbits were used [154–160], and another 7 ones in rats where used, two Wistar strain [161,162], four Spargue-Dawley [163–166] and in one the breed was not specificized [167]. According to the definition made by Brunello et al. [12], an intrabony defect of critical dimensional is not expected by definition, to heal spontaneously within the lifetime of the animal. All the defects made in rats were performed in calvaria, but only 3 could be considered as critical-sized bone defects (CSD). However, the ones in rabbits were performed in femur and radius, but only the ones in radius could be considered as CSD (Table 2). Zhang et al. [159], in contrast, did not make a defect, but rather developed a in vivo bioreactor model crossing the scaffold with a vascular bundle and transplanted it to tibial periosteum.

Table 1
Main Reason for exclusion after full-text screening.

Main Reason for Exclusion	No.	References
Language	2	[36,37]
Implants' characterization and/or in vitro study	48	[9,16,20,38–82]
No additive manufacturing fabrication	3	[83–85]
Ectopic bone formation model	2	[86,87]
PLA Copolymers	32	[19,88–118]
No PLA bioceramic composites	34	[119–152]
Internal Fixation Clip	1	[153]

As mentioned before, PLA is one of the main polymeric materials used in bone tissue engineering, and its isomeric composition may vary its characteristics. Only four out of fourteen articles specify the isomeric, L- or D-LA, composition PLLA (pure poly L-LA, $n = 3$) [158,160,164] and PDLA (poly-D,L-LA, $n = 1$) [165]. Likewise, hydroxyapatite is the main bioceramic chosen for the synthesizing composites ($n = 10$) [154–161,163,166], being used as powders mixed in different ratios with the polymeric material. Besides, the HA particles' size varies among the publications, showing a nanometric size in 5 [154,156–158,163]. Other bioceramic materials employed are CaP ($n = 1$) [162] as a biomimetic coating, β-TCP ($n = 1$) [164], AW ($n = 1$) [165] or OCP ($n = 1$) [167].

Regarding the morphology of the scaffolds, the fabrication of 3D porous interconnected structures with different shapes and sizes has been the election in all the studies. These were probably selected for their advantages and crucial role in bone regeneration, simulating the properties of an extracellular matrix, to create a microenvironment conducive to optimal tissue regeneration. Among the wide range of production methods, additive manufacturing techniques can be divided in the following groups.

- Extrusion-based techniques, where the material is deposited using a nozzle fixed on a robotic arm, such as fused deposition modelling (FDM) or fused filament fabrication (FFF), robocasting, dispense plotting or bioplotting, multi-head deposition system (MHDS) or mini-deposition (MDS) system [7,11]. FDM or FFF is the most commonly used, as seen in 11 of the papers included in this review [154,156–163,165,166]. However, other alternatives when manufacturing 3D implants were utilized, such as micro-extrusion based 3D-printing technology ($n = 1$) [167] or 3D bioplotting ($n = 2$) [155,164].
- Other group is powder-based techniques, where particles constituting a powder are sintered or chemically bounded, such as inkjet printing, selective laser sintering (SLS), selective laser melting (SLM), binder jetting/sintering, direct metal laser sintering (DMLS) and electron beam melting (EBM) [7,11]. Binder jetting/sintering (indirect 3D-printing) technique was selected for the synthesis of apatite-wollastonite (AW) disks [165].
- Finally, vat photopolymerization techniques, where a liquid resin is photopolymerized using UV light.

Another important feature when synthesizing implants is the sterilization process since it is essential to prevent unsterile medical devices and also required to obtain regulatory approval [11,168]. Among the different sterilization techniques, ethylene oxide sterilization was selected to sterilize PLA-bioceramic composite scaffolds in 7 of the included manuscripts [154,159–163,166]; another paper utilized γ-irradiation [165] and in the remaining 6 studies the sterilization process was not reported [155–158,164,167]. Besides, Tcacencu et al. [165] used steam sterilization (also called autoclaving) to sterilize the apatite-wollastonite disks.

Scaffold characterization is an essential step in bone tissue engineering due to the importance of key parameters that may influence the biological response and the bone healing process, such as mechanical strength, porosity, degradability, or in vitro trials (summarized in Table 3). First, mechanical strength, in terms of compressive strength and/or elastic modulus, is included in approximately 57% of the studies, and its importance lies in its ability to withstand the existing loads after implantation and pro-

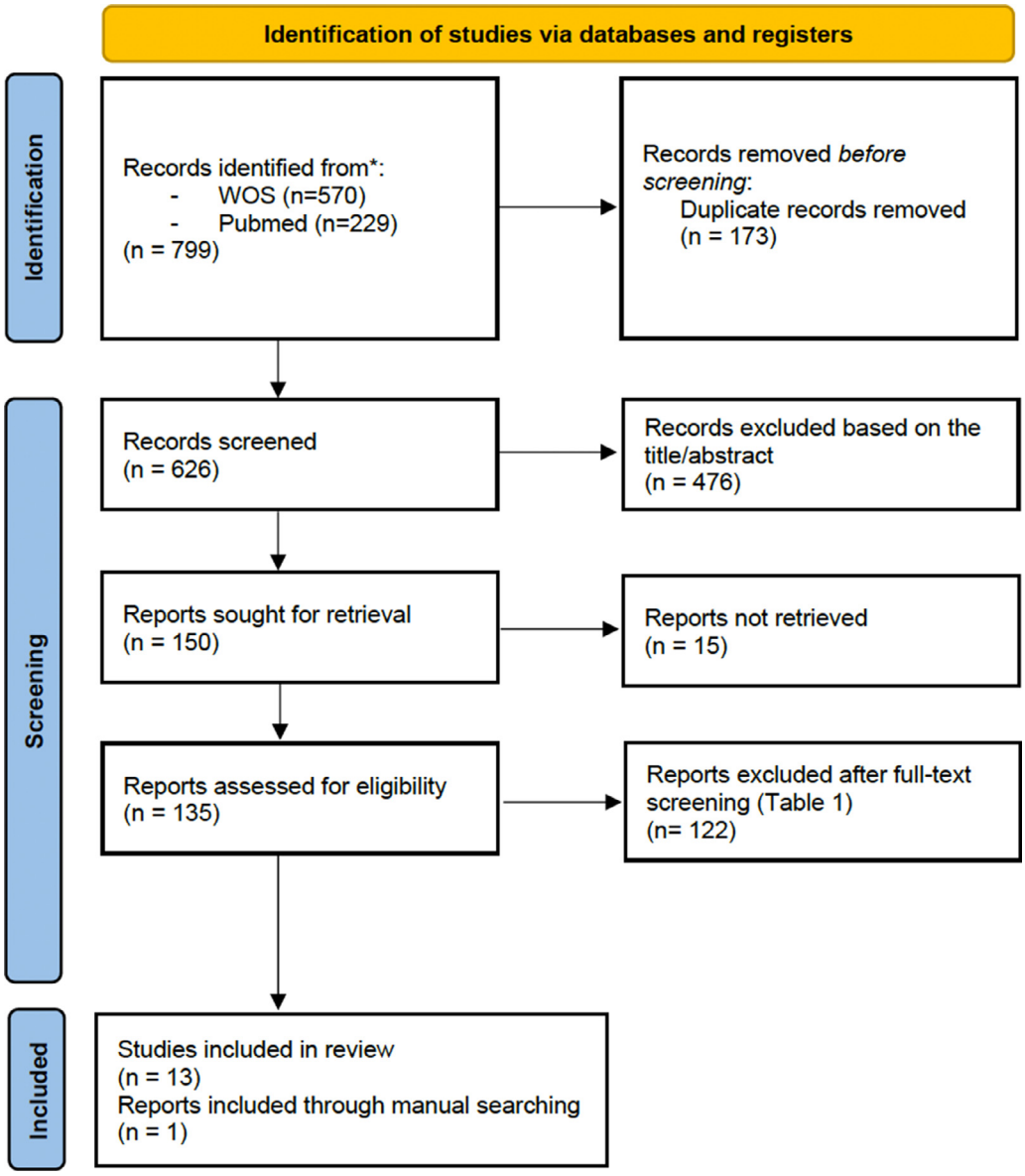

Fig. 2. Flow chart of the article selection procedure.

Table 2
Animal defects.

Animal	Study Model	Number of Publications	Critical-Sized Defects	References
Rats ($n = 7$)	Calvarial Bilateral Defect	1	1/1	[161]
	Calvarial Unilateral Defect	6	2/6	[162–167]
Rabbits ($n = 5$)	Femoral diaphysis defect (cylindrical)	4	0/4	[154,156–158]
	Radius diaphysis segmental defect	2	2/2	[155,160]

vide sufficient support to bone growth. So it should be as similar as possible to the bone: Compressive strength of Trabecular bone 0.1-16 MPa and Compressive strength of Cortical Bone 130-200 MPa [169,170]. Likewise, porosity and/or pore size have been reported in all the articles included in the present review as a consequence of its main role in cell spreading and effective transport of nutrients, oxygen, waste, etc., favoring continuous ingrowth of bone tissue from the periphery into the inner part of the scaffold [6,171,172]. Indeed, high porosity and pore size promote bone regeneration, but reduce the mechanical properties of the implant [172,173]. The results include values of porosity and pore size ranging between 26.4% and 70%, and 100 and 500 μm respectively (See Table 3). However, the degradability of the scaffolds was only measured by 3 studies [156,158,164], even though it is an important parameter, as well as the degradation products derived from it, which can influence the environment affecting bone formation and healing time. Furthermore, the degradability will also be related to porosity and mechanical strength, as higher porosity leads to higher degradability and, consequently, a lower mechanical resistance [172,173]. In two of them, the samples were soaked into PBS media (pH 7.4 +- 0.2) at an established temperature, and variations in weight, molecular weight and/or pH were measured at various time points [156,158]. And in the other one, the analysis was performed in vivo, through the measurement

Table 3
Characterization of the scaffolds in the studies.

References	Biomaterials (s)	Mixing ratio (wt PLA: wt Bioceramic)	Bioceramic particle size	Production Method	Morphology	Porosity (%)	Pore Size (μm)	Elastic Modulus (GPa or MPa)	Compressive Strength (MPa)	In vitro	Degradability	Sterilization	Scaffolds analysis
[161]	PLA + HA	90: 10	50 μm	FFF	3D porous interconnected structure	58	450	-	-	-	-	Ethylene Oxide	SEM
[162]	PLA + CaP Coating	Uncoated 98: 2	-	FDM	3D porous interconnected structure	49.93+ -5.28 49.09±3.2	-	0.512±0.24 GPa 0.510±0.11 GPa	20.50±1.95 MPa 18.22±2.67 MPa	Yes	-	Ethylene Oxide	SEM, FTIR, XRD, TGA, Mechanical Test
[163]	PLA + n-HA	80:20	-	FDM	3D porous interconnected structure	70±2.23	-	10.12±1.24 GPa	31.18±4.86 MPa	Yes	-	Ethylene Oxide	SEM, Mechanical Test, Porosity evaluation
[164]	PLLA + β-TCP	100: 0 90: 10 70: 30	250 μm	3D Bioplotter	3D porous interconnected structure	~62	100		258±102MPa 310±40MPa 349±51MPa	Yes	PLLA/TCP30 % Remaining scaffold Week GPC NIR 4 ~87 ~91 8 ~79 ~84 12 ~71 ~69	-	SEM, μCT, Mechanical Test, Degradability test (GPC, NIR fluorescence imaging)
[165]	PLA + AW	70% AW AW+30%MD powder (maltodextrin) 50:50	55% - 90 μm 15% - 0-53 μm	AW- Binder jet-ting/sintering (Indirect 3D-printing) PLA-FFF	3D porous interconnected structure	AW disks 41.85+ -0.94% PLA 60%	-	-	-	Yes	-	AW – Autoclave PLA and composite – gamma radiation	SEM, μCT, Digital Microscope, XDR, Porosity evaluation (Archimedes method)
[166]	PLA + HA	85: 15	2.1±0.4 μm	MDS	3D porous interconnected structure.	60±1.5	500± 20	-	-	Yes	-	Ethylene oxide	SEM
[167]	PLA + OCP (octacalcium phosphate)	40: 60	-	MEB	3D porous interconnected structure.	-	500	-	1 MPa	Yes	-	-	FESEM, Mechanical Test
[156]	PLA + n-HA	100: 0 90: 10 80: 20 70: 30 60: 40 50: 50	50-80 nm	FDM	3D porous interconnected structure.	~50	-	-	~35MPa ~29MPa ~28MPa ~25 MPa ~23 MPa ~17 MPa	Yes	Degradation rate: Pn50>Pn 30>Pn0	-	SEM, XDR, TEM, Mechanical Test; Porosity evaluation (Archimedes method), Degradability test (GPC)
[157]	PLA + n-HA	100:0 50: 50	75±20 nm	FDM	3D porous interconnected structure.		300-400	-	35.41±2.07 MPa 17.8±1.92 MPa	Yes	-	-	TEM, AFM, SEM, EDS, μCT, Mechanical Test
[158]	PLLA + n-HA	100: 0 70: 30 50: 50	50-80 nm	FDM	3D porous interconnected structure.	60	-	43±0.09 MPa 45.54±0.11 MPa 44.31±0.10 MPa	44.02±6.85 MPa 29.68±1.92 MPa 14.22±0.20 MPa	Yes	Degradation rate and mass change: 50%n-HA>30%n-HA>0%n-HA	-	SEM, Contact angle, Mechanical test, Degradability test (GPC)
[155]	PLA + HA	70: 30	50 μm	3D Bioplotter	3D porous interconnected structure.	60	500	-	-	No	-	-	μCT, SEM
[154]	PLA + n-HA	90: 10	63±1.5nm	FDM	3D porous interconnected structure.	26.4	292±1.8	-	23.36±0.48 MPa	Yes	-	Ethylene oxide	SEM, EDS, Mechanical test, Porosity evaluation
[159]	PLA + HA	85: 15	2.1 ±1 μm	MDS	3D porous interconnected structure.	60	500	-	-	Yes	-	Ethylene oxide	-
[160]	PLA + HA	-	-	FDM	3D non-porous structure	-	-	-	-	No	-	Ethylene oxide	-

PLA: polylactic-acid); HA: hydroxyapatite; n-HA: nanohydroxyapatite; β-TCP: Beta-tricalcium phosphate; AW: apatite-wollastonite; OCP: octacalcium phosphate; wt: percentage by mass; FDM: Fused Deposition Modeling = FFF: Fused Filament Fabrication; MDS: Mini-Deposition System; MEB: Micro-extrusion based 3D-printing; SEM: scanning electron microscope; FTIR: Fourier transform infrared spectroscopy; XDR: X-ray diffraction; TGA: Thermogravimetric analysis; FESEM: field emission scanning electron microscope; TEM: Transmission Electron Microscope; AFM: Atomic Force Microscope; EDS: Energy-dispersive X-ray spectroscopy; μCT - Micro-computed tomography

of non-degradation-related molecular weights by gel permeation chromatography (GPC) and near-infrared (NIR) fluorescence images [164]. Finally, in vitro trials were carried out in all studies except three (see Table 3); though no information was collected, they represent an essential intermediate step between material synthesis and characterization, and in vivo testing. Scanning electron microscopy (SEM) is the most common characterization technique for scaffolds. However, others can be found in Table 3, such as Micro-Computed Tomography (μCT), mechanical testing, Fourier Infrared Spectroscopy (FTIR), Energy Dispersive Spectroscopy (EDS), X-ray Diffraction Analysis (XDR), etc.

Furthermore, different substances can be applied to scaffolds to improve bone healing and regeneration by affecting bone metabolism. Two studies used bone marrow-derived stem cells (BMSCs) [159,163], one used dental pulp stem cells (DPSC) [161] and one used enhanced bone marrow (eBM) [155]. Human osteoblastoma cell line (MG-63 cell line) was also used in one of the reports [164], as well as recombinant human bone morphogenetic protein-2 (rhBMP-2) [162]. Substances such as lanthanum (La), a rare earth element with an important role in the bone remodeling cycle that can promote the proliferation of bone-building osteoblast, were used in one paper [167]. Specifically in this case, La may influence the hydrolysis of OCP to an HA structure, thus influencing OCP mediated formation.

Likewise, many few procedures can also favor bone regeneration, such as sinusoidal electromagnetic fields (EMF) [163] or induced membrane technique (IMT) [155]. EMF triggered a higher new bone formation and vascularization. And IMT generated membranes similar to the periosteum, giving interesting results for treating large bone defects when combined with autografts [174].

There are different methods to assess bone healing in clinical trials. The ones utilized in selected studies are summarized in Tables 4 and 5. Histological evaluation was the most frequently used ($n = 14$), being able to distinguish between a qualitative histological analysis ($n = 13$), describing the results without the use of objective measurement techniques, and a quantitative or histomorphometric analysis ($n = 5$), that supplies objective data about the parameters analyzed such as angiogenesis or osteogenesis. In addition, these procedures can be carried out by decalcifying the bone and embedding it in paraffin ($n = 10$) or dehydrating and embedding it in a resin ($n = 4$). Likewise, micro-computed tomography analysis is widely used ($n = 9$), providing objective measurements to quantify bone regeneration. Other methods are radiographic evaluation, fluorescence imaging, immunohistochemistry (osteocalcin (OC), type I collagen (COL-1) or CD31) or biochemical analysis. Follow-ups varied between 4 and 16 weeks; a single observation time was reported in 4 out of 13 studies [158,160,161,165,167] and in the other ones, multiple observation times were chosen.

3.2.1. Studies in rats- main features

In vivo trials in the included reports for testing biomaterials were conducted through unilateral or bilateral defects in the calvaria of adult rats without any adverse reactions to the implanted scaffolds reported. The main characteristics and results of the studies are summarized in Table 4.

First, regarding the anesthetic protocols, different drugs and combinations were utilized by the different authors. Intraperitoneal injection of pentobarbital was administered in two studies, as a single drug [167], or in combination with inhaled isoflurane [163]. Ketamine was used alone [166], combined with xylazine [161,165], or with xylazine and midazolam [162]. Kwon et al. [164] chose a mixture of tiletamine, zolazepam and xylazine. Besides, only one study reports the use of local anesthesia, with lidocaine, and/or postoperative analgesia, in this case, buprenorphine [161]. Given the importance of the anesthetic protocol, both from an ethical point of view and the experimental process, it will be analyzed in more in detail in the discussion section.

HA is the main bioceramic added to a PLA matrix for synthesizing composites, which will be later used to produce 3D porous scaffolds via 3D-printing. They were tested in rats in three selected studies [161,163,166]. Gendviliene et al. [161] manufactured PLA/HA scaffolds showed a low potential to induce bone growing (BV (mm3) μCT: male 3.86±0.99, new bone (mm2) histology: 2.90±0.06), that is slightly higher PLA alone scaffolds and negative control, but less than the one showed by the Bio-Oss (BV (mm3) μCT: male 4.24±0.51, new bone (mm2) histology: 4.15±0.58). However, these results can be improved by adding dental pulp stem cells to obtain a cellularized scaffold (PLA/HA cells), or the production of decellularized extracellular matrix PLA/HA (PLA/HA ECM) scaffolds from the first. Thus, achieving a bone formation in vivo similar o even superior to that obtained with the Bio-Oss (PLA/HA cells- BV (mm3) μCT: male 4.11±0.72, new bone (mm2) histology: 3.66±0.29; PLA/HA ECM- BV (mm3) μCT: male 5.09±1.27, new bone (mm2) histology: 3.80±0.24). Interestingly, significant differences between male and female groups can be appreciated in relation to bone growth (Figure 3).

Nevertheless, Zhang et al. [166] demonstrated the osteogenic capability of 3D-printed PLA/HA scaffolds, as confirmed by histological examination and the results of the tomographic analysis, which was performed at 4 and 8 weeks, showing that scaffolds' bone volume per total volume (BV/TV) presented values around 45% at 8 weeks. On the other hand, defects filled with β-TCP presented the highest BV/TV value, almost reaching 50%, and those filled with demineralized bone matrix (DBM) and the empty ones got the lowest values.

Tu et al. [163] utilized nano-grade HA to manufacture 3D-printed PLA/HA composite scaffolds. μCT results at 4 weeks after surgery indicate a BV/TV of about 10% approximately, a lower value than that obtained by Zhang et al. [166] at the same time point, approximately 20%. Histological and μCT results of the PLA/HA scaffold group are superior to the control group at both time points (PLA/HA BV/TV and New Bone Area Fraction (%) 4w and 8w: ∼10% and ∼20%). However, Tu et al. [163] applicated two different treatments to PLA/HA scaffolds to improve their bone regeneration capability, seeding rat bone marrow mesenchymal stem cells (BMSCs), applying electromagnetic fields (EMF) or both, thus generating another 3 experimental groups. The results showed a higher percentage of bone growth in all groups, being more notable in the one that combined BMSCs and EMF (PLA/HA BMSCs + EMF BV/TV; 4w and 8w: ∼35% and ∼70%; New Bone Area Fraction (%) 4w and 8w: ∼30% and ∼60%). When used independently, the amount of new bone is lower without significant differences between PLA/HA BMSCs and PLA/HA EMF groups at any time point (Figure 4).

Almost no direct comparisons could be performed among papers that used HA in rat's calvaria model [161,163,166], because of differences in time points, PLA/HA mixing ratios and the defects' number and/or size.

Likewise, octacalcium phosphate (OCP) powders, which is thought to be one of the precursors for the formation of bone apatite crystals and can be converted to HA under physiological environments, were synthesized and mixed with PLA to create 3D-printed porous scaffolds [167]. OCP powders with different concentrations of Lanthanum (0.2/0.5/1La-OCP) were prepared via co-precipitation methods. In vivo trials showed that OCP promoted positive bone formation, an 0.2 La-OCP/PLA scaffolds showed an improvement in bone defect regeneration compared with the other groups.

β-tricalcium phosphate (β-TCP) was added to PLLA scaffolds by Kwon et al. [164], demonstrating effective support of bone regeneration. Micro-computed tomography showed a higher percentage of bone regeneration when a weight fraction (w.f.) of 30 TCP (∼25%

Table 4
Main features of studies in rats.

Reference	Animal	Anesthetic Protocol	Biomaterial groups	Sample Size	Defect	CSD	Empty Control	Groups	Bone metabolisms substances	Sacrifice Weeks	Assessment method	Main findings
[161]	Rat Wistar 300 gr 4 m/o 1/2 female y 1/2 male	Anesthesia: Ketamine 2.4 ml/kg, and Xylacine 5 mg/kg (IP) Local anesthesia: 2% Lidocaine 0.25 ml (SC) Postoperative Analgesia: Buprenorphine 0.01 mg/kg(SC)	PLA/HA	24	Calvarial Bone Circular bilateral defect ø 5.5 mm.	Yes	Yes	Empty $n = 8$ Bio-Oss $n = 8$ PLA $n = 8$ PLA/HA ($n = 8$) PLA/HA + DPSC ($n = 8$) PLA/HA + ECM ($n = 8$)	DPSC ECM	8 w	µCT analysis Qualitative histological analysis Quantitative histological analysis Paraffin	PLA/HA ECM scaffolds presented bone-forming ability comparable to that of Bio-Oss, based on histology and µCT analysis. Otherwise, PLA/HA scaffolds can potentially be used in bone tissue engineering, especially combined with the ECM.
[162]	Rat Wistar 300-400 gr	Anesthesia: Ketamine 100 mg/kg, Xylazine 10 mg/kg and Midazolam 5 mg/kg (IM)	PLA/CaP	45	Calvarial Bone Circular unilateral defect ø 8 mm	Yes	No	PLA $n = 15$ PLA/CaP $n = 15$ PLA/CaP + rhBMP2 $n = 15$	rhBMP-2	1, 3 and 6 m	Qualitative histological analysis Histomorphometric analysis Paraffin	The clinical trials have shown that the PLA-CaP scaffolds have proven to be biocompatible, promoting new bone formation after 6 months, even without rhBMP-2, based on histological results.
[163]	Rat Sprague-Dawley 280-320 g weight 12-13 w/0 male	Anesthesia: Pentobarbital 35 mg/kg and Inhaled Isofluorane	PLA/n-HA	126	Calvarial Bone Circular unilateral defect ø 6 mm	No	Yes	Empty=24 PLA/n-HA $n = 24$ PLA/n-HA + EMF $n = 24$ PLA/n-HA + BMSCs $n = 24$ PLA/n-HA + EMF + BMSCs $n = 24$	BMSCs Sinusoidal EMF: 15 Hz, 1mT. 4h/day)	4 and 12 w	µCT analysis Quantitative histological analysis Paraffin	The histological and microtomographic analysis revealed that PLA+HA scaffolds + BMSCs with EMF exposure present the best bone integration among all the groups, positioning itself as a promising candidate for craniofacial reconstruction.
[164]	Rat Sprague-Dawley 320-350 g. 8 w/o	Anesthesia: Combination of tiletamine and zolazepam, and Xylazine, 1:1, 1,5 ml/kg	PLLA/β-TCP	90	Calvarial Bone Circular unilateral defect ø 5 mm	No	No	PLLA $n = 15$ PLLA/TCP10 $n = 15$ PLLA/TCP30 $n = 15$ PLLA+MG63 $n = 15$ PLLA/TCP10 + MG63 $n = 15$ PLLA/TCP30 + MG63 $n = 15$	MG-63	4,8 and 12 w	µCT analysis Qualitative histological analysis Paraffin	3D-printed PLLA+TCP scaffold effectively supports bone regeneration in rats. The results show a greater bone regeneration rate in those animals with higher percent of TCP, and after adding of MG-63 to the scaffolds.
[165]	Rat Sprague-Dawley 350 g. adult male	Anesthesia: Ketamine and Xylacine	PLA/AW	15	Calvarial Bone Circular unilateral defect ø 8 mm	Yes	No	PLA dics $n = 3$ AW discs $n = 6$ AW/PLA discs $n = 6$	-	12 w	Qualitative histological analysis Histomorphometric analysis Paraffin	All three types of scaffolds were biocompatible. AW/PLA, the ones with the largest amount of new formed bone. AW scaffolds showed excellent osseointegration with the formation of new bone, and PLA ones have been well tolerated but were not osteogenic.
[166]	Rat Sprague-Dawley 300-350 g. 8 w/o Male	Anesthesia: Ketamine	PLA/HA	32	Calvarial Bone Circular unilateral defect ø 5 mm	No	Yes	3DP PLA/HA $n = 8$ β-TCP $n = 8$ DBM $n = 8$ Blank control $n = 8$	-	4 and 8 w	µCT analysis Qualitative histological analysis Immunohistochemistry (OC and COL-1) Paraffin	The percentage of new bone area in 3DP PLA/HA scaffolds was larger than in DBM (demineralized bone matrix) and control groups but less than β-TCP (Beta-Tricalcium phosphate) groups. The same tendencies were found at 4 and 8 weeks. So, PLA/HA scaffolds might be a promising candidate for bone defect repair, with little inflammation response, relatively larger resorption rate and superior osteoinductive activity.
[167]	Rat 6-8 w/o	Anesthesia: Pentobarbital (IP)	PLA/OCP	?	Calvarial Bone Circular unilateral defect. ø 5 mm	No	Yes	Control $n = ?$ PLA/OCP $n = ?$ PLA/OCP + 0.2La $n = ?$ PLA/OCP + 0.5La $n = ?$ PLA/OCP + 1La $n = ?$	La	8 w	Qualitative histological analysis Paraffin	The scaffolds enhanced bone defect regeneration in vivo. 0.2La-OCP/PLA scaffolds are significantly more likely to enhance bone defect regeneration in vivo than other groups. Our study suggests that La-OCP/PLA porous scaffolds have markedly potential in clinical bone tissue engineering.

m/o: months old; w/o: weeks old; PLA: polylactic-acid; HA: hydroxyapatite; n-HA: nanohydroxyapatite; β-TCP: Beta-tricalcium phosphate; AW: apatite-wollastonite; OCP: octacalcium phosphate; IP: intraperitoneal injection; SC: subcutaneous injection; IM: intramuscular injection; PLA:; HA:; n-HA:; OCP:; DPSC: dental pulp stem cells; ECM: extracellular matrix; rhBMP-2: recombinant human bone morphogenetic protein-2; BMSCs: bone marrow mesenchymal stem cells; EMF: electromagnetic fields; MG-63: human osteoblastoma cell line; DBM: demineralized bone marrow; La: Lanthanum; months: m; weeks: w; OC: osteocalcin; COL-1: type I collagen; µCT: micro-computed tomography.

Table 5
Main features of studies in rabbits.

Reference	Animal	Anesthetic Protocol	Biomaterial	Sample Size	Defect	CSD	Empty Control	Groups	Bone metabolisms substances	Sacrifice Weeks	Assessment method	Main findings
[156]	Rabbit New Zealand White 2-3 kg, male	Anesthesia: Pentobarbital 40 mg/kg (IV)	PLA/n-HA	18	Femoral Diaphysis Circular Unilateral Defect ø 5 mm	No	No	PLA $n = 9$ PLA/n-HA30% $n = 9$	-	4, 8 and 12 w	µCT analysis Qualitative histological analysis Resin	PLA/n-HA can be printed when the n-HA ratio is less than or equal 50%, the increasing incorporation of n-HA doesn't affect significantly the overall mechanical strength in a limited range (0-30%), but it really enhances the osteogenesis in vivo.
[157]	Rabbit New Zealand White 2-3 kg, male	Anesthesia: Pentobarbital 40 mg/kg	PLA/n-HA	-	Femoral Diaphysis Circular ¿Unilateral? Defect ø 5 mm	No	No	PLA $n = ?$ PLA/n-HA 50% $n = ?$	-	1,2 and 3 m	µCT analysis Qualitative histological analysis Resin	The new bone growth of the composite material (PLA+50%n-HA) is significantly higher than that of the PLA group. Consequently, it has a high potential for use as implant for the critical bone defects
[158]	Rabbit New Zealand White 2-3 kg, male	Anesthesia: Pentobarbital 40 mg/kg (IV)	PLLA/n-HA	9	Femoral Diaphysis Circular bilateral Defect ø 5 mm	No	No	PLLA $n = 3$ PLLA/30%nHA $n = 3$ PLLA/50%nHA $n = 3$	-	4 w	Qualitative histological analysis Resin	The PLLA/50%n-HA has shown a preferable capability of bone regeneration, also supported by the discovery of the Harversian Canals, compared with the PLLA-30%n-HA specimens, which in turn have presented a bigger amount of new bone tissue than the PLLA ones.
[155]	Rabbit New Zealand White 2,5 +/- 0.25 kg, 6 m/o	Anesthesia: Pentobarbital 30 mg/kg (IM)	PLA/HA	36	Diaphysis Left Radius Segmental Unilateral Defect 15 mm	Yes	No	ICBG + IM $n = 9$ PLA/HA $n = 9$ IM + PLA/HA $n = 9$ IM + PLA/HA + eBM $n = 9$	eBM ICBG IMemb	4, 12 and 16 w	µCT analysis Qualitative histological analysis Histomorphometric Analysis Paraffin	The IM combined with 3D-printed PLA-HA scaffold and eBM has a bigger efficiency for treatment of large bone defects than the PLA-HA and the IM/PLA-HA groups, and similar to the IM/ICBG group (Gold Standard), based on the X-ray, µCT and histological results.
[154]	Rabbit New Zealand White 4.2+/-0.18 kg, male, adult	Anesthesia: Xylazine 0,.1 ml/kg (IM)	PLA/n-HA	3	Distal Right Femur Circular Unilateral Defect ø 4.5 mm and Depth 10-13 mm	No	No	PLA/HA $n = 3$	-	4, 8 and 12 w	µCT analysis Qualitative histological analysis Resin	In vivo trials confirmed that the printed PLA/n-HA scaffold can enhance osteogenesis and osteoconductivity. It was showing bone formation within the femoral defect at 4,8 and 12 weeks, and no inflammation signs.
[159]	Rabbit New Zealand White 2.5+/-0.2 kg., 6 m/o	-	PLA/HA	24	Tibial Diaphysis Periosteum. Cuboid shaped periosteal pockets 10 mm in length and 7.5 mm in diameter.	-	No	Experimental Group (EG) PLA/HA +BMSCs with blood vessel Control Group (CG) PLA/HA + BMSCs without blood vessel	BMSCs	4 and 8 w	µCT analysis Qualitative histological analysis Immunohistochemistry (OC and CD31) Paraffin	3D-printed PLA-HA composite scaffolds in an in vivo bioreactor prove to be a promising tool for the prefabrication of large volume, customized, vascularized bone tissues. Besides, adding a vascular bundle allows the construction of large vascularized bone grafts that translate into a bigger BV/TV, Tb.N and Tb.Th in the in vivo trials.
[160]	Rabbit 4-5.5 kg, female, > 7 m/o	Anesthesia: Ketamine 20 mg/kg, midazolam 2 mg/kg, and morphine 2 mg/kg (IM). Inhaled isoflurane Local anesthesia: 2% Lidocaine 6 mg/kg – Right brachial plexus block Postoperative Analgesia: Tramadol 4 mg/kg and meloxicam 0.1 mg/kg (SC)	PLA/HA	60	Diaphysis Right Radius Segmental Unilateral Defect 15 mm	Yes	Yes	Control Group $n = 20$ ICBG $n = 20$ PLA/HA Group $n = 20$	-	2, 4, 8 y 12 w	Radiographic analysis Qualitative histological analysis Paraffin	Scaffold created with anatomical characteristics similar to the radios proved to be biocompatible and allow cell multiplication around the composite. Despite of the fact that less bone callus and bone bridge was formed compared to the gold standard method (ICBG).

m/o: months old; w/o: weeks old; PLA: polylactic-acid; PLLA: poly-L-lactic-acid; HA: hydroxyapatite; n-HA: nanohydroxyapatite; IM: intramuscular injection; IV: intravenous injection; BMSCs: bone marrow mesenchymal stem cells; DBM: demineralized bone marrow; La: Lanthanum; eBM: enhanced bone marrow; ICBG: iliac crest bone graft; IMemb: induced membranes; w: weeks; m: months; OC: osteocalcin; µCT: micro-computed tomography; BV/TV: Bone Volume/Tissue Volume; Tb. N: Trabecular Number; Tb. Th: Trabecular thickness.

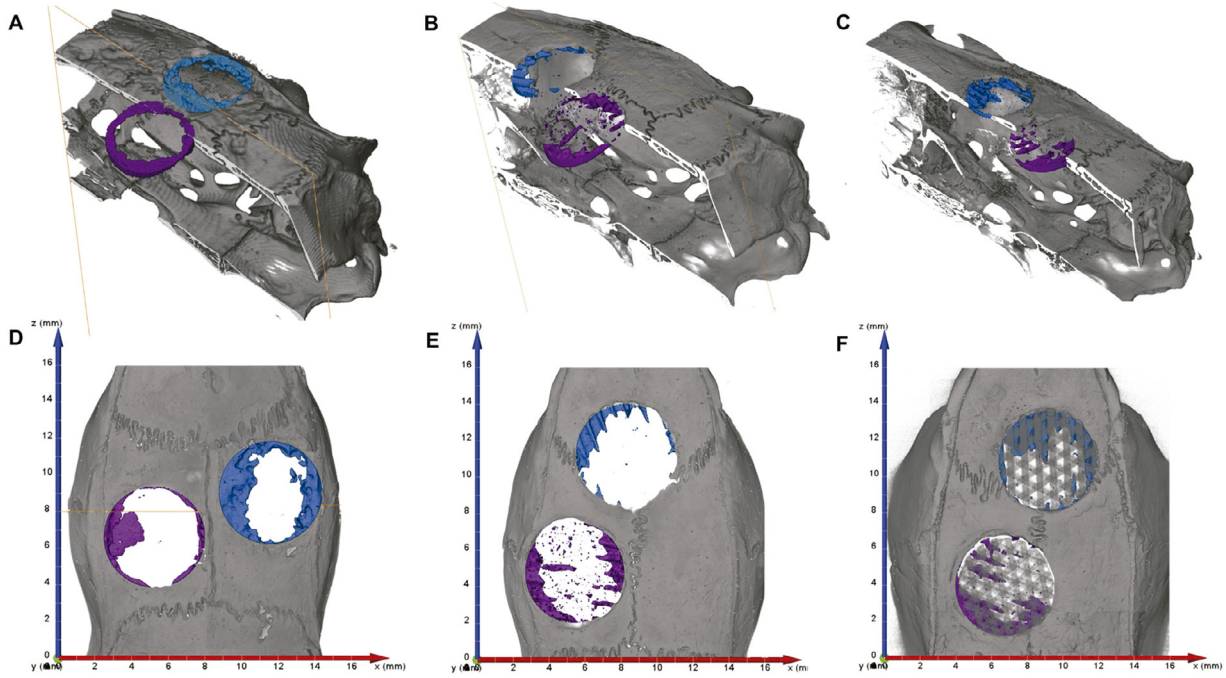

Fig. 3. µCT and histology results according to gender (All parameters are presented as mean SD). Processed µCT images taken with an X-Ray 3D Computer tomograph RayScan 250E. (a,d) Negative control (purple) and Geistlich Bio-Oss® (blue). (b,e) Pure PLA (blue) and PLA/HA (purple) scaffolds. (c,f) PLA/HA cellularized with dental pulp stem cells (blue) and PLA/HA Extra Cellular Matrix scaffolds (purple) [161]. "Reprint with permission from [161] under the terms of the Creative Commons Attribution 4.0 International License, CC BY-NC.ND 4.0."

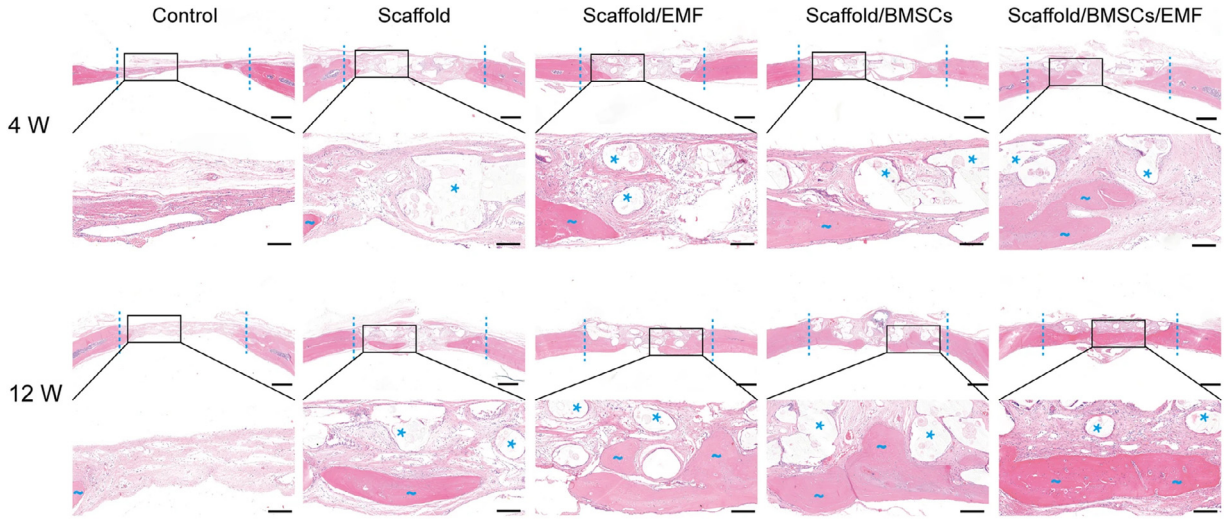

Fig. 4. Bone regeneration evaluated by HE staining. Coronal HE stained sections in the calvarial defect region of different groups were taken 4 and 12 weeks post-operation. The dotted line indicates the boundary of the 6-mm defect. Blue wary lines designate newly formed bone, and asterisks point to residual scaffolds. Scale bars in lower magnification images represent 1000 μm, and scale bars in higher magnification images represent 250 μm [163]. "Reprint with permission from [163] under the terms of the Creative Commons Attribution 4.0 International License, CC BY-NC.ND 4.0."

at 12 weeks) was used compared with PLLA/TCP10 w.f. (~10% at 12 weeks) or PLLA (~0% at 12 weeks) at all time points. The same trend was maintained when MG-63 cells were added to the scaffold, reaching 45% of bone regeneration values in the PLLA/30TCP group at 12 weeks. Besides, Massons's trichrome staining of cranial bone shows the formation of new bone tissue with a typical mature bone structure when MG-63 cells are added.

CaP biomimetic coatings have shown their capability to confer osteoconductivity properties to scaffolds. Maia-Pinto et al. [162] developed and evaluated PLA scaffolds biomimetically coated with apatite, with and without loading rhBMP-2. After 6 months, trim bone formation levels were appreciated in PLA group (New formed bone: 11.2%), compared with PLA-CaP and PLA-CaP-BMP2 groups, which presented significantly better biological responses of newly formed bone, 31.2 and 44.85 respectively. Besides, PLA-CaP-BMP2 groups presented bone tissue formed with a more advance degree of maturity and large area, as compared to PLA-CaP group; and there was no significant degradation of the implants.

Finally, Tcacencu et al. [165] created a composite structure by manufacturing PLA and apatite-wollastonite (AW) disks combined with thermal bonding creating AW/PLA porous composite structures. Despite the confirmation by histological assessment of the in vivo biocompatibility of PLA, AW and AW/PLA scaffolds, the AW/PLA implants resulted in the most considerable amount of

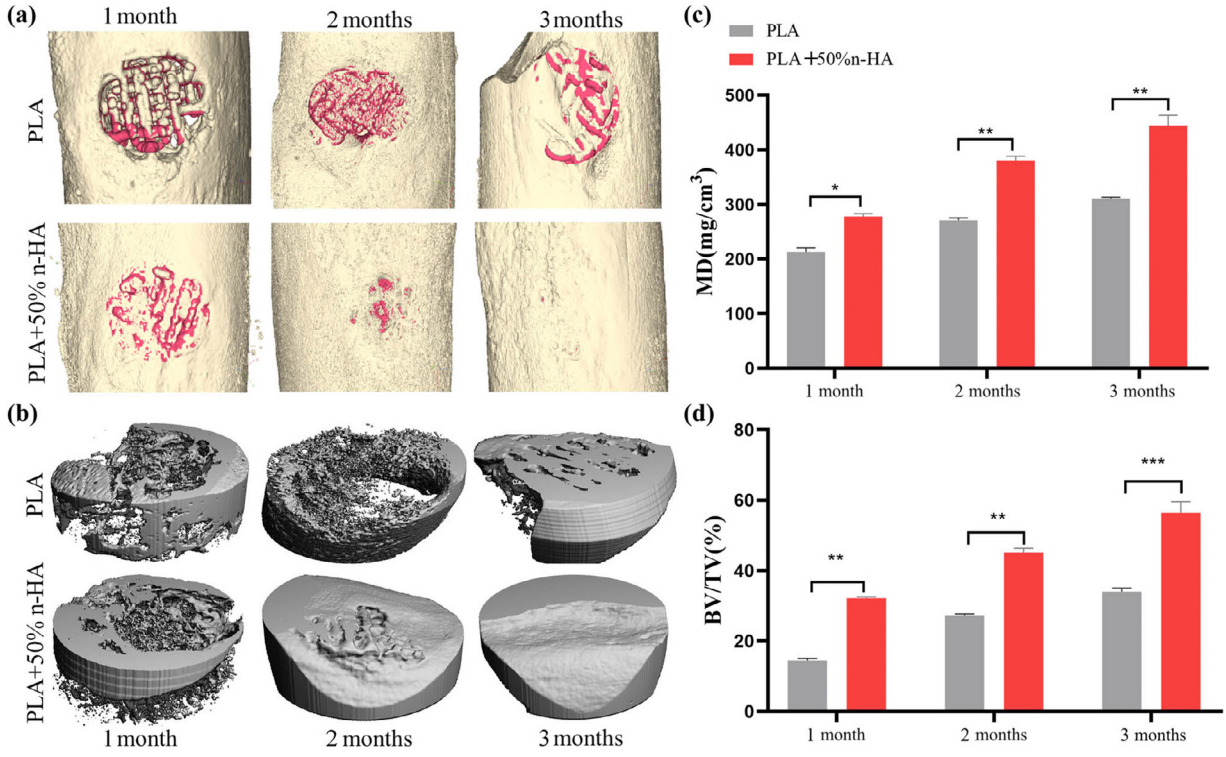

Fig. 5. Micro-CT analysis of the implanted scaffolds. The PLA and PLA/n-HA composite scaffolds were implanted into the rabbit femoral defect. (a) At 1,2 and 3 months after scaffold implantation, the bone defect area was scanned using micro-CT, and 3D reconstruction was performed. The reconstructed scaffold was shown in red and the bone in gold; (b) the scaffold-implanted area of the cortical bone (5 mm in diameter and 2 mm in depth) was reconstructed in 3D; and (c and d) quantitative calculation of new bone growth based on CT data, mineral density (MD), and bone tissue volume (BV)/total tissue volume (TV). $^{*}p < 0.05$; $^{**}p < 0.01$;$^{***}p < 0.001$. [157]. "Reprint with permission from [157] under the terms of the Creative Commons Attribution 4.0 International License, CC BY-NC.ND 4.0."

newly formed bone, with a percentage of newly formed bone between 15 and 25%, versus the 1-2% showed by AW implants.

3.2.2. Studies in rabbits

Studies in rabbits were performed on appendicular limbs, including the femur, tibia, and radius. No adverse effects were found when evaluating the behavior of the biomaterials. The main characteristics and results of the reports are summarized in Table 5.

Curiously, 4 out of the 7 anesthetic protocols selected in rabbits [155–158] included only an injection of pentobarbital, without the complementary administration of any drug. Regarding the other 3 studies, one reported using xylazine [154], and in the other one [159], no information about the anesthetic protocol was provided. Eventually, Minto et al. [160] selected combination of ketamine, midazolam and morphine for preanesthetic medication, besides they administered isoflurane for the induction and maintenance of the general anesthesia, and performed a right brachial plexus block using lidocaine. Likewise, authors used tramadol and meloxicam for postoperative pain control.

As it was mentioned above, HA is the most commonly used bioceramic, having been selected in all the studies in rabbits [154–160]. Specifically nano-HA, was utilized in 4 reports [154,156–158]; and 3 of them used a 5-millimeter circular defect in the femoral diaphysis to assess their bone regeneration properties [156–158]. Wang et al. [156] synthetized PLA/30%n-HA scaffolds and compared them with PLA/0%n-HA scaffolds. In vivo trials showed new bone tissue growing in all groups at any time points without inflammatory reaction or tissue necrosis, demonstrating the biocompatibility of the implant. µCT results indicate a higher bone growing in PLA/30%n-HA groups at 4, 8 and 12 weeks, with BV/TV percentages of 40% vs 30% in PLA/0%n-HA group. Wang et al. [157] manufactured 3D-printed porous scaffolds with a 5:5 mass ratio PLA/n-HA showing that high n-HA content composite materials were biocompatible and osteogenic inductors conducting new bone growth at 1,2 and 3 months. Statistical differences ($p < 0.001$) were found when comparing BV/TV between PLA (~35% BV/TV at 3 months) and PLA/50%n-HA groups (~60% BV/TV at 3 months) (Figure 5). Likewise, these results were superior to those obtained by Wang et al. [156] at the same time point, 40% BV/TV PLA/30%n-HA vs 60% BV/TV PLA/50%n-HA, so a higher amount of n-HA on composites is related with a better bone regeneration of femoral defects. Zhang et al. [158], for their part, reported the implantation during 4 weeks of porous PLLA/n-HA scaffolds loaded with 0, 30 and 50% n-HA, and despite not having performed a quantitative analysis of the results, histological observations demonstrated that all the specimens utterly integrated with surrounding host tissue, with a little bone tissue formation in the internal pores of PLA/30% n-HA scaffolds and even less in PLLA ones, which presented the least new bone tissue. However, in the PLLA/50%n-HA scaffolds, all the pores were filled with new bone tissue, with signs indicating bone maturation. This reaffirms what was previously indicated about the relation between the presence of HA, and bone regeneration (Figure 6). The latest report on n-HA composites is the one carried out by Chen et al. [154], who developed porous PLA/n-HA composite scaffolds with the following PLA/n-HA mixing ratio 9:1 m/m, and evaluate its in vivo osteogenic effects by means of circular defects in the distal part of the femur. Quantitative analysis of µCT showed that BV/TV increased with the increased implant time, from 6% at 4 weeks to 20% at 12 weeks; besides the histological section indicated no inflammation signs and the presence of bone in bone/implant contact region and inside the pores.

No nano-hydroxyapatite powders were utilized in 3 reports in rabbits. Liu et al. [155] designed a 3D-printed scaffold with a PLA/HA mass ratio of 7:3, and tested it in long bone defects,

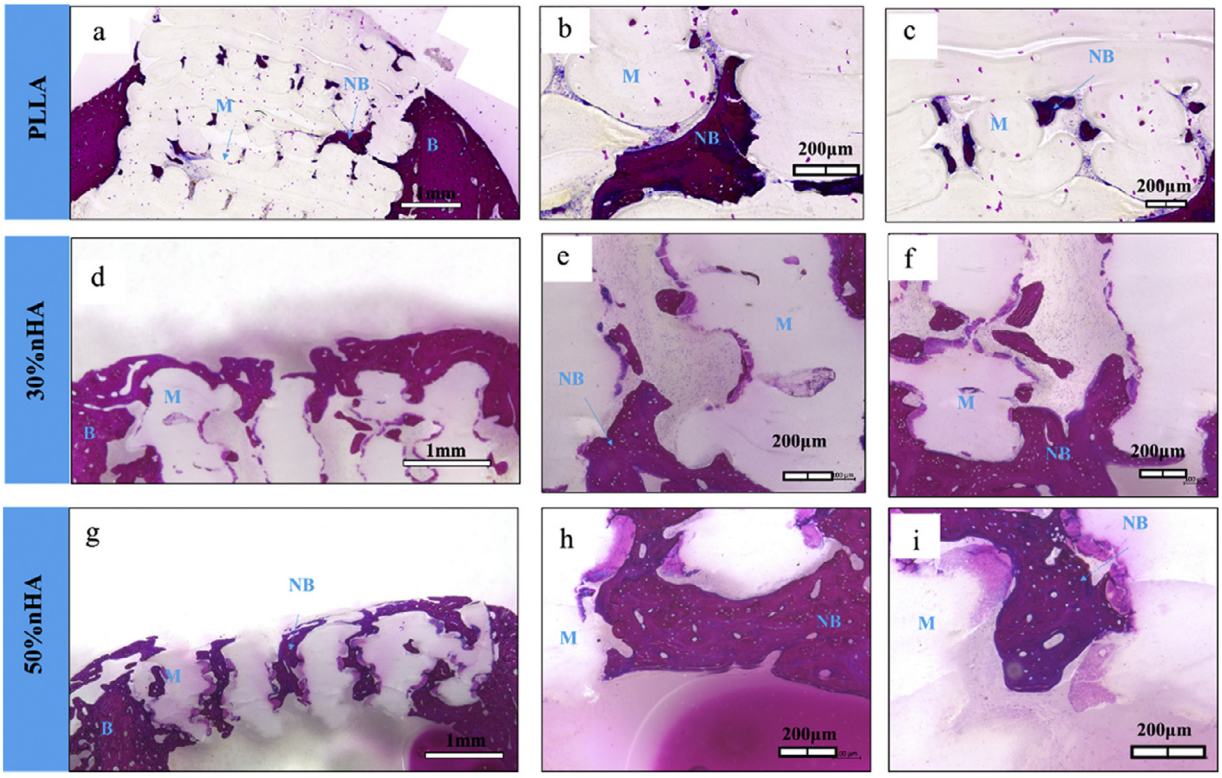

Fig. 6. HE evaluation of PLLA/nHA scaffolds in vivo for 4 weeks (a,d,g) cross-section HA histological images of PLLA, 30%nHA explants; (b,c) high magnification images of PLLA cross-sections and new bone; (e,f) high magnification images of 30%nHA cross-section and new bone; (h,i) high magnification images of 50%nH cross-sections and new bone (M: materials cross-sections, NB: new bone) [158]. "Reprint with permission from [158] under the terms of the Creative Commons Attribution 4.0 International License, CC BY-NC.ND 4.0."

specifically in a segmental defect in the middle of the left radius. Besides, they studied the effect of its use with induced membranes (IM), alone and combined with enhanced bone marrow (eBM), or iliac crest bone graft (ICBG), considered the gold standard in bone regeneration, to improve the bone healing process. Micro-tomographic analysis was performed at 16 weeks and showed the following results: PLA/HA group obtained the lowest BV/TV values (~30%), then IM+PLA/HA group (~50%), and finally IM+ICBG (~70%) and IM+PLA/HA+eBM (~70%), which had demonstrated the best effects on bone regeneration, without significative differences between them. Thus, IM and eBM significantly enhanced bone repair, achieving greater ratios of woven bone than PLA/HA and IM+PLA/HA groups. Likewise, histomorphometry results showed the same trend, with the following area ratios of WB at 8 weeks: PLA/HA (~20%) < IM+PLA/HA (~40%) < IM + ICBG (~70%) = IM + PLA/HA + eBM (~70%).

Minto et al. [160] manufactured a 3D-printed PLLA/HA nonporous scaffolds to fill a defect in the right radius diaphysis, and compared with empty control and iliac crest autologous graft groups. No severe lameness was detected in any of the groups, however, the implant groups showed grater lameness, edema, and pain, compared with the others. Likewise, radiographic and histopathologic studies showed smaller bone callous and grater inflammation signs, respectively, when animals included in PLLA/HA group were analyzed. Therefore, graft group was the one which led to superior results, since it is the gold standard for bone regeneration.

Finally, 3D-printed PLA-HA composites scaffolds were combined with in vivo bioreactor strategies to generate vascularized tissue-engineered bone of customizable size and geometry by Zangh et al. [159]. The scaffolds were seeded with autologous BMSCs, crossed with a vascular bundle (experimental group, EG) or not (control group, CG) and inserted in a tibial periosteum capsule. The histological examination revealed neovascular formation and ossified tissue regeneration in both groups at 4 and 8 weeks. Microangiography and μCT measurements showed a higher vessel number and volume in the EG than CG at any time point. In the same way, BV/TV analysis of the EG was significantly greater than CG, 35% vs 20% at 4 weeks, and 70% vs 30% at 8 weeks.

3.3. Study quality and risk of bias assessment

The quality assessment of the studies was performed according to the essential items of the ARRIVE guidelines, which are summarized in Figure 7. The individual analysis of the manuscripts showed that at item 3. "Inclusion and exclusion criteria", 6. "Outcome measures", 8. "Experimental Animals", 9. "Experimental Procedures", and 11. "Results" the information was adequate and reported with percentages of 85.7%, 78.6%, 85.7%, 64.3% and 64.3%; thus, it graded as "reported". However, items 4. "Randomisation", 5. "Blinding" and 10. "Adverse events" were considered as "not reported" because there is an evident lack of information in the reported studies, with frequencies 35.7%, 100% and 64.3%. Other items, such as 1. "Study Design", 2. "Sample Size" and 7. "Statistical Methods", were classified as "unclear reported", due to incomplete items reported, insufficient experimental details provided, or no subitems included.

The risk of bias was evaluated using the SYRCLE in all the included reports and is shown in the Figure 8, as a frequency distribution percent. Most of the questions were graded as "Low Risk of Bias", as shown in item 2. "Baseline characteristics", 6. "Random outcome assessment", 8. "Incomplete outcome data addressed", 9. "Free from selective outcome reporting" and 10. "Free from other sources of Bias", with percentages from 64.3% to 100%. By contrast,

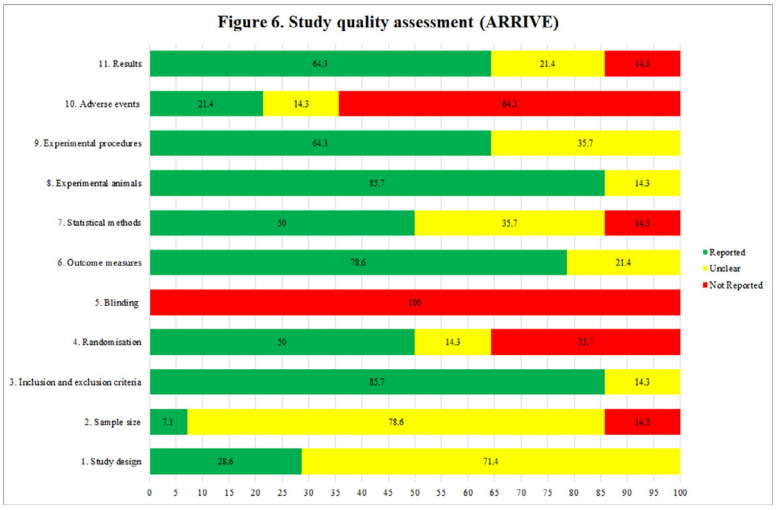

Fig. 7. Study quality assessment (ARRIVE).

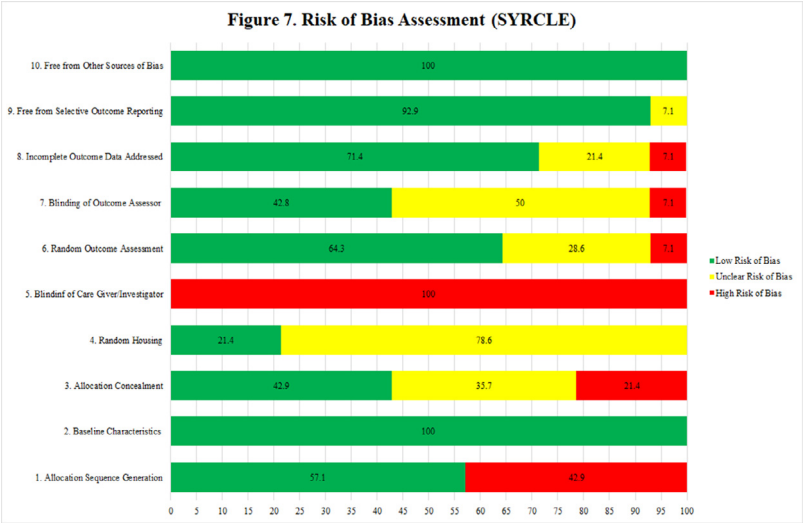

Fig. 8. Risk of Bias Assessment (SYRCLE).

items 1. “Allocation sequence generation” and 5 “Blinding of care giver/investigator”, were assigned as “High Risk of Bias” showing frequencies of 42.9% and 100%. Finally, “Unclear Risk of Bias” was detected at items 3 “Allocation concealment”, 4 “Random housing” and 7 “Blinding of Outcome Assessor” with frequencies of 35.7%, 78.6% and 50%, respectively.

4. Discussion

This systematic review aimed to evaluate the possible use, as bone graft substitutes, of 3D-printed scaffolds synthesized from PLA/bioceramic composites in preclinical studies with animal models as a promising approach to bone repair and reconstruction. Bone tissue engineering is one of the main fields of study in biomedicine, due to the tremendous impact of this pathology on people’s quality of life. Thus, the results positioned 3D-printing technology and composite materials as alternatives to heal impaired fractures, supporting and favoring the growth of new bone and vascular tissue. In addition, its implantation does not trigger and inflammatory response that could harm bone regeneration. Other authors have corroborated these findings, confirming that the use of 3D-printed templates showed more significant bone tissue regeneration than conventional porous templates fabricated from the same material [8]. Likewise, bioceramic scaffolds, alone or combined with polymeric materials, demonstrated better supported new bone formation, compared to untreated empty defects, and a similar bone growth compared to defects filled with deproteinized bovine-derived bone mineral [12].

The importance of using scaffolds in bone tissue engineering has increased in recent years, with the main goals of filling bone defects and supporting and inducing the growth of bone tissue [154]. At the same time, the utilization of additive manufacturing techniques for their synthesis has risen notably since it allows their customization when dealing with complicated and irregular geometries [175], as well as, precisely controlled architectures, high reproductivity and accuracy of produced parts [162,166]. In addition, scaffold architecture is critical for bone regeneration [161], because it is related to its ability to stimulate cellular responses and is essential for regulating cell adhesion, proliferation, migration, and differentiation.

Some of the scaffold’s main studied parameters in the papers were the pore interconnection, overall porosity and pore size. A wide range of pore sizes can be selected for bone regeneration. Generally, macroporosity promotes osteogenesis and microporosity improves surface area for protein adsorption, providing attachment points for osteoblasts. Hence, studies suggested that pore

size should range from 200 to 500 micrometers. Typically, pores should be higher than 300 µm to facilitate osteoblast proliferation and enhance neovascularization, and 100 µm is the very minimum size, since it is associated with the formation of non-mineralised osteoid or fibrous tissue, limiting oxygen and nutrient diffusion throughout the scaffolds [4,161,171–173]. Likewise, pore interconnectivity positively influences bone deposition rate and depth of infiltration, improving nutrient and oxygen supply to the inner part of the scaffold and allowing cell infiltration [172,173]. Another feature that influences bone regeneration rate is the pore's geometry, due to different morphologies giving rise to differences in pore width and curvature of the surface, leading to variations in tissue morphology and growth rate. For example, tissue formation favors concave surfaces compared with flat and convex regions [172].

The bioactive properties are also important, and in all the studied publications, it was demonstrated that the addition of an appropriate amount of calcium phosphate to a PLA matrix provides the implant an improvement in its biological activity [156], by reducing possible inflammatory reactions that could limit PLA applications [166]. Likewise, the addition of bioceramics influenced mechanical properties and biodegradability. Balancing PLA's ductility and Ca-P's brittleness is the key issue regulating composite's mechanical properties [158]. Kwon et al. [164] observed that adding β-TCP in mixture ratios of 10 and 30%, increased the compressive strength of the implants from approximately 258 MPa (PLA alone), to 310 and 349 MPa respectively. However, other studies observed that when higher concentrations of hydroxyapatite were added to a PLA matrix, the compressive strength of the implants decreased [156–158]. Zhang et al. [158] showed that PLA scaffolds had a compressive strength of around 44.02 MPa, which decreased progressively as hydroxyapatite was added, with values of 29.68 and 14.22 MPa for 30 and 50%HA concentrations, respectively.

A critical property when manufacturing bone scaffold is its biodegradability. An ideal biodegradable material should be comparable to the rapid replacement rate by the new bone formation, providing support while leaving space for tissue growth [166]. Indeed, the degradation ratee should match the growth of native ECM to ensure mechanical support throughout the lifecycle of the scaffold [173]. PLA is degraded by simple hydrolysis, and the degradation products are then transformed into nontoxic subproducts that are eliminated through regular cellular activity and urine [13]. Nevertheless, lactate's releasing triggers the acidification of the environment affecting the defect site's acid-base balance, which can lead to hampered biological response towards the scaffold [24,156]. Like other bioceramics, HA performed the neutralizing capacity to the acidic products form in vivo degraded polymers and partially blocked the unfavorable acidic environment [154,176]. Besides, HA is hydrophilic, increasing the ability to absorb the water, and accelerating the degradation process [156,161]. Wang et al. [156] observed that Pn50 group (PLA/50%HA) degraded faster than the other groups (Pn30, PLA/30%HA and Pn0, PLA/0%HA) after 7 days. Zhang et al. [158] also obtained similar results with higher mass and molecular weight losses in PLA/50%HA scaffolds than PLA/30% HA and PLA/0%HA ones. Furthermore, the last studied changes in the solution pH values that before day 11 were significantly lower in PLA/50%HA and PLA/30%HA groups, corresponding to the degree of mass reduction. However, in the later stage, the high content of HA seemed to alleviate environmental acidity, and the lowest pH values were found in samples without HA. By contrast, Kwon et al. [164] concluded from their in vivo degradability analysis that 71% of the original molecular weight of the PLA scaffolds remains 12 weeks post-implantation, with similar results and consequently similar changes in the profiles, if the measures were obtained by GPC or NIR intensity. Besides, the degradation-related molecular weights of PLLA, PLLA+TCP10, and PLLA+TCP30 scaffolds did not vary significantly.

Regarding modifying the characteristics of PLA scaffolds, it is worth highlighting some of the available possibilities that may be interesting for bone tissue engineering. Shuai et al. [107] concluded in their work that the addition of poly (glycolic acid) (PGA) to PLLA/HA scaffolds results in an improvement of the hydrophilic behavior, with higher water absorption and the degradation rate, increasing the contact area between PLLA and body fluid. Consequently, there is a higher exposure of the HA embedded in the PLA matrix, which contacts with body fluids to exchange ions, and therefore the bone like apatite deposition, providing a suitable environment for osteoblastic growth and proliferation. Another possibility is using a copolymer of the PLA, derived from natural monomers of lactide and glycolide, such as poly (lactic-co-glycolic acid) (PLGA). Its amorphous structure allows water molecules to diffuse easily into the scaffold, providing greater degradability and bioactivity compared to the ones made by PLA [177].

Generally, when manufacturing the implants, the bioceramic powders were mixed or dissolved with PLA solution to be later printed using additive manufacturing techniques. However, Tcacencu et al. [165] synthesized apatite-wollastonite disks independently and then adhered them to PLA porous disks through a thermal bonding process, and Maia-Pinto et al. [162] biomimetically coated with apatite a 3D-printed polylactic acid scaffolds. Regarding the manufacturing process of PLA-HA implants, the most frequent combination, and the variations among the mixing ratios, it could be seen that most of the studies chose one proportion [154,155,157,159,161,163,166], but readers do not know why it was selected. However, others tested different concentrations of HA to evaluate the influence on scaffolds' performance [156,158]. At this point, it was observed that when HA ratio was more significant than 50%, the composite material could not be printed coherently and stably due to its high brittleness, but values less than or equal to 50% can be printed satisfactorily by FFF [156–158]. Zhang et al. [158] achieved a successful impression of a composite with 50% HA by using a silane couple agent called dodecyl trimethoxy silane (WD-10), which can combine with the polymer molecular chain more effectively. By contrast, Wang et al. [156] were able to print PLA/50%HA scaffolds but did not test them in vivo, probably because of the presence of apparent fractures in the cuboids and the negative effects of proportions of HA higher than 30% had over the ductility, as they reported.

HA particles' size is also another important aspect when synthesizing composites. Nano-hydroxyapatite has been demonstrated to overcome the shortcomings of the micro-sized one. It increases surface activity due to its size similar to apatite in natural bones, has better dispersibility to attach to the cell membrane and is more suitable as a filler or a coating material. Furthermore, it is less brittleness [156,157].

Likewise, sterilization processes have a major significance when manufacturing scaffolds for bone regeneration and need to be raised at the beginning of implant development. For this purpose, there are many available options as steam sterilization (also called autoclaving), ethylene oxide sterilization, hydrogen peroxide sterilization, γ-irradiation, electron-beam irradiation (also called β-irradiation) and UV sterilization. However, not all of them can be used on biodegradable polymers and/or bioceramics, because it may produce adverse reactions such as physico-chemical and morphological changes and the formation of toxic byproducts by degrading the material [11,168]. UV exposure, γ-irradiation and β-irradiation are suitable processes to sterilize biodegradable polymers. Nevertheless, autoclaving, plasma sterilization and ethylene oxide, the most used process in the included papers, should be avoided because they produce respectively, a shrinkage of the materials, physical alterations, and toxicity [11,178–180]. Regarding bioceramics, γ-irradiation has been shown to be the most indicate sterilization process. However, autoclaving and ethylene ox-

ide have been demonstrated to degrade some calcium phosphate phases [11,30]. Therefore, neither has proven suitable techniques for sterilizing composites synthesized from PLA and bioceramics.

Zeiter et al. [181] reported in their manuscript the massive variations in the chosen models used to test bone substitutes, for example, animal species, strain or breed, age and gender. Rabbits and rats were the most frequently used models but without a clear preference for a specific gender. Besides, there is a high variability in the age of the animals, something with critical influence regarding the closure of growth plates and the skeletal maturity. Literature revealed that important information such as age or gender, was missed in many studies, hindering the interpretation and replicability of the results. These results were in agreement with those obtained in the present review. Al-allaq and Kashan [33] also reported more trials in rodents (rats, mice), than in the rest of the models, probably because of the ease of handling and their small size. However, large animal models should be considered for future investigations, due to the similarities between human clinical conditions and animal models are essential for investigating bone scaffold interactions.

Among the species available for the evaluation of bone formation, rats and rabbits were selected for testing different composite materials in this review, and information about age or gender was variable between them or was not reported or specified [154–167]. Calvaria and femur were, respectively, the main anatomical regions selected to make the defects. However, because of protocol differences such as defect size, the number of defects, observation times or scaffolds composition, no cross-study comparisons could be performed, and the generalizability of the results was limited. Furthermore, the following limitations were found when evaluating the preclinical trials with animal models of the different reports. The sample size was not specified in two [157,167] and another one utilized only 3 animals [154], which is a deficient number of specimens to obtain significative statistical results. The critical-sized defect (CSD) model, commonly proposed for the evaluation of bone healing, was just observed in 5 papers [155,160–162,165]. The lack of control groups, since empty controls were only utilized in 5 of 14 studies [160,161,163,166,167], and iliac crest bone graft control or positive control in 2 [155,160]. The low report of adverse effects, usually present in this kind of procedure, was poorly reported, as seen in the study quality assessment. And finally, the absence of quantitative methods when evaluating bone regeneration among the different groups, such as μCT analysis, quantitative histologic analysis or histomorphometric analysis, was identified in 2 reports [158,160,167].

The choice of the anesthetic protocol is an essential step in the design of any animal experiment, and it must reach a state of unconsciousness, analgesia, and muscle relaxation. Scientists sometimes decide to leave the animals' pain untreated since using potent anesthetic and analgesic drugs may strongly affect the animals' biology. However, animal pain management in laboratories is an ethical imperative [182], specifically when performing most orthopedic and wound healing models, since they produce moderate to severe pain [183]. Below, we will analyze some of the main features of the drugs used for surgical procedures. Since pentobarbital is a barbiturate that produces hypnosis but has poorly analgesic properties, it is typically not used alone in painful procedures. It was administered alone in rabbits [155–158] and rats [167], although in the latter, it was combined in one case with isoflurane [163], an inhalational anesthetic with little or no analgesic activity. Ketamine is a dissociative anesthetic that reaches somatic analgesic levels. It was utilized in rats alone [166] or combined with other drugs, such as xylazine [161,165], xylazine and midazolam [162] or midazolam and morphine [160]. Xylazine is an alpha-2 agonist with powerful tranquillizing properties and moderate visceral analgesic action; midazolam, a benzodiazepine with relatively low tranquillizing-sedative effects and no analgesic properties, is usually utilized as an adjunctive drug to ketamine; and morphine, a pure opioid with potent analgesic action and bad hypnotic properties, which is very useful given its lasting effects for animal's premedication, but also for the postoperative period. Tiletamine, as well as ketamine, is a dissociative anesthetic used in conjunction with zolazepam, a benzodiazepine drug; the combination provides a sedation, but no so potent analgesia. It was administered to rats in combination with xylazine [164]. Furthermore, only one two reports included the use of local anesthesia or postoperative analgesia. Gendviliene et al. [161] selected respectively, lidocaine, a short-acting local anesthetic commonly applied through the infiltration of the tissue, and buprenorphine, a partial agonist opioid which provides analgesia and is considered as an effective treatment for postsurgical pain. It is one of laboratory animals' most widely used analgesics [184]. Likewise, Minto et al. [160] administered lidocaine to perform a right brachial plexus block, a local anesthesia technique; and used meloxicam and tramadol for the control of the pain during the postsurgical period. Meloxicam is a non-steroidal anti-inflammatory drug (NSAID) which provides a moderate analgesic action, usually used for the treatment of pain or inflammatory processes. And tramadol is another opioid commonly administered in rabbits to treat mild acute and chronic pain, it has a low activity at the mu opioid receptor and inhibits noradrenaline and serotonin reuptake [185]. Doses and administration routes are highly important aspects when designing a protocol, although they will not be discussed in this paper. Once reviewed all the drugs included in the anesthetic protocol of the different studies, we can conclude that pain management is deficient in most of the articles, especially in the ones in rabbits. In addition, the use of local anesthesia techniques and postoperative pain control are non-standardized practices, at least in the papers included in the present review. But, what are the implications of choosing an ideal anesthetic protocol that includes an effective pain management, when designing an in vivo preclinical trial for the evaluation of biomaterials? Physiologic response to surgery and pain has been described as "surgical stress response". This phenomenon induced several changes in animals' physiology, such as muscle wasting, weight loss, impaired wound healing and a generalized state of immunosuppression, leading to the appearance of septic complications in the postoperative period. Furthermore, untreated pain can produce a reduction of food and water intake, disrupted sleep and changes in activity and behavior in rodents, which also can delay bone healing [183]. In matter of orthopedic procedures, pain control is also essential, because it favors continued limb usage, and thus, stimulate bone healing [183,186]. So, this is the reason why the concepts of balanced anesthesia and multimodal analgesia become important, since on the one hand they will help us to achieve a quick recovery and bone healing, and prevent chronic pain [183]. And on the other hand, it will allow us to reduce the possible bias outcomes that pain and stress can exert on the bone regeneration process in animals. The results of Carbone and Austin [182] also suggest that animal post-surgical pain is likely undertreated, likewise poor reporting of pain management can lead to the belief that analgesics are not or cannot be used, and as a consequence, other researchers published their work whit referring neither to pain or its treatment; so finally "under-reporting encourages under-treatment".

The urgent need to provide safe and effective biomaterials for clinical applications creates a demand for reproducible and technically simple bioassay for biomaterials' screening, which need to be tested at all stages of preclinical development [187,188]. Animal models play a key role in basic medical research, and many different ones have been used for different applications. [189,190]. However, they encounter ethical, practical, and technical problems which limit their use [190]. For this reason, other alternative pre-

clinical models have gained importance in recent years, thus promoting the incorporation of the 3Rs (Reduction, Replacement and Refinement) in submitted research proposals [188]. Cell cultures have been used as in vitro models for over a century and represents an indispensable tool to improve the understanding of cell biology and in vivo cell behavior mechanisms [189]. Different cell culture techniques have been developed. 2D monolayer models are simple and efficient to assess a biomaterial's biocompatibility, characterization and functionality. However they not accurately mimic the natural 3D organization of cells and their extracellular matrix [188,189], and consequently do not fully predict in vivo outcomes. This is why 3D cell cultures were developed, offering an opportunity to replace animal models due to their success to replicate a higher number of in vivo features by mimicking living organ's organization and microarchitecture (organotypic culture/organoids) [188,189]. Thus, 3D cell cultures allow the study of cell-cell and cell-environment interactions mimicking in vivo physiology [188]. Likewise, the chorioallantoic-membrane (CAM) of the chick embryo have demonstrated to be a valuable, short-term, simple and cost-effective assay to test biomaterials, with results comparable with the ones obtained in mouse trials [187,188,190]. The CAM functions as an organ for gas exchange between the embryo and the environment [187]. Its most common application is examining the angiogenic response as an early indicator of biomaterials' performance in vivo [188], because of the close connection between osteogenesis and angiogenesis during bone healing [190]. But this model also allows the evaluation of biocompatibility based on the survival rate of the chick embryos at the experimental end-point, the integration of the implant within the CAM and the presence of a primitive inflammatory response [188]. Finally, another option for the study of angiogenesis is the generation or an arteriovenous loop. This model is useful for investigating the angiogenesis and biocompatibility but also for the axial vascularization of scaffolds for tissue engineering purposes, in which engineered tissue can be transplanted with its vascular axis and connected to local vessels at the recipient site. The model provides the tissue with oxygen and nutrients immediately after transplantation [191].

3D-printed templates have been shown to have characteristics for their use in bone regeneration when composite originated from the addition of HA, β-TCP or octacalcium phosphate to a PLA matrix, the combination between PLA and apatite-wollastonite discs or the use of biomimetic CaP coatings; were utilized for their synthesis. Starting from this, we can extract certain ideas. First of all, we could see that higher concentrations of HA [156,158] or β-TCP [164], as expected, will lead to higher percentages of new bone area. Furthermore, the addition of different substances to functionalize the scaffolds, showed an improvement in the results compared with not functionalized groups, as Minto et al. [160] described in their paper "A factor that could assist the scaffold would be the use of precursor cells for osteogenesis to optimize bone healing, since biologically active 3D implants are promising in tissue regeneration". Dental pulp stem cells [161], bone marrow stem cells [159,163] or enhanced bone marrow [155], which increase the migration of the stem cells to the site of the injury, and induce angiogenesis and osteogenic differentiation by the release of growth factors. Indeed, grown factors with the greatest osteoinductive potential can also be applied, such as bone morphogenetic proteins (BMP) [162], which stimulate bone formation via recruiting osteoprogenitor cells. BMP-2 has been widely studied because of its ability to directly target BMP receptors at the cell surface and trigger stem cell differentiation in bone, and it has been demonstrated to be an alternative to stem cell implantation [192]. Likewise, other substances have demonstrated a positive effect on bone growth, such as human osteoblastoma cell lines [164], a potential osteoblast-like source. This potential osteoblast-like source allows rapid bone proliferation, and lanthanum, a foreign ion capable of enhancing bone formation by influencing the hydrolysis of OCP to HA. Nevertheless, functionalizing substances is not the only strategy different authors use to stimulate bone regeneration. The application of electric fields [163] and induced membranes technique [155] have also benefited bone healing. Among the substances that can be added to scaffolds to improve the biological effects, even the use of metals has been reported. Wang et al. *[193]* recently published the addition of lithium to PLA/n-HA composites, which plays an important role in bone development, homeostasis, osteoblast differentiation and bone formation via the activation of Wnt signaling pathway. Likewise, in vivo trials have demonstrated that in lithium doped groups presented higher osteogenic induction than not doped ones.

As it could be seen in the results section, none of the papers matching the search criteria have used bioglass, however they have also been demonstrated to neutralize the acidic degradation of the PLA, improve the mechanical properties of the composites, as well as their bioactivity, cytocompatibility and biological fixation, defined as the capability of bonding to both hard and soft tissues. Furthermore, bioglass release inhibits the growth of various bacterial strains, reducing the risk of infections and implant encapsulation, as mentioned before [16,17]. Alksne et al. [20] in their work compared in vitro 3D-printed PLA/HA and PLA/BG composite scaffolds, and concluded that BG composites are more suitable for bone regeneration demonstrating better biofriendly and osteoinductive properties compared to pure PLA and PLA/HA scaffolds, since the ions dissociated from BG such as soluble silica, calcium, sodium and phosphate, stimulate osteogenesis and angiogenesis, affecting cell fate, biological response and osteogenic commitment more than HA, that only ensure bone building material accessibility acting as a nucleating site for bone minerals. Thus, BG is presented as another interesting option for the synthesis of composites for bone regeneration, as it was demonstrated by Sultan et al. [17] who implanted PLA/BG scaffolds subcutaneously in rats and reported the potential of these scaffolds in bone tissue engineering.

5. Conclusion

All included studies concluded that 3D-printed composite scaffolds provide a promising alternative for treating of bone defects. Tested implants showed to be biocompatible without the appearance of adverse reactions that could impair bone growth. They are also mechanically resistant, and bone formation was positively related to adding higher bioceramics to the PLA matrix. Furthermore, adding different substances to functionalize the scaffolds or using several procedures improved their biological activity and, consequently, the appearance of better newly bone formation results. However, most of the reports focused on the synthesis and characterization of the implant. Finally, they neglected the design and performance of in vivo trials with animal models, mainly in aspects related to anesthetic protocol, which is vital in this kind of study. Likewise, there is a lack of standardization in the design of these procedures that allows the comparison of the results obtained among the different reports, specifically when regarding the animal species, age and gender, the number and size of performed defects, the use of empty control groups, the establishment of critical defects as essential in the study of bone healing and the unification of formed bone quantification methods. These changes will lead to refining the surgical processes and procuring quality information without the risk of bias, which will help the rest of the research community working in this research area.

Funding sources

This research received no external funding.

Declaration of Competing Interest

The authors declare that they have no competing of interests.

Acknowledgements

I.A. acknowledges the XUNTA de Galicia for his pre-doctoral contract (Ref. ED481A 2021/137) from Galician Government Consellería de Cultura, Educación e Universidades.

References

[1] G. Fernandez de Grado, L. Keller, Y. Idoux-Gillet, Q. Wagner, A.-M. Musset, N. Benkirane-Jessel, F. Bornert, D. Offner, Bone substitutes: a review of their characteristics, clinical use, and perspectives for large bone defects management, J. Tissue Eng. 9 (2018) 204173141877681, doi:10.1177/2041731418776819.
[2] A. Ho-Shui-Ling, J. Bolander, L.E. Rustom, A.W. Johnson, F.P. Luyten, C. Picart, Bone regeneration strategies: engineered scaffolds, bioactive molecules and stem cells current stage and future perspectives, Biomaterials 180 (2018) 143–162, doi:10.1016/j.biomaterials.2018.07.017.
[3] M. Majidinia, A. Sadeghpour, B. Yousefi, The roles of signaling pathways in bone repair and regeneration, J. Cell. Physiol. 233 (2018) 2937–2948, doi:10.1002/jcp.26042.
[4] H.J. Haugen, S.P. Lyngstadaas, F. Rossi, G. Perale, Bone grafts: which is the ideal biomaterial? J. Clin. Periodontol. 46 (2019) 92–102, doi:10.1111/jcpe.13058.
[5] Y. Li, S.K. Chen, L. Li, L. Qin, X.L. Wang, Y.X. Lai, Bone defect animal models for testing efficacy of bone substitute biomaterials, J. Orthop. Transl. 3 (2015) 95–104, doi:10.1016/j.jot.2015.05.002.
[6] G. Brunello, S. Sivolella, R. Meneghello, L. Ferroni, C. Gardin, A. Piattelli, B. Zavan, E. Bressan, Powder-based 3D printing for bone tissue engineering, Biotechnol. Adv. 34 (2016) 740–753, doi:10.1016/j.biotechadv.2016.03.009.
[7] A.V. Do, R. Smith, T.M. Acri, S.M. Geary, A.K. Salem, 3D Printing Technologies for 3D Scaffold Engineering, Elsevier Ltd, 2018, doi:10.1016/B978-0-08-100979-6.00009-4.
[8] M.N. Hassan, M.A. Yassin, S. Suliman, S.A. Lie, H. Gjengedal, K. Mustafa, The bone regeneration capacity of 3D-printed templates in calvarial defect models: a systematic review and meta-analysis, Acta Biomater. 91 (2019) 1–23, doi:10.1016/j.actbio.2019.04.017.
[9] A. Saberi, A. Behnamghader, B. Aghabarari, A. Yousefi, D. Majda, M.V.M. Huerta, M. Mozafari, 3D direct printing of composite bone scaffolds containing polylactic acid and spray dried mesoporous bioactive glass-ceramic microparticles, Int. J. Biol. Macromol. 207 (2022) 9–22, doi:10.1016/j.ijbiomac.2022.02.067.
[10] Tumedei, Savadori, Del Fabbro, Synthetic blocks for bone regeneration: a systematic review and meta-analysis, Int. J. Mol. Sci. 20 (2019) 4221, doi:10.3390/ijms20174221.
[11] C. Garot, G. Bettega, C. Picart, Additive manufacturing of material scaffolds for bone regeneration: toward application in the clinics, Adv. Funct. Mater. 31 (2021) 2006967, doi:10.1002/adfm.202006967.
[12] G. Brunello, S. Panda, L. Schiavon, S. Sivolella, L. Biasetto, M.D. Fabbro, The impact of bioceramic scaffolds on bone regeneration in preclinical in vivo studies: a systematic review, Materials 13 (2020) 1–26, doi:10.3390/ma13071500.
[13] M.S. Singhvi, S.S. Zinjarde, D.V. Gokhale, Polylactic acid: synthesis and biomedical applications, J. Appl. Microbiol. 127 (2019) 1612–1626, doi:10.1111/jam.14290.
[14] V. DeStefano, S. Khan, A. Tabada, Applications of PLA in modern medicine, Eng. Regen. 1 (2020) 76–87, doi:10.1016/j.engreg.2020.08.002.
[15] E.H. Tümer, H.Y. Erbil, Extrusion-based 3D printing applications of PLA composites: a review, Coatings 11 (2021) 390, doi:10.3390/coatings11040390.
[16] E. Schätzlein, C. Kicker, N. Söhling, U. Ritz, J. Neijhoft, D. Henrich, J. Frank, I. Marzi, A. Blaeser, 3D-Printed PLA-bioglass scaffolds with controllable calcium release and MSC adhesion for bone tissue engineering, Polymers 14 (2022) 2389, doi:10.3390/polym14122389.
[17] S. Sultan, N. Thomas, M. Varghese, Y. Dalvi, S. Joy, S. Hall, A.P. Mathew, The design of 3D-printed polylactic acid–bioglass composite scaffold: a potential implant material for bone tissue engineering, Molecules 27 (2022) 7214, doi:10.3390/molecules27217214.
[18] M. Cannio, D. Bellucci, J.A. Roether, Dino.N. Boccaccini, V. Cannillo, Bioactive glass applications: a literature review of human clinical trials, Materials 14 (2021) 5440, doi:10.3390/ma14185440.
[19] Y. Zhang, T. Lin, H. Meng, X. Wang, H. Peng, G. Liu, S. Wei, Q. Lu, Y. Wang, A. Wang, W. Xu, H. Shao, J. Peng, 3D gel-printed porous magnesium scaffold coated with dibasic calcium phosphate dihydrate for bone repair in vivo, J. Orthop. Transl. 33 (2022) 13–23, doi:10.1016/j.jot.2021.11.005.
[20] M. Alksne, M. Kalvaityte, E. Simoliunas, I. Rinkunaite, I. Gendviliene, J. Locs, V. Rutkunas, V. Bukelskiene, In vitro comparison of 3D printed polylactic acid/hydroxyapatite and polylactic acid/bioglass composite scaffolds: Insights into materials for bone regeneration, J. Mech. Behav. Biomed. Mater. 104 (2020) 103641, doi:10.1016/j.jmbbm.2020.103641.
[21] S. Dorozhkin, Medical application of calcium orthophosphate bioceramics, BIO 1 (2011) 1–51, doi:10.5618/bio.2011.v1.n1.1.
[22] S. Fukuba, M. Okada, K. Nohara, T. Iwata, Alloplastic bone substitutes for periodontal and bone regeneration in dentistry: current status and prospects, Materials 14 (2021) 1096, doi:10.3390/ma14051096.
[23] C. Stacchi, T. Lombardi, F. Oreglia, A. Alberghini Maltoni, T. Traini, Histologic and histomorphometric comparison between sintered nanohydroxyapatite and anorganic bovine xenograft in maxillary sinus grafting: a split-mouth randomized controlled clinical trial, BioMed Res. Int. 2017 (2017) 1–10, doi:10.1155/2017/9489825.
[24] J.-W. Kim, B.-E. Yang, S.-J. Hong, H.-G. Choi, S.-J. Byeon, H.-K. Lim, S.-M. Chung, J.-H. Lee, S.-H. Byun, Bone regeneration capability of 3D printed ceramic scaffolds, Int. J. Mol. Sci. 21 (2020) 4837, doi:10.3390/ijms21144837.
[25] S. Bose, S. Vahabzadeh, A. Bandyopadhyay, Bone tissue engineering using 3D printing, Mater. Today. 16 (2013) 496–504, doi:10.1016/j.mattod.2013.11.017.
[26] L. Roseti, V. Parisi, M. Petretta, C. Cavallo, G. Desando, I. Bartolotti, B. Grigolo, Scaffolds for bone tissue engineering: state of the art and new perspectives, Mater. Sci. Eng. C. 78 (2017) 1246–1262, doi:10.1016/j.msec.2017.05.017.
[27] A. Stavropoulos, A. Sculean, D.D. Bosshardt, D. Buser, B. Klinge, Pre-clinical *in vivo* models for the screening of bone biomaterials for oral/craniofacial indications: focus on small-animal models, Periodontol 68 (2015) 55–65, doi:10.1111/prd.12065.
[28] N. Donos, X. Dereka, N. Mardas, Experimental models for guided bone regeneration in healthy and medically compromised conditions, Periodontol 68 (2015) 99–121, doi:10.1111/prd.12077.
[29] A.T. Khalaf, Y. Wei, J. Wan, J. Zhu, Y. Peng, S.Y. Abdul Kadir, J. Zainol, Z. Oglah, L. Cheng, Z. Shi, Bone tissue engineering through 3D bioprinting of bioceramic scaffolds: a review and update, Life 12 (2022) 903, doi:10.3390/life12060903.
[30] N. Eliaz, N. Metoki, Calcium phosphate bioceramics: a review of their history, structure, properties, coating technologies and biomedical applications, Materials 10 (2017) 334, doi:10.3390/ma10040334.
[31] B.I. Oladapo, S.A. Zahedi, S.O. Ismail, D.B. Olawade, Recent advances in biopolymeric composite materials: future sustainability of bone-implant, Renew. Sustain. Energy Rev. 150 (2021) 111505, doi:10.1016/j.rser.2021.111505.
[32] R.A. Ilyas, S.M. Sapuan, M.M. Harussani, M.Y.A.Y. Hakimi, M.Z.M. Haziq, M.S.N. Atikah, M.R.M. Asyraf, M.R. Ishak, M.R. Razman, N.M. Nurazzi, M.N.F. Norrrahim, H. Abral, M. Asrofi, Polylactic acid (Pla) biocomposite: processing, additive manufacturing and advanced applications, Polymers 13 (2021), doi:10.3390/polym13081326.
[33] A.A. Al-allaq, J.S. Kashan, A review: in vivo studies of bioceramics as bone substitute materials, Nano Sel. 4 (2023) 123–144, doi:10.1002/nano.202200222.
[34] N. Percie du Sert, V. Hurst, A. Ahluwalia, S. Alam, M.T. Avey, M. Baker, W.J. Browne, A. Clark, I.C. Cuthill, U. Dirnagl, M. Emerson, P. Garner, S.T. Holgate, D.W. Howells, N.A. Karp, S.E. Lazic, K. Lidster, C.J. MacCallum, M. Macleod, E.J. Pearl, O.H. Petersen, F. Rawle, P. Reynolds, K. Rooney, E.S. Sena, S.D. Silberberg, T. Steckler, H. Würbel, The ARRIVE guidelines 2.0: updated guidelines for reporting animal research, PLOS Biol. 18 (2020) e3000410, doi:10.1371/journal.pbio.3000410.
[35] C.R. Hooijmans, M.M. Rovers, R.B. de Vries, M. Leenaars, M. Ritskes-Hoitinga, M.W. Langendam, SYRCLE's risk of bias tool for animal studies, BMC Med. Res. Methodol. 14 (2014) 43, doi:10.1186/1471-2288-14-43.
[36] F. Ze-wen, Z. Xin-yu, Q. Shuai, W. Yan, G. Jing, Q. Hui-xin, X. Lan-juan, 3D printing of polylactic acid/poly ethylene glycol/hydroxyapatite porous bone scaffolds and their biocompatibility, J. Mater. Eng. 49 (2021) 135–141, doi:10.11868/j.issn.1001-1381.2020.000390.
[37] S.M. Lebedev, D.M. Chistokhin, S. Shchadenko V, A.N. Dzuman, O.O. Nikolaeva, D. Mitrichenko V, A.B. Prosolov, I.A. Khlusov, Biodegradable polymer composites with osteogenic potential, Byulleten Sib. Meditsiny. 19 (2020) 119–129, doi:10.20538/1682-0363-2020-4-119-129.
[38] N. Ranjan, R. Singh, I.P.S. Ahuja, R. Kumar, D. Singh, S. Ramniwas, A.K. Verma, D. Mittal, 3D printed scaffolds for tissue engineering applications: mechanical, morphological, thermal, in-vitro and in-vivo investigations, CIRP J. Manuf. Sci. Technol. 32 (2021) 205–216, doi:10.1016/j.cirpj.2021.01.002.
[39] B. Ashwin, B. Abinaya, T.P. Prasith, S.V. Chandran, L.R. Yadav, M. Vairamani, S. Patil, N. Selvamurugan, 3D-poly (lactic acid) scaffolds coated with gelatin and mucic acid for bone tissue engineering, Int. J. Biol. Macromol. 162 (2020) 523–532, doi:10.1016/j.ijbiomac.2020.06.157.
[40] W. Clifton, E. Nottmeier, A. Damon, C. Dove, S.G. Chen, M. Pichelmann, A feasibility study for the production of three-dimensional-printed spine models using simultaneously extruded thermoplastic polymers, CUREUS 11 (2019), doi:10.7759/cureus.4440.
[41] M. Wan, S. Liu, D. Huang, Y. Qu, Y. Hu, Q. Su, W. Zheng, X. Dong, H. Zhang, Y. Wei, W. Zhou, Biocompatible heterogeneous bone incorporated with polymeric biocomposites for human bone repair by 3D printing technology, J. Appl. Polym. Sci. 138 (2021), doi:10.1002/app.50114.
[42] H. Belaid, S. Nagarajan, C. Barou, V. Huon, J. Bares, S. Balme, P. Miele, D. Cornu, V. Cavailles, C. Teyssier, M. Bechelany, Boron nitride based nanobiocomposites: design by 3D printing for bone tissue engineering, ACS Appl. Bio Mater. 3 (2020) 1865–1874, doi:10.1021/acsabm.9b00965.
[43] C.R. Moreno, E.M. Santschi, J. Janes, J. Liu, D. Kim, A.S. Litsky, Compression generated by cortical screws in an artificial bone model of an equine medial femoral condylar cyst, Vet. Surg. 51 (2022) 833–842, doi:10.1111/vsu.13814.
[44] H. Belaid, S. Nagarajan, C. Teyssier, C. Barou, J. Barés, S. Balme, H. Garay, V. Huon, D. Cornu, V. Cavaillès, M. Bechelany, Development of new biocompatible 3D printed graphene oxide-based scaffolds, Mater. Sci. Eng. C 110 (2020) 110595, doi:10.1016/j.msec.2019.110595.

[45] C.-H. Cheng, Y.-W. Chen, A. Kai-Xing Lee, C.-H. Yao, M.-Y. Shie, Development of mussel-inspired 3D-printed poly (lactic acid) scaffold grafted with bone morphogenetic protein-2 for stimulating osteogenesis, J. Mater. Sci. Mater. Med. 30 (2019), doi:10.1007/s10856-019-6279-x.
[46] M.-M. Liu, Y. Zhong, Y. Chen, L.-N. Wu, W. Chen, X.-H. Lin, Y. Lei, A.-L. Liu, Electrochemical monitoring the effect of drug intervention on PC12 cell damage model cultured on paper-PLA 3D printed device, Anal. Chim. ACTA. 1194 (2022), doi:10.1016/j.aca.2021.339409.
[47] Z. Huan, H.K. Chu, H. Liu, J. Yang, D. Sun, Engineered bone scaffolds with Dielectrophoresis-based patterning using 3D printing, Biomed. Microdevices. 19 (2017) 102, doi:10.1007/s10544-017-0245-5.
[48] R. Donate, M.Elena Aleman-Dominguez, M. Monzon, J. Yu, F. Rodriguez-Esparragon, C. Liu, Evaluation of aloe vera coated polylactic acid scaffolds for bone tissue engineering, Appl. Sci. 10 (2020), doi:10.3390/app10072576.
[49] K.S. Manjunath, K. Sridhar, V. Gopinath, K. Sankar, A. Sundaram, N. Gupta, A.S.S.J. Shiek, P.S. Shantanu, Facile manufacturing of fused-deposition modeled composite scaffolds for tissue engineering-an embedding model with plasticity for incorporation of additives, Biomed. Mater. Bristol. Engl. 16 (2020) 15028, doi:10.1088/1748-605X/abc1b0.
[50] A. Souness, F. Zamboni, G.M. Walker, M.N. Collins, Influence of scaffold design on 3D printed cell constructs, J. Biomed. Mater. Res. B 106 (2018) 533–545, doi:10.1002/jbm.b.33863.
[51] F. Caronna, N. Glimpel, G.-P. Paar, T. Gries, A. Blaeser, K. Do, E.B. Dolan, W. Ronan, Manufacturing, characterization, and degradation of a poly(lactic acid) warp-knitted spacer fabric scaffold as a candidate for tissue engineering applications, Biomater. Sci. 10 (2022) 3793–3807, doi:10.1039/D1BM02027G.
[52] M.P. Bernardo, B.C.R. da Silva, A.E.I. Hamouda, M.A.S. de Toledo, C. Schalla, S. Rütten, R. Goetzke, L.H.C. Mattoso, M. Zenke, A. Sechi, PLA/Hydroxyapatite scaffolds exhibit in vitro immunological inertness and promote robust osteogenic differentiation of human mesenchymal stem cells without osteogenic stimuli, Sci. Rep. 12 (2022) 2333, doi:10.1038/s41598-022-05207-w.
[53] P. Kowalczyk, P. Trzaskowska, I. \Lojszczyk, R. Podgórski, T. Ciach, Production of 3D printed polylactide scaffolds with surface grafted hydrogel coatings, Colloids Surf. B 179 (2019) 136–142, doi:10.1016/j.colsurfb.2019.03.069.
[54] R. Chung, D.M. Kalyon, X. Yu, A. Valdevit, Segmental bone replacement via patient-specific, three-dimensional printed bioresorbable graft substitutes and their use as templates for the culture of mesenchymal stem cells under mechanical stimulation at various frequencies, Biotechnol. Bioeng. 115 (2018) 2365–2376, doi:10.1002/bit.26780.
[55] M.J. Dewey, E.M. Johnson, D.W. Weisgerber, M.B. Wheeler, B.A.C. Harley, Shape-fitting collagen-PLA composite promotes osteogenic differentiation of porcine adipose stem cells, J. Mech. Behav. Biomed. Mater. 95 (2019) 21–33, doi:10.1016/j.jmbbm.2019.03.017.
[56] K. Dave, Z. Mahmud, V.G. Gomes, Superhydrophilic 3D-printed scaffolds using conjugated bioresorbable nanocomposites for enhanced bone regeneration, Chem. Eng. J. 445 (2022) 136639, doi:10.1016/j.cej.2022.136639.
[57] M. Alksne, E. Simoliunas, M. Kalvaityte, E. Skliutas, I. Rinkunaite, I. Gendviliene, D. Baltriukiene, V. Rutkunas, V. Bukelskiene, The effect of larger than cell diameter polylactic acid surface patterns on osteogenic differentiation of rat dental pulp stem cells, J. Biomed. Mater. Res. A. 107 (2019) 174–186, doi:10.1002/jbm.a.36547.
[58] S. Swetha, K. Balagangadharan, K. Lavanya, N. Selvamurugan, Three-dimensional-poly(lactic acid) scaffolds coated with gelatin/magnesium-doped nano-hydroxyapatite for bone tissue engineering, Biotechnol. J. 16 (2021) e2100282, doi:10.1002/biot.202100282.
[59] S. Pant, S. Thomas, S. Loganathan, R.B. Valapa, 3D bioprinted poly(lactic acid)/mesoporous bioactive glass based biomimetic scaffold with rapid apatite crystallization and in-vitro Cytocompatability for bone tissue engineering, Int. J. Biol. Macromol. 217 (2022) 979–997, doi:10.1016/j.ijbiomac.2022.07.202.
[60] B. Oladapo I, S.O. Ismail, M. Zahedi, A. Khan, H. Usman, 3D printing and morphological characterisation of polymeric composite scaffolds, Eng. Struct. 216 (2020), doi:10.1016/j.engstruct.2020.110752.
[61] F. Gang, W. Ye, C. Ma, W. Wang, Y. Xiao, C. Liu, X. Sun, 3D printing of PLLA/biomineral composite bone tissue engineering scaffolds, MATERIALS. 15 (2022), doi:10.3390/ma15124280.
[62] I. Buj-Corral, A. Bagheri, O. Petit-Rojo, 3D Printing of porous scaffolds with controlled porosity and pore size values, MATERIALS 11 (2018), doi:10.3390/ma11091532.
[63] L. He, X. Liu, C. Rudd, Additive-manufactured gyroid scaffolds of magnesium oxide, phosphate glass fiber and polylactic acid composite for bone tissue engineering, Polymers 13 (2021), doi:10.3390/polym13020270.
[64] C. Amnael Orozco-Diaz, R. Moorehead, G.C. Reilly, F. Gilchrist, C. Miller, Characterization of a composite polylactic acid-hydroxyapatite 3D-printing filament for bone-regeneration, Biomed. Phys. Eng. Express. 6 (2020), doi:10.1088/2057-1976/ab73f8.
[65] R. Donate, M. Monzon, Z. Ortega, L. Wang, V. Ribeiro, D. Pestana, J.M. Oliveira, R.L. Reis, Comparison between calcium carbonate and beta-tricalcium phosphate as additives of 3D printed scaffolds with polylactic acid matrix, J. Tissue Eng. Regen. Med. 14 (2020) 272–283, doi:10.1002/term.2990.
[66] E.H. Backes, L. de N. Pires, H.S. Selistre-de-Araujo, L.C. Costa, F.R. Passador, L.A. Pessan, Development and characterization of printablePLA/beta-TCPbioactive composites for bone tissue applications, J. Appl. Polym. Sci. 138 (2021), doi:10.1002/app.49759.
[67] M.P. Bernardo, B.C. Rodrigues da Silva, L.H. Capparelli Mattoso, Development of three-dimensional printing filaments based on poly(lactic acid)/hydroxyapatite composites with potential for tissue engineering, J. Compos. Mater. 55 (2021) 2289–2300, doi:10.1177/0021998320988568.
[68] V. Nadarajan, S.W. Phang, H.L. Choo, Fabrication of 3d-printed bone scaffold of natural hydroxyapatite from fish bones in polylactic acid composite, in: 13TH Int. Eng. Res. Conf. 13TH EURECA 2019, 2020, p. 2233, doi:10.1063/5.0001497.
[69] E.H. Backes, L.D.N. Pires, C.A.G. Beatrice, L.C. Costa, F.R. Passador, L.A. Pessan, Fabrication of biocompatible composites of poly(lactic acid)/hydroxyapatite envisioning medical applications, Polym. Eng. Sci. 60 (2020) 636–644, doi:10.1002/pen.25322.
[70] E. Salamanca, T.-C. Tsao, H.-W. Hseuh, Y.-F. Wu, C.-S. Choy, C.-K. Lin, Y.-H. Pan, N.-C. Teng, M.-C. Huang, S.-M. Lin, W.-J. Chang, Fabrication of polylactic acid/beta-tricalcium phosphate FDM 3D printing fiber to enhance osteoblastic-like cell performance, Front. Mater. 8 (2021), doi:10.3389/fmats.2021.683706.
[71] G. Dubinenko, A. Zinoviev, E. Bolbasov, A. Kozelskaya, E. Shesterikov, V. Novikov, S. Tverdokhlebov, Highly filled poly(l-lactic acid)/hydroxyapatite composite for3Dprinting of personalized bone tissue engineering scaffolds, J. Appl. Polym. Sci. 138 (2021), doi:10.1002/app.49662.
[72] S. Gnanamani Sankaravel, R.B. Syed, V. Manivachakan, In vitro and mechanical characterization of PLA/egg shell biocomposite scaffold manufactured using fused deposition modeling technology for tissue engineering applications, Polym. Compos. 43 (2022) 173–186, doi:10.1002/pc.26365.
[73] N. Soehling, S. Al Zoghool, E. Schaetzlein, J. Neijhoft, K.M.C. Oliveira, L. Leppik, U. Ritz, E. Doersam, J. Frank, I. Marzi, A. Blaeser, D. Henrich, In vitro evaluation of a 20% bioglass-containing 3D printable PLA composite for bone tissue engineering, Int. J. BIOPRINTING. 8 (2022) 65–81, doi:10.18063/ijb.v8i4.602.
[74] Y. Zamani, G. Amoabediny, J. Mohammadi, B. Zandieh-Doulabi, J. Klein-Nulend, M.N. Helder, Increased osteogenic potential of pre-osteoblasts on three-dimensional printed scaffolds compared to porous scaffolds for bone regeneration, Iran. Biomed. J. 25 (2021) 78–87, doi:10.29252/ibj.25.2.78.
[75] H. Hwangbo, J. Lee, G. Kim, Mechanically and biologically enhanced 3D-printed HA/PLLA/dECM biocomposites for bone tissue engineering, Int. J. Biol. Macromol. 218 (2022) 9–21, doi:10.1016/j.ijbiomac.2022.07.040.
[76] X. Lacambra-Andreu, N. Dergham, M. Magallanes-Perdomo, S. Meille, J. Chevalier, J.-M. Chenal, A. Maazouz, K. Lamnawar, Model composites based on poly(lactic acid) and bioactive glass fillers for bone regeneration, POLYMERS 13 (2021), doi:10.3390/polym13172991.
[77] A. Smieszek, K. Marycz, K. Szustakiewicz, B. Kryszak, S. Targonska, K. Zawisza, A. Watras, R.J. Wiglusz, New approach to modification of poly (l-lactic acid) with nano-hydroxyapatite improving functionality of human adipose-derived stromal cells (hASCs) through increased viability and enhanced mitochondrial activity, Mater. Sci. Eng. C 98 (2019) 213–226, doi:10.1016/j.msec.2018.12.099.
[78] C.-A. Dascalu, F. Miculescu, A.-C. Mocanu, A.E. Constantinescu, T.M. Butte, A.M. Pandele, R.-C. Ciocoiu, S.L. Voicu, L.T. Ciocan, Novel synthesis of core-shell biomaterials from polymeric filaments with a bioceramic coating for biomedical applications, Coatings 10 (2020), doi:10.3390/coatings10030283.
[79] C.E. Corcione, F. Scalera, F. Gervaso, F. Montagna, A. Sannino, A. Maffezzoli, One-step solvent-free process for the fabrication of high loaded PLA/HA composite filament for 3D printing, J. Therm. Anal. Calorim. 134 (2018) 575–582, doi:10.1007/s10973-018-7155-5.
[80] M. Bayart, M. Dubus, S. Charlon, H. Kerdjoudj, N. Baleine, S. Benali, J.-M. Raquez, J. Soulestin, Pellet-Based Fused Filament Fabrication (FFF)-derived process for the development of polylactic acid/hydroxyapatite scaffolds dedicated to bone regeneration, Materials 15 (2022), doi:10.3390/ma15165615.
[81] I. Fernandez-Cervantes, M.A. Morales, R. Agustin-Serrano, M. Cardenas-Garcia, P.V. Perez-Luna, B.L. Arroyo-Reyes, A. Maldonado-Garcia, Polylactic acid/sodium alginate/hydroxyapatite composite scaffolds with trabecular tissue morphology designed by a bone remodeling model using 3D printing, J. Mater. Sci. 54 (2019) 9478–9496, doi:10.1007/s10853-019-03537-1.
[82] T. Distler, N. Fournier, A. Gruenewald, C. Polley, H. Seitz, R. Detsch, A.R. Boccaccini, Polymer-bioactive glass composite filaments for 3D scaffold manufacturing by fused deposition modeling: fabrication and characterization, Front. Bioeng. Biotechnol. 8 (2020), doi:10.3389/fbioe.2020.00552.
[83] N.W. Pensa, A.S. Curry, P.P. Bonvallet, N.F. Bellis, K.M. Rettig, M.S. Reddy, A.W. Eberhardt, S.L. Bellis, 3D printed mesh reinforcements enhance the mechanical properties of electrospun scaffolds, Biomater. Res. 23 (2019), doi:10.1186/s40824-019-0171-0.
[84] H. Chen, H. Zhang, Y. Shen, X. Dai, X. Wang, K. Deng, X. Long, L. Liu, X. Zhang, Y. Li, T. Xu, Instant in-situ tissue repair by biodegradable PLA/gelatin nanofibrous membrane using a 3d printed handheld electrospinning device, Front. Bioeng. Biotechnol. 9 (2021) 684105, doi:10.3389/fbioe.2021.684105.
[85] V. Guduric, C. Metz, R. Siadous, R. Bareille, R. Levato, E. Engel, J.-C. Fricain, R. Devillard, O. Luzanin, S. Catros, Layer-by-layer bioassembly of cellularized polylactic acid porous membranes for bone tissue engineering, J. Mater. Sci. Mater. Med. 28 (2017) 78, doi:10.1007/s10856-017-5887-6.
[86] X. Liang, J. Gao, W. Xu, X. Wang, Y. Shen, J. Tang, S. Cui, X. Yang, Q. Liu, L. Yu, J. Ding, Structural mechanics of 3D-printed poly(lactic acid) scaffolds with tetragonal, hexagonal and wheel-like designs, Biofabrication 11 (2019), doi:10.1088/1758-5090/ab0f59.
[87] F. Azadmanesh, M. Pourmadadi, J. Zavar Reza, F. Yazdian, M. Omidi, B.F. Haghirosadat, Synthesis of a novel nanocomposite containing chitosan as a three-dimensional printed wound dressing technique: emphasis on gene expression, Biotechnol. Prog. 37 (2021) e3132, doi:10.1002/btpr.3132.
[88] J.A. Driscoll, R. Lubbe, A.E. Jakus, K. Chang, M. Haleem, C. Yun, G. Singh, A.D. Schneider, K.M. Katchko, C. Soriano, M. Newton, T. Maerz, X. Li, K. Baker, W.K. Hsu, R.N. Shah, S.R. Stock, E.L. Hsu, 3D-printed ceramic-demineralized

bone matrix hyperelastic bone composite scaffolds for spinal fusion, Tissue Eng. Part A 26 (2020) 157–166, doi:10.1089/ten.TEA.2019.0166.
[89] D. Gao, Z. Wang, Z. Wu, M. Guo, Y. Wang, Z. Gao, P. Zhang, Y. Ito, 3D-printing of solvent exchange deposition modeling (SEDM) for a bilayered flexible skin substitute of poly (lactide-co-glycolide) with bioorthogonally engineered EGF, Mater. Sci. Eng. C 112 (2020) 110942, doi:10.1016/j.msec.2020.110942.
[90] R. Fairag, L. Li, J.L. Ramirez-GarciaLuna, M.S. Taylor, B. Gaerke, M.H. Weber, D.H. Rosenzweig, L. Haglund, A composite lactide-mineral 3D-printed scaffold for bone repair and regeneration, Front. Cell Dev. Biol. 9 (2021), doi:10.3389/fcell.2021.654518.
[91] Y. Dou, J. Huang, X. Xia, J. Wei, Q. Zou, Y. Zuo, J. Li, Y. Li, A hierarchical scaffold with a highly pore-interconnective 3D printed PLGA/n-HA framework and an extracellular matrix like gelatin network filler for bone regeneration, J. Mater. Chem. B. 9 (2021) 4488–4501, doi:10.1039/d1tb00662b.
[92] H. Kang, X. Jiang, Z. Liu, F. Liu, G. Yan, F. Li, Biodegradable 3D printed scaffolds of modified poly (trimethylene carbonate) composite materials with Poly (L-lactic acid) and hydroxyapatite for bone regeneration, Nanomaterials 11 (2021), doi:10.3390/nano11123215.
[93] S. Kurt, S. Selviler-Sizer, B. Onuk, M. Kabak, Comparison of sheep scapula models created with polylactic acid and thermoplastic polyurethane filaments by three-dimensional modelling, Anat. Histol. Embryol. 51 (2022) 244–249, doi:10.1111/ahe.12784.
[94] M. Micic, D. Antonijevic, S. Milutinovic-Smiljanic, D. Trisic, B. Colovic, D. Kosanovic, B. Prokic, J. Vasic, S. Zivkovic, J. Milasin, V. Danilovic, M. Djuric, V. Jokanovic, Developing a novel resorptive hydroxyapatite-based bone substitute for over-critical size defect reconstruction: physicochemical and biological characterization and proof of concept in segmental rabbit's ulna reconstruction, Biomed. Tech. 65 (2020) 491–505, doi:10.1515/bmt-2019-0218.
[95] J.W. Yun, S.Y. Heo, M.H. Lee, H.B. Lee, Evaluation of a poly(lactic-acid) scaffold filled with poly(lactide-co-glycolide)/hydroxyapatite nanofibres for reconstruction of a segmental bone defect in a canine model, Vet. Med. 64 (2019) 531–538, doi:10.17221/80/2019-VETMED.
[96] B. Zhang, S. Shen, H. Xian, Y. Dai, W. Guo, X. Li, X. Zhang, Z. Wang, H. Li, L. Peng, X. Luo, S. Liu, X. Lu, Q. Guo, Fabrication of poly (lactic-co-glycolic acid)/decellularized articular cartilage extracellular matrix scaffold by three-dimensional printing technology and investigating its physicochemical properties, J. Reparative Reconstr. Surg. 33 (2019) 1011–1018, doi:10.7507/1002-1892.201901082.
[97] B. Li, C. Ruan, Y. Ma, Z. Huang, Z. Huang, G. Zhou, J. Zhang, H. Wang, Z. Wu, G. Qiu, Fabrication of vascularized bone flaps with sustained release of recombinant human bone morphogenetic protein-2 and arteriovenous bundle, Tissue Eng. Part A. 24 (2018) 1413–1422, doi:10.1089/ten.TEA.2018.0002.
[98] S. Pitjamit, W. Nakkiew, K. Thongkorn, W. Thanakulwattana, K. Thunsiri, Finite element analysis of traditional and new fixation techniques of the 3D-printed composite interlocking nail in canine femoral shaft fractures, Appl. Sci.-BASEL. 10 (2020), doi:10.3390/app10103424.
[99] S. Camarero-Espinosa, L. Moroni, Janus 3D printed dynamic scaffolds for nanovibration-driven bone regeneration, Nat. Commun. 12 (2021) 1031, doi:10.1038/s41467-021-21325-x.
[100] M. Deng, J. Tan, C. Hu, T. Hou, W. Peng, J. Liu, B. Yu, Q. Dai, J. Zhou, Y. Yang, R. Dong, C. Ruan, S. Dong, J. Xu, Modification of PLGA scaffold by MSC-derived extracellular matrix combats macrophage inflammation to initiate bone regeneration via TGF-β-induced protein, Adv. Healthc. Mater. 9 (2020) e2000353, doi:10.1002/adhm.202000353.
[101] Y. Lai, Y. Li, H. Cao, J. Long, X. Wang, L. Li, C. Li, Q. Jia, B. Teng, T. Tang, J. Peng, D. Eglin, M. Alini, D.W. Grijpma, G. Richards, L. Qin, Osteogenic magnesium incorporated into PLGA/TCP porous scaffold by 3D printing for repairing challenging bone defect, Biomaterials 197 (2019) 207–219, doi:10.1016/j.biomaterials.2019.01.013.
[102] W.-X. Cheng, Y.-Z. Liu, X.-B. Meng, Z.-T. Zheng, L.-L. Li, L.-Q. Ke, L. Li, C.-S. Huang, G.-Y. Zhu, H.-D. Pan, L. Qin, X.-L. Wang, P. Zhang, PLGA/β-TCP composite scaffold incorporating cucurbitacin B promotes bone regeneration by inducing angiogenesis, J. Orthop. Transl. 31 (2021) 41–51, doi:10.1016/j.jot.2021.10.002.
[103] W. Yu, R. Li, J. Long, P. Chen, A. Hou, L. Li, X. Sun, G. Zheng, H. Meng, Y. Wang, A. Wang, X. Sui, Q. Guo, S. Tao, J. Peng, L. Qin, S. Lu, Y. Lai, Use of a three-dimensional printed polylactide-coglycolide/tricalcium phosphate composite scaffold incorporating magnesium powder to enhance bone defect repair in rabbits, J. Orthop. Transl. 16 (2019) 62–70, doi:10.1016/j.jot.2018.07.007.
[104] J. Wei, Y. Yan, J. Gao, Y. Li, R. Wang, J. Wang, Q. Zou, Y. Zuo, M. Zhu, J. Li, 3D-printed hydroxyapatite microspheres reinforced PLGA scaffolds for bone regeneration, Mater. Sci. Eng. C (2021) 112618, doi:10.1016/j.msec.2021.112618.
[105] W. Chen, L. Nichols, L. Teer, K. Clinton, L.B. Priddy, A hybrid coating of polydopamine and nano-hydroxyapatite enhances surface properties of 3D printed poly(lactic-co-glycolic acid) scaffolds, J. Mater. Sci. 57 (2022) 13011–13026, doi:10.1007/s10853-022-07442-y.
[106] M. Lian, Y. Han, B. Sun, L. Xu, X. Wang, B. Ni, W. Jiang, Z. Qiao, K. Dai, X. Zhang, A multifunctional electrowritten bi-layered scaffold for guided bone regeneration, Acta Biomater. 118 (2020) 83–99, doi:10.1016/j.actbio.2020.08.017.
[107] C. Shuai, W. Yang, P. Feng, S. Peng, H. Pan, Accelerated degradation of HAP/PLLA bone scaffold by PGA blending facilitates bioactivity and osteoconductivity, Bioact. Mater. 6 (2021) 490–502, doi:10.1016/j.bioactmat.2020.09.001.
[108] R. Donate, M. Monzon, M.E. Aleman-Dominguez, Additive manufacturing of PLA-based scaffolds intended for bone regeneration and strategies to improve their biological properties, E-Polym. 20 (2020) 571–599, doi:10.1515/epoly-2020-0046.
[109] J. Babilotte, B. Martin, V. Guduric, R. Bareille, R. Agniel, S. Roques, V. Héroguez, M. Dussauze, M. Gaudon, D. Le Nihouannen, S. Catros, Development and characterization of a PLGA-HA composite material to fabricate 3D-printed scaffolds for bone tissue engineering, Mater. Sci. Eng. C 118 (2021) 111334, doi:10.1016/j.msec.2020.111334.
[110] Z. Xu, N. Wang, P. Liu, Y. Sun, Y. Wang, F. Fei, S. Zhang, J. Zheng, B. Han, Poly(Dopamine) coating on 3D-printed poly-lactic-co-glycolic acid/β-tricalcium phosphate scaffolds for bone tissue engineering, Molecules 24 (2019), doi:10.3390/molecules24234397.
[111] P.-C. Chang, H.-T. Luo, Z.-J. Lin, W.-C. Tai, C.-H. Chang, Y.-C. Chang, D.L. Cochran, M.-H. Chen, Preclinical evaluation of a 3D-printed hydroxyapatite/poly(lactic-co-glycolic acid) scaffold for ridge augmentation, J. Formos. Med. Assoc. Taiwan Yi Zhi. 120 (2021) 1100–1107, doi:10.1016/j.jfma.2020.10.022.
[112] S.-S. Cao, S.-Y. Li, Y.-M. Geng, K. Kapat, S.-B. Liu, F.H. Perera, Q. Li, H. Terheyden, G. Wu, Y.-J. Che, P. Miranda, M. Zhou, Prefabricated 3D-printed tissue-engineered bone for mandibular reconstruction: a preclinical translational study in primate, ACS Biomater. Sci. Eng. 7 (2021) 5727–5738, doi:10.1021/acsbiomaterials.1c00509.
[113] P.-C. Chang, H.-T. Luo, Z.-J. Lin, W.-C. Tai, C.-H. Chang, Y.-C. Chang, D.L. Cochran, M.-H. Chen, Regeneration of critical-sized mandibular defect using a 3D-printed hydroxyapatite-based scaffold: an exploratory study, J. Periodontol. 92 (2021) 428–435, doi:10.1002/JPER.20-0110.
[114] S.K. Lee, C.-M. Han, W. Park, I.H. Kim, Y.K. Joung, D.K. Han, Synergistically enhanced osteoconductivity and anti-inflammation of PLGA/β-TCP/Mg(OH)(2) composite for orthopedic applications, Mater. Sci. Eng. C 94 (2019) 65–75, doi:10.1016/j.msec.2018.09.011.
[115] H. Liu, H. Zhu, L. Cheng, Y. Zhao, X. Chen, J. Li, X. Xv, Z. Xiao, W. Li, J. Pan, Q. Zhang, C. Zeng, J. Guo, D. Xie, D. Cai, TCP/PLGA composite scaffold loaded rapamycin in situ enhances lumbar fusion by regulating osteoblast and osteoclast activity, J. Tissue Eng. Regen. Med. 15 (2021) 475–486, doi:10.1002/term.3186.
[116] R. Duan, Y. Wang, D. Su, Z. Wang, Y. Zhang, B. Du, L. Liu, X. Li, Q. Zhang, The effect of blending poly (l-lactic acid) on in vivo performance of 3D-printed poly(l-lactide-co-caprolactone)/PLLA scaffolds, Biomater. Adv. 138 (2022) 212948, doi:10.1016/j.bioadv.2022.212948.
[117] E. Akerlund, A. Diez-Escudero, A. Grzeszczak, C. Persson, The effect of PCL addition on 3D-printable PLA/HA composite filaments for the treatment of bone defects, Polymers 14 (2022), doi:10.3390/polym14163305.
[118] S. Pitjamit, K. Thunsiri, W. Nakkiew, T. Wongwichai, P. Pothacharoen, W. Wattanutchariya, The possibility of interlocking nail fabrication from FFF 3D printing PLA/PCL/HA composites coated by local silk fibroin for canine bone fracture treatment, Materials 13 (2020), doi:10.3390/ma13071564.
[119] J. Pizzicannella, F. Diomede, A. Gugliandolo, L. Chiricosta, P. Bramanti, I. Merciaro, T. Orsini, E. Mazzon, O. Trubiani, 3D Printing PLA/gingival stem cells/EVs upregulate miR-2861 and -210 during osteoangiogenesis commitment, Int. J. Mol. Sci. 20 (2019), doi:10.3390/ijms20133256.
[120] Z.B. Velioglu, D. Pulat, B. Demirbakan, B. Ozcan, E. Bayrak, C. Erisken, 3D-printed poly(lactic acid) scaffolds for trabecular bone repair and regeneration: scaffold and native bone characterization, Connect. Tissue Res. 60 (2019) 274–282, doi:10.1080/03008207.2018.1499732.
[121] N. Söhling, J. Neijhoft, V. Nienhaus, V. Acker, J. Harbig, F. Menz, J. Ochs, R.D.R.D. Verboket, U. Ritz, A. Blaeser, E. Dörsam, J. Frank, I. Marzi, D. Henrich, N. Soehling, J. Neijhoft, V. Nienhaus, V. Acker, J. Harbig, F. Menz, J. Ochs, R.D.R.D. Verboket, U. Ritz, A. Blaeser, E. Doersam, J. Frank, I. Marzi, D. Henrich, N. Söhling, J. Neijhoft, V. Nienhaus, V. Acker, J. Harbig, F. Menz, J. Ochs, R.D.R.D. Verboket, U. Ritz, A. Blaeser, E. Dörsam, J. Frank, I. Marzi, D. Henrich, 3D-Printing of hierarchically designed and osteoconductive bone tissue engineering scaffolds, MATERIALS. 13 (2020), doi:10.3390/ma13081836.
[122] A. Lauer, P. Wolf, D. Mehler, H. Goetz, M. Ruezgar, A. Baranowski, D. Henrich, P.M. Rommens, U. Ritz, Biofabrication of SDF-1 functionalized 3D-printed cell-free scaffolds for bone tissue regeneration, Int. J. Mol. Sci. 21 (2020), doi:10.3390/ijms21062175.
[123] S.H. Han, M. Cha, Y.-Z. Jin, K.-M. Lee, J.H. Lee, BMP-2 and hMSC dual delivery onto 3D printed PLA-Biogel scaffold for critical-size bone defect regeneration in rabbit tibia, Biomed. Mater. 16 (2021) 15019, doi:10.1088/1748-605X/aba879.
[124] C.-H. Yao, Y.-H. Lai, Y.-W. Chen, C.-H. Cheng, Bone morphogenetic protein-2-activated 3D-printed polylactic acid scaffolds to promote bone regrowth and repair, Macromol. Biosci. 20 (2020) e2000161, doi:10.1002/mabi.202000161.
[125] R.T. Anbu, V. Suresh, R. Gounder, A. Kannan, Comparison of the efficacy of three different bone regeneration materials: an animal study, Eur. J. Dent. 13 (2019) 22–28, doi:10.1055/s-0039-1688735.
[126] M. Zhu, J. Tan, L. Liu, J. Tian, L. Li, B. Luo, C. Zhou, L. Lu, Construction of biomimetic artificial intervertebral disc scaffold via 3D printing and electrospinning, Mater. Sci. Eng. C 128 (2021), doi:10.1016/j.msec.2021.112310.
[127] M. Alksne, M. Kalvaityte, E. Simoliunas, I. Gendviliene, P. Barasa, I. Rinkunaite, A. Kaupinis, D. Seinin, V. Rutkunas, V. Bukelskiene, Dental pulp stem cell-derived extracellular matrix: autologous tool boosting bone regeneration, Cytotherapy 24 (2022) 597–607, doi:10.1016/j.jcyt.2022.02.002.
[128] B.N. Teixeira, P. Aprile, R.H. Mendonça, D.J. Kelly, R.M.D.S.M. Thiré, Evaluation of bone marrow stem cell response to PLA scaffolds manufactured by 3D printing and coated with polydopamine and type I collagen, J. Biomed. Mater. Res. Part B 107 (2019) 37–49, doi:10.1002/jbm.b.34093.

[129] X. Zhang, Q. Lou, L. Wang, S. Min, M. Zhao, C. Quan, Immobilization of BMP-2-derived peptides on 3D-printed porous scaffolds for enhanced osteogenesis, Biomed. Mater. Bristol Engl. 15 (2019) 15002, doi:10.1088/1748-605X/ab4c78.
[130] L. Perez-Sanchez, M.A.O. De la O, P. Gonzalez-Alva, L.A. Medina, D. Masuoka-Ito, M.A. Alvarez-Perez, J. Serrano-Bello, In vivo study on bone response to 3D-printed constructs designed from microtomographic images, J. Mater. Eng. Perform. 30 (2021) 5005–5012, doi:10.1007/s11665-021-05585-8.
[131] A. Sharma, S. Gupta, T.S. Sampathkumar, R.S. Verma, Modified graphene oxide nanoplates reinforced 3D printed multifunctional scaffold for bone tissue engineering, Biomater. Adv. 134 (2022) 112587, doi:10.1016/j.msec.2021.112587.
[132] K.-S. Liu, W.-H. Chen, C.-H. Lee, Y.-F. Su, Y.-W. Liu, S.-J. Liu, Novel biodegradable 3D-printed analgesics-eluting-nanofibers incorporated nuss bars for therapy of pectus excavatum, Int. J. Mol. Sci. 23 (2022) 2265, doi:10.3390/ijms23042265.
[133] J.L. Chakka, T. Acri, N.Z. Laird, L. Zhong, K. Shin, S. Elangovan, A.K. Salem, Polydopamine functionalized VEGF gene-activated 3D printed scaffolds for bone regeneration, RSC Adv. 11 (2021) 13282–13291, doi:10.1039/d1ra01193f.
[134] P. Wang, H.-M. Yin, X. Li, W. Liu, Y.-X. Chu, Y. Wang, Y. Wang, J.-Z. Xu, Z.-M. Li, J.-H. Li, Simultaneously constructing nanotopographical and chemical cues in 3D-printed polylactic acid scaffolds to promote bone regeneration, Mater. Sci. Eng. C 118 (2021), doi:10.1016/j.msec.2020.111457.
[135] J. Yun, J. Lee, C.W. Ha, S.J. Park, S. Kim, K. Koo, Y. Seol, Y. Lee, The effect of 3-D printed polylactic acid scaffold with and without hyaluronic acid on bone regeneration, J. Periodontol. (2022) 1–11, doi:10.1002/jper.21-0428.
[136] M. Bahraminasab, A. Talebi, N. Doostmohammadi, S. Arab, A. Ghanbari, S. Zarbakhsh, The healing of bone defects by cell-free and stem cell-seeded 3D-printed PLA tissue-engineered scaffolds, J. Orthop. Surg. 17 (2022) 320, doi:10.1186/s13018-022-03213-2.
[137] F. Diomede, A. Gugliandolo, P. Cardelli, I. Merciaro, V. Ettorre, T. Traini, R. Bedini, D. Scionti, A. Bramanti, A. Nanci, S. Caputi, A. Fontana, E. Mazzon, O. Trubiani, Three-dimensional printed PLA scaffold and human gingival stem cell-derived extracellular vesicles: a new tool for bone defect repair, Stem Cell Res. Ther. 9 (2018), doi:10.1186/s13287-018-0850-0.
[138] M. Cha, Y.-Z. Jin, J.W. Park, K.M. Lee, S.H. Han, B.S. Choi, J.H. Lee, Three-dimensional printed polylactic acid scaffold integrated with BMP-2 laden hydrogel for precise bone regeneration, Biomater. Res. 25 (2021), doi:10.1186/s40824-021-00233-7.
[139] H. Chen, Q. Shi, H. Shui, P. Wang, Q. Chen, Z. Li, Degradation of 3D-printed porous polylactic acid scaffolds under mechanical stimulus, Front. Bioeng. Biotechnol. 9 (2021), doi:10.3389/fbioe.2021.691834.
[140] P. Karimipour-Fard, R. Pop-Iliev, H. Jones-Taggart, G. Rizvi, G.U. Erinc, Design of 3D scaffold geometries for optimal biodegradation of poly(lactic acid)-based bone tissue, in: Proc. 35TH Int. Conf. Polym. Process. Soc. PPS-35, 2020, p. 2205, doi:10.1063/1.5142977.
[141] H. Shui, Q. Shi, N.M. Pugno, Q. Chen, Z. Li, Effect of mechanical stimulation on the degradation of poly(lactic acid) scaffolds with different designed structures, J. Mech. Behav. Biomed. Mater. 96 (2019) 324–333, doi:10.1016/j.jmbbm.2019.04.028.
[142] S.C. Cifuentes, L. Saldana, J.Luis Gonzalez-Carrasco, R. Benavente, A. Garcia-Penas, Effect of thermal processing on the dynamic/isothermal crystallization and cytocompatibility of polylactic acid for biomedical applications, Macromol. Chem. Phys. 222 (2021), doi:10.1002/macp.202100274.
[143] E. Mohan, M.S. Kumar, Experimental investigation on mechanical and tribological properties of the fused filament fabrication of poly-lactic acid parts with various print orientations, Appl. Phys. 128 (2022), doi:10.1007/s00339-022-05579-w.
[144] Y. Zhang, C. Wang, L. Fu, S. Ye, M. Wang, Y. Zhou, Fabrication and application of novel porous scaffold in situ-loaded graphene oxide and osteogenic peptide by cryogenic 3D printing for repairing critical-sized bone defect, Molecules 24 (2019), doi:10.3390/molecules24091669.
[145] A.C.D. Nascimento Jr., R.C.D.A.G. Mota, L.R.D. Menezes, E.O.D. Silva, Influence of the printing parameters on the properties of Poly(lactic acid) scaffolds obtained by fused deposition modeling 3D printing, Polym. Polym. Compos. 29 (2021) S1052–S1062, doi:10.1177/09673911211040770.
[146] B. Gao, H. Jing, M. Gao, S. Wang, W. Fu, X. Zhang, X. He, J. Zheng, Long-segmental tracheal reconstruction in rabbits with pedicled Tissue-engineered trachea based on a 3D-printed scaffold, Acta Biomater. 97 (2019) 177–186, doi:10.1016/j.actbio.2019.07.043.
[147] C. Pagano, L. Rebaioli, F. Baldi, I. Fassi, G.U. Erinc, Mechanical behavior of scaffold-like structures: research of relationships between properties and geometry, in: Proc. 35TH Int. Conf. Polym. Process. Soc. PPS-35, 2020, p. 2205, doi:10.1063/1.5142979.
[148] R. Baptista, M. Guedes, Morphological and mechanical characterization of 3D printed PLA scaffolds with controlled porosity for trabecular bone tissue replacement, Mater. Sci. Eng. C 118 (2021), doi:10.1016/j.msec.2020.111528.
[149] R. Baptista, M. Guedes, Porosity and pore design influence on fatigue behavior of 3D printed scaffolds for trabecular bone replacement, J. Mech. Behav. Biomed. Mater. 117 (2021), doi:10.1016/j.jmbbm.2021.104378.
[150] D. Singh, A. Babbar, V. Jain, D. Gupta, S. Saxena, V. Dwibedi, Synthesis, characterization, and bioactivity investigation of biomimetic biodegradable PLA scaffold fabricated by fused filament fabrication process, J. Braz. Soc. Mech. Sci. Eng. 41 (2019), doi:10.1007/s40430-019-1625-y.
[151] K.-C. Feng, A. Pinkas-Sarafova, V. Ricotta, M. Cuiffo, L. Zhang, Y. Guo, C.-C. Chang, G.P. Halada, M. Simon, M. Rafailovich, The influence of roughness on stem cell differentiation using 3D printed polylactic acid scaffolds, Soft Matter 14 (2018) 9838–9846, doi:10.1039/c8sm01797b.
[152] A. Grivet-Brancot, M. Boffito, G. Ciardelli, Use of polyesters in fused deposition modeling for biomedical applications, Macromol. Biosci. 22 (2022), doi:10.1002/mabi.202200039.
[153] Y.K. Yeon, H.S. Park, J.M. Lee, J.S. Lee, Y.J. Lee, Md.T. Sultan, Y.B. Seo, O.J. Lee, S.H. Kim, C.H. Park, New concept of 3D printed bone clip (polylactic acid/hydroxyapatite/silk composite) for internal fixation of bone fractures, J. Biomater. Sci. 29 (2018) 894–906, doi:10.1080/09205063.2017.1384199.
[154] X. Chen, C. Gao, J. Jiang, Y. Wu, P. Zhu, G. Chen, 3D printed porous PLA/nHA composite scaffolds with enhanced osteogenesis and osteoconductivity in vivo for bone regeneration, Biomed. Mater. 14 (2019), doi:10.1088/1748-605X/ab388d.
[155] Z. Liu, Y. Ge, L. Zhang, Y. Wang, C. Guo, K. Feng, S. Yang, Z. Zhai, Y. Chi, J. Zhao, F. Liu, The effect of induced membranes combined with enhanced bone marrow and 3D PLA-HA on repairing long bone defects in vivo, J. TISSUE Eng. Regen. Med. 14 (2020) 1403–1414, doi:10.1002/term.3106.
[156] W. Wang, B. Zhang, M. Li, J. Li, C. Zhang, Y. Han, L. Wang, K. Wang, C. Zhou, L. Liu, Y. Fan, X. Zhang, 3D printing of PLA/n-HA composite scaffolds with customized mechanical properties and biological functions for bone tissue engineering, Compos. Part B 224 (2021) 109192, doi:10.1016/j.compositesb.2021.109192.
[157] W. Wang, B. Zhang, L. Zhao, M. Li, Y. Han, L. Wang, Z. Zhang, J. Li, C. Zhou, L. Liu, Fabrication and properties of PLA/nano-HA composite scaffolds with balanced mechanical properties and biological functions for bone tissue engineering application, Nanotechnol. Rev. 10 (2021) 1359–1373, doi:10.1515/ntrev-2021-0083.
[158] B. Zhang, L. Wang, P. Song, X. Pei, H. Sun, L. Wu, C. Zhou, K. Wang, Y. Fan, X. Zhang, 3D printed bone tissue regenerative PLA/HA scaffolds with comprehensive performance optimizations, Mater. Des. 201 (2021) 109490, doi:10.1016/j.matdes.2021.109490.
[159] H. Zhang, X. Mao, D. Zhao, W. Jiang, Z. Du, Q. Li, C. Jiang, D. Han, Three dimensional printed polylactic acid-hydroxyapatite composite scaffolds for prefabricating vascularized tissue engineered bone: an in vivo bioreactor model, Sci. Rep. 7 (2017) 15255, doi:10.1038/s41598-017-14923-7.
[160] B.W. Minto, A.G. Sprada, J.A. Gonçalves Neto, B.M. de Alcântara, T.A.S. de S. Rocha, A.C.V. Hespanha, C. Quarterone, M. da R. Sartori, A. Hataka, R.A.R. Uscategui, L.G.G.G. Dias, Three-dimensional printed poly (L-lactide) and hydroxyapatite composite for reconstruction of critical bone defect in rabbits, Acta Cirúrgica Bras 36 (2021) e360404, doi:10.1590/acb360404.
[161] I. Gendviliene, E. Simoliunas, M. Alksne, S. Dibart, E. Jasiuniene, V. Cicenas, R. Jacobs, V. Bukelskiene, V. Rutkunas, Effect of extracellular matrix and dental pulp stem cells on bone regeneration with 3D printed PLA/HA composite scaffolds, Eur. Cell. Mater. 41 (2021) 204–215, doi:10.22203/eCM.v041a15.
[162] M.O.C. Maia-Pinto, A.C.B. Brochado, B.N. Teixeira, S.C. Sartoretto, M.J. Uzeda, A.T.N.N. Alves, G.G. Alves, M.D. Calasans-Maia, R.M.S.M. Thiré, Biomimetic mineralization on 3D printed PLA scaffolds: on the response of human primary osteoblasts spheroids and in vivo implantation, Polymers 13 (2020) 74, doi:10.3390/polym13010074.
[163] C. Tu, J. Chen, C. Huang, Y. Xiao, X. Tang, H. Li, Y. Ma, J. Yan, W. Li, H. Wu, C. Liu, Effects of electromagnetic fields treatment on rat critical-sized calvarial defects with a 3D-printed composite scaffold, Stem Cell Res. Ther. 11 (2020) 433, doi:10.1186/s13287-020-01954-7.
[164] D.Y. Kwon, J.H. Park, S.H. Jang, J.Y. Park, J.W. Jang, B.H. Min, W.-D. Kim, H.B. Lee, J. Lee, M.S. Kim, Bone regeneration by means of a three-dimensional printed scaffold in a rat cranial defect, J. Tissue Eng. Regen. Med. 12 (2018) 516–528, doi:10.1002/term.2532.
[165] I. Tcacencu, N. Rodrigues, N. Alharbi, M. Benning, S. Toumpaniari, E. Mancuso, M. Marshall, O. Bretcanu, M. Birch, A. McCaskie, K. Dalgarno, Osseointegration of porous apatite-wollastonite and poly(lactic acid) composite structures created using 3D printing techniques, Mater. Sci. Eng. C 90 (2018) 1–7, doi:10.1016/j.msec.2018.04.022.
[166] H. Zhang, X. Mao, Z. Du, W. Jiang, X. Han, D. Zhao, D. Han, Q. Li, Three dimensional printed macroporous polylactic acid/hydroxyapatite composite scaffolds for promoting bone formation in a critical-size rat calvarial defect model, Sci. Technol. Adv. Mater. 17 (2016) 136–148, doi:10.1080/14686996.2016.1145532.
[167] Z. Xu, B. Lin, C. Zhao, Y. Lu, T. Huang, Y. Chen, J. Li, R. Wu, W. Liu, J. Lin, Lanthanum doped octacalcium phosphate/polylactic acid scaffold fabricated by 3D printing for bone tissue engineering, J. Mater. Sci. Technol. 118 (2022) 229–242, doi:10.1016/j.jmst.2021.09.069.
[168] N.P. Tipnis, D.J. Burgess, Sterilization of implantable polymer-based medical devices: a review, Int. J. Pharm. 544 (2018) 455–460, doi:10.1016/j.ijpharm.2017.12.003.
[169] L.-C. Gerhardt, A.R. Boccaccini, Bioactive glass and glass-ceramic scaffolds for bone tissue engineering, Materials 3 (2010) 3867–3910, doi:10.3390/ma3073867.
[170] K. Hayashi, M.L. Munar, K. Ishikawa, Effects of macropore size in carbonate apatite honeycomb scaffolds on bone regeneration, Mater. Sci. Eng. C. 111 (2020) 110848, doi:10.1016/j.msec.2020.110848.
[171] A.R. Amini, C.T. Laurencin, S.P. Nukavarapu, Bone Tissue Engineering: Recent Advances and Challenges, 2013.
[172] N. Abbasi, S. Hamlet, R.M. Love, N.-T. Nguyen, Porous scaffolds for bone regeneration, J. Sci. Adv. Mater. Devices. 5 (2020) 1–9, doi:10.1016/j.jsamd.2020.01.007.
[173] S.G. Pedrero, P. Llamas-Sillero, J. Serrano-López, A multidisciplinary journey towards bone tissue engineering, Materials 14 (2021) 4896, doi:10.3390/ma14174896.

[174] K.-W. Chong, C.Y.-L. Woon, M.-K. Wong, Induced membranes—a staged technique of bone-grafting for segmental bone loss: surgical technique, J. Bone Jt. Surg. 93 (2011) 85–91, doi:10.2106/JBJS.J.01251.
[175] B. Zhang, L. Wang, P. Song, X. Pei, H. Sun, L. Wu, C. Zhou, K. Wang, Y. Fan, X. Zhang, 3D printed bone tissue regenerative PLA/HA scaffolds with comprehensive performance optimizations, Mater. Des. 201 (2021), doi:10.1016/j.matdes.2021.109490.
[176] R.-S. Chen, S.-H. Hsu, H.-H. Chang, M.-H. Chen, Challenge tooth regeneration in adult dogs with dental pulp stem cells on 3D-printed hydroxyapatite/polylactic acid scaffolds, CELLS 10 (2021), doi:10.3390/cells10123277.
[177] A.M. Maadani, E. Salahinejad, Performance comparison of PLA- and PLGA-coated porous bioceramic scaffolds: mechanical, biodegradability, bioactivity, delivery and biocompatibility assessments, J. Controlled Release 351 (2022) 1–7, doi:10.1016/j.jconrel.2022.09.022.
[178] Y. Zhao, B. Zhu, Y. Wang, C. Liu, C. Shen, Effect of different sterilization methods on the properties of commercial biodegradable polyesters for single-use, disposable medical devices, Mater. Sci. Eng. C 105 (2019) 110041, doi:10.1016/j.msec.2019.110041.
[179] N.S. Turker, A.Y. Özer, Ş. Çolak, B. Kutlu, R. Nohutçu, ESR investigations of gamma irradiated medical devices, Appl. Radiat. Isot. 130 (2017) 121–130, doi:10.1016/j.apradiso.2017.09.026.
[180] S. Pérez-Davila, L. González-Rodríguez, R. Lama, M. López-Álvarez, A.L. Oliveira, J. Serra, B. Novoa, A. Figueras, P. González, 3D-Printed PLA medical devices: physicochemical changes and biological response after sterilisation treatments, Polymers 14 (2022) 4117, doi:10.3390/polym14194117.
[181] S. Zeiter, K. Koschitzki, M. Alini, F. Jakob, M. Rudert, M. Herrmann, Evaluation of preclinical models for the testing of bone tissue-engineered constructs, Tissue Eng. Part C 26 (2020) 107–117, doi:10.1089/ten.tec.2019.0213.
[182] L. Carbone, J. Austin, Pain and laboratory animals: publication practices for better data reproducibility and better animal welfare, PLoS ONE 11 (2016) e0155001, doi:10.1371/journal.pone.0155001.
[183] M.K. Huss, S.A. Felt, C. Pacharinsak, Influence of pain and analgesia on orthopedic and wound-healing models in rats and mice, Comp. Med. 69 (2019) 535–545, doi:10.30802/AALAS-CM-19-000013.
[184] M. Guarnieri, C. Brayton, L. DeTolla, N. Forbes-McBean, R. Sarabia-Estrada, P. Zadnik, Safety and efficacy of buprenorphine for analgesia in laboratory mice and rats, Lab. Anim. 41 (2012) 337–343, doi:10.1038/laban.152.
[185] L. Benato, N.J. Rooney, J.C. Murrell, Pain and analgesia in pet rabbits within the veterinary environment: a review, Vet. Anaesth. Analg. 46 (2019) 151–162, doi:10.1016/j.vaa.2018.10.007.
[186] P. Leucht, J.-B. Kim, R. Wazen, J.A. Currey, A. Nanci, J.B. Brunski, J.A. Helms, Effect of mechanical stimuli on skeletal regeneration around implants, Bone 40 (2007) 919–930, doi:10.1016/j.bone.2006.10.027.
[187] N. Mangir, S. Dikici, F. Claeyssens, S. MacNeil, Using *ex Ovo* Chick Chorioallantoic Membrane (CAM) assay to evaluate the biocompatibility and angiogenic response to biomaterials, ACS Biomater. Sci. Eng. 5 (2019) 3190–3200, doi:10.1021/acsbiomaterials.9b00172.
[188] I. Moreno-Jiménez, J.M. Kanczler, G. Hulsart-Billstrom, S. Inglis, R.O.C. Oreffo, The chorioallantoic membrane assay for biomaterial testing in tissue engineering: a short-term *in vivo* preclinical model, Tissue Eng. Part C 23 (2017) 938–952, doi:10.1089/ten.tec.2017.0186.
[189] P. Bédard, S. Gauvin, K. Ferland, C. Caneparo, È. Pellerin, S. Chabaud, S. Bolduc, Innovative human three-dimensional tissue-engineered models as an alternative to animal testing, Bioengineering 7 (2020) 115, doi:10.3390/bioengineering7030115.
[190] E. Petrovova, Preclinical alternative model for analysis of porous scaffold biocompatibility in bone tissue engineering, ALTEX 36 (2019) 121–130, doi:10.14573/altex.1807241.
[191] A. Weigand, J.P. Beier, A. Arkudas, M. Al-Abboodi, E. Polykandriotis, R.E. Horch, A.M. Boos, The Arteriovenous (AV) loop in a small animal model to study angiogenesis and vascularized tissue engineering, J. Vis. Exp. 54676 (2016), doi:10.3791/54676.
[192] M. Bouyer, C. Garot, P. Machillot, J. Vollaire, V. Fitzpatrick, S. Morand, J. Boutonnat, V. Josserand, G. Bettega, C. Picart, 3D-printed scaffold combined to 2D osteoinductive coatings to repair a critical-size mandibular bone defect, Mater. Today Bio 11 (2021) 100113, doi:10.1016/j.mtbio.2021.100113.
[193] W. Wang, J. Wei, D. Lei, S. Wang, B. Zhang, S. Shang, B. Bai, C. Zhao, W. Zhang, C. Zhou, H. Zhou, S. Feng, 3D printing of lithium osteogenic bioactive composite scaffold for enhanced bone regeneration, Compos. Part B 256 (2023) 110641, doi:10.1016/j.compositesb.2023.110641.

La regeneración de tejidos óseos continúa siendo en la actualidad un importante problema clínico y socioeconómico, tanto en medicina humana como en veterinaria. La falta de sustitutos óseos clínicamente relevantes hace patente la necesidad de investigar nuevos métodos alternativos que puedan ser utilizados en el proceso de curación ósea. El objetivo de esta Tesis Doctoral fue la síntesis de andamiajes compuestos de ácido poliláctico y bioapatitas derivadas de dientes de tiburón fabricados mediante tecnología de impresión 3D, y la evaluación de su potencial para lograr la regeneración de defectos óseos, modificando su composición o su patrón de impresión.